A Sheffield Hallam University thesis

Spectroscopic and Thermal Analysis of Clay Mineral-Organic Composites

Nigel D'Mello

A thesis submitted in partial fulfilment of the requirements of
Sheffield Hallam University
for the degree of Doctor of Philosophy

June 2003

Abstract

Composites of clay minerals have been prepared with organic monomers for subsequent study upon polymerisation. Particular combinations of clays and organic species have enabled three unique systems to be studied.

The first involves the intercalation of the clay minerals Kaolin and Halloysite with Phenylphosphonic Acid (PPA). The intercalation process proceeds via the use of an acetone / water entraining agent and subsequent analysis by Diffuse Reflectance Infrared Fourier transform Spectroscopy (DRIFTS), X-Ray Diffraction (XRD), Thermogravimetric Analysis (TGA) and Evolved Gas Analysis (EGA) using TG-Mass Spectrometry. This has revealed the remarkable thermal stability of these intercalates; they are stable to above 450 °C, and exhibit interlayer spacings of 15.4 Å. Furthermore, the fate of the water as the entraining agent is determined and is found to be hydrogen bonded to the phosphonic acid moiety of PPA and also weakly bound to the inner surface hydroxyls in these clays. This water represents an opportunity for displacement by an organic monomer, and the lone pair of electrons on the oxygens also provide scope for coordination. Hence, the PPA intercalates were treated with the monomer N-vinylformamide (VFA) and evaluated for subsequent polymerisation.

In the second system, montmorillonite was intercalated with VFA and then treated with a polar activator (Propylene Carbonate) prior to polymerisation. The polar activator interacts with the bifunctional VFA molecules causing the clay to swell further prior to polymerisation. This produces significant differences in the XRD traces with and without polymerisation of VFA in the presence of the clay. If the polar activator is absent the $d_{(001)}$ spacing is 21.0 Å. If the polar activator is present then no $d_{(001)}$ is observed , in a situation reminiscent of an exfoliated nanocomposite.

In the last system studied an *in – situ* intercalative approach was employed. Montmorillonite was treated with dialdehydes and diamines capable of reacting together to form amino resins oligomers and polymers. The molar ratio of the two reactants determines the intermediate and hence the subsequent product that is formed as characterised by DRIFTS. In a binary mixture where both reactants are simultaneously added to the clay, if the aldehyde is in excess, then dimethylol condensation products are formed. If the amine is in excess then monomethylol condensation products are formed. Sequentially adding these two reactants to clay (i.e. treating the clay first with one reactant and washing to remove any excess, then adding a second reactant) also has a bearing on the results. If the amine is added first, then the aldehyde is able to displace it from the clay interlayer. If however, the aldehyde is added first, then monomethylol reaction product is seen and this together with DRIFTS TGA and XRD analysis indicates that some of the aldehyde has been removed during the washing process.

Acknowledgments

Yes, I know, I took far too long to write up so I'll just get right on with it. First of all people at Hallam. I would like to acknowledge my supervisor Prof. Chris Breen and also Prof. Jack Yarwood for their help. For teaching me how to make polymers, I thank Dr. Neil Bricklebank. For his help with XRD and fixing the thing numerous times when it was down a lot of thanks to Dr. Brain Lewis. I had a great deal of help too from my colleagues with various aspects of my work from synergy to VT-DRIFTS etc so I'd also like to thank Jeff Forsyth, Scott Taylor and Francis Clegg for the time they put in for me and for confusing me no end with the synergy.

Now to thank my friends also, especially Dr. Joe Jaegar without whom I would never have had the confidence to submit. I'd like also to thank a lot of my friends for the support and encouragement which really made a difference before my viva – thanks to Al (Dr. Evil), Craig ("looks like a Koala Bear" Williams) and Helen (Hanson Haircut) for coming down to Sheffield on the day. Sound words of encouragement too from Andy were very timely as were the long conversations with James many times in Manchester. I'm sure too I should be thanking Kev probably for endless beers on a Friday afternoon and for being an A1 lopper who can growl.

I'd like lastly to thank my family (even if none of you understood what I was doing so long) especially Cait who helped in many, many ways not least for listening to my griping, sage advice and being my better half. The only thing that would make it all perfect would be to share it with my Dad, who is never far from memory.

Table of Contents

Abbreviations

TGA – Thermogravimetric Analysis

DTG – Derivative Thermogram

FTIR – Fourier Transform Infrared Spectroscopy

DRIFTS – Diffuse Reflectance Infrared Fourier Transform Spectroscopy

XRD – X- Ray Diffraction

EGA – Evolved Gas Analysis

CEC – Cation Exchange Capacity

TIC – Total Ion Chromatogram

PPA – Phenylphosphonic Acid

KPPA – Intercalate prepared from Kaolin and Phenylphosphonic Acid

HPPA – Intercalate prepared from Halloysite and Phenylphosphonic Acid

VFA – N-vinylformamide

DMF –N, N- Dimethylformamide

NMF – N-methylformamide

3NH2 – 3, 3-diamino – N – methyldipropylamine

DAP – 1, 3 – diaminopropane

EDA – Ethylenediamine

PC – Propylene Carbonate

Chapter One – Introduction

1.1 Aims and Objectives

Clay mineral – organic composites have been studied within this thesis using a selection of layered minerals and organic species. Particular combinations of clays and organic species used enabled unique systems to be studied, and permitted the formation of clay mineral - nanocomposites from these materials. The systems studied can be divided into three areas, each related but with differing objectives.

1.1.2 Kaolin / Halloysite – Phenylphosphonic Acid

The clay minerals kaolin and halloysite were modified with phenylphosphonic acid to form intercalation compounds. These products were then subjected to thermal and spectroscopic analysis to ascertain their stability versus temperature and also the nature of the interaction between the clay mineral and phenylphosphonic acid.

Furthermore, the resultant intercalation products and untreated minerals were then treated with N-vinylformamide with the aim of forming nanocomposites.

1.1.3 Amine – Aldehyde Clay Composites

This work was undertaken as an exploratory study for Schlumberger Cambridge Research (SCR). Montmorillonite (SWy-2) was treated with various amines and aldehydes (in aqueous solutions) to form a (nano) composite capable of shale stabilisation. The reaction product between these two organics may be an imine and it was hoped to form a polyimine between the clay layers. Alternatively this reaction may also form an amino resin, hence it was necessary to examine any evidence for imine or amino resin formation. The montmorillonite – single reactant systems were also studied.

1.1.3 Montmorillonite – N-vinylformamide Composites

Montmorillonite was treated with the monomer n-vinylformamide with the aim of polymerising this monomer within the layers of the clay to form a nanocomposite. Most nanocomposites

are formed via the use of an organoclay, but the aim here was to investigate a system that had not been organfunctionalised. Furthermore the use of a polar activator to aid in nanocomposite formation was investigated.

1.2 Shale Stabilisation

The market for oilfield chemicals has been estimated at approximately £100 million p.a. in the North Sea sector alone and ten times this value elsewhere. When drilling for oil, shale is one of the most common rock types encountered, making up more than 75% of drilled formations and causing more than 90% of borehole instability problems.[1] Some of the common wellbore instability problems are illustrated in Figure 1:-
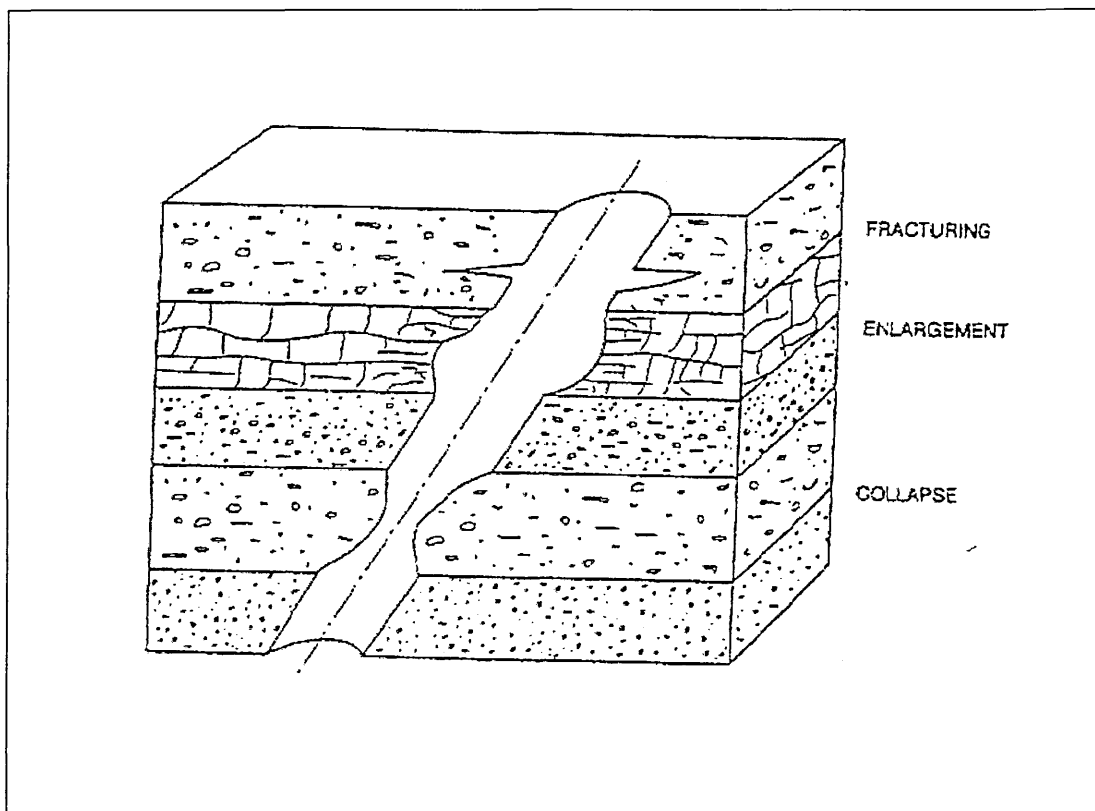
Figure 1.0 Common Borehole Instability Types.

Shales are rocks that have been formed by the compaction of marine sediments over time. Water is squeezed out of the rock as the sediment is buried deeper and deeper by the deposition of further sediment layers. Such marine sediments become more compact as the depth of burial increases. In turn, this compaction will increase as long as excess water is

2

able to escape from the shale. Consequently older shales are more compact, retain less water and as a result are hard and less easily dispersed into water, whereas younger shales, are softer and disperse easily in water[2].

Shale is typically composed of quartz, feldspar, pyrite, gypsum, moisture and a large amount of clay – kaolinite, illite and mainly montmorillonite. Montmorillonite is a swelling clay – it is able to intercalate a large amount of water which penetrates between the layers of the clay thus causing it to expand. Conversely, non swelling clays such as kaolinite and illite swell to a much less degree if at all in the presence of water. The amount of clay found in shale is dependant on the composition of the shale sediments as they are deposited on the seabed. The type of clay encountered in shale not only depends on the composition of marine sediments at the time of deposition but also the conditions to which the sediment is subjected once buried.

The presence of montmorillonite in shale is indicative of younger less compacted shales. When these sediments age and the depth to which they are buried increases, the percentage of illite in the shale increases. Illite is formed from the conversion of montmorillonite by a process called diagenesis. The driving force for diagenesis is thought to be the temperature attained as the sediments are buried deeper, rather than the pressure exerted by such burial[3]. The adsorption of water can be seen in the enlargement of the borehole in Figure 1.0, and this also causes collapse[4-5]. Both these problems reflect the property of montmorillonite to adsorb vast quantities of water and, hence, why this clay is the most troublesome found in shale. As the montmorillonite in rocks swells on contact with water the sides of the borehole also swell leading to fragments dislodging themselves and leaving behind enlarged spaces within the borehole or subsequent fracturing. These fragments may fall further down the hole causing blockages. In addition the swelling may be so great as to cause narrowing of the hole in more extreme conditions.

It should also be noted that temperatures in boreholes may reach as much as 60 – 80 °C in the North Sea and even up to 150 °C off the coast of Saudi Arabia and in the Gulf.

1.2.1 Solutions to Borehole Instability

The destructive effect of montmorillonite on borehole stability has made it very desirable to find a solution to this problem. The collapse of a borehole ultimately leads to downtime and simply inserting a pipeline / steel casing is not economically viable i.e. bore hole instability is costly.

The mechanisms by which reactive shales may be stabilised include chemical adsorption, reducing clay dispersion in drilling fluids, prevention of water invasion, binding together of shale particles to improve mechanical strength and increasing mud lubricity (thus reducing mechanical damage from the drillstring)[2].

In order to address these mechanisms, drilling muds have been employed. The use of such drilling muds may enable drilling to continue for longer periods without the need for steel casing. Using less casing may also enable as much as £500000 per well to be saved. The main desirable properties identified in such muds include the following[6]:

- Control of density – prevents blowouts from the borehole which occur when porous rocks are drilled.

- Rheology – required for the efficient removal of suspended drilled solids (cuttings) from the drill bit to the drill platform.

- Filtration – This is effected by the use of solids in the drilling mud which form a thin layer of low permeability on the inside of the borehole. This reduces the amount of fluid permeating into the shale pore spaces and therefore prevents excessive wall cake accumulation and fluid loss.

1.2.2 Drilling Muds.

Oil based muds (OBM) contain, as the name implies oil, barite as a weighting agent and drilled solids such as clay to improve the filtration and rheological properties. As the clays are hydrophilic surfactants are added to counteract this. OBMs were first used in the late 1970's and their use quickly became widespread due to their high effectiveness attained during shale drilling[2,7]. In addition, OBMs satisfy the criteria laid out above for drilling muds. However, OBM produce oily wastes which have a lasting environmental impact and has resulted in the banning of OBM or the reduction of waste to near zero levels[8].

4

This has lead to considerable research into the development of water based muds (WBM). WBM again contain barite for reasons discussed above but also polymers and surfactants to maintain borehole stability. Clays / water suspensions also provide high-shear velocity, yield stress and fluid loss control. Soluble salts such as KCl are also added to reduce the dispersion of clays and promote shale inhibition by shielding the negative charges on the clay[9]. Polyacylamide was commonly used as the polymer additive, but these WBM proved less effective than OBM in promoting shale stability and also not nearly as cost effective.

Cationic polymers have also been used as shale inhibitors in WBM but (although the performance was good), these proved incompatible with other mud additives[10], have an environmental impact on marine species and have high depletion rates that increase drilling costs[11].

Research carried out in this study has investigated the possibility of forming a polymer that will prevent a shale from swelling and effecting mud rheology. Such a polymer may be a polyimine, formed from the reaction between an aldehyde and amine. The polymer may interact with the clay thus forming a clay mineral - polymer nanocomposite.

1.3 Nanocomposites.

If the market for polymer nanocomposites is examined the projected figures show how important this class materials is becoming (Table 1.0).

	Global Market million lb	
Market Sector	Year - 2004	Year - 2009
Packaging	105.9	367.6
Automotive	50.6	345.7
Building & Construction	13.3	151.5
Coatings	21.9	63.5
Industrial	18.2	48.1
Other Markets	19.9	67.3

Table 1.0 – Market Analysis of the Projected Growth of Polymer Nanocomposites.

The projected growth for polymer nanocomposites serves to show not only the importance of this material but also the diversity and growth of an important market.

A composite material usually comprises of two or more materials possessing complementary physical and chemical properties. Together these materials are expected to produce a synergistic property, which is difficult to attain separately from that of the individual components. Usually one component serves as the matrix in which particles of the other are uniformly dispersed. A polymer is one of the primary components and an inorganic particle (a filler) the other.

These polymer composites (sometimes called macro or microcomposites) are commonplace and are used in diverse applications such transportation vehicles, construction materials, electronics, sporting goods, and many other consumer products[12]. The new property obtained from such a composite can be illustrated by looking at the construction industry where such materials offer the advantage of low weight but high strength, stiffness and durability.

The resulting properties depend largely on the interfacial interactions and mixing between the organic polymer phase and the dimensions and microstructure of the particulate inorganic filler phase. As such these phases are generally incompatible, but a better interfacial interaction will impart better properties to a polymer composite such as high modulus, tensile strength, and hardness as well as resistance to fatigue, cracking and corrosion[13-14]. In a worst case scenario the phases would be immiscible resulting in a coarsely blended macrocomposite with chemically distinct phases. This results in poor physical attraction between the organic phase and the inorganic filler phase. Indeed, when the phases are still compatible to a degree, micometer size filler particles may still act as stress concentrators.

Nanocomposites are often described as "new class" of materials, where again, there is a combination of two or more phases containing different compositions or structures but, more importantly, at least one dimension of the dispersed phase is in the nanometer range[15]. The phases may be inorganic – inorganic, inorganic – organic, or organic – organic[12]. The resulting material may be amorphous, crystalline or semicrystalline.

Similarly, nanocomposites enjoy a wide range of similar applications to their macro and micro counterparts such as enhanced mechanical and barrier properties, fire retardation, magnetic, electronic and optical properties. Biological, polymer based nanocomposites are also

widespread. Examples of these include bones, cartilage cobwebs, cuticles, scales, teeth, shells, and wood. These are derived from inorganic phases such as carbonate and phosphate minerals and from biological polymers such as carbohydrates, lipids and proteins[16].

These improved properties are generally thought to make nanocomposites better than their counterparts due to the nanometer size characteristics of the dispersed phase. Arguments supporting this include that they maximise the interfacial adhesion, due to the small size of the phase and therefore the high surface to volume ratio[17]; the inorganic phase is now too small to be a stress concentrator; quantum size effects; coulombic charging effects originating from the nanometer sizes and morphology[18-19].

Alexandre and Dubois[15], in their comprehensive review, identify three different types of nanocomposites, dependant on the number of dimensions of the dispersed particles that are in the nanometer range,:-

1. Isodimensional nanoparticles. These have three dimensions in the order of nanometers such as spherical slica nanoparticles and semiconductor nanoclusters[20]. These are obtained by in situ sol – gel methods or by polymerisation promoted directly from their surface[21-23].

2. Nanotubes or "whiskers". These have two dimensions in the nanoscale with a third larger one forming an elongated structure. Included here are carbon nanotubes or cellulose whiskers[24-26]. These have been extensively studied as reinforcing nanofillers.

3. Polymer layered crystal nanocomposites. Here, only one dimension is in the nanometer range. The filler is present in the form of sheets of one to a few nanometers thick and hundreds to thousands of nanometers long. This class of material is obtained by intercalation of the polymer (or monomer which is subsequently polymerised) inside the galleries of the layered inorganic crystals. This class of nanocomposite offers an extensive range of improved properties as previously discussed.

One of the most widely studied layered host crystals in the third category above are clay minerals. They are easily available, relatively cheap and their intercalation chemistry is well studied. Furthermore the smectite group of clay minerals, which includes montmorillonite, can

readily accommodate either polymers or monomers within their galleries, and effectively form nanoscale building blocks. Clay mineral nanocomposites are reviewed in more detail in later chapters.

One of the main advantages of using clay minerals as fillers is their ability to swell when accommodating an organic phase such as a polymer. In order to overcome the hydrophilicity of clays and enable them to swell more, they are often treated with an organic to form an organoclay. Organoclays are commonly used to subsequently form nanocomposites due to their enhanced swelling abilites. The use of phenylphosphonic acid (PPA) has been investigated to such an end by treating kaolinite with this organic, and subsequently treating this intercalated clay with the monomer N – vinylformamide, prior to polymerisation.

In this thesis the formation of nanocomposites have also been investigated without the use of such organoclays. The use of N – vinylformamide has been employed as a route to nanocomposite formation without the use of organoclays, as this monomer swells montmorillonite to a large extent.

Chapter Two – Clay Mineral Structures

2.0 An Introduction to Clay Minerals

Clay minerals are the product of chemical weathering of minerals formed deep within the earth such as feldspars and other silicate minerals. The weathering is initiated when minerals meet the atmosphere and react with it. However, they may also be formed by deposition as a sediment or by hydrothermal action.

As a result they are the major components of soils, sedimentary rocks, the outcrops of which cover about 75% earth's land surface, and of the pelagic oozes blanketing the ocean basins. Clay minerals are composed of silica, alumina, water and usually a quantity of iron, alkalis and alkaline earth metals.

In terms of size, clay minerals are generally thought of as less than 2µm to a geologist and less than 4µm to engineers and soil scientists, 2µm being the generally accepted size. Indeed, one of the ways in which clays are separated from their bulk rock or soil constituents employs size fractionation.

Clays have, and continue to be one of the most important industrial minerals, enjoying a wide range of uses. They are important in geology, agriculture, construction, engineering, process industries, and environmental applications. Traditional applications are many. Some of the more important include ceramics, paper, paint, plastics, drilling fluids, foundary bondants, chemical carriers, liquid barriers, decolourisors and catalysis[27-28].

Research and development activities in academia, government and industry are continually resulting in new and innovative clay products. Many of these new applications are the result of improved processing, which provides clays of higher purity, more precise particle size and distribution, whiter and brighter colour, modified surface chemistry and other physical and chemical modifications. Some new and improved clay products include tailored or engineered paper coating kaolins, enhanced paper thickeners, nanofillers for plastics, pillared clays as special absorbents and catalysts, clays for fertilizer suspensions, clays for the adsorption of

animal wastes, calcined kaolins with high brightness and low abrasion, faster casting clays, and clays with a high modulus of rupture[27].

The diverse usage of clay minerals is directly attributable to their variation in structure. It was not until the 1920s that clays were first analysed and discovered to be crystalline materials by X –ray diffraction (XRD) studies, although in the late 1800s clays were already gaining interest beyond the traditional applications of the time such as ceramics. As other techniques such as infrared spectroscopy, thermal analysis and electron microscopy came to the fore in the middle of the 20th century the chemical and physical properties, and, more importantly, their structure were then more clearly understood[29].

2.1 Clay Structure

Most clay minerals have a characteristic arrangement of their constituent atoms in interlinked planes. This gives rise to the sheet structure within clays and hence clays are generally known as sheet silicates or phyllosilicates. These sheets when linked together form layers within the clay. These layers are polymerised or stacked to give two dimensional structures in a clay particle. It is the arrangement and composition of the layers that give rise to differing clays. Essentially, two types of sheets are found in clays.

2.1.1 The Tetrahedral Sheet

A tetrahedral sheet is comprised of SiO_4^{4-} units, in which each Si is surrounded by four O to form a tetrahedron. Bonding to achieve the sheet – like structure is through sharing of basal oxygens (Figure 2.0). The sheet is flat with all the tetrahedral bases lying in the same plane.
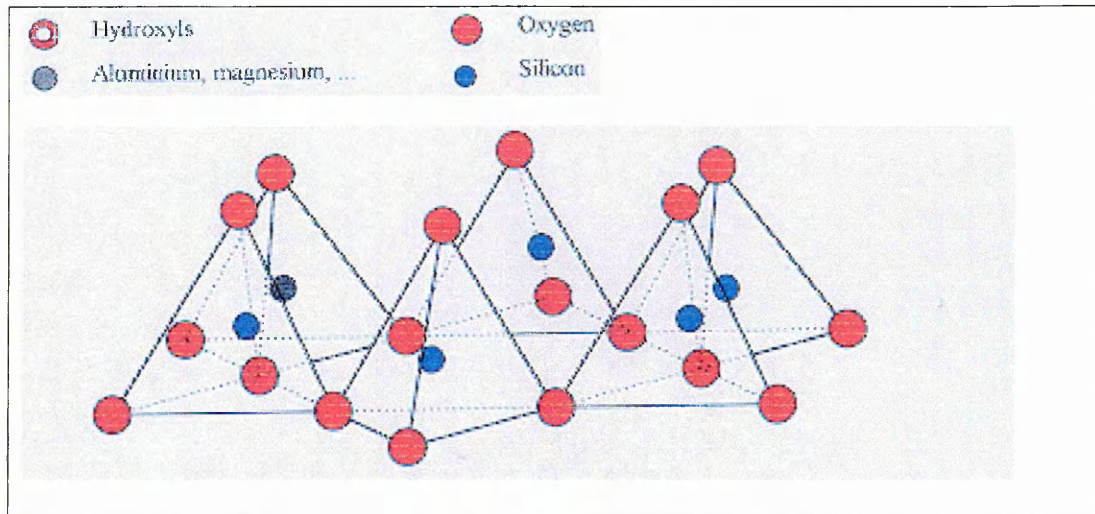
Figure 2.0 – Basal arrangement of silica tetrahedral

The arrangement of the interlinked basal oxygens of the tetrahedra occurs in such a way as to leave a hexagonal "hole" in the network of oxygen atoms, called the ditrigonal cavity. On the opposite side of the linked tetrahedra are what are called the apical oxygens of this sheet. Quite often the tetrahedral sheet is represented schematically as in Figure 2.1:-
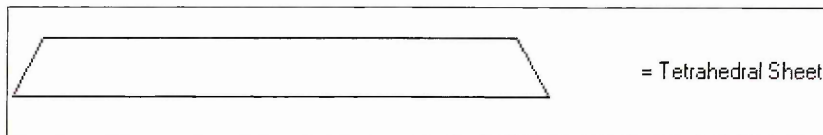
= Tetrahedral Sheet

Figure 2.1. Schematic representation of tetrahedral sheet.

2.1.2 The Octahedral Sheet

An octahedral sheet contains cations which are coordinated with six oxygens or hydroxyl units in an octahedral polyhedron (Figure 2.2).
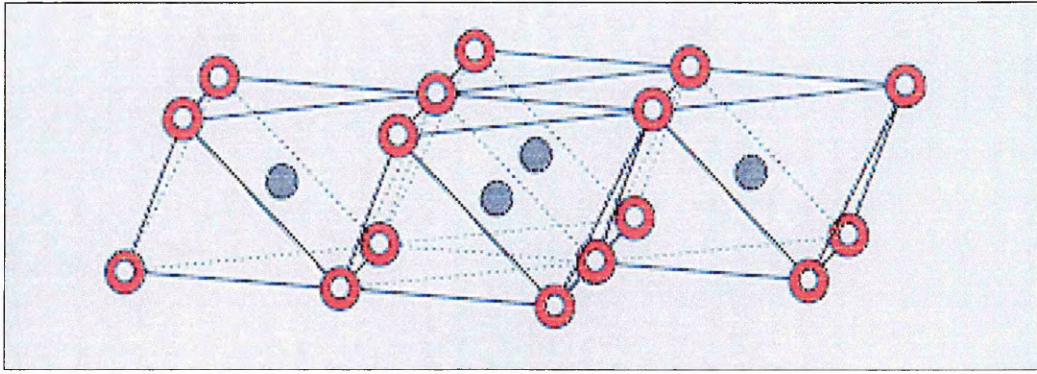
Figure 2.2 – The arrangement of atoms in the octahedral sheet.

As in the case of the tetrahedra, the octahedrally coordinated cations (commonly Mg^{2+} or Al^{3+}) are interlinked with shared anions in a two dimensional structure. When aluminium is present, only two thirds of the positions in the lattice are filled, whereas when magnesium is present, all the positions are filled to balance the structure.. Again the octahedral sheet can be represented schematically (Figure 2.3)
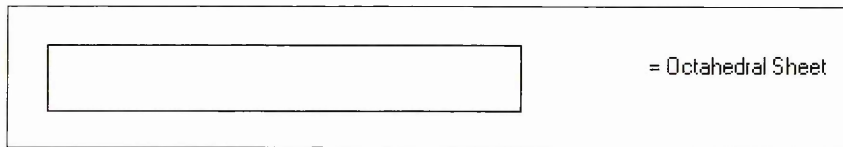
= Octahedral Sheet

Figure 2.3. Schematic representation of the octahedral sheet.

2.1.3 Forming the Layer Structure

The octahedral sheet is linked to the tetrahedral sheet via sharing of the apical oxygens from the Si tetrahedra. Herein lie the differences between the various types of clay, as it is also the ratio in which they are present in one layer of clay which forms the basis for the classification of clay minerals.

For example, when one tetrahedral and one octahedral sheet combine a 1:1 type clay is formed such as kaolin. One octahedral sheet sandwiched between two tetrahedral sheets gives rise to 2:1 type clays such as the smectite, montmorillonite.

2.1.4 Isomorphous Substitution

Isomorphous substitution occurs in clay minerals when cations of the same charge but different valency (usually lower) replace ions in both the octahedral and tetrahedral sheet. This results in a negatively charged structure and this positive charge deficiency is neutralised by sorption of interlayer cations between the layers of the clay (see below). These hold the sheets together. Typical substitutions are Mg for Al in the octahedral sheet and Al for Si in the tetrahedral sheet.

2.1.5 Interlayer Cations

The interlayer cations (or exchange cations) influence the surface and colloidal properties of clays and may themselves be exchanged by other cations (metallic or organic). They are present when isomorphous substitution occurs and neutralise the negative charge imparted on the structure caused by isomorphous substitution. The interlayer cations may be hydrated and the addition of more water or an organic may cause the interlayer space of a clay to swell; this is termed intercalation. Such a clay may now have different properties depending on the intercalant. The charge (and size) of the interlayer cation will determine the capacity of the intercalate e.g. a Na^+ exchanged montmorillonite will expand in water to interlayer spacings of greater than 20 Å, whereas a Ca^{2+} exchanged montmorillonite due to its greater attractive forces exerted between layers by the Ca^{2+} ion will only expand to 17 Å. When formed naturally, calcium is a predominant interlayer cation, while sodium and magnesium are common.

2.1.6 Cation Exchange Capacity

The cation exchange capacity (CEC) is the maximum number of these ions that may be exchanged. It is determined by immersing a quantity of clay in an aqueous solution containing a salt, usually chloride, or ammonium hydroxide. The clay is extracted from the solution after being washed several times to ensure that there is no residual salt present, and therefore that all of the cations are fixed on the surface or in the clay (hence exchange capacity). The washing step is carried out to homogenise the ionic species present in the sample in order to quantify the amount of material present naturally. In this way, the CEC reflects the overall charge imbalance on the

layer structure and the exchange capacity of the clay – it is an estimate of both the number of ions adsorbed between the layers of a clay structure and of those adsorbed on the outer surfaces. It is measured in terms of the quantity of ions present in milliequivalents per 100g of dried clay.

2.1.7 Classification of Clay Minerals

Some of the differences in clay minerals arise therefore, from the arrangement of the sheets, the layer charge and the extent of isomorphous substitution, and the nature of the interlayer cations. These properties also determine a clays ability to intercalate other species into the layer structure. Clays to be classified into seven groups, according to their layer charge: -

1. **The kaolinite and serpentine group.** Has a 1:1 arrangement, and an overall layer charge of zero. There is no isomorphous substitution and hence no interlayer cations. Intercalation is possible but relatively difficult to achieve. Typical examples of minerals of this group include kaolinite , $Al_4(Si_4O_{10})OH_8$ and halloysite, $Al_4Si_4O_8$ $OH_8.4H_2O$.

2. **The pyrophyllite and talc group.** This group contains non – swelling 2:1 minerals, with a layer charge of zero, resulting from the lack of isomorphous substitution. Hence intercalation and cation exchange are not possible. Typical examples include talc $Mg_6(Si_8O_{20})(OH)_4$, and pyrophyillite $Al_4(Si_8O_{20})OH)_4$.

3. **The smectite group.** This group of strongly swelling clays have a 2:1 ratio (octahedral to tetrahedral sheet) and a layer charge of $0.5 – 1.2$ per unit cell. Isomorphous substitution readily occurs with interlayer cations adsorbed to balance the layer charge. Examples include montmorillonite $Na_{0.6}(Al_{3.4}Mg_{0.6})Si_8O_{20}(OH)_4$. Na is shown here as the main interlayer cation though this may be mixed with other cations such as Ca^{2+}, and easily exchanged not only with other cations but organo-cations such as tetramethylammonium.

4. **The vermiculite group.** Again a 2:1 layer arrangement. The overall layer charge is 0.5 – 1.2 per unit cell. Here, isomorphous substitution occurs only in the tetrahedral sheet, and

14

cation exchange is difficult. Intercalation of water and other molecules is possible. Examples include vermiculite $(Mg, Fe^{2+}, Fe^{3+})_6 (Si>Al)_8 O_{20}(OH)_4.nH_2O$.

5. **Illite.** The structure is the same as that for montmorillonite except that some of the silicon ions are replaced by aluminium ions and the resultant charge deficiency is balanced by potassium ions. The small size of the potassium ions allows short range Van der Waals forces to contribute along with the electrostatic forces to an increased strength in the bonding between the layers. Thus the clay layers are held tightly together making swelling difficult. An ideal structural formula is $KAl_2(Sl_3Al)O_{10}(OH)_2$, but Mg and Fe may also be present. Other formulae are $KAl_2(Sl_3Al)O_{20}(OH)_4$.

6. **The chlorites.** Chlorites have an unusual arrangement of two tetrahedral sheets sandwiching an octahedral sheet, but also another octahedral sheet together comprising one layer. This results in a layer charge of 1.1 – 3.3 per unit cell. Intercalation of water occurs only when the hydrogen bonding between the layers is disrupted. Examples include donbassite $Al_4(Si_8O_{20})(OH)_4Al_4(OH)_{12}$.

7. **The mica group.** Has a 2:1 arrangement, and a layer charge of ≤2 per unit cell. There is isomorphous substitution of Si^{4+} by Al^{3+} in the tetrahedral sheet and this is balanced by sorption of K^+. These K^+ ions are in twelve – fold coordination, being situated centrally on the lines of the centres joining the ditrigonal network of oxygen ions of adjacent silicate layers. This arrangement together with the high charge per formula unit makes it difficult to expand the layers due to the strong electrostatic attraction, especially for ions of large size and low hydration energy (NH_4^+, Cs^+) Examples include muscovite.

8. **The palygorskite and sepiolite group.** These minerals are composed of trimorphic layers arranged in chains, or bands which are joined through the oxygen atoms. The tetrahedral sheets are continuous but the apices of the SiO_4 in adjacent chains point in opposite directions, giving rise to a corrugated surface with open channels running parallel to the chains. Examples include palygorskite $Mg_5(Si_8O_{20})(OH)_2(OH)_4.4H_2O$.

The minerals studied in this thesis include kaolin, halloysite and montmorillonite and these are described in further detail below.

2.2 Detailed Structures

2.2.1 The Structure of Kaolin

Kaolin has a structural formula of $Al_2Si_2O_5(OH)_4$, (Figure 2.4) and comprises of one tetrahedral sheet and one octahedral sheet. There are no interlayer cations in kaolin and the layers are held together via hydrogen bonding of the hydroxl groups of the octahedral sheet and the oxygens of the tetrahedral sheet. Organic interaction (see later) is thus through bonding to the external surface (relatively easy) or through intercalation (harder as there are

no interlayer cations). If intercalation takes place (section 2.4.2) then this necessitates disrupting the strong hydrogen bonding network holding the layers together and the intercalate itself must be capable of hydrogen bonding with the surfaces of the octahedral and tetrahedral sheets.
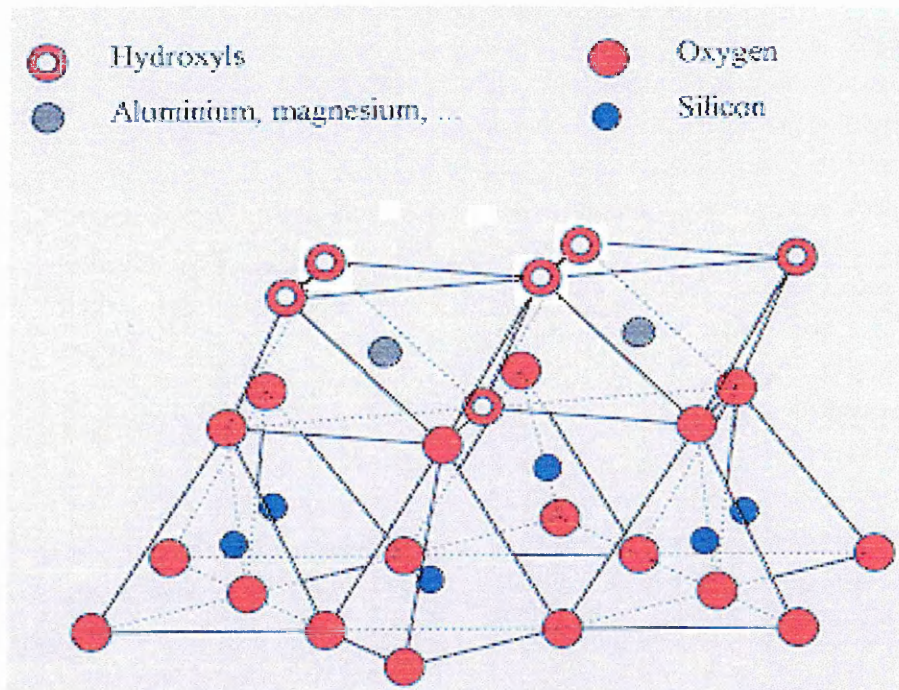
Figure 2.4 The Structure of Kaolin

The thickness of the kaolin layer is calculated from XRD and in particular the first reflection – (called the $d_{(001)}$ or basal spacing), and is measured in Å. Hence in this instance the $d_{(001)}$ spacing for kaolin (which is the octahedral and tetrahedral sheet combined) is 7.2 Å (Figure 2.5)

16
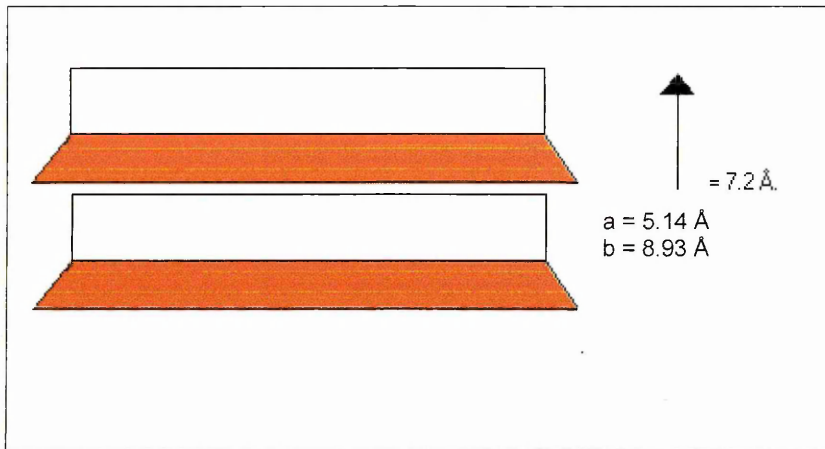
Figure 2.5. The $d_{(001)}$ spacing in kaolin

2.2.1 The Structure of Halloysite

Halloysite has a structural formula of $Al_4Si_4O_8.4H_2O$. It is often considered a polytype of kaolin. Halloysite possesses the same 1:1 arrangement of layers – one tetrahedral and one octahedral, but occurs naturally as an expanded phase with a $d_{(001)}$ spacing of 10.0 Å. This is a result of the incorporation of water into the interlamellar space (Figure 2.6). Furthermore there are differences in the dimensions of the octahedral and tetrahedral sheets which cause the layers to curl[29-31]. As compared with kaolin, stacking of successive layers within a single crystal is disordered. The interlayer water molecules are thought to be arranged in a hexagonal network, linked to each other and to adjacent halloysite layers by hydrogen bonding.
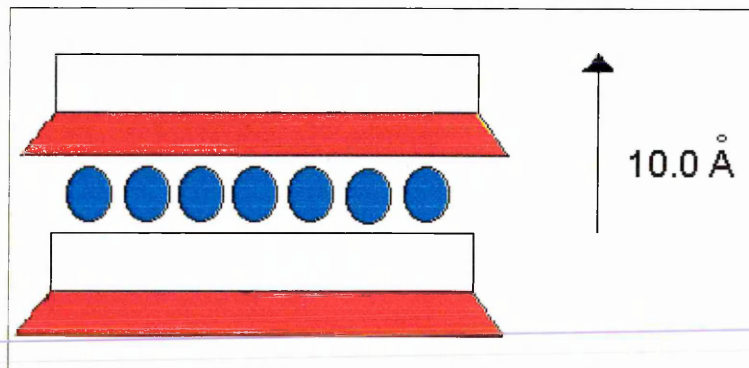
Figure 2.5 – Halloysite structure showing naturally occurring water in interlayer space (blue).

Electron microscopy reveals that kaolin particles are arranged as flat, hexagonal plates. Halloysite however is often seen as tubular. This difference is morphology is attributed to a difference in the b dimension of the octahedral and tetrahedral sheets, which causes the layers to curl when the restraint imposed by the close proximity of adjacent layers is removed by the presence of interlayer water. The halloysite morphology i.e. tubes or plates etc may be due to the elemental composition of the octahedral sheet. This is what alters the b dimension.

2.3   The Structure of Montmorillonite

A typical structural formula for montmorillonite is $Na_{0.3}(Al_{1.7}Mg_{0.3})Si_4O_{10}(OH)_2$. It can be seen that the structure (Figure 2.6) comprises an octahedral sheet sandwiched between two tetrahedral sheets. Isomorphous substitution readily occurs of Al^{3+} in the octahedral layer by other cations such as Mg^{2+}, Fe^{2+} and less frequently Al^{3+} for Si^{4+} in the tetrahedral sheet.
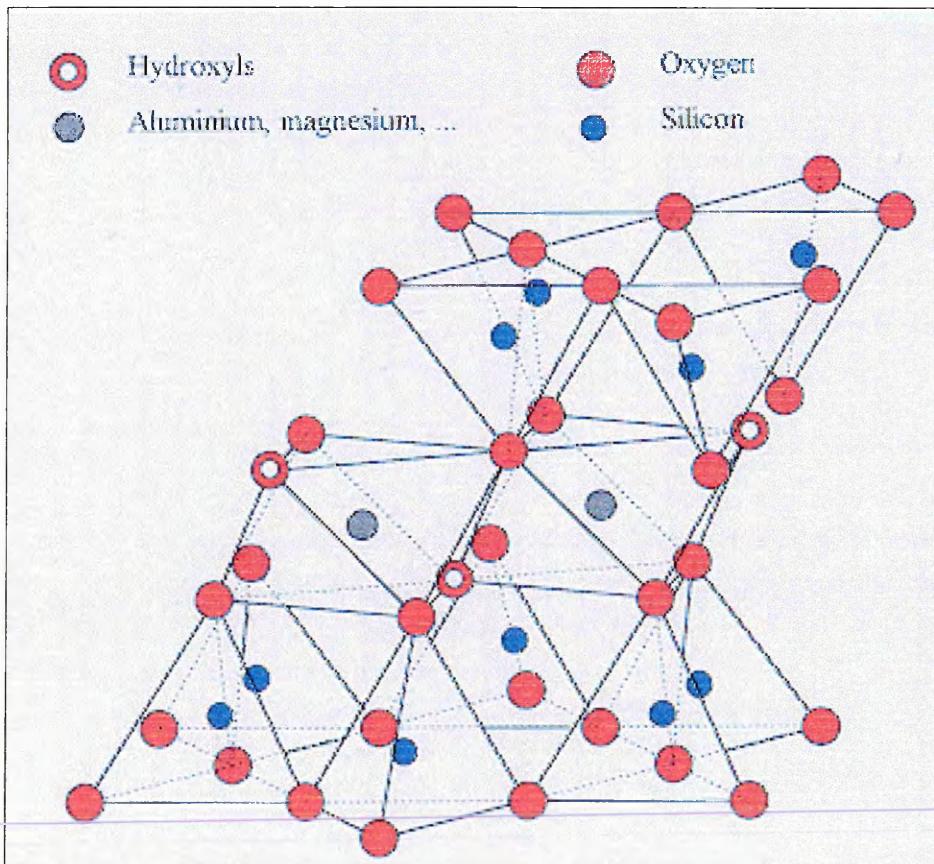
Figure 2.6 Montmorillonite Structure.

18

Hence cations (e.g. Na^+ which can be exchanged) are sorbed between the layers. This results in weak electrostatic interactions, due to a lowering of the charge density, between the layers allowing easy swelling and intercalation by water and other polar molecules.

The interlayer cations present in montmorillonite will readily bind water and this reflected in the $d_{(001)}$ spacing of montmorillonites. However, as the interlayer cation varies in montmorillonites, this is also reflected in the $d_{(001)}$ spacing. Without the presence of water the $d_{(001)}$ spacing of montmorillonite is 9.6 Å (with an interlayer cation such as Na^+). With large monovalent or divalent interlayer cations present water will swell the clay to a $d_{(001)}$ spacing of 19.0 Å. If however, the interlayer cation is small and monovalent (Na^+, Li^+), swelling due to water adsorption may be as much as 40.0 Å, reflecting the ability of these cations to hold together the clay layers.

2.4   Clay-Organic Interaction Sites

Clay minerals undergo a varied range of interactions with many organics[32], which may result in specific properties being imparted to the clay; hence the need for a clear understanding of the source of these interactions before a description of the resulting properties and reactions can be undertaken.

Johnston[32] provides a comprehensive review and identifies six predominant active sites.

1. The Neutral Siloxane Surface - This is the SiO_4^{4-} tetrahedral sheet in a clay. It occurs in 2:1 layer silicates where no isomorphous substitution has taken place (*e.g.* talc and pyrophylite) and in 1:1 layer silicates such as kaolin. Each of the surface oxygens are co-ordinated to two Si atoms and, as previously stated, the oxygen atoms are arranged in a hexagonal network. This type of surface has a low affinity for water and in terms of surface reactivity the siloxane surface in clay minerals is considered to be inert and unreactive due to the strong bond formed between the Si and O atoms.

2. Isomorphous Substitution Sites - This site occurs as a result of isomorphous substitution in 2:1 layer silicates and are characterised by a permanent negative charge. Some of the sites are situated on the basal surfaces of 2:1 layer silicates *i.e.* the tetrahedral sheet. To compensate

19

for this negative charge exchangeable cations (interlayer cations) are sorbed. If present, organic cations and protonated organic bases can also participate in cation exchange reactions. The location of these sites has a large influence on the sorption of polar and charged organic solutes. Substitution in the octahedral sheet creates a soft Lewis base which changes to a harder Lewis base when the substitution is in the tetrahedral sheet. Selectivity for inorganic and organic cations, degree of swelling and accessibility of the interlamellar region are all influenced by the extent and type of isomorphous substitution in layer silicates. For example substitution of Al^{3+} for Si^{4+} in the siloxane surface increases reactivity and surface acidity. Repulsion between non - bonding electron pairs on the oxygen surface increases due to Al substitution and the overall basic strength increases. The potential for polar organic molecules to hydrogen bond directly to the clay surface will thus increase as this substitution increases.

3. Exchangeable Metal Cations and Exposed Undercoordinated Metal Atoms - In these sites, an organic solute co-ordinates directly to the metal cation. The degree of metal - organic interaction will depend on the ability of the organic solute to compete for co-ordination sites around the metal centre and the size and charge of the exchange cation. A larger cation will accommodate larger molecules as it creates more space between the layers due to its large size such as Cs^+ or Ba^{2+}. A small highly charged cation such as Al^{3+} will more easily polarise incoming molecules - such as water for example - than Ni^{2+} and Na^+.

4. Polarised Water Molecules Surrounding Exchangeable Cations - Two types of sorbed water are present in this site. There are water molecules directly co-ordinated to exchangeable cations and interlamellar spaces between the exchange cations, physisorbed water occupying interstitial pores, or polar sites on external surfaces. The polarised water molecules surrounding exchange cations can donate protons to adjacent organic solutes and promote a variety of chemical reactions. Thus organic species may co-ordinate with the metal cation via a water bridge.

5. Hydrophobic Sites - Sorption of organic molecules on clay surfaces can impart a hydrophobic nature to the clay surface. For example, exchanging of alkyl-ammonium cations for inorganic

20

cations on montmorillonite. This creates an organo-clay with unique surface properties with respect to the original clay, resulting in an organophilic surface. Such a surface on an organo - clay makes it an efficient sorbent for non polar compounds and helps in nanocomposite formation.

6. Broken Edge Sites - see section 2.4.1.below on kaolin surface adsorption.

2.4.1 Surface Adsorption on Kaolin

Kaolin has available a siloxane surface (from the SiO_4 tetrahedral sheet), and an opposing surface of hydroxyls (from the octahedral sheet) - available for hydrogen bonding. Thus organics must be able to interact strongly with OHs. In addition, the edges of kaolinite crystals are also important, as these contain 'broken bonds' or broken edge sites. These sites occur at the end of sheets and layers. The broken edges leave coordinatively unsaturated ions (Si^{4+}, Al^{3+}) which may react with water molecules to form more surface OH groups. In turn, these surface OH groups may form inner-sphere complexes with metal species and hydrogen bond to adsorptive or solvent molecules accumulated at an interface or be influenced by inorganic or organic cations through electrostatic interactions. At low pH these hydroxylated edge sites develop a positive charge due to the adsorption of protons. This allows organic acids and oxyanions to interact strongly with these positively charged sites at low pH. As the pH increases, these sites develop a neutral charge and ultimately a negative charge when the pH value is greater than the point of zero charge of the kaolin surface.

These edge sites contribute to the cation exchange capacity (CEC) of the clay and the extent of the contribution depends on the particle size. Large particles contribute only a minimal amount, and as the particle size decreases the contribution increases. This is a significant site in kaolin as kaolin does not have any isomorphous substitution and hence has no exchange cations.

2.4.2 Kaolin Intercalation

As previously described, it is relatively difficult to intercalate organic molecules into kaolin - the oxygen and hydroxyl planes of successive layers in a single crystal results in interlayer hydrogen

bonding. Nevertheless, intercalation remains possible, usually with the aid of an organic solvent containing the intercalating molecule, which itself, must be able to hydrogen bond with hydroxyl surface of the octahedral sheet. At high temperatures (100°C) the organic solvent first penetrates the layers. In time this is replaced by the intercalant of interest. Intercalation can also be achieved without the use of such solvents and using small polar molecules alone such as dimethyl sulfoxide (DMSO), N-methylformamide and hydrazine[29,33].

2.4.2.1 Intercalation in Halloysite

As might be expected, intercalation in halloysite is easier and generally quicker than in kaolin as the layers are already separated by the interlayer water. Intercalation of a variety of species is facilitated by replacement of this water, often in less extreme conditions than needed for kaolin. This is analogous to the use of 10.0 Å hydrated kaolin, which can be used as an intermediate for the intercalation of other organic species (see Chapter 4)

2.4.3 Intercalation in Montmorillonites

Intercalation in montmorillonites primarily involves the interlayer cations. Organic solutes may co-ordinate directly with the metal cations as previously described. However, at high water contents, organic solutes have a limited ability to compete for co-ordination positions around the hydrated cation. At lower water contents, however, this barrier is removed and unsaturated organic solutes can participate in electron transfer and subsequent polymerisation reactions.

Non polar organic solutes interact with montmorillonite at four sites in relation to the active sites previously described - the hydrophobic site (the interaction of non - polar organic compounds will be greatly enhanced by the presence of hydrophobic "coatings" on clay surfaces), the neutral siloxane surface, with hydrated cations (weak interaction) and with exchangeable metal cations or exposed undercoordinated metal cations (Lewis acid sites). Polar organic compounds may interact with the exchange cation and broken edge sites on montmorillonite.

Organic cations readily replace exchange cations and have characteristically high selectivity. In terms of active sites, organic cations are stabilised by electrostatic interaction with charge in the

clay and broken edge sites, via ion exchange and through van der Waals interactions of the hydrophobic part of the organic cation with the neutral portion of the siloxane surface. Sorption of organic cations is often irreversible due to the high selectivity of a clay surface for organic cations over metal cations. The size of the organic cations is an important factor to consider - if molecules are too large, steric hindrance can limit the amount sorbed when the cations become too large to fit into the interlamellar region.

Organic bases favour interaction in montmorillonites, via cation exchange (in their cationic form), with exchangeable metal cations (Lewis acid sites), with water molecules surrounding exchange cations (Bronsted acid sites) and hydrophobic sites.

2.4.3.1 The Intercalation of water in Montmorillonite

Diagrammatically, intercalation in montmorillonites may be shown in Figure 2.7 which illustrates the swelling caused by water:-
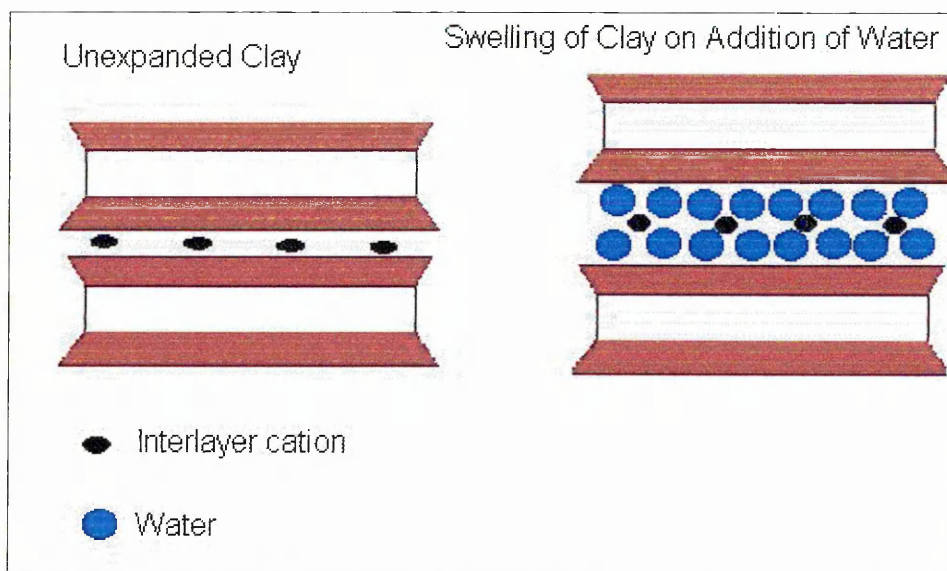
Figure 2.7 - The intercalation of Montmorillonite by water.

As discussed previously montmorillonite occurs naturally with water present in the interlamellar space, though it should be noted that montmorillonite can also adsorb water onto its external surfaces. Generally montmorillonite is able to adsorb water to a greater extent than many other

clays. Kaolin for example, can only adsorb water onto its external surfaces and intercalate water only under extreme conditions, via an entraining agent. The $d_{(001)}$ spacing caused by the swelling of montmorillonite with water imparts a larger area to the clay thus facilitating intercalation by other species, perhaps by replacement of interlayer water.

The driving force for this is the interlayer cation and its associated properties – its size, valency, electronegativity and hydration energy. These properties may also determine the amount of water intercalated by a clay. For example a clay with predominantly sodium in the interlayer may expand up to 40 Å, whereas one with predominantly calcium may only expand to 17 Å.

However, the charge density of the clay also has a limited affect on the quantity of water adsorbed. Montmorillonite with a low layer charge intercalates a large quantity of water, whereas clay minerals with a high layer charge intercalate water less readily – the increase electrostatic interaction between the layers and cations make it difficult for an intercalating molecule to separate the layers.

2.5 Mechanisms of Reactions Used in Composite Synthesis.

2.5.1 Free Radical Polymerisation

A free radical is an atomic or molecular species whose normal bonding system has been modified such that an unpaired electron remains associated with the new structure. Such a radical is capable of reacting with an olefinic monomer to generate a chain carrier which can retain activity long enough to propagate a macromolecular chain under the appropriate conditions.

In order to generate free radicals an initiator is often used. An effective initiator is a molecule which, when subjected to heat, electromagnetic radiation, or chemical reaction, will readily undergo homolytic fission into radicals of greater reactivity than the monomer radical (Figure 2.8).
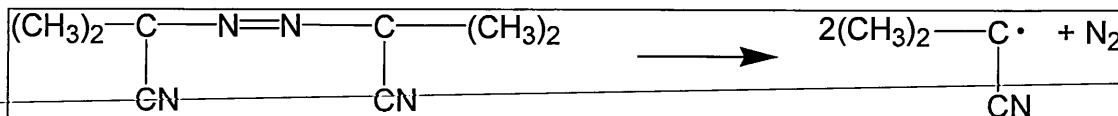
Figure 2.8 – Radical formation illustrated by the Initiator AIBN

These radicals must also be stable long enough to react with a monomer and create an active centre. The special reactivity of π – bonds in the C=C double bond makes them susceptible to rearrangement if activated by free radicals (Figure 2.9) or ionic initiators. The active centre
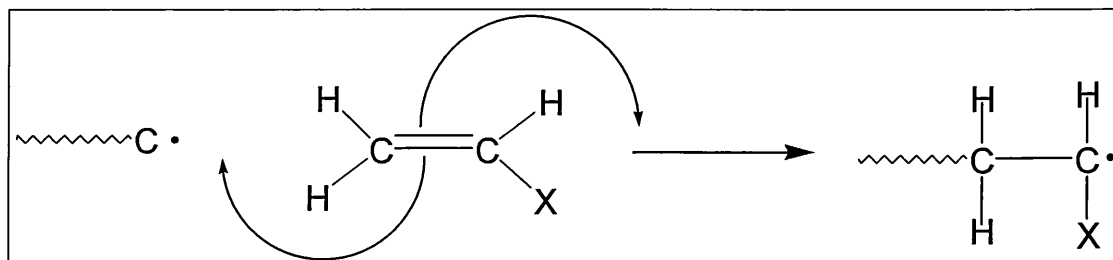
Figure 2.9 – Creation of active centre by free radical.

created by this reaction then propagates a kinetic chain which leads to the formation of a single macromolecule whose growth is stopped when the active centre is neutralised by a termination reaction.

The complete polymerisation process – whether initiated by free radical or cationic initiators – proceeds in three distinct stages:-

1. Initiation – when the active centre which acts as a chain carrier is created (Figure 2.9).

2. Propagation – involving growth of the macromolecular chain by a kinetic chain mechanism and characterised by a long sequence of identical events, namely the repeated addition of a monomer to the growing chain.

3. Termination – whereby the kinetic chain is brought to a halt by the neutralisation or transfer of the active centre (Figure 2.10).
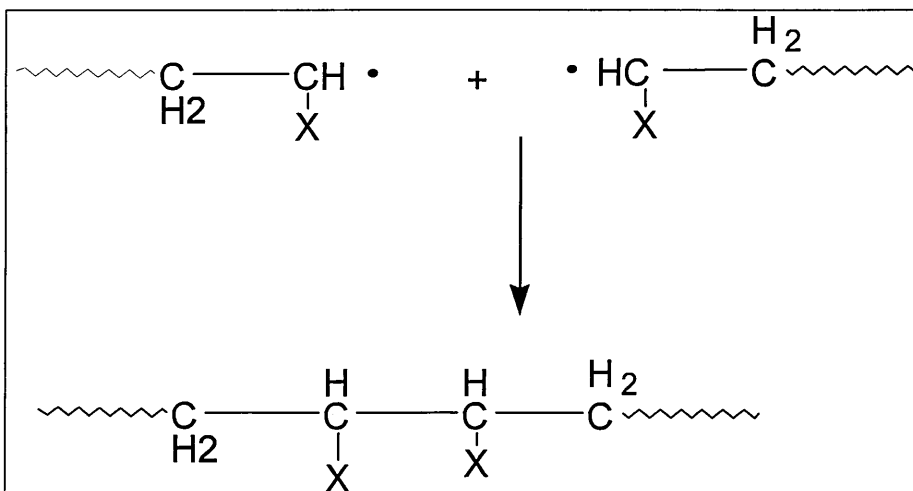
Figure 2.10 – Termination of growing chain by reaction with similar chain.

2.5.2 Cationic Polymerisation

Cationic polymerisation occurs with the same three steps as per free radical polymerisation, the obvious difference being that the active centre is cationically generated (Figure 2.11)
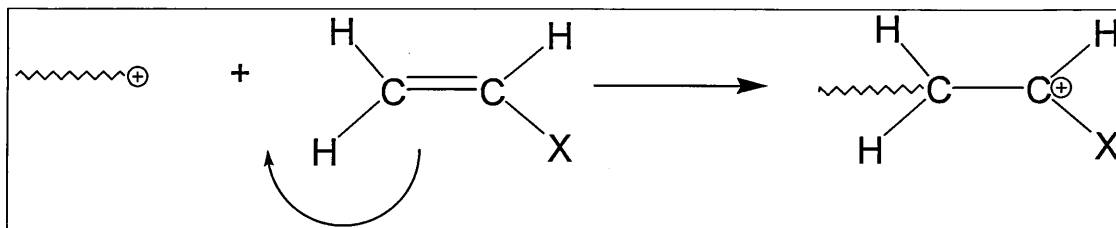
Figure 2.11 – Cationic initiation of active centre.

Chain growth takes place through the repeated addition of a monomer in a head to tail manner, to the carbenium ion, with retention of ionic character throughout.

2.5.3 Reactions between Aldehydes and Amines

The general reaction between an aldehyde and an amine can be summarised as:-

$RCHO + R'NH_2 \leftrightarrow RCH=NR' + H_2O$
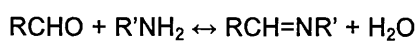
The functional group C=N is what is characterised as an imine and in the above equation the product is a substituted imine or Schiff base. Imines readily hydrolyse back to their constituent aldehydes and amines unless a stabilising aromatic group is present, or they are able to polymerise. The above reaction proceeds readily at room temperature.

An alternate product of this reaction is however, the formation of an amino resin or aminoplast via a two-step reaction (these are discussed further to specific reactants in chapter 7) : -

1. $RNH_2 + HCHO \rightarrow RNHCH_2OH$ (a methylol unit) with further heating: -

2. $RNHCH_2OH \rightarrow RNHCH_2OCH_2NHR + H_2O$ (a condensation reaction).

Alternatively the methylol groups can react further with amino groups, also evolving a molecule of water in what as another condensation reaction:-

3. $RNHCH_2OH + H_2N \rightarrow RNHCH_2NHR + H_2O$

Chapter 3 – Basic Principles of Spectroscopic Analysis of Clays

3.1 Fourier Transform Infrared Spectroscopy (FTIR)

FTIR spectroscopy is now the preferred method of infrared spectral analysis and has several advantages over the traditional dispersive methods. In a dispersive instrument a prism or grating is used to resolve the infrared radiation into separate components whereas in a Fourier transform instrument a Michelson Interferometer is used (see below). This allows all the infrared frequencies of the source to be recorded in the time domain as an interferogram. A Fourier transform can be applied to convert the spectrum to the frequency domain. During the mathematical conversion an apodisation function is used to truncate the interferogram which removes unnecessary data. Apodisation can affect both the resolution and signal to noise ratio of the spectrum.

FTIR has been used extensively in clay mineral characterisation yielding information on structure, interactions and composition[34,35]. FTIR, as a technique for clay mineral characterization, has the following advantages:

* Speed of analysis

* Requires only a small amount of sample (e.g. 5% w/w in KBr)

* Provides information yielding immediate recognition of functional groups

* Applicable to a wide range of sample types due to the various sampling accessories available – powder (hence well suited in this aspect for clays), liquid, suspension and film.

Several possible infrared techniques have been used for measuring the infrared spectra of powdered samples, these include: -

1. transmission spectroscopy (halide discs and mineral oil mulls)

2. diffuse reflectance spectroscopy

3. emission spectroscopy

4. photoacoustic spectroscopy

Work carried out in studies in this thesis use only diffuse reflectance techniques and this is discussed in more detail further in this chapter.

3.1.1 The Electromagnetic Spectrum and Infrared Frequencies

In the electromagnetic spectrum the mid – infrared range (4000 – 400 cm^{-1}) is the most frequently used and is located as follows (Figure 3.0)[36,37]:-
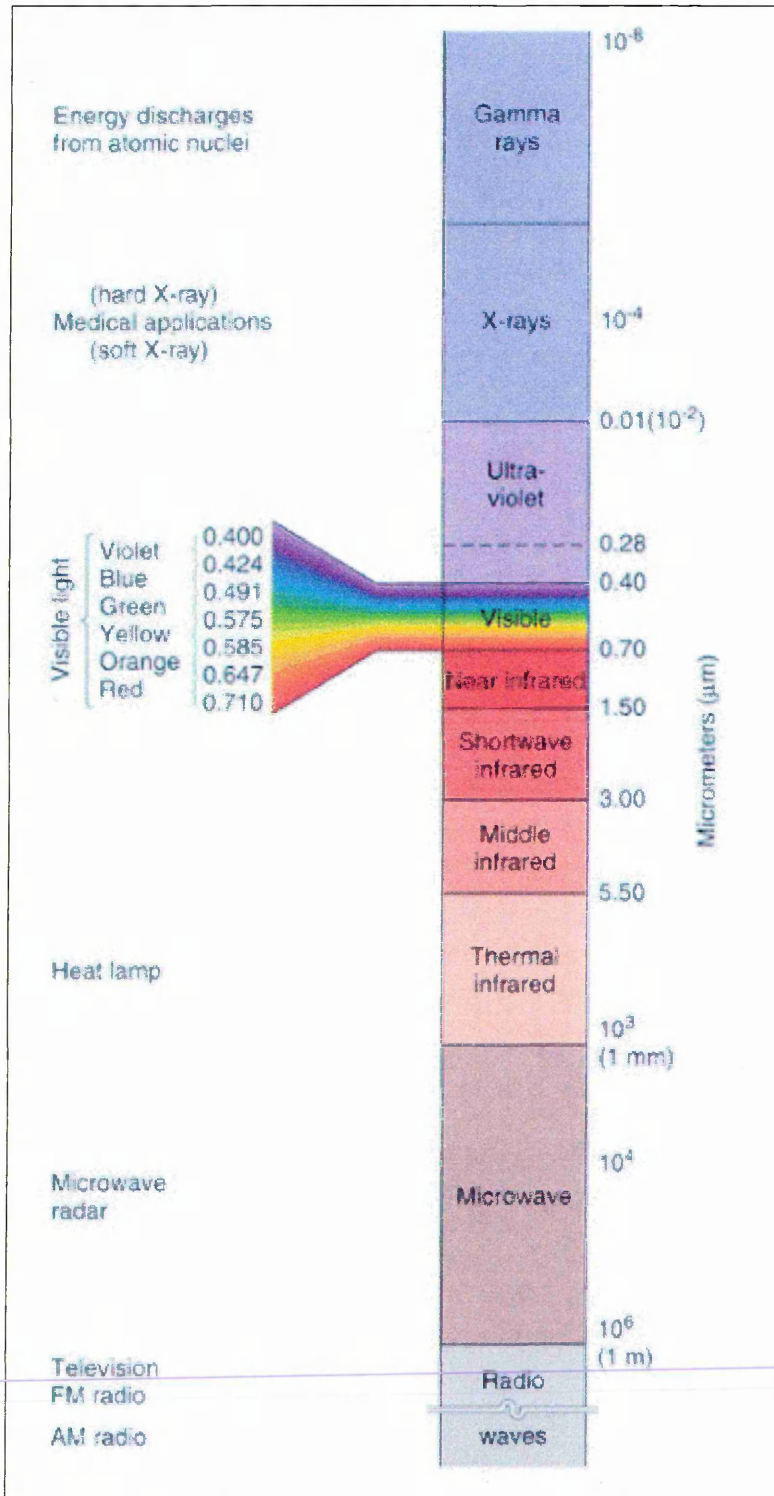
Figure 3.0 – The Electromagnetic Spectrum

Molecules vibrate (and rotate) when struck by a photon (converting electromagnetic energy to kinetic energy). If the frequency (↔) and hence the energy (E) of the photon matches a fundamental vibration (as defined by an anharmonic oscillator) of the molecule and causes resonance, the molecule absorbs energy from the photon (Figure 3.1).
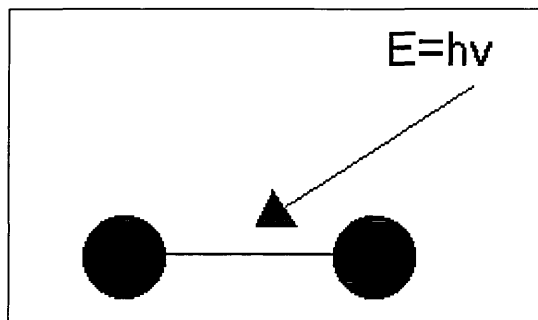
Figure 3.1 – Simple schematic depicting a photon molecule interaction.

In the above equation ν is the frequency of the wave (photon) and h is Plancks constant. The underlying principle of infrared spectroscopy is the interaction of electromagnetic waves / photons with the electrons in a chemical bond. As the wavelength is varied, a spectrum of infrared absorption energies can be recorded.

In energy level terms, the transition from the ground state to the next energy level – the first excited state - by the absorption of one quantum of light is a fundamental vibration. This is the mechanism that causes the appearance of absorption bands in the IR spectrum, when a sample is exposed to polychromatic light.

3.1.2. Modes of Vibration

A polyatomic molecule can be looked upon as a system of masses joined by bonds with spring – like properties. The position of each of these atoms can be described using three numbers, which indicates its position relative to a set of axes at right angles (the x, y and z axes). An atom has three degrees of freedom, which means it can move relative to each of these axes. This is known as translational movement. Hence molecules have more degrees of freedom because their many atoms can move relative to each other. This gives rise to rotational and vibrational degrees of freedom. This can be predicted for small molecules using the following equation:-

$$B = 3N - 6 \text{ or for a linear molecule } B = 3N - 5$$

Where B is the number of normal vibrations and N is the number of atoms in the molecule.

For example, a linear triatomic molecule, such as CO_2 (Figure 3.2) has three fundamental modes of vibration, a symmetric stretch (υ_1), a bending or deformation mode (υ_2) and an antisymmetric stretch (υ_3).
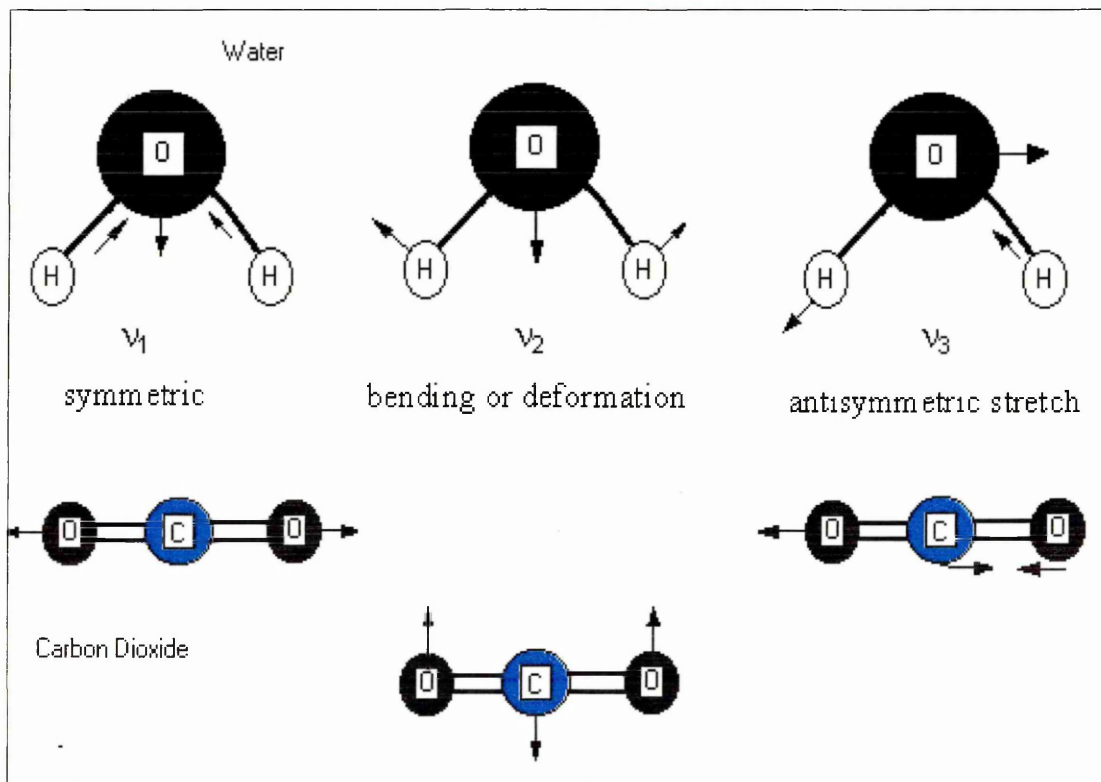
Figure 3.2 - Models of fundamental vibrations for water and carbon dioxide molecules.

A "bent" molecule, such as water, has four normal modes of vibration, two of which (orthogonal bending motions) are degenerate (i.e. of identical frequency). Other vibrational modes in molecules include the scissor mode, common in NH_2 groups for example.

If a molecule is to absorb infrared radiation it must undergo a net change in dipole moment due to its vibrational motion. A dipole moment is the product of the magnitude of the localised electrical charges within any molecule and the distance separating the positive and negative components of these charges (i.e. atoms). If the frequency of the incident radiation is the same as the frequency of the molecular vibration then a net transfer of energy occurs which results in a change in the amplitude of the molecular vibration, and absorption of the radiation occurs.

3.1.3. Instrumentation

3.1.3.1. Overview

For the work carried out in this thesis a single beam Fourier Transform Infrared (FTIR) spectrometer was used. The basic building blocks for such a spectrometer[38] are a source of radiation, collection optics, a means to discriminate between wavelengths and a detector. In such an instrument an infrared beam is passed from a source through an interferometer, then through the sample, and onto the detector. An interferogram is recorded, by a single scan, over the full wavenumber range, in a few seconds or less. To improve signal to noise ratio, several scans are recorded, co-added and then averaged, which reduces the noise contribution. The interferogram (see later) is transformed by Fourier transform mathematics into an infrared absorption spectrum. The spectrum is recorded as a single beam spectrum, so bands due to atmospheric water vapour and carbon dioxide are also present. FTIR spectrometers operate with a fixed resolution and a variable energy profile. The sample spectrum is superimposed on that background shape. A FTIR sample spectrum is generated by ratioing it against a background spectrum, which has been recorded under the same conditions as the sample spectrum, but without the sample in place.

3.1.3.2. Sources

Sources for infrared are most commonly broad band emitters, thermal for the mid – infrared, with the sample itself sometimes acting as the radiation source. Sources are usually a rod – like element of a refractory material which is heated to a high enough temperature to emit continuous radiation across the mid – infrared region. Ideally, sources need to be stable, long – lived, preferably rugged and of high emissivity. Examples include nichrome coils, silicon carbide rods and tunable laser diodes.

3.1.3.3. Detectors

Infrared detectors are essentially of two types; thermal or quantum. Thermal detectors sense and respond to a change in temperature. They are usually operated at room temperature and have wide wavelength coverage, but compared to quantum detectors are slow and less sensitive. Common thermal detectors include pyroelectric detectors, which detect a change in

32

the degree of polarisation as a consequence of a temperature change caused by incident radiation. These include detectors such as triglycine sulphate (TGS) and deuterated triglycine sulphate (DTGS).

Quantum (or photon) detectors are both sensitive and fast. They depend on the interaction between quanta of the incident radiation and the electrons in a solid, which for most infrared purposes is a semiconductor. The incident photons must be able to excite electrons in the semiconductor from one state to another, thereby raising it from a non – conducting state to a conducting state. The excited electrons in the conduction band and the holes in the valence band can then generate a current via the photoelectric effect. The sensitivity of these detectors tend to fall off rapidly close to their wavelength limit, since each photon has an energy (E) which is directly proportional to its frequency ($\leftrightarrow$), (E = h$\leftrightarrow$ = h(c/λ). For operation or optimum performance the elements of many of these infrared photon detectors must be cooled; for some, simple thermoelectrical cooling is sufficient, others need to be maintained at liquid nitrogen temperatures (77 K). Examples of quantum detectors include PbS, PbSe, InGaAs, InSb, and CdHgTe. The latter is most commonly referred to as the MCT (mercury cadmium telluride) detector, and has a response time as low as 20ns and must also be maintained at liquid nitrogen temperatures.

3.1.3.4 The Interferometer

IR spectrometers are normally required to interrogate as much of the spectral range as possible. In FTIR instruments this may achieved by the use of the interferometer. Unlike a dispersive monochromator, which spatially separates the spectral radiation into individual components for successive measurement, an interferometer measures all of the spectral radiation simultaneously; a spectrometer based on an interferometer is a multiplex detection system. This offers very distinct advantages over a wide range of applications for infrared spectrometers.

The most common interferometer used in commercial vibrational spectrometers is a Michelson type, or a derivation thereof (Figure 3.3).
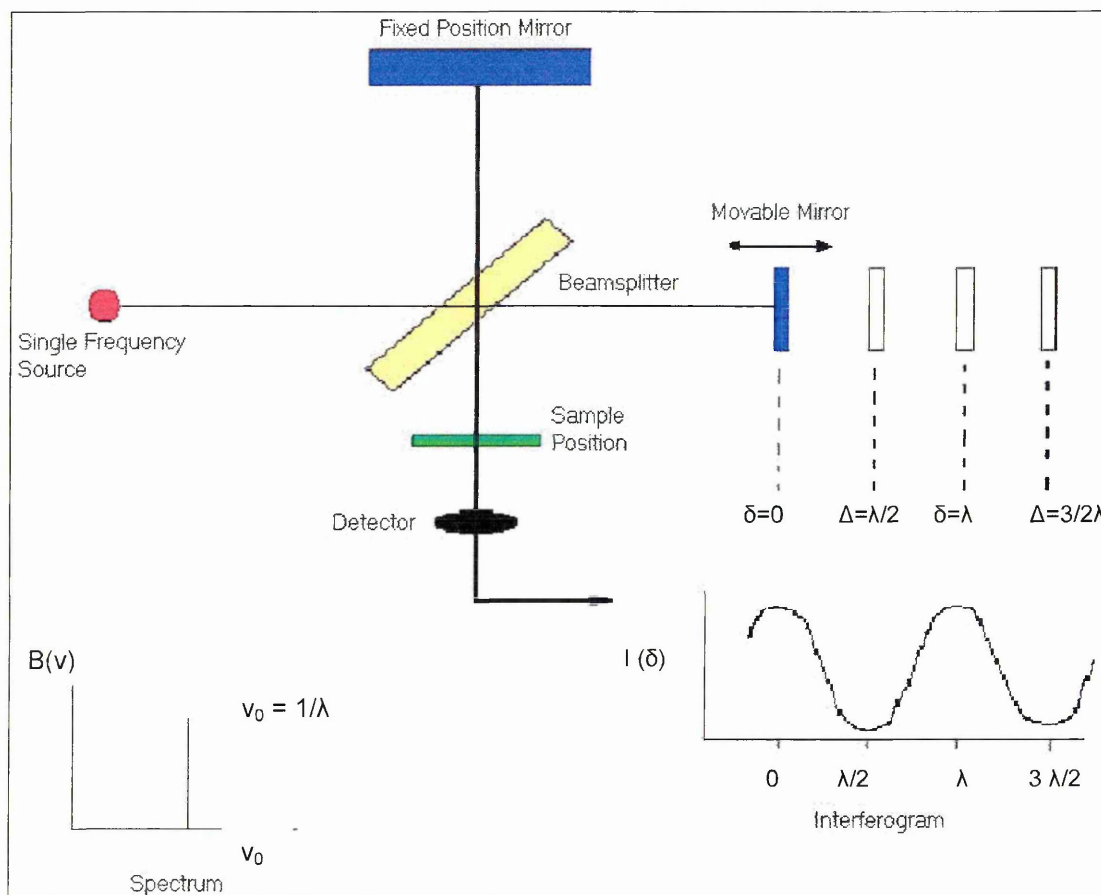
Figure 3.3 – Schematic of a Michelson interferometer. The diagram also shows the spectrum of an infinitely narrow line source and how its cosine function interferogram is generated as the moving mirror is translated.

The principle of action of the interferometer is best illustrated initially by considering its action with a monochromatic (i.e. single wavelength λ) radiation source. The components of a Michelson interferometer comprise a beam splitter and two mirrors, one fixed in position, while the other is scanned back and forth. Collimated monochromatic radiation incident on an ideal beamsplitter will be divided into two equal intensity beams, such that 50% is transmitted to one of the mirrors (e.g. the fixed mirror), while 50% is reflected to the other mirror. These two beams are reflected back and returned to the beam splitter, where they are recombined and 50% is sent to the detector via the sample component, while the other 50% is essentially lost as it is returned to the source. As the moving mirror is scanned, the path difference between the two recombined beams will be varied. When this path difference is an integral number of wavelengths, then the beams will be in phase and constructive interference will

occur between the recombined beams, i.e.. their intensities will be additive. Destructive interference results when the optical path difference between the two beams is λ / 2, i.e. the moving mirror has moved (been displaced) a distance equivalent to λ / 4 for the inphase position. The optical path difference is sometimes referred to as the retardation (or optical retardation). If the moving mirror is scanned at constant velocity, the detector will measure a sinusoidally varying signal as the beams move in and out of phase. The intensity measured by the detector is therefore a function of the moving mirror displacement.

The Interferogram. As the moving mirror travels away from the position of zero path difference (Figure 3.3) between the two recombined interferometer beams the intensity of radiation reaching the detector varies as a cosine function of the optical retardation, which may be expressed as an equation of the form:

$I(\delta) = B(v) \cos (2\pi\delta / \lambda) = B(v) \cos (2\pi\delta v)$

Where $I(\delta)$ is the intensity of radiation at the detector, δ is the optical retardation and $B(v)$ represents the single beam spectrum intensity at wavenumber v. $I(\delta)$ is the cosine fourier transform of $B(v)$. The single beam spectrum $B(v)$ is calculated by computing the cosine fourier transform of $I(\delta)$. The monochromatic source of wavelength λ (the spectrum), and the cosine wave (its interferogram), represent a Fourier transform pair.

This process is best illustrated as in Figure 3.4. Consider an infrared source emitting a wide range of wavenumbers. Figure 3.4 (a) shows how the idealised wavenumber domain spectrum of this source emitting continuously between $\ddot{v}_1$ and $\ddot{v}_2$ might appear. We can regard this spectrum as comprising a very large number of wavelengths between $\ddot{v}_1$ and $\ddot{v}_2$ so that the corresponding detector signal, as a function of retardation, will be the result od adding together very many cosine waves of different wavelengths. The signal is large at $\delta = 0$ since all the waves are in phase, but else where they are out of phase, interfere with each other and produce total cancellation of the signal. The intense signal at $\delta = 0$ is known as the centre – burst (Figure 3.4 (b)). (Because of slight dispersion by the beamsplitter B the waves at $\delta = 0$ are not quite in-phase resulting in asymmetry of the centre – burst about $\delta = 0$).
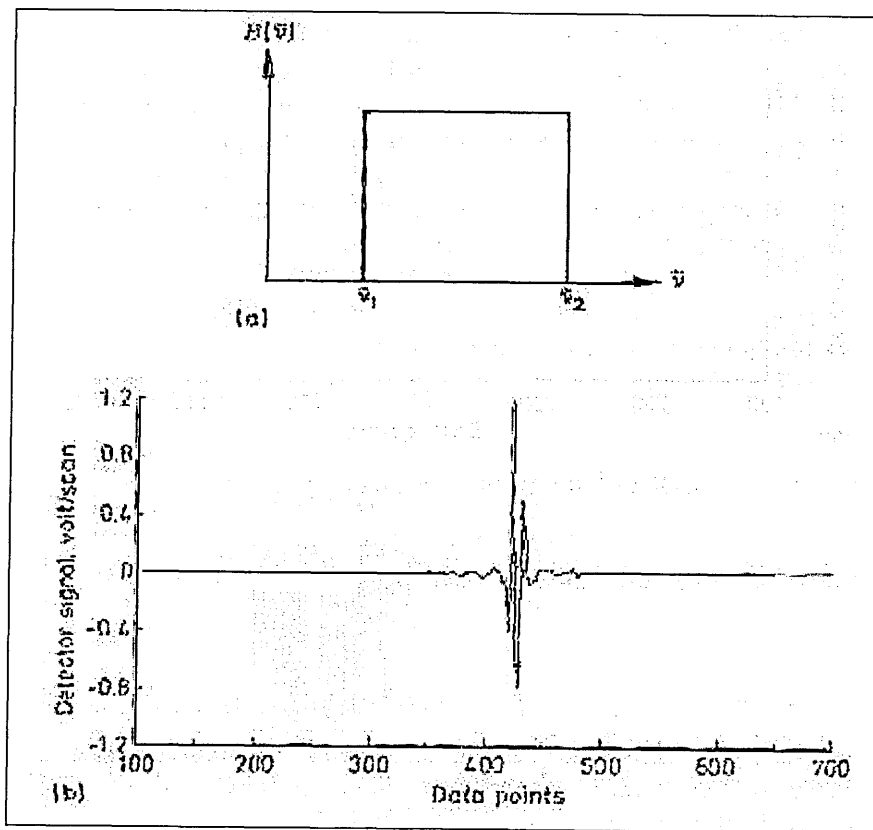
Figure 3.4 – (a) Wavenumber domain spectrum of a broad band source and (b) the corresponding interferogram.

If a single sharp absorption occurs at a wavenumber v_a between $\bar{v}_1$ and $\bar{v}_2$ the cosine wave corresponding to v_a is not cancelled out and remains in the interferogram (Figure 3.5).

For a continuum source the equation becomes:-

$$I(\delta) = \int_{-\infty}^{+\infty} B(v) \cos(2\pi\delta/\lambda) = B(v) \cos(2\pi\delta\, v).$$

And its spectrum is calculated from :-

$$B(v) = \int_{-\infty}^{+\infty} I(\delta) \cos(2\pi\bar{v}\delta)\, d\delta$$

Since the magnitude of the centre is large compared to that in the wings of the interferogram, where, comparatively, the signal to noise may be low but much of the spectrally important information is encoded, the ADC (analogue –to-digital converter) of the detection system must have a large dynamic range, typically 10^6 or better.

36
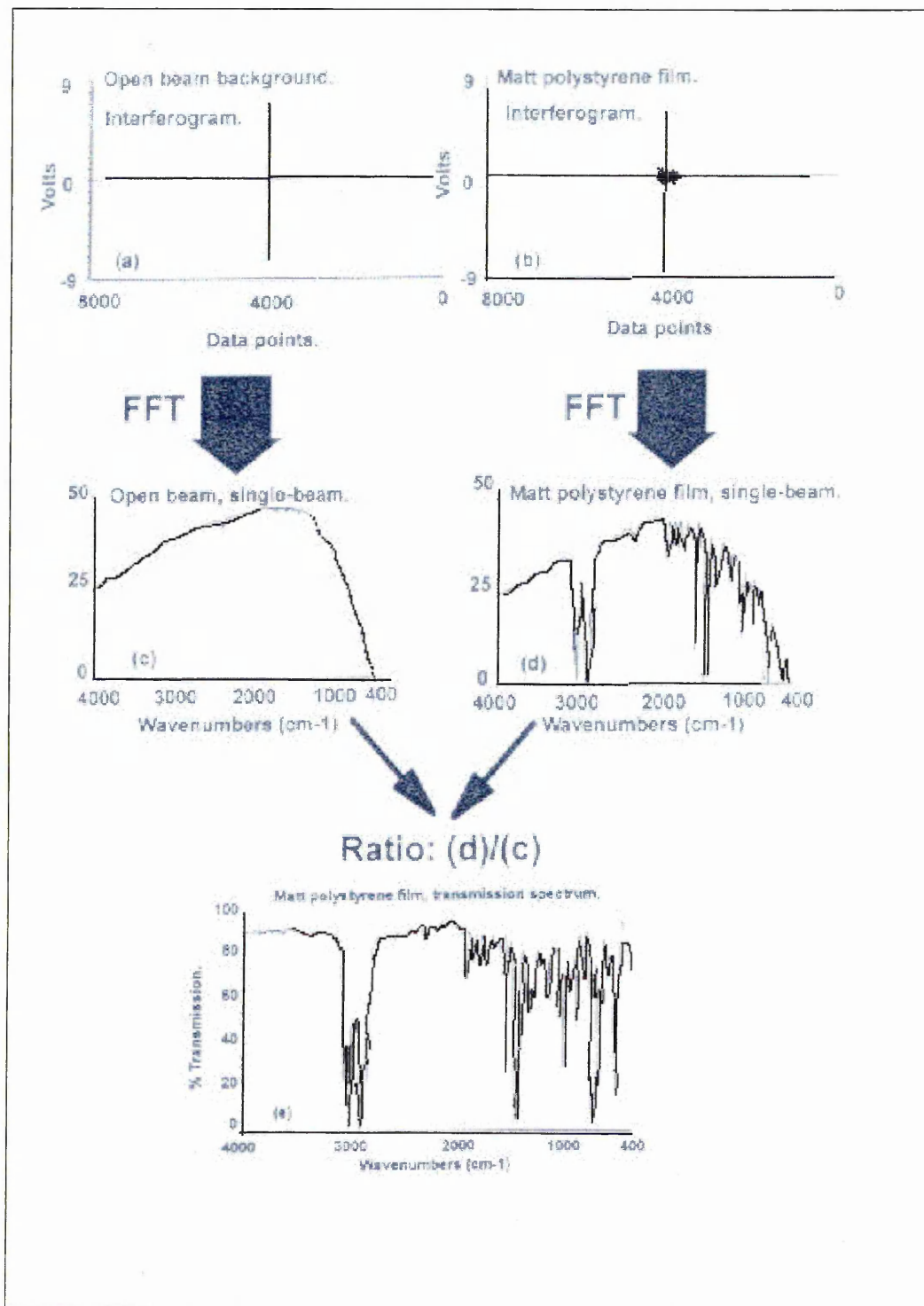
Figure 3.5 – Summary diagram of the principal steps involved in generating a FTIR spectrum from, in this example, a matt polystyrene film (FFT = fast Fourier transform).

Apodisation. The moving mirror only moves a finite distance, since it cannot travel from minus infinity to plus infinity, so the interferogram is truncated by a boxcar function (Figure 3.6) the Fourier transform of which is a sinc function.
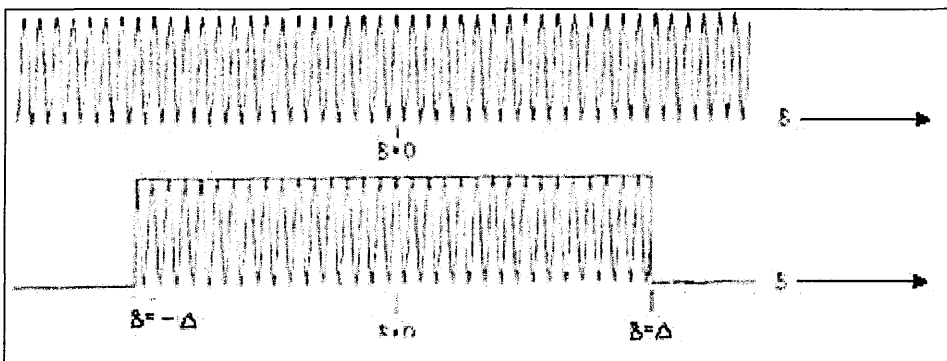
Figure 3.6 – Schematic of Boxcar truncation of the interferogram for a single frequency source. The interferogram is recorded for optical retardation δ cm between $-\Delta$ and $+\Delta$, $\delta = \frac{1}{2}$ x optical path difference.

The effect of convoluting the spectrum with this sinc function is to introduce positive and negative lobes to spectral bands. These lobes may be minimised (or effectively eliminated) to greater or lesser extents (depending on the true bandshape) at the expense of (increased) band width and (decreased) band intensity, by replacing the boxcar truncation function with another algebraic (weighting) function. These functions are known as apodisation functions. They may be operator selective.

3.1.3.5 Spectral Resolution

The spectral resolution of a Fourier transform spectrum depends on how far the moving mirror of the interferometer has travelled. To resolve two bands in a spectrum, the extent of travel of the moving mirror must equal or exceed that necessary to register one complete beat pattern generated between the two cosine waves in the interferogram that represent the wavenumber position of the two bands. For a conventional Michelson interferometer the spectral resolution (cm^{-1}) is given by:-

$\Delta \nu = 1/\Lambda_{max}$

Where λ_{max} is the maximum optical retardation, equal to twice the distance travelled by the moving mirror from its position at zero path – length distance (ZPD) between the beams, thus: a mirror travel from ZPD of ~ 0.25 cm will yield a spectrum of 2 cm^{-1} resolution. A mirror travel of ~ 2 cm will yield a spectrum of 0.25 cm^{-1} resolution.

3.1.4 Potential Advantages of Interferometric Measurements of Vibrational Spectra.

Three important and often quoted primary advantages of FTIR spectrometers over dispersive infrared spectrometers are frequently referred to by the names of the pioneer scientists who first defined or were closely associated with the principles. They are known as the Fellgett, Jacquinot and Connes advantages. These are concerned with the multiplex, throughput and wavenumber precision aspects of interferometric measurements respectively.

3.1.4.1 The Fellgett or Multiplex Advantage.

In a monochromator dispersive spectrometer the single – channel detector only observes one resolution element at a time, scanning successively through consecutive wavelength / wavenumber elements until it has built up a spectrum; to cover the normal mid infrared range this may typically take 10 – 20 minutes. In an interferometer all of the wavelengths / wavenumbers are being scanned continuously and for the equivalent range this may take 1 second. (Clearly there is a significant time advantage here).

Furthermore, in a system which is limited by detector noise then, providing precise data point triggering is retained between successive scans (see Connes advantage below), successive interferograms may be co – added (superimposed) in order to improve the S/N characteristic of the resultant spectrum. If the spectrum recorded from a scanning dispersive single – channel spectrometer is composed of M resolution elements, then the spectrum recorded at the same resolution transformed from a set of co – added interferograms recorded on an interferometer over the same time period will show a $\sqrt{M}$ better S/N all other parameters being equal.

3.1.4.2 The Connes, or Wavelength Repeatability Advantage

Modern spectrometers employ the use of the He − Ne reference laser to monitor the position of the moving mirror and trigger data acquisition. This ensures exact correspondence between consecutive data points in successive interferograms. Also, since the wavelength of the laser is known very precisely, the wavenumber positions of the data points in the FTIR spectrum can be determined very accurately. This precision in data point repeatability and wavenumber position is critical to successful co − addition of interferograms, and the subsequent superimposition of spectra. They are invaluable spectral properties for the application of spectral subtraction processes and prerequisites for many analyses involving the comparison of closely matched spectra.

3.1.4.3 The Jacquinot, or Throughput Advantage

The Jacquinot advantage is contained within the fact that in an interferometer the ability to accept radiation is determined by the collimating area of the interferometer mirrors or the diameter of the interferometer circular entrance aperture, or the Jacquinot stop. The area of the Jacquinot stop is generally considered greater than that of the slits within the optical train of a monochromator system, and hence the etendue and thus the throughput are much greater in an interferometer. The extent of the gain will be both wavenumber and resolution dependant, but improvements in the order of 50 − 100 times are typical mid − range values.

3.2 Diffuse Reflectance Infrared Fourier Transform Spectroscopy (DRIFTS)

Diffuse reflectance has long been employed as a versatile sampling technique for ultraviolet, visible, and infrared spectroscopic analyses[40,41]. As a sampling technique DRIFTS offers a number of advantages including[42]:-

* Minimal or no sampling preparation.
* Very high sensitivity (ppm levels)
* Applicability across a wide range of sample concentrations from ppm to neat.
* Ability to analyse most non − reflective materials, including highly opaque or weakly absorbing materials.

- Ability to analyse irregular surfaces or coatings on glass fibres.

- Suitability for very large, intractable samples through the use of specialised sampling devices.

3.2.1 Theory of DRIFTS

When an infrared beam is focused onto a fine particulate material, three different events, which yield three classes of reflected radiation, can occur[43,44] (Figure 3.7).
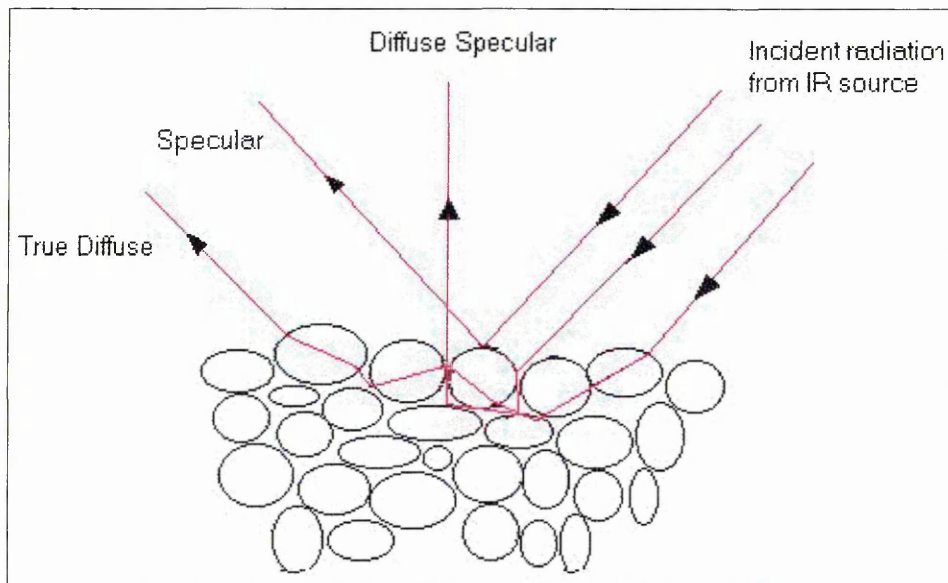
Figure 3.7 Schematic diagram of the three modes of reflection in DRFITS.

The first class results from the simple reflection of incident radiation at a sample grain interface that is parallel to the macroscopic surface of the sample; this is called Specular reflectance, and the angle of reflection is equal to the angle of incidence. It is also referred to as front-surface, regular or Fresnal reflectance.

The second class of reflected radiation is similar to the first in that it is not transmitted through any sample grains, but merely undergoes multiple reflections at particle surfaces. This radiation carries no information about the sample, but it is diffusely reflected in the sense that it is isotropically scattered and its polarization is scrambled relative to that of the incident radiation. This radiation is called diffuse specular reflectance and is distributed in all directions

The third and final class of radiation reflected from the sample is called true diffuse reflectance. This radiation has been transmitted through at least one sample grain, contains

41

all the information regarding the analyte that is available in the reflected radiation, is isotropically scattered and its polarization is scrambled relative to the incident field.

The sample concentration is related to the intensity of the measured infrared spectrum thus: -

$$f(R_\infty) = (1 - R_\infty)^2 / 2 R_\infty k / s$$

where R_∞ is the absolute reflectance of an 'infinitely thick' sample, $f(R_\infty)$ represents the value of the function, k is the absorption coefficient and s is a scattering coefficient defined for purely scattering samples by $I = I_0 e^{-sx}$.

It is generally assumed that s is a constant or at most a slowly varying function of analyte concentration. An infinitely thick sample is one through which no light is transmitted. All light is either reflected or absorbed. The infinitely thick criterion is general satisfied for samples 3 – 5mm thick.

3.2.2 Sampling Considerations In DRIFTS

The major drawbacks in DRIFTS arise from the specular component (specular and diffuse specular) of the reflected radiation. As they do not penetrate the sample it becomes a particular problem in spectral regions where there is a highly absorbing species and the surface effects dominate the bulk leading to Restrahlen bands (see below). This can lead to the distortion and inversion of bands.

The amount of specular component in the spectrum is governed by the refractive index (n') which is the complex sum of the index of refraction (n) (called the real component) and the absorption index (k') (called the imaginary component):

$$n' = n + ik' \text{ (for non-absorbing materials } k' =)$$

The difference in refractive indices leads to reflection and these differences can be real or imaginary components.

The absorption index, k', is related to the absorption coefficient, K i.e.

$$K' = K/4\pi v$$

where v is the frequency of radiation (cm^{-1}).

The absorption coefficient, K, is related to the absorptivity, a, by

$$K = 2.303ac$$

where c is concentration.

If the sample absorbs, the absorption coefficient, K (≠ k') has an effect on the amount of specular reflectance near the wavelength where absorption occurs. The appearance of the features produced in the infrared spectrum depends on the value of the absorption index and hence the absorptivity.

If the absorptivity is very small, very little if any change in the spectrum results. If the absorptivity is intermediate, as is for most organic compounds, the increased specular reflectance can result in an anomalous dispersion feature. This lead to a derivative shaped feature or a shift in the peak maximum to higher wavenumber of the band in question. If the absorptivity is large, such as the strong bands in some minerals, a large reflectance maximum, or restrahlen band results.

These effects can also be minimised by dilution of the sample in a non – absorbing matrix (sometimes referred to as reference material) such as KBr.

In addition, accessory design can help to reduce the specular reflectance contributions and such an accessory is shown in Figure 3.8 which is the accessory used to collect DRIFTS spectra in this thesis.
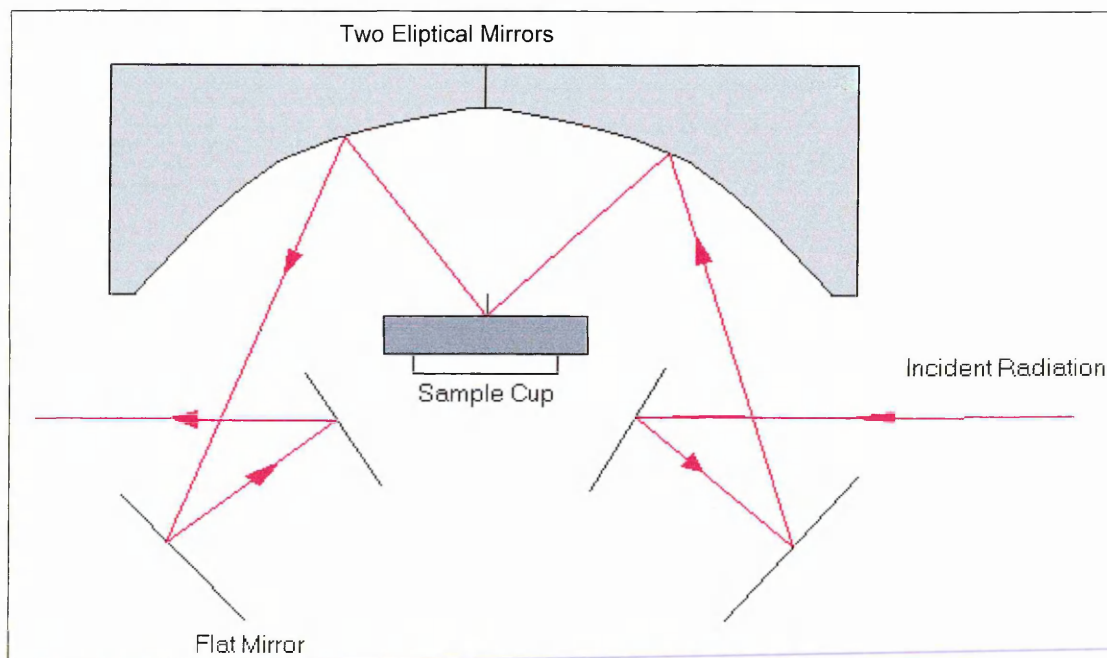
Figure 3.8 Schematic Diagram illustrating common DRFITS Accessory

The alignment of the DRIFTS accessory (in particular the mirrors) is critical because typically only 10 – 15% of the energy throughput is available for DRIFTS analysis compared to the transmission mode.

Other factors to consider include: -

- Particle Size – a major consideration when performing DRFITS on solids[45]. The amount and type of reflectance encountered in DRIFTS is largely dependant on the particle size of not only the sample but also the reference / diluent material used. As the particle size of the sample decreases band heights increase and band widths decrease. The change in diffuse reflectance spectra is due mainly to the amount of specular reflectance collected, since the greater the particle size of the sample, the greater the proportion of the specularly reflected component. In addition, as the specular component increases, less of the beam penetrates into the powdered sample and thus less refraction, scattering and absorption occurs of which the latter results in loss of information about the sample. Similar effects are also noted with regard to band height and width with reference materials.

- Sample Homogeneity – a higher concentration of sample near the surface results in variation in relative peak intensities[46]. Therefore it is necessary to distribute the sample as uniformly as possible within the non – absorbing matrix.

- Concentration and Reference Materials – at high concentrations, there is a dramatic increase in the specular contribution to the spectral data. As a result some sample data will be uninterpratable without adequate sample dilution – hence the need for a reference material. This will reduce anomalous dispersion effects and also Restrahlen bands. As the single beam spectrum is ultimately ratioed against the reference (background) spectrum the reference material needs to be a good diffuse reflector, non – absorbing and highly scattering material. Most commonly used reference materials are alkali halides, in particular KBr. They have been found to have fewest interferences and the highest overall reflectance[47]. However, such alkali halides are prone to adsorb atmospheric water and organics so care must be taken to keep them dry and free from contaminants.

- The Depth of the Sample Matrix — when the depth of any absorbing material is increased a subsequent increase in its absorption bands will be observed until a certain depth is reached[45]. At this depth, any further increase will result in no change in the diffuse reflectance spectra and the sample is said to be of "infinite thickness". The actual depth depends on both the absorption and scattering coefficients of the sample under investigation[48]. For a pure KCl matrix overlaying a sample, the point of infinite thickness occurs at 5mm, i.e. no bands due to the sample are observed in the spectra. However, the difference in band intensity between 2 and 5mm is not very great. If a sample is dispersed in KBr at 5% and is weakly absorbing, then the expected depth at which no further change in the diffuse reflectance spectrum occurs will be approximately 3mm. For strongly absorbing materials the emerging beam will probably originate from less than 1mm below the surface of the sample. If the sample is insufficiently deep, the incident beam will be reflected off the sample cup bottom travelling back up through the sample. As a result, part of the radiation will interact twice with the absorbing sample giving rise to increased absorption.

- Sample Packing — In the DRIFTS experiment, the sample mixed with the reference material is packed and the surface carefully levelled in the sample cup. Studies regarding the pressure as a result of such packing[49,50] show that as the pressure increases the variability in the scattering coefficient decreases from sample to sample. This may aid in reproducing diffuse reflectance spectra. Levelling the surface is also important as this affects the particle orientation at the top surface and enhances specular reflection — the height with respect to the incident beam and the focal point should be the same.

- Sample Height — The sample should be positioned so that maximum radiation throughput is observed.

- Absorptivity and Refractive Index — The absorptivity and refractive index (n) can have a related effect on the types of reflection and thus appearance of the diffuse relectance spectra. For a given particle size distribution (50 - 90µm) over a wide range of refractive indices the diffusely reflected energy increases from 0 for n=1, to a maximum for n close to 2, and then decreases for higher refractive index values. KBr

has a refractive index of 1.54 and is therefore a good choice for the diluting material used in DRIFTS.

3.2.3 Variable Temperature DRIFTS

Variable Temperature DRIFTS (VT-DRIFTS), involves the heating of a solid sample and subsequent collection of diffuse reflection spectra over a range of temperatures. Not only does this technique provide spectral data on the sample as it is heated, but it may also be correlated with other thermal analysis techniques such as Thermogravimetirc Analysis, Thermochemical Analysis, Differential Thermal Analysis and Differential Scanning Calorimetry. Two types of VT-DRIFTS experiments exist – stepped and ramped. For the purposes of this thesis, only the former is discussed here.

In the stepped experiment, the sample is placed in an environmental chamber, which is capable of heating the sample, accommodating the DRIFTS optics and is also purged with an inert gas. The sample is heated to a selected temperature and a spectrum recorded at each temperature after equilibration at that temperature.

However, the major drawback results from baseline variation. Such variation results from instrumental fluctuations occurring between collection of reference and sample spectra. This is a result of the fact that some FTIR instrument parameters vary with time[51,52] e.g. source output, interferometer instabilities and fluctuations in detector pre-amplification and filter electronics. Also unmodulated infrared radiation emitted from the heated sample may effect the DRIFTS spectrum, especially if a liquid nitrogen cooled MCT detector is used. Baseline artefacts are typically broad-features superimposed on DRIFTS spectra.

Additionally heating of the sample results in significant thermal expansion of the sample holder which changes the characteristics of the incident-beam-sample interface and may result in baseline shifts[53].

Quite simply, these temperature dependant effects may be minimised by recording the sample and background spectra at the same temperatures as those at which the samples are recorded at.

3.3 Thermogravimetric Analysis

Thermogravimetric analysis (TGA) is an instrumental technique by means of which a sample for analysis is weighed continuously as it is heated at a constant temperature rate with time in a nitrogen purged furnace (Figure3.9).
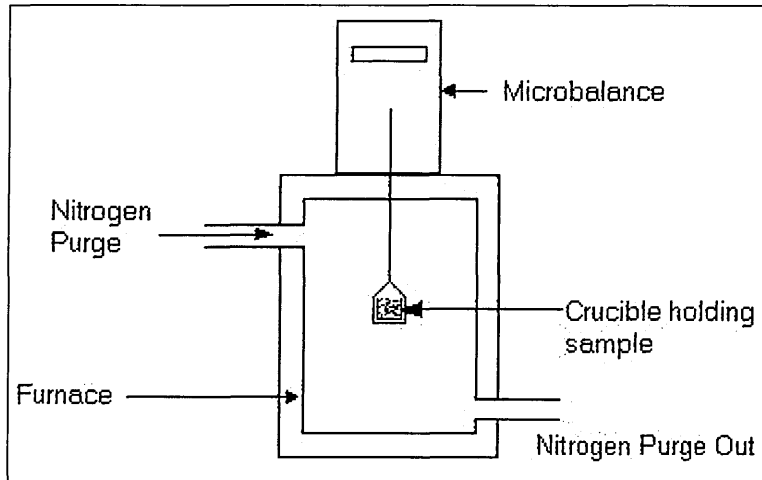
Figure 3.9 – Thermogravimetric Balance

3.3.1 Principle of Operation

The sample to be analysed is weighed into a refractory crucible (typically alumina) which is placed onto the receptacle of a thermal balance, residing inside an electric furnace with adjustable and uniform temperature rise per unit time. The temperature is measured by means of a thermocouple inside the furnace[54]. The nitrogen purge ensures that the sample does not undergo oxidation reactions as the temperature increases.

As the sample is heated at various temperatures it may undergo a series of transformations which are accompanied by a change in mass. By graphically plotting the change in mass vs. temperature ($m = f$ (T)) a thermogravimetric curve may be obtained. Factors influencing the shape of such a curve include particle size and distribution, the depth of packing (too deep and this may induce "deep bed" effects) and the heating rate.

Quite commonly these curves are represented as negative derivatives (DTG) enabling weight losses to be displayed as maxima.

There are several factors that influence the shape of a TG curve which are related to the sample, the apparatus and experimental conditions. They must be considered to achieve reproducibility:-

1. particle size distribution and packing density

2. use of inert atmospheres, for example nitrogen and / or helium which may be used to suppress oxidation of organic materials in clays.

3. the sample holder which must enable product gases in the immediate vicinity of the sample to be efficiently removed.

4. a heating rate of 10 °C / min has become standard, but only due to historical factors. The resolution of maxima decreases with increasing heating rate. The maxima size also increase with heating rate. It is important that the heating rate must be identical for sample comparison.

3.4 X – Ray Diffraction (XRD)

As previously discussed, X-rays are part of the electromagnetic spectrum (Figure 3.0) and therefore have properties of both particles and waves. The energy of an electromagnetic beam interacting with a medium is partly transmitted, partly refracted and scattered, and partly absorbed[55]. The packets of radiation, or photons, can "bounce" and transfer energy, which is a property of a discrete particle. They can also be diffracted by a grating of appropriate size within the dimensions of the incoming X-ray travel. Spacing in a crystal structure can serve as a diffraction grating. The relationship between the wavelength of the radiation λ, the angle θ between the incident beam of radiation and the parallel planes of atoms causing the diffraction, and the spacing d between these planes is called Bragg's Law:-

$$n \lambda = 2d \sin \theta$$

Scattered radiation from a crystal behaves as if the diffracted beam were "reflected" from a plane passing through points of the crystal lattice in a manner that makes these crystal-lattice planes analogous to mirrors. Such lattice planes are directions in the crystal lattice that are rich in lattice points. Each diffracted beam is considered as a "Bragg reflection" from a crystal lattice plane, so that the angle of the incident x-ray beam (incident radiation) equals the angle of reflection (Figure 3.10).

48
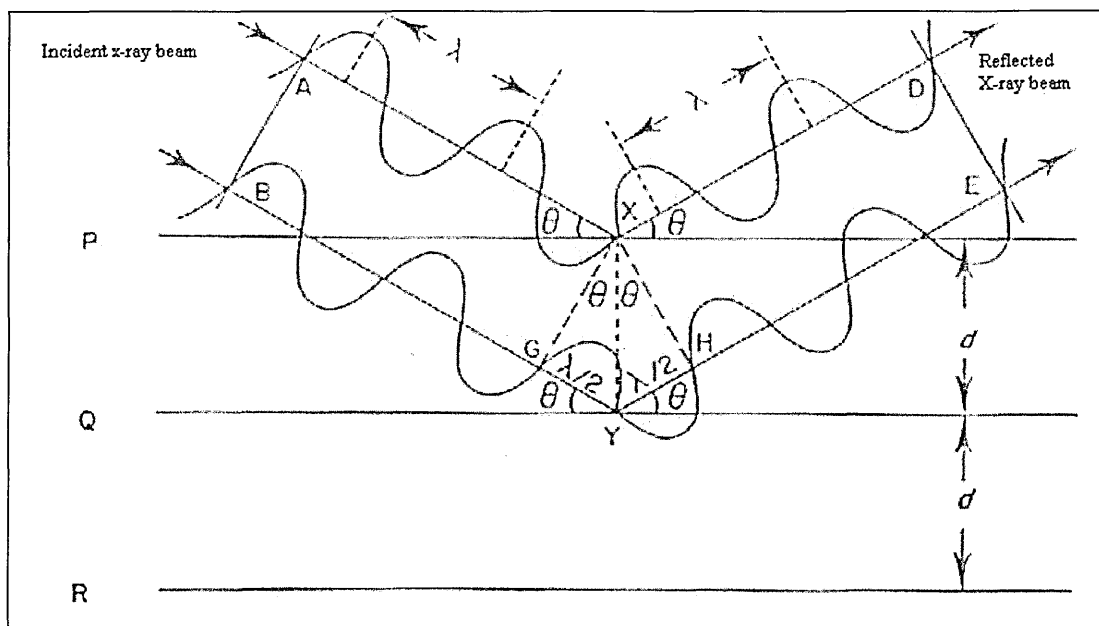
Figure 3.10 – Geometry of diffraction and its relationship to Braggs Law.

The distance between families of planes in a crystal is of the same order of magnitude as the wavelength of x-rays. For example Cu K_α radiation has a wavelength of 1.5418 Å and the value of a for NaCl is 5.65 Å. Consequently crystals act as diffraction gratings for x-rays. If the above diagram (Figure 3.10) the ray BYE travels a longer distance than ray AXD. Therefore, if these two rays are to constructively interfere then the distance (GY + YH) must be an integral number of wavelengths. Simple trigonometry shows that GY = HY = XY sinθ. However, XY = d (the interplanar spacing) hence the integral number of wavelengths must equal 2d sinθ. Hence this is the Bragg equation and coherent diffraction will occur when, and only when, the Bragg equation is satisfied. Thus if values of θ and λ are known d may be determined, which in clay minerals is the distance between the layers of the clay. Indeed clay minerals are often orientated so that diffraction will take place only from the 001 plane. The resultant value of d is known as the $d_{(001)}$ spacing, d-spacing or interlayer spacing in clay minerals. These values can be used to determine for example if intercalation upon treatment with an organic compound has been successful or not e.g. in untreated kaolin the d-spacing is 7.2 Å. On treatment with an intercalant, this value will be expected to increase.

For x-rays of a single wavelength and for a specific orientation of the crystal, very few Bragg reflections satisfy this condition (unless the unit cell is very large). Therefore it is usual to oscillate or rotate the crystal through an angular range or to use multiple wavelength, in order

to bring more diffracted beams in to the necessary diffraction geometry for measurement (Figure 3.11).
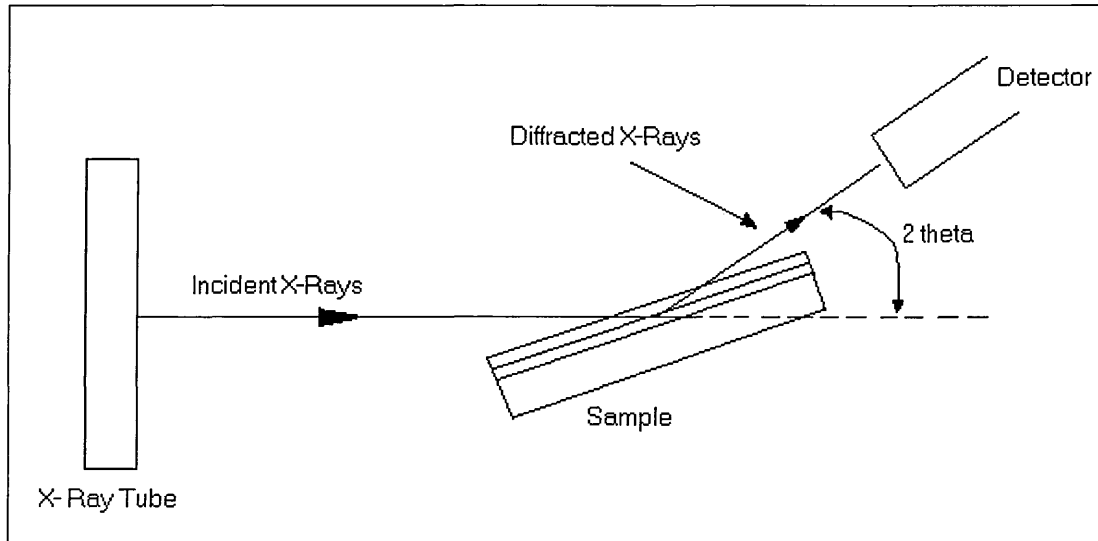
Figure 3.11 – Basic Features of a Diffractometer.

The detector and sample are rotated by a goniometer in order to reach the required angles. Typically, the diffracted intensity of the scattered X – rays that obey Bragg's Law, is measured as a function of the diffracted angle (2θ) and the orientation of the sample which yields the diffraction pattern. Hence diffraction will only occur if a beam of x- rays falls on a series of atom bearing planes each with a distance apart d and at an angle θ.

Samples such as clays may be mounted for analysis as powdered samples or deposited as a thin film cast onto a glass slide. The latter presentation may also be mounted onto a heated stage, thus enabling variable temperature measurements to be made.

X- rays are usually produced by the sudden deceleration of fast moving electrons. They are generated in X-ray tube when electrons are emitted from a glowing tungsten filament (the cathode), accelerated through the vacuum of the tube by an applied voltage, usually from 15 to 60 kV, and strike a metal target (the anode). Within the target the electrons encounter crowds of other electrons which causes a sudden deceleration. The result is X – radiation of two major varieties: one form has a broad, continuous spectrum of wavelengths (the Bremsstrahlung), and the other has very sharp peaks, of discrete wavelengths, characteristic of the target material (Figure 3.12).

The equipment generally used to produce x-rays consists of a cathode that produces an electron beam and a stationary metal anode that is the target for this beam and from which the x-rays are emitted. These components are enclosed in a glass tube under vacuum. Large amounts of heat accompany the production of x-rays, and therefore the x-ray target must be cooled by a stream of water circulating in a jacket enclosing it.
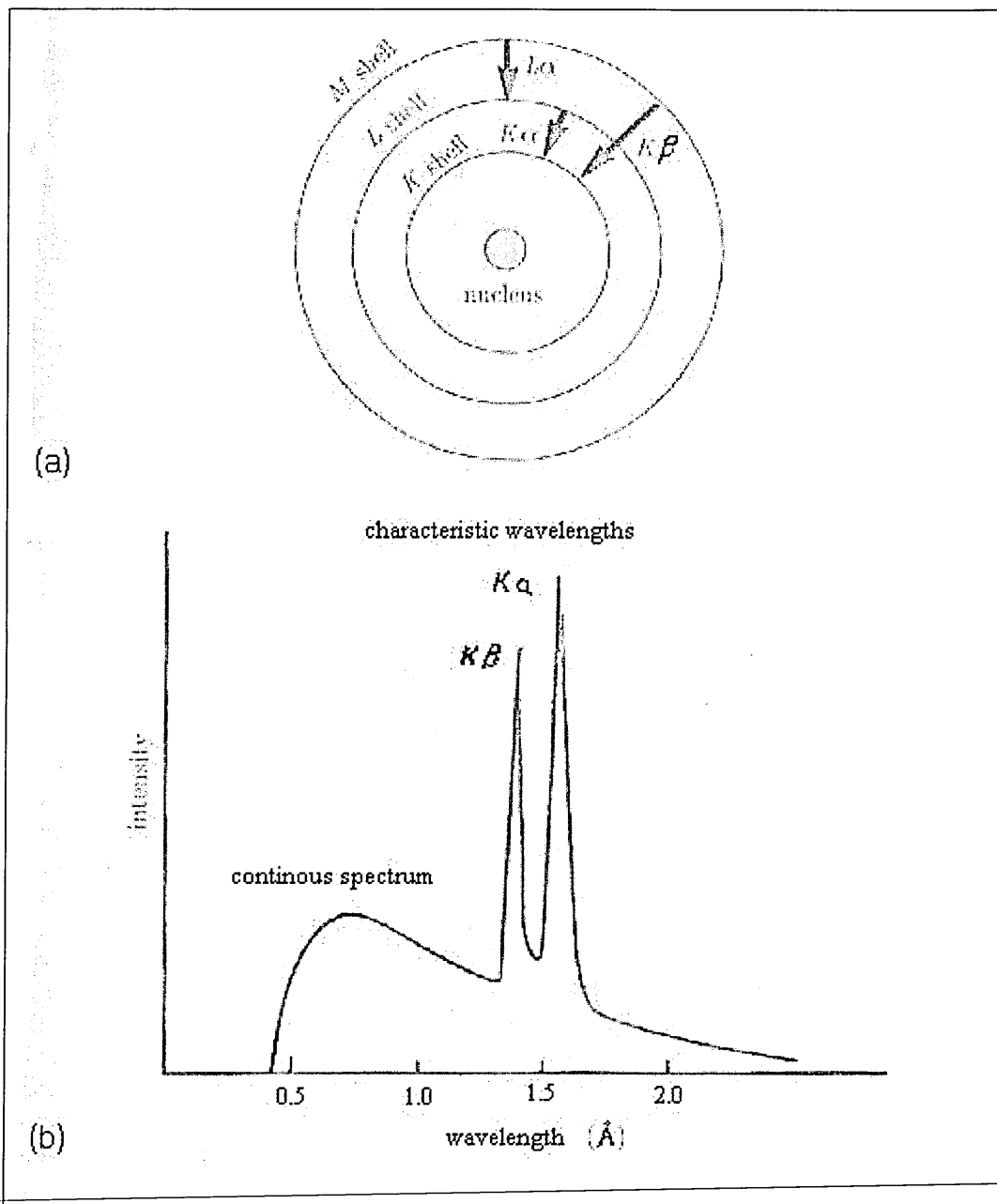
Figure 3.12 – The X radiation emitted when an electron falls from an outer to an inner level (a) Electronic energy levels involved (b) Characteristic X-ray spectrum for copper radiation.

As previously stated, two types of radiation are produced when the anode target is bombarded by fast-moving electrons in this way. A continuum of radiation referred to as white radiation, is produced by simple collisions between electrons and target (Figure 3.12b). In addition to simple energy exchange on collision metal atoms in the target may become ionised by the loss of an inner – shell electron. An outer shell electron then moves to an inner shell, and radiation of a wavelength specific to the target material is emitted (Figure 3.12a). these x-rays produced are called characteristic x-rays because their nature is dependant on the atomic character of the material used to make the target. Common targets incude copper or molybdenum. Molybdenum radiation has a shorter wavelength and higher penetration through a crystal, and it is less readily absorbed. In practice, the characteristic x radiation is not of a single wavelength but contains several sharp lines, as shown in Figure 3.12b which illustrates the characteristic spectrum from a copper target. All but one of these spectral lines need to be filtered out in order to obtain a monochromatic beam. Usually Kα radiation is selected. In addition, the white radiation described above, must be eliminated or minimised.

3.4 Evolved Gas Analysis using Synergic Chemical Analysis

A synergic chemical analysis system[56] consists of a thermobalance, infrared gas cell, organic trap module (OTM), gas chromatograph (GC), and mass spectrometer (MS). (Figure 3.13). The thermobalance is fitted with two outlets, which are connected to heated transfer lines. One transfer line is connected to the infrared gas cell (path length 40cm) connected to an FTIR spectrometer. The outlet from the infrared gas cell flows into a second transfer line which is connected to an absorbent trap contained within the organic trap module. The outlet from OTM is also connected to a GC-MS. The third transfer line is connected directly to the MS.

This enables the user to operate in various modes:- TG-FTIR, TG-FTIR-real time MS, TG-FTIR-OTM-GC-MS. As can be seen in all cases the TG is employed, and it is the gases evolved during the TG analysis which are subsequently analysed.
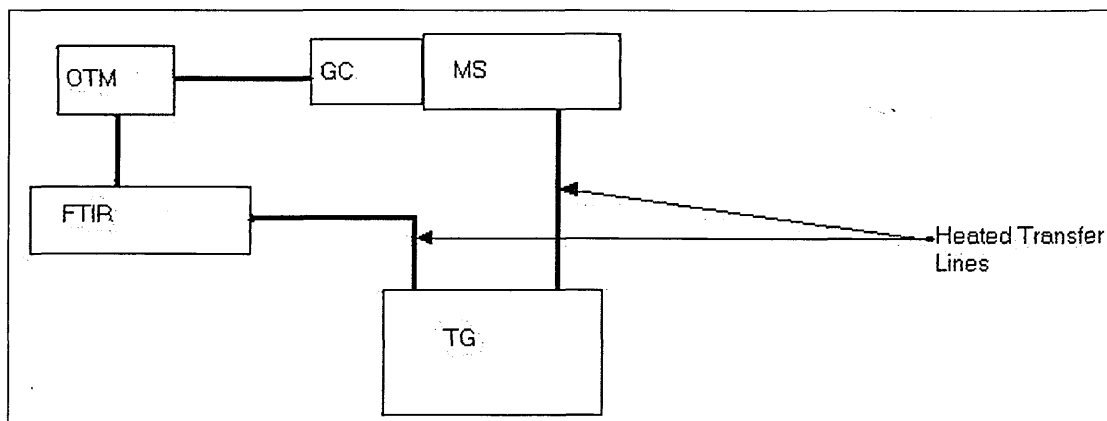
Figure 3.13 Synergic Chemical Analysis

The mass spectrometer used in the synergic chemical analysis system is an ATI Unicam Automass System 2 quadropole MS. The MS is operated in the electron impact (EI), positive ionisation mode. There are three main sections in the quadrupole mass spectrometer:-

1. The Ion Source – The Ion Source is where the sample is introduced into the MS. The sample passes through an electron beam (70eV) and ionisation of the sample occurs (i.e. electron removal leaving a positive ion). The molecular ions may also fragment to form charged and neutral fragments. Only positively charged fragments will be detected. The ions are then accelerated by an electric field towards the quadrupole mass analyser.

2. Quadrupole Mass Analyser – This is used to select the required mass range of molecular ions to be detected.

3. Detector – The ions which have travelled through the quadrupole are then sent towards the detector. The ions strike a dynode which emits secondary electrons, which are transformed into photons and then detected by a photo – multiplier. This amplifies the photon signal.

Chapter 4 – Clay Mineral Organic Interactions and Characterisation.

4.1 Vibrational Spectroscopy of Kaolin and Halloysite

The IR, (and recently) Raman spectra of the kaolinite clay minerals, have been studied extensively over the past four decades, and has attracted considerable interest due to its applications in structural studies of such minerals. Among the IR spectroscopic techniques for studying clay minerals there are

1. The absorption (KBr) technique.

2. IR emission spectroscopy (IES).

3. The reflectance technique, including diffuse and specular reflectance

4. Attenuated total reflectance (ATR).

5. IR microscopy.

6. Photoacoustic FTIR spectroscopy (PAS).

The selection of technique depends on the particular problem at hand. For example IES is suitable for studying kaolinite dehydroxylation and thermal changes in kaolinites at elevated temperatures[57]. The pressing of a KBr pellet may alter the spectrum through absorption or exchange of K into the clay structure. ATR is limited in its use with powders by the signal to noise ratio determined by the energy throughput. PAS is a non – destructive technique useful for handling clays but is limited by the number of samples that can be studied in a given period of time. Specular reflectance is not readily applicable to clay minerals, as the technique normally applies to flat polished shiny surfaces. Hence, for the reasons discussed previously, DRIFTS remains particularly useful in the study of clay minerals.

Some of the earliest IR studies were undertaken by Farmer[58,59] and since then there has been extensive debate with regards to band assignments of these minerals, in particular the hydroxyl stretching region of kaolin. This is an important region to study in the vibrational spectra of the kaolinite clay minerals as this represents the hydroxyls of the aluminium octahedral sheet which are involved in hydrogen bonding between the layers of kaolin and

also with any intercalated species that may be intercalated between the layers. Furthermore, hydroxyl group vibrations are sensitive probes for distinguishing between different kaolin clay minerals and determining their structure[60]. Figure 4.0 shows the DRIFTS spectrum of kaolin.
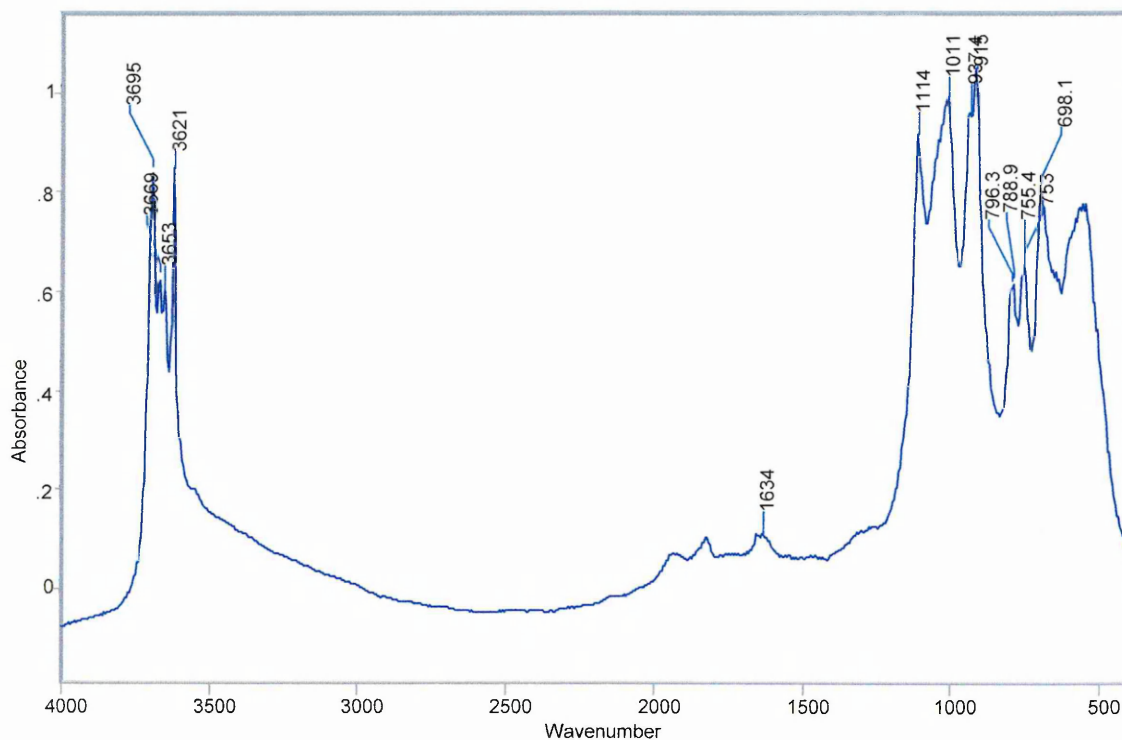
Figure 4.0 DRIFTS spectrum of English China Clays Kaolin.

The band assignments for this spectrum are as follows:-

Band (cm^{-1})	Assignment
698	Si-O-Al Stretch
755	Si-O-Al Stretch
788	OH bend
796	OH Bend
915	Inner OH bend
937	Outer OH bend
1011	Si – O Stretch
1114	Si – O Stretch
1653	OH Bend (water)
3621	Inner OH stretch
3653	Outer OH Stretch
3669	Outer OH Stretch
3695	Outer OH Stretch

Table 4.0 – Band assignments for Kaolin DRIFTS spectrum[60].

4.1.1. The OH stretching region in kaolin and halloysite.

As previously stated the OH stretching region is of particular importance in the kaolinite minerals, and therefore merits further investigation and discussion. The unit cell of kaolin was determined by Bish[61] to have four different OH groups and hence four different OH vibrations, it is assumed that these can give rise to four different stretching frequencies. (Figure 4.1).
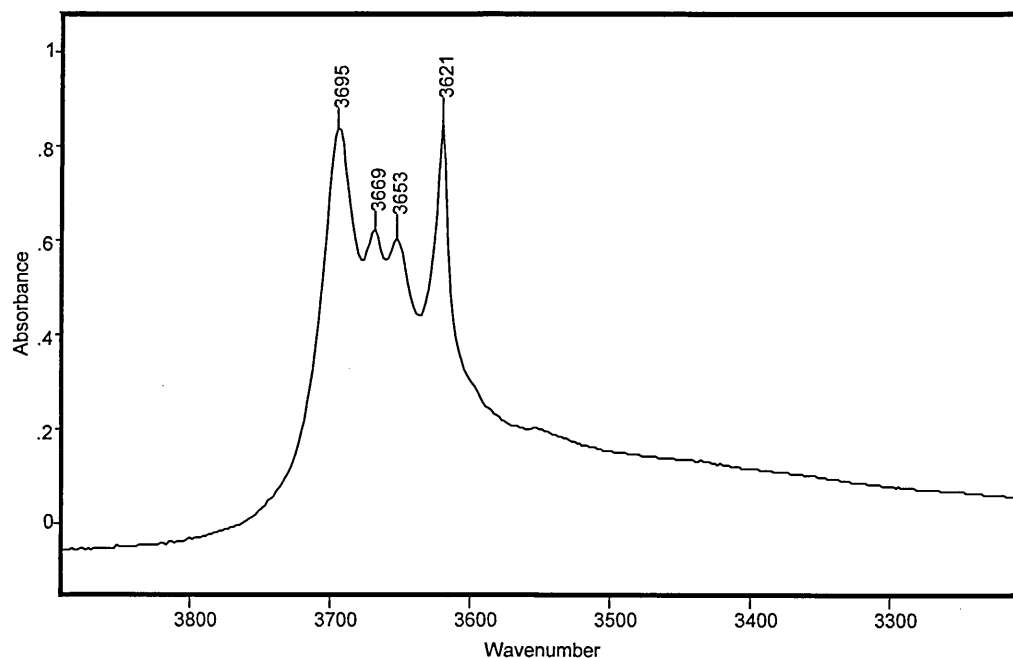
Figure 4.1 – OH stretching in kaolin DRIFTS spectrum.

Much debate has been generated by the exact assignments of these four bands using both conventional IR and raman spectroscopy. The accepted band positions for the IR OH stretching frequencies are 3697, 3670, 3652 – corresponding to the outer hydroxyl groups (or "inner surface hydroxyls") – and 3620 cm^{-1} which corresponds to the inner sheet hydroxyl where the tetrahedral and octahedral sheets are joined and is considered not to participate in hydrogen bonding. The band near 3697 cm^{-1} is strong and the other inner surface hydroxyl bands at 3670 and 3552 cm^{-1} are weaker absorption bands. This intensity distribution can be explained if the stretching vibrations of the three inner surface hydroxyls couple to give one in

– phase vibration at 3697 cm^{-1} and two anti – phase vibrations vibrations at 3670 and 3552

56

cm^{-1} [57,58,62]. Moreover, the hydroxyl deformation modes of kaolin at 959, 938 and 915 cm^{-1} of kaolin, which, as shown by Frost[63], can be of equal importance.

The OH stretching region of halloysite generally contains two distinct bands at 3695 and 3620 cm^{-1} (Figure 4.2). The presence of water in the interlayer reduces the intensity and broadens 3695, 3688 and 3652 cm^{-1} bands.
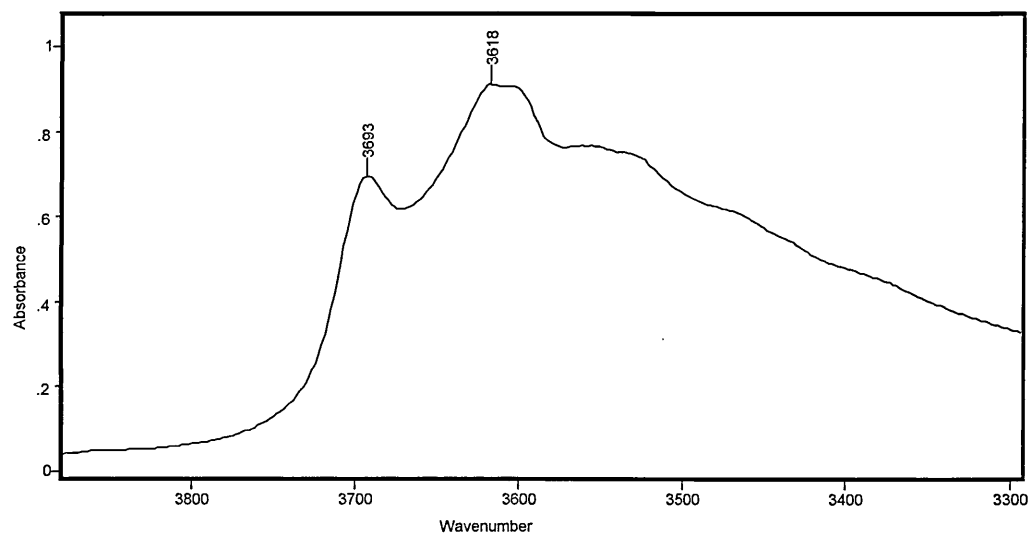
Figure 4.2 – OH stretching region of Halloysite (Chinese origin)

As kaolin and halloysite both utilise the inner surface hydroxyls in intercalation, it therefore follows that perturbation via bands shifts, reduction in intensity or even the evolution of new bands in the OH stretching region may by observed when studying such intercalates.

4.2 Intercalates of Kaolinite Clay Minerals

The formation of intercalation compounds has many points of interest. For example, the basal spacing of the complexes may be used to distinguish, by XRD, different kaolin polymorphs as illustrated by Range et al.,[64] and Wada[65]; differences among kaolinites with varying degrees[64] of ordering may also be investigated by XRD. Lagaly[66] has shown that intercalation reactivity may be an important factor controlling the technical applicability of kaolinite.

Intercalates may be obtained in three ways:-

1. By direct intercalation.
2. Via an entraining agent.

3. Via displacement of preformed complexes.

4.2.1 Direct Intercalation.

Direct intercalation occurs with alkali metal salts of short chain fatty acids, in particular acetates, and small polar compounds including hydrazine, formamide and amines. Intercalates of potassium and caesium acetate have been extensively studied by Frost *et al.*,[67-70] and also Ruiz Cruz *et al.*,[71] who utilised DRIFTS and Raman spectroscopy (as well as XRD and thermal techniques) in elucidating the structure of the complexes formed. In all cases the complexes were formed by stirring kaolin in solutions of the acetates for varying periods of time. Clearly seen in the hydroxyl stretching region, is a reduction in the intensity of the original kaolin bands (as these are now involved in hydrogen bonding with the intercalate) and the formation of new bands at 3604 cm^{-1} (narrow) and 3450 cm^{-1} (broad). The latter was thought to represent the contribution of at least three bands, one wide band centred at 3450 cm^{-1}, and some higher frequency bands, the more intense at 3561 and 3520 cm^{-1} which were obtained upon heating the complex.. These latter bands according to Frost[72] represent different types of water molecules in the intercalate (as will be discussed later), but which Ruiz Cruz[71] thought to represent the shift of the OH stretching bands due hydrogen bonding between intercalated water and inner surface OH. The 3604 cm^{-1} band observed was attributed to the splitting of the inner OH stretch which is not modified by partial dehydration as this band remains unchanged upon heating. Additionally new bands were observed in the spectrum of the intercalate at 1586 and 1410 cm^{-1} which arise from the symmetric and antisymmetric stretches respectively of the COO$^-$ moiety. The d(001) spacing of this complex was determined to be 14.06 Å which decreased to 9.35 Å when heated.

Similarly, changes in the OH stretching of kaolin have been observed with intercalates of hydrazine[73] and formamide[74-75]. For the hydrazine intercalates, the positions and relative intensities of the OH bands of kaolin were affected as seen by a reduction in the intensities of the 3695, 3668 and 3652 cm^{-1} bands and by the appearance of two new bands at 3568 and 3463 cm^{-1}. The appearance of two such red shifted OH stretches with a separation of 103 cm^{-1} indicates the formation of hydrogen bonds with two distinct N – O bond lengths. According

to published correlations[76] this 103 cm^{-1} separation corresponds to N – O (N $_{hydrazine}$ – O $_{Al-OH}$

$_{of\ kaolinite}$) distances which differ by 0.07 Å i.e. there are two unique environments for the

nitrogen atoms of hydrazine. Perturbation in bands of the intercalate are also observed here

in the N – H stretches. A band in the kaolin – hydrazine complex were observed at 2975 cm^{-1}

which is a red shift of 275 cm^{-1} from the same band in liquid hydrazine, indicating that these

NH$_2$ groups are significantly more strongly hydrogen bonded than those in liquid hydrazine.

Similarly shifts in the lower frequency twisting and scissor modes of H-N-H in hydrazine were

also observed. In hydrazine the twisting mode occurs at 1305 cm^{-1} but this shifts to 1276 cm^{-1}

in the complex with kaolin and was attributed to isolated hydrazine molecules where

intermolecular hydrogen bonding has been reduced.

Frost[75] has used DRIFTS and Raman spectroscopy to study intercalates of kaolin with

formamide. Here kaolin was mixed with 50% aqueous formamide for 80 hours at room

temperature. The consequence of using an aqueous mixture is apparent in the DRIFTS

results obtained. Additional bands in the OH stretching region are observed at 3606 and 3629

cm^{-1}, which are attributed to the intercalated water and to the inner surface hydroxyl groups

bonded to the formamide respectively. A band at 1595 cm^{-1} is also attributed to adsorbed

water which is merely "space filling" in the expended interlayer. However bands are also

observed in this region at 1715, 1695, and 1674 cm^{-1}, any one of which could be the HOH

bend from water or the C=O stretch and the amide I and II deformations. These bands are

assigned as – 1715 cm^{-1} C=O stretch and 1695, and 1674 cm^{-1} to the N-H deformations. The

band positions of these groups suggest that there is interaction between the C=O of

formamide and the kaolin inner surface hydroxyls and also the NH of formamide and the

siloxane surface of kaolin. The position of the 1595 cm^{-1} band suggests that this is therefore

water and not interacting with anything but merely space filling as the liquid water HOH bend

is normally observed at 1630 cm^{-1}. A small intensity of ~1% at 1624 cm^{-1} is attributed to

adsorbed water. VT-DRIFTS (variable temperature DRIFTS) analysis here would have been

useful to ascertain the assignments of the 1800 – 1500 cm^{-1} region.

It is interesting to note here Frost's interpretation of the reduction in intensity of the inner

surface hydroxyl stretching bands and the results obtained from XRD. The (XRD) results

show an intercalation ratio of 100%, which means that all of layers in the kaolin – formamide complex are expanded. (The intercalation ration is a measure of the expanded versus non – expanded layers in the clay and is expressed as a percentage of layers expanded). However, this may imply that all of the inner surface hydroxyls are involved in hydrogen bonding with formamide. This is not true and Frost explains this due to the residual intensity in the hydroxyl stretching region from the inner surface OH groups of kaolin. Such intensity implies that not all of these OH groups are involved in hydrogen bonding. This may be due to the size and orientation of the formamide molecules in the interlayer of kaolin, which makes it impossible for all of the OH groups to participate in hydrogen bonding i.e. it is a question of space.

Halloysite shows similar changes to that of kaolin, but as deposits of this mineral are less prevalent than kaolin this is reflected in literature. Using DRIFTS but mainly Raman spectroscopy Frost[77,78] has examined intercalates of halloysite with urea and potassium acetate. With potassium acetate an additional band at 3605 cm^{-1} is observed and attributed to the inner surface hydroxyls bonded to the acetate ion. Again with urea there is a significant decrease in intensity of the hydroxyl stretching bands in halloysite, with urea intercalates exhibiting additional bands at 3387, 3410 and 3497 cm^{-1} all attributed to hydrogen bonds between the N-H of urea and halloysite (i.e. N-H stretching modes).

Not to be overlooked is the use of the OH bending modes in the vibrational spectra of kaolin and halloysite, sometimes referred as the librational or deformation mode. These offer another, complementary means of studying changes in the intercalation of such minerals. Kaolin has OH deformation bands at 940 and 915 cm^{-1} which are attributed to inner surface and inner sheet OH's respectively. Halloysite also has the same bands but are less resolved and weaker.

Returning to the earlier example of hydrazine[73] intercalates of kaolin show that the intensity of the 940 cm^{-1} is strongly reduced (inner surface OH hydrogen bonded to hydrazine) and the 915 cm^{-1} is shifted to 904 cm^{-1} showing that the inner surface OH group is perturbed by the presence of hydrazine. Formamide intercalated kaolin[75] exhibits similar decreases in intensity for the OH deformation modes with an additional band observed at 905 cm^{-1} assigned to inner surface hydroxyls hydrogen bonded to the C=O of the formamide.

Finally, halloysite intercalates with urea[79] were shown to have reduced OH deformation intensity as one would expect with a new band at 897 cm^{-1}.

4.2.2 Intercalation via Entraining Agents.

As previously discussed, direct intercalation into kaolinites involves the use of small polar molecules. However, the intercalation of other larger molecules is possible but it generally involves the prior intercalation of precursors followed by the intercalation of the required molecule[80]. This process occurs as one reaction mixture and the intercalated precursor complex is not isolated prior to displacement. Such a precursor is called an entraining agent. The entraining agent effectively opens the interlamellar space allowing organofunctionalisation of kaolinite by the required species. For example, these reactions may be performed using water as the entraining agent in order to intercalate alcohols[81-83].

In these reactions, called topotactic, the basic unit of the kaolinite remains intact with the exception of the substitution of the hydrogen atoms of the octahedral sheet by the appropriate organic groups. After the functionalisation process, ether – type bonds (Al-O-R) are formed on the gibbsite side of the lamellae. Quite often this reaction will require heat to facilitate the process.

The hybrid materials obtained through this process combine the physical, chemical, structural and mechanical properties of the silicate with the particular properties of the organic compound. Thus they find applications in industry such as chromatographic columns, catalyst supports, coloured kaolinite for use in the paper industry, ionic exchangers and adsorbent materials.

Water is commonly used an entraining agent, and the fate of such water in the resultant intercalate has been studied extensively. Water intercalates themselves are made via an entraining agent / displacement reaction. Water in clay minerals has three principal vibrational spectroscopic regions:-

1. the hydroxyl stretching region 3600 – 3000 cm^{-1}.

2. the H-O-H bending region centred at 1630 cm^{-1} (lower frequencies imply free molecular water in the structure

61

3. the deformation (or librational) region 700 – 400 cm^{-1}.

Frost[84,85] and co. workers have studied such water in intercalates of kaolin with formamide and hydrazine. In the case of formamide (prepared from a 1:1 % wt formamide : water solution) TG showed that compared to kaolin intercalated directly with formamide the water – formamide intercalated kaolin intercalated greater amounts of formamide. Additional differences attributable to water were increases in a band at 3605 cm^{-1} which was significantly more intense in the water intercalated complex than the formamide one. This was identified as being a contribution from the interlamellar water now incorporated into the structure. Bands at 1630 and 1595 cm^{-1} (fairly intense) were observed and attributed to adsorbed and free water in the complex respectively, which implies that there is some water which is not hydrogen bonded and may simply be acting as a space filling molecule in the expanded interlayer space.

Similarly, it was found that water plays a significant role in the intercalation of hydrazine into kaolin when mixed with hydrazine hydrate at 85°C (as this is the aqueous from of hydrazine). Here OH stretches attributed water were observed at 3413, 3469 and 3599 cm^{-1} and OH bends for water at 1578, 1598, 1612, 1627, 1650 and 1679 cm^{-1} after curve fitting. The 1578, 1598, 1612, 1627 cm^{-1} bands were attributed to free or non-hydrogen bonded water held in the interlayer spaces of kaolin (1578 and 1598 cm^{-1}), water in the hydration sphere of hydrazine (1612 cm^{-1}) and adsorbed water on the kaolin surface (1627 cm^{-1}). The 1650 and 1679 cm^{-1} were assigned to water coordinated to the siloxane surface or strongly hydrogen bonded due to their appearance at higher wavenumber. These results correlate with the XRD results which show a broad d$_{(001)}$ with a shoulder implying that there is more than one phase present. Two were clearly identified ay 10.28 and 9.48 Å and these are thought to be due to hydrazine intercalating with a significant hydration sphere. In addition, a band at 3628 cm^{-1} is attributed to the inner surface hydroxyl group hydrogen bonded to the hydrazine. As hydrazine is present as a base such as [NH$_2$-NH$_3$]$^{\delta+}$OH$^{\delta-}$ the authors suggest that no HNH bends in the region 1700 – 1600 cm^{-1} are observed. Furthermore, on exposure to air for 6 hours the 1650 cm^{-1} increases in intensity whilst the 3628 cm^{-1} band decreases in intensity. As the sample is left exposed to air for 24 hours the XRD shows a collapse in the interlayer

spacing, whilst the 1650 cm^{-1} band remains but decreases in bandwidth. Such an observation is thought to be due to water getting into a fixed orientation as might occur in a "crystalline like" lattice. The 1679 cm^{-1} displays similar behaviour, whilst the 1612 cm^{-1} (water in the hydration sphere of hydrazine) band decreases in intensity over the exposure time.

Wypych and co workers[86] combine several techniques to obtain an interesting result using TG-DSC, XRF, XRD and FTIR (KBr) in their study of phenylphosphonic acid (PPA) intercalated kaolin. Here the entraining agent was a mixture of 1:1 (v/v) acetone: water, which was refluxed with phenylphosphonic acid and kaolin for a period of 20 days at 95°. The reaction can be written as :-

$$Al_2Si_2O_5(OH)_4 + 3H_2O_3PPh \rightarrow Al_2Si_2O_5(OH)(HO_3PPh)_3.2H_2O + 3H_2O$$
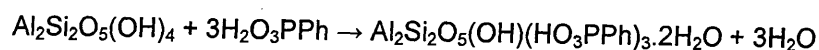
This implies the formation of a hydrated intercalate. One phase was isolated, with a d$_{(001)}$ of 15.02 Å which represents considerable layer expansion for kaolin from 7.12 Å. The TGA results show a 5% weight loss by 164°C which was attributed to loss of water of crystallisation and an overall weight loss of 15%. The authors also state that the decomposition of the complex shows that the organic (PPA) part of the structure is only eliminated at temperatures as high as the dehydroxylation temperature of 500°C, suggesting that this complex displays extremely high thermal stability. PPA itself has a melting point of 250 °C.

The FTIR results show a decrease in the intensity of the OH stretching bands of kaolin, as well as new bands at 3537, 3056, 3015, 1199, 883, 850 669 and 580 cm^{-1} for which no assignment was given. A band at 1642 cm^{-1} was observed to be an O-H bend but a band at 1595 cm^{-1} was incorrectly assigned to a vibration arising from PPA. This could be free spacing filling water trapped within the interlayer. Furthermore the hydroxyl deformation region shows an intensification of the peaks attributed to inner hydroxyl groups in comparison to the outer surface hydroxyl groups (915 and 942 cm^{-1}). A significant background contribution in the OH stretching region was also observed (though not commented on by the authors), which is indicative of a large amount of hydrogen bonding.

Wypych and co workers[87] took this work further by replacing the water molecules in their hydrated PPA intercalate of kaolin with hexylamine. This was achieved by mixing the PPA intercalate with hexylamine for 72 hours at room temperature, as the already expanded kaolin

should not need extreme conditions to accommodate another species. This increases the interlayer spacing to 16.36 Å, but on heating the hexylamine grafted onto the kaolin-PPA host was lost (230 °C), though the resultant dehydrated host intercalate was found again to be stable to 498°C.

4.2.3 Intercalation via Displacement of Preformed Complexes.

Intercalation via preformed complexes involves the intercalation of a species commonly DMSO or NMF and then subsequent displacement of this intercalate with another species, that would not be possible to intercalate directly or via the use of an entraining agent. Characterisation of the resultant intercalate yields similar results to those previously discussed in terms in IR band shifts and intensities and increased layer spacings observed through XRD. However, this type of intercalation in kaolin is of interest, as it has opened up a new opportunity for the utilisation of kaolin in nanocomposites. Strategies for the manufacture of nanocomposites from kaolin rely on this approach, hence it will be discussed briefly here. Quite often, though not always it is desirable to be able to expand the gallery of the host clay mineral to as high a degree as possible when manufacturing a nanocomposite.

Intercalates of kaolin with DMSO and NMF were used Detellier[88] to intercalate methoxy groups into kaolin. It was found that by heating the DMSO or NMF intercalates with methanol at various temperatures greater than 150 °C resulted in a new intercalate of 8.2 Å spacing. TG analysis showed that the new intercalate was stable to 515 °C and both the XRD traces and FTIR spectra were identical after heating to 210°C for 1 hour. Some intensity was lost in the OH stretching region of the FTIR spectrum and a new band at 3646 cm^{-1} was attributed to kaolin – MeOH. Detellier reinforces the fact that the loss in intensity is related to the steric packing of the methanol in the interlayer space of kaolin. The distance between the adjacent surface hydoxyl groups is approximately 2.8 Å and the van der Waals diameter of a methyl group is 3.9 Å so a completely methoxylated surface would be sterically forbidden. Such a kaolin intercalate (with methanol) itself has been used to facilitate the intercalation of alkylamines[89] and water into kaolin yielding $d_{(001)}$ spacings of as much as 27 – 57 Å.

Hydrated kaolin[90] made from a kaolin / DMSO intercalate, was washed by centrifugation with methanol and then water to produce a 10.0 Å hydrated kaolin which was only stable in water. This was used to ultimately intercalate a range of amino acids into kaolin[91]. Intercalation was found to dependant on the chain length, pH and the concentration of the amino acid zwitterions. The resultant intercalates displayed $d_{(001)}$ spacing of 10.3 to 14.2 Å and were stable to 250 – 300 °C.

Perhaps of more relevance to nanocomposites are the intercalates of benzamide (14.29 Å) and 1-methyl-2-pyrrolidone (12.31 Å) reported by Wypych and co workers[91.92], who in both instances once again used a kaolin DMSO intercalate as the starting material.

4.2.4 Intercalates of Phenylphosphonic Acid.

As previously discussed the work of Wypych[86] has shown that phenylphosphonic acid forms intercalates of kaolin which possess high thermal stability. As this work has been extended and complemented on in this thesis this enhanced thermal stability will be briefly discussed further here, as it has been recorded in layered double hydroxides[93,94], layered γ zirconium phosphate[95] and layered $AlH_3(PO_4)_2$[96].

The structure of an LDH derives from that of brucite $Mg(OH)_2$, where the metal atoms are octahedrally surrounded by the hydroxy groups. These octahedra share edges to form infinite sheets. In LDHs a fraction of the divalent metal is substituted by a trivalent metal, thus generating a positive charge in the brucite like sheets. This charge is compensated by the formation of a layered structure in which the positive ordered sheets, are separated from each other by a disordered layer of counter anions, and water molecules, forming a lamellar structure with alternating positive and negative layers. (For this reason these compounds are also known as mixed layered hydroxides). Usually the most stable anion in the interlayer region is carbonate, but LDHs with other anions can be prepared by various methods.

Temperatures of 25 – 75 °C were used to intercalate PPA into Cd/Al LDHs (with NO_3 and CO_3 anions) from water[93]. This produced an interlayer spacing of 14.59 Å, whilst the original interlayer spacings of the starting complexes were 8.24 and 7.54 Å for the NO_3 and CO_3 compounds respectively. FTIR results show that the P=O stretch at 1220 cm^{-1} in the acid has

disappeared in the intercalate suggesting that there is formation of PO_3^{2-} groups that present ionic interactions with the positive layers. P-O stretching bands are also observed in the region of 1180 - 900 cm^{-1}. These bands are somewhat narrower and more intense than in the acid as there is intermolecular hydrogen bonding in the acid. Mg, Al, and Zn LDHs[94] show interlayer spacings of 15.8 Å but more importantly the authors performed TGA experiments to show that the stabilities were stable up to 500 °C. In addition, the reported IR bands were at 3054 and 3076 cm^{-1} : C-H vibrations of the aromatic group, 1438 cm^{-1} ; P-C stretch and 1140, 1068, 1040 and 990 cm^{-1} : vibrations of the O_3P-C group.

In layered γ zirconium phosphate (interlayer spacing − 8.55 Å)[95] the intercalation reaction was performed in a similar fashion to Wypych[86] in that a 1:1 (v/v) mixture of acetone : water at 80 °C was used for reaction times varying from 5 mins to 40 days. The resultant interlayer spacing of the intercalate is again in a similar range to those previously discussed here and reported − 15.3 Å, but the authors found that the reaction proceeded faster in a mixture of water and acetone than just water alone. Similarly in layered $AlH_3(PO_4)_2$[96] the interlayer spacing is determined to be 15.2 Å and the thermal stability is again in the region of 500 °C. Other intercalates of PPA displaying similar properties include bayerite $Al(OH)_3$[97] (14.35 Å, stable to 600 °C) and it should also be noted that Zinc and Cobalt[98] phenylphosphonates also display this high thermal stability.

4.2.5 Kaolin and Halloysite Nanocomposites.

Most work on nanocomposites, as will be seen in later, involves the use of smectites rather than 1:1 clay minerals such as kaolin. This is mainly because smectites are more easily intercalated. Nevertheless, some work has been reported with kaolin and halloysite.

Some of the first studies on kaolin − polymer interactions were carried out by Sugahara[99,100] and co workers who looked at the intercalation of monomers and subsequent polymerisation between the layers of kaolin (an in situ intercalative approach). The monomers used were acrylonitrile[99] and acrylamide[100]. Both were first intercalated into kaolin by displacement of a kaolin − ammonium acetate intercalate and kaolin − NMF intercalate respectively. The intercalated monomers also contained 0.7% of initiator. Polymerisation of these monomers

was then carried out by heating the complexes to the required temperature to initiaite polymerisation, and the reaction mixture left stirring for 24 hours. As will be seen later this is termed in situ polymerisation. The kaolin – polyacrylonitrile (PAN) complex was found to have a $d_{(001)}$ spacing of 13 – 14 Å, whilst the spacing of the kaolin – polyacylamide complex was 11. 0 Å. IR analysis however showed that not all the original kaolin intercalate had been displaced after initiation as well as the presence some unreacted initiator. The authors also made good use of the kaolin OH stretching region in IR analysis to further show hydrogen bonding with the $C \equiv N$. For example in the PAN intercalate where the $C \equiv N$ stretch shifted from 2245 to 2253 cm^{-1}, furthermore proving that some polymerisation had also taken place (further supported by NMR). This was also observed in the kaolin – polyacrylamide intercalation compound, where the C=C stretch at 1658 cm^{-1} was shown to decrease in intensity after polymerisation. Both these complexes were found to be stable to >300 °C.

Direct intercalation of a polymer into kaolin has also been reported using poly(vinylprrolidone) (PVP)[101] and poly(ethylene glycol) (PEG)[102]. Both of these methods use the displacement method from intercalates of kaolin and methanol and DMSO respectively, but unlike the previous examples, in this instance, the polymer as a whole is intercalated into kaolin. In the case of PEG the polymer was intercalated via the melt, which is a common method of intercalating polymers into clay minerals especially with smectities. Again, these nanocomposites were characterised by a mixture of XRD, IR, NMR and TGA. The kaolin – PEG intercalate was found to have an interlayer spacing of 11.0 Å and indicates a monolayer within the interlayer of kaolin. IR analysis of the kaolin – PEG intercalate revealed not only perturbance of the hydroxyl stretching region (not unexpected) but also the fact that at least a portion of the intercalated ($O-H_2CH_2-O$) groups of the intercalated PEG polymer were in the trans conformation as indicated by a band at 1326 cm^{-1}. Furthermore, TGA/DSC measurements revealed that the complete decomposition of the organic component of the oxymethylene based organokaolinite did not occur until greater than 1000 °C.

The kaolin – PVP composite produced an interlayer spacing of 12.4 Å. FTIR analysis here showed new bands at 3634, 3599 and 3555 cm^{-1} which the authors attribute to OH hydrogen bonded to PVP.

Lastly polymerisation of aniline within the tubular structure of halloysite has been reported[103]. This was achieved by intercalation of aniline into halloysite via aniline vapour. However, in order to polymerise polyaniline (PANI) within halloysite the halloysite first had to be exchanged with Cu(II) to allow the oxidative polymerisation of aniline to de driven by the Cu(II)/ Cu(I) couple. This can be visually followed in a colour change from grey to red, and simply occurs over a period of time, during which there is continued exposure to aniline which in this case resulted in studies over two weeks. As the polymerisation was hoped to take place within the tubular structure of halloysite the resultant layer spacing of 7.1 Å was not unexpected.

IR showed that intercalation of aniline results in the formation of peaks between 1700 and 1200 cm^{-1} that are characteristic of polyaniline. All forms of polyaniline have bands at 1500 cm^{-1} (C-C breathing mode of the phenyl ring) and 1300 cm^{-1} (Ph – N stretch). An increase in intensity of both of these bands are observed over a two week period. The presence of weak bands at 3386 and 3319 cm^{-1} are assigned to the symmetric NH_2 stretching modes of aniline. The existence of these peaks at values shifted from those of neutral aniline (3481 and 3360 cm^{-1}) suggested that aniline is coordinated to metal centres or bound to the halloysite surface by hydrogen bonding. Further analysis by XPS and TEM confirmed that polyaniline was formed on the internal and external surfaces of halloysite.

4.3 Clay Mineral - Polymer Nanocomposites

4.3.1 Classification of Nanocomposite Structures

One of the most comprehensive reviews on clay – mineral nanocomposites, has been compiled by Alexandre and Dubois[15]. Identified, within this are the four types of nanocomposite structure obtained (Figure 4.3), depending on the components used – clay mineral (layered silicate), organic cation and polymer matrix.
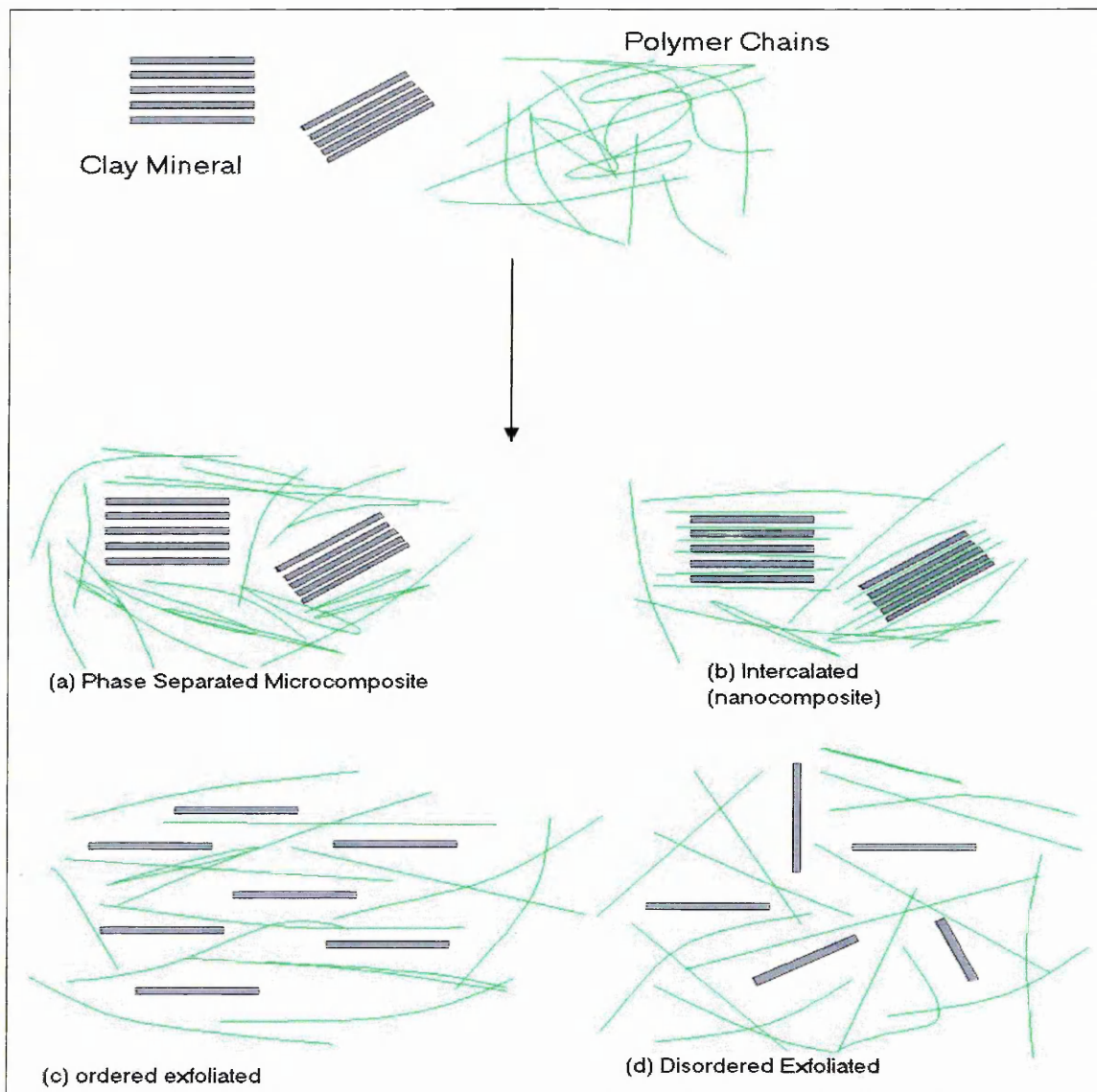
Figure 4.3 – Schematic of different types of composite arising from the intercalation of clay minerals with polymers.

When the polymer is unable to intercalate between the layers of the clay (Figure 4.3a), a phase separated composite is obtained – a microcomposite. The properties of these offer somewhat better interaction than a macrocomposite. If the polymer is able to intercalate the clay mineral with a single (and sometimes more than one) polymer chain an intercalated structure is obtained. A well ordered multilayer morphology is obtained alternating between organic polymer and inorganic clay mineral layers (Figure 4.3b). When the clay mineral layers are completely and uniformly dispersed in a continuous polymer matrix, an exfoliated or

delaminated structure is obtained (Figure 4.3c or d). This type of structure is considered especially desirable for improved properties because of the homogeneous dispersion of the clay and large interfacial area between polymer and clay.

Two complementary techniques are used to characterise these structures. XRD is used to identify intercalated structures as the repetitive, (but intercalated) structure of the clay mineral remains intact. However, no diffraction peaks are visible in the exfoliated structure either because of too large a spacing between the layers (exceeding 80 Å), or because the nanocomposite does not present ordered layers anymore. In the latter case transmission electron microscopy (TEM) is used to characterise the nanocomposite morphology.

4.3.2 Nanocomposite Preparation

Four main methods are used to prepare clay – mineral nanocomposites[104].

1. Exfoliation – adsorption. The clay mineral is exfoliated into single layers using a solvent in which the polymer is soluble. The polymer then adsorbs onto the delaminated sheets and when the solvent is evaporated (or the mixture precipitated), the sheets reassemble, sandwiching the polymer to form, in the best case, an ordered multilayer structure (Figure 4.3b). Under this process are also grouped the nanocomposites which are obtained through emulsion polymerisation where the clay mineral is dispersed in the aqueous phase.

2. In situ intercalative polymerisation. In this case the clay mineral is intercalated within the liquid monomer (or monomer solution) so as the polymer formation can occur in the interlamellar space of the clay mineral. Polymerisation is then initiated within the interlayer via heat or radiation, by the diffusion of a suitable initiator or by an organic initiator or catalyst fixed through cationic exchange inside the interlayer before swelling the structure with the monomer.

3. Melt intercalation. The clay mineral is mixed with the polymer matrix in the molten state, and effectively this allows the polymer to diffuse into the interlayer space. No

70

solvent is required. An intercalated or exfoliated polymer may be obtained via this method.

4. Template Synthesis. This is a less well developed technique for clay minerals where the mineral is formed in situ in an aqueous solution containing the polymer and structural units for the clay mineral. The polymer aids nucleation and growth of the inorganic host crystals and gets trapped within the layers as they grow.

4.3.3 Organoclays and Intercalation

A practical problem in the synthesis of clay mineral nanocomposites is to disperse an inorganic clay in an organic medium on a molecular scale. This can be addressed by treating the clay so that it becomes organophilic. In order to make a clay organophilic the hydrated interlayer cations in smectites, for example, may be exchanged with commonly used cationic surfactants such as alkylammonium or alkylphosphonium (onium) species. The modified clay – now an organoclay - is organophilic as its surface energy is lowered and it becomes more compatible with organic polymers and monomers. The structure is now to some extent already swollen by the presence of the onium ion giving a larger interlayer spacing, especially when more bulky alkylammonium ions are used.

The arrangement of the alkylammonium ions within the interlayer of the clay are dependant on the charge density of the clay and the chain length of the alkylammonium surfactant (Figure 4.4). In general, the longer the surfactant chain length, and the higher charge density of the clay, the further apart the clay layers will be forced.

71
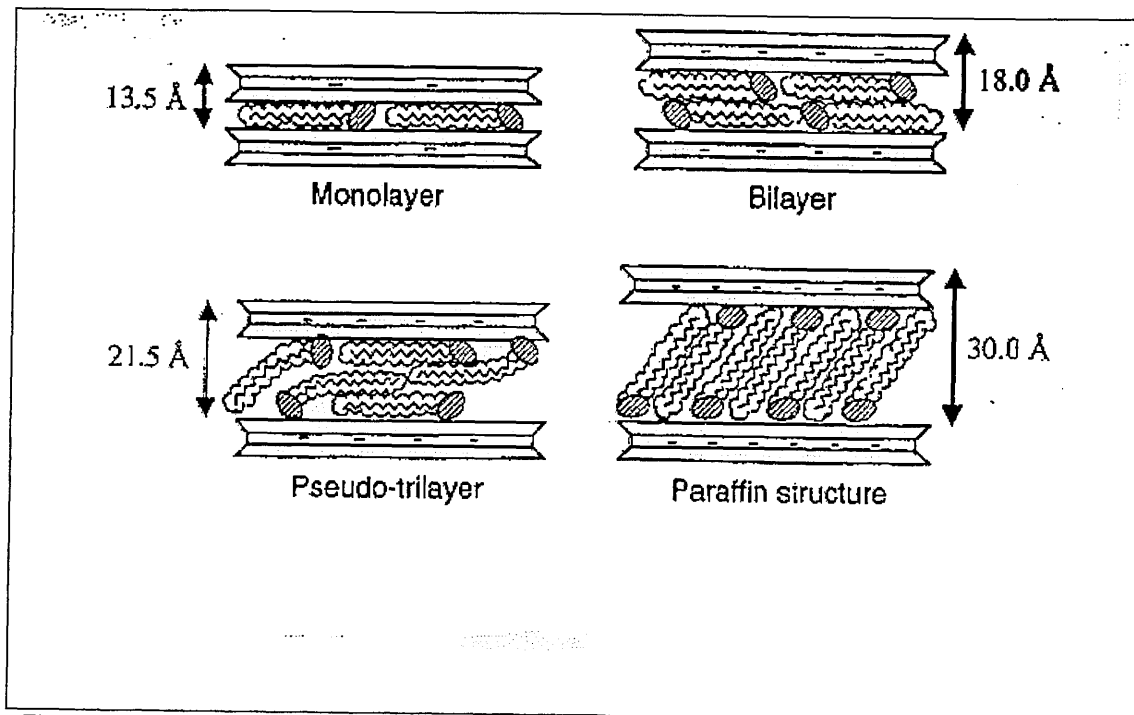
Figure 4.4 – Effect of charge density on the expansion of clay layers by alkylammonium ions

As the negative charge originates in the silicate sheet, the cationic head of the alkylammonium molecule preferentially resides at the layer surface leaving the organic tail radiating away from the surface. Depending on the charge density of the clay the onium ions may lie parallel to the clay surface as a monolayer, a lateral bilayer, a pseudo trimolecular layer, or an inclined paraffin structure, as has been determined by IR[105], XRD[105,106] and modelling experiments[107].

If the polarity of the organoclay sufficiently matches the monomer or polymer then it will intercalate into the clay further spreading the layers apart. This is a common approach in the manufacture of clay mineral nanocomposites as will be seen in the forthcoming discussion.

4.3.4 In Situ Intercalative Approaches

Methods to synthesise nanocomposites in this thesis focus on the in situ intercalative approach, hence this review concentrates on this approach to the manufacture of nanocomposites. This approach has been described by Lagaly[108] in his review of nanocomposite production methods as one of the most promising reactions to create clay

mineral - polymer nanocomposites, and was one of the first methods employed by the Toyota[109,110] research group who were one of the first groups to study clay mineral – polymer nanocomposites (see later).

For this type of nanocomposite preparation the conditions must be such that the monomers polymerising within the interlayer of the clay disperse the silicate layers uniformly in the polymer matrix. The enthalpy involved during the interlamellar polymerisation provides an essential contribution to exfoliation.

A typical procedure will involve the use of an organoclay as one of the starting materials. This is then swollen with the required monomer (which is also used as the solvent) and a curing agent may be added. Polymerisation may be initiated by a number of means, as will be illustrated in the following discussion.

4.3.4.1 Epoxy – Clay Nanocomposites.

Epoxy clay nanocomposites make use of these methods to good effect, the clay mineral providing very effective reinforcement in these systems[111-113]. These authors found that the it is effective to first load the clay interlayer with hydrophobic alkylammonium ions, and then expand the interlayer further by diffusing in the epoxide monomer, the curing agent or a mixture of the two. The acidic interlayer alkylammonium ions catalyse interlayer polymerisation at a rate that is competitive with polymerisation outside the confines of the clay structure. This is important because if the rate of polymerisation is greater in the bulk monomer polymerisation within the interlayer may not occur to a great extent within the interlamellar spaces available. Thus (provided the intragallery polymerisation occurs at a rate comparable to the extragallery polymerisation), an exfoliated nanocomposite can be formed. If the extragallery rate polymerisation is more rapid than the intragallery diffusion and polymerisation or if intragallery polymerisation is retarded, an intercalated structure will result.[111]. The study of epoxy – clay nanocomposites illustrates many of these factors together.

Lan et al.,[114] studied epoxy self – polymerisation in smectite clays. Na$^+$ monmorillonite, hectorite, fluorohectorite and vermicullite which were exchanged with alkylammonium ions of

varying chain length $(CH_3 (CH_2)_{n-1}NH_3^+)$ were used, with the increasing chain length producing increasing basal spacings. The organoclay was then mixed with the monomer – the diglycidyl ether of bisphenol A, (the epoxy resin Epon – 828) for 30 minutes at 75°C after which time it was determined that the organoclay had swollen even further. This is because the orientation of the alkylammonium chain in the interlayer does not affect the final structure of the epoxy monomer in the clay (Figure 4.5). When the epoxy monomers intercalate into the organoclay, the orientation of the interlayer organo cations change from initial state (parallel or inclined to the clay layers) to a perpendicular orinetation. This perpendicular orientation of the alkylammonium ions optimises the solvation interaction between the alkyl groups and the epoxy monomer, allowing enough monomer into the interlayer to aid exfoliation (discussed in more detail later).
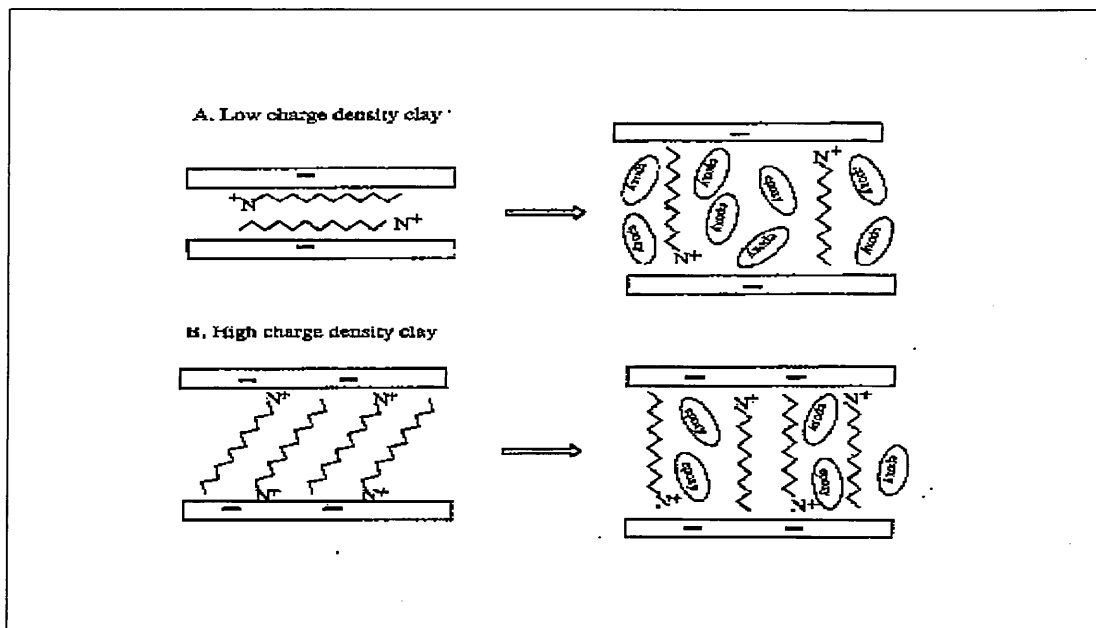
Figure 4.5 – Swelling of clay in monomer precursor.

From these mixtures the nanocomposites were prepared by heating at a rate of 10°C/min, to the polymerisation temperature range of 120 °C to 200 °C, which was self initiated due to the acidic form of the clay, or more specifically the protonated primary amine cations on the exchange sites of the clay. Additionally the onset of polymerisation within the clay interlayer occures at a considerably lower temperature than that of the resin alone – 350 °C. As the

74

temperature increases the viscosity also increases resulting finally in the formation of a powder. The formation of the powder was also accompanied by a strong exotherm, which increases the temperature by as much as 50 °C (which could, as previously discussed, aid exfoliation). Subsequent analysis by XRD and TEM revealed that exfoliated nanocomposites were produced there was complete lack of $d_{(001)}$ reflections in the XRD trace and TEM revealed a layer spacing of greater than 80 Å. DSC results however, showed that two exothermic processes were taking place. A lower temperature process is attributed to the interlayer polymerisation where the proton concentration is higher. This was confirmed by the relative intensities of the high and low temperature exotherms upon varying the amount of clay present in the mixture. The higher temperature exothermic process is attributed to bulk polymerisation.

An important model for such a reaction is also proposed by the authors[114]. It is suggested that the epoxy monomers swell the organoclay galleries at 75 °C with retention of a liquid like suspension. With increasing temperature the intercalated epoxy monomers undergo polymerisation by catalytic reaction with the acidic protons associated with the alkylammonium cations. After this initial step, a gel if formed with no significant change in volume. Upon further heating more epoxy monomers diffuse into the clay galleries and polymerise. The reaction is complete when all mobile monomers undergo polymerisation on the clay surface.

This approach to epoxy - clay mineral nanocomposites has variants that will determine the structure and properties of the final product[115.]. Berglund et al[116] have demonstrated the influence of the nature of the clay on structure. They were specifically interested in the influence of the cation exchange capacity (CEC) of the clay on the synthesis and structure of epoxy clay nanocomposites. The CEC of the clay determines the amount of alkylammonium ions present between the clay layers and therefore controls the space available for diffusion of epoxy monomer. The highest CEC provides the minimum space. Hence, they used clays with a high CEC (CWC – 140 meq/100g) and low CEC (SWy-2 – 94 meq/100g). The interlamellar spacing for the high CEC exchanged clay was 21.4 Å and the low CEC clay 17.2 Å. The difference in interlamellar spacing between these two organoclays, according to

Weiss[117] arises because the high CEC clay has a higher layer charge than the lower CEC clay (Figure 4.5). On exposure to the monomer (Epon - 828) the layer spacing of these two clays was investigated over a period of 24 hours. The low CEC clay rapidly increases in basal spacing and eventually exfoliates accompanied with a dramatic increase in viscosity. In contrast the high CEC clay increases to 34.0 Å after 3 hours and remains constant . These observations suggest that it is the low CEC clay that initiates a reaction with the monomer that affects the structure of the clay, and not the high CEC clay. Furthermore, the authors claim that the increase in viscosity during the mixing is due to a combination of two distinct phenomena: the homopolymerisation of the epoxy monomer as well as an decrease in effective clay particle size, due to increasing separation of the clay layers. The difference in layer charge greatly affects the structure of the two clays during the swelling phase. This might be explained by the amount of space occupied by the alkylammonium ions in the clay galleries. Indeed, due to the relatively low layer charge density (i.e. low CEC) the lower CEC clay contains a lower amount of amount of alkylammonium ions. This means that there is more space for the epoxy monomer in the clay galleries (see Figure 4.5).

Another interesting feature of epoxy clay nanocomposites is the addition of a curing agent after the initial swelling of the organoclay with epoxy monomer. Such a curing agent is added to promote cross linking in the final polymer and aids properties such as mechanical strength. This has been investigated by various authors [112,118 - 120]. All authors report that on addition of the curing agent there is an increase (dependant on the structure of the curing agent) in the interlayer spacing of the organoclay.

Berglund et al[118], have shown that the reactivity and chemical structure of the curing agent can have a direct effect on the extent of exfoliation of the organoclay, and also demonstrate that the choice of curing agent and curing conditions (such as temperature), can be optimised in order to obtain an exfoliated nanocomposite. Intercalated nanocomposites were obtained with curing agents of relatively high reactivity, but when a curing agent of lower reactivity was used the nanocomposite obtained was exfoliated. Hence the lower the reactivity, the higher the degree of exfoliation. From this observation it was concluded that lowering the temperature of curing for the higher reactive curing agents would facilitate exfoliation, but this

is not proved to be correct. In fact raising the curing temperature promotes exfoliation in these systems, and this is thought to aid diffusion of both epoxy monomer and curing agent into the interlayer.

Russell et al[119] investigated the effects of the amount of curing agent and clay used in the manufacture of epoxy clay nanocomposites. It was found that the lower the amount of the curing agent the higher the extent of exfoliation. An excess amount of curing agent resulted dominantly in the extragallery crosslinking of epoxy monomer and curing agent with insufficient diffusion of materials into the intragallery regions. The rapid rate of extragallery crosslinking in comparison to the slower intragallery diffusion limited the exfoliation. Furthermore, they determined that the higher the clay concentration the lower the rate of increase in layer spacing. As the concentration of clay was increased from 1 –20 wt. % the maximum spacing obtained decreased.

The nature of the alkylammonium cation used was investigated by Brown et al[120], with an aim of investigating the reaction rate and viscosity of reaction mixtures – high viscosity and component reactivity inhibit the incorporation of the inorganic clay into the component mixture. To make the organoclay they used hydroxyl - substituted quaternary ammonium surfactants (able to initiate the polymerisation) together with a low boiling point solvent – acetone. The use of the acetone enhanced mixability by lowering the viscosity. The lower viscosity allows intimate homogeneous mixing of components at lower temperatures than that at which reactions between reagents occur. This also enables the production of nanocomposites containing as much as 25% clay (as compared to 5 – 10%). The use of acetone did not alter the curing reaction or the final mechanical properties of the nanocomposite. It should also be noted that the use of acetone may also cause it to act as a polar activator, which may alter the swelling characteristics of the clay, swelling it more before polymerisation can be initiated. No measurement was made however of the basal spacing of the reaction mixtures containing acetone. The hydroxyl – substituted quaternary ammonium surfactants were found to increase miscibility towards the epoxy monomer and increase the intragallery reaction rate, but at the cost of increasing the viscosity of the reaction mixtures. Hence the use of acetone to counteract this.

4.3.4.2 Polystyrene – Clay Nanocomposites.

In situ polymerisation has also been largely used in the manufacture of polystyrene nanocomposites. Akelah and Moet[121] used (vinylbenzyl)trimethyl ammonium chloride (VDAC) exchanged Na and Ca montmorillonite obtaining increased layer spacings of 5.4Å. In contrast to methods deployed with epoxy nanocomposites the organoclay was then dispersed and swollen in various solvents and cosolvent mixtures such as acetonitrile, acetonitrile / toluene and acetonitrile / THF (tetrahydrfuran). These clay were then treated with the styrene monomer and subsequently polymerised with N,N – azobis(isobutyronitrile) (AIBN) at 80 °C for five hours. The composites were isolated by precipitation of the colloidal suspension in methanol, filtered off and dried. The product all cases was an intercalated nanocomposite with spacings varying between 17.2 and 24.5 Å, depending on the solvent used.

Using more conventional organoclays – three tetraalkyammonium cation exchanged clays – Do and Cho[122] compared the ability of the alkylammonium cation to promote the intercalation of styrene through the free radical polymerisation of styrene at 50 °C. They found that a benzyl tetraalkylammonium exchanged clay gave the best intercalated structure ($d_{(001)}$ = 34.0 Å) due to better affinity between styrene and benzyl groups. They also found that this nanocomposite exhibited a higher thermal stability compared with either pure polystyrene or a polystyrene – montmorillonite composite. This technique allows extensive intercalation of polystyrene chains, but no control over the chain length (hence molecular weight) produced or exfoliation.

Such control had been achieved by Weimer et al[123]. Here, a Na montmorillonite was modified by anchoring an ammonium cation bearing a nitroxide moiety known for its ability to mediate the controlled / "living" free radical polymerisation of styrene. Styrene polymerisation was carried out in the absence of solvent at 125 °C for 8 hours yielding an exfoliated product. Desorbing of the polymer from the clay layers also revealed that the molecular weight (M_n) was in perfect agreement with the theoretical molecular weight expected from the initial monomer to nitroxide initiator molar ratio, assuming a living polymerisation. The tailoring of the polystyrene molecular weight can be achieved by varying the amount of fixed initiator. For doing so, variable quantities of an inactive alkylammonium was added together with the

nitroxide bearing ammonium species during the ion exchange. Thus, this strategy allows some control of the molecular weight of the polystyrene while producing an exfoliated structure.

Another approach to an exfoliated structure was developed by Fu et al[124], albeit the final product was a copolymer of styrene. As in the approach of Alkelah and Moet [121] they used a polymerisable cationic surfactant, vinylbenzyldimethyldodeceylammonium chloride (VDDAC). This organoclay was then dispersed in the styrene monomer stirred by vortex and sonicated for 4 hours prior to polymerisation. The product was indeed exfoliated and determined by TGA to be stable to 500 °C. Furthermore they were successful in using both Na and Ca exchanged montmorillonite.

4.3.4.3 Polyolefin – Clay Nanocomposites

Polyolefins present yet another different approach to in situ intercalative nanocomposite preparation. Soluble metallocene catalysts were intercalated into clays by Tudor et al[125] to promote the coordination polymerisation of propylene. Such an approach begins with the clay – a synthetic hectorite – first treated with methylaluminoxane (MAO) in order to remove all the acidic protons and to prepare the clay interlayer to receive the transition metal catalyst. This step produces no increase in interlayer spacing, but an increase in Al content and IR data show complete disappearance of bands assignable to Si – OH vibrations. Addition of the metallocene catalyst via cation exchange results in an increase in interlayer spacing. When treated with propylene this clay polymerises the monomer, but no characterisation of the final product is given.

Bergman et al[126] use a similar method, but in this case the catalyst is intercalated into an organically modified fluorohectorite. Here an increase in interlayer spacing is shown upon going from the organoclay to the organoclay + catalyst. A further increase is observed upon addition of ethylene until the clay is exfoliated following polymerisation.

Polyethylene – clay nanocomposites have also been prepared[127,128] by using a method called the polymerisation – filling technique[129]. This method consists of anchoring a Ziegler – Natta type catalyst or any other coordination catalysts, on the clay surface, and then in situ

polymerising ethylene and or α-olefins directly from the surface. A mixture of exfoliated and intercalated nanocomposites resulted.

4.3.4.4 Polyamide / – Clay Nanocomposites.

As with epoxy – clay nanocomposites there has been considerable work performed with polyamide / Nylon nanocomposites, as they produce particularly useful products – they find commercial applications in the automotive industry as they are tough and light, and also as barrier films, coatings and packaging materials. Hence some of the more relevant approaches are described here.

Some of the first work on nanocomposites, as previously mentioned, was carried out by the group at Toyota Research [109.110,130,131], who studied nylon – 6 based nanocomposites. Their strategy was to use a Na montmorillonite which was cation exchanged with ω-amino acid ($^+H_3N-(CH_2)_{n-1}$ where n = 2,3,4,5,6,8,11,12,18). These produced interlayer spacings of 12.7 – 28.2 Å with increasing chain length. The 12- aminolauric acid was chosen initially because, as well as being the most commercially available, it swelled more when treated with monomer. The organoclay was then swollen with the monomer, ε-caprolactam (M.P. = 70°C), by heating to 100 °C. The maximum layer expansion of a clay with an n<8 ω-amino acid was found to be 26.2 Å when treated with the monomer. However, if n > 8 swelling will be greater than this (Figure 25) and n = 12 it is 31.5 Å, indicating that a longer alkyl chain will intercalate more monomer. Heating to 250 °C allows the ω-amino acid to catalyse the ring opening polymerisation of ε-caprolactam to form Nylon-6, after which the product is cooled, crushed and washed in water at 80 °C and dried. The final product was found to be exfoliated.
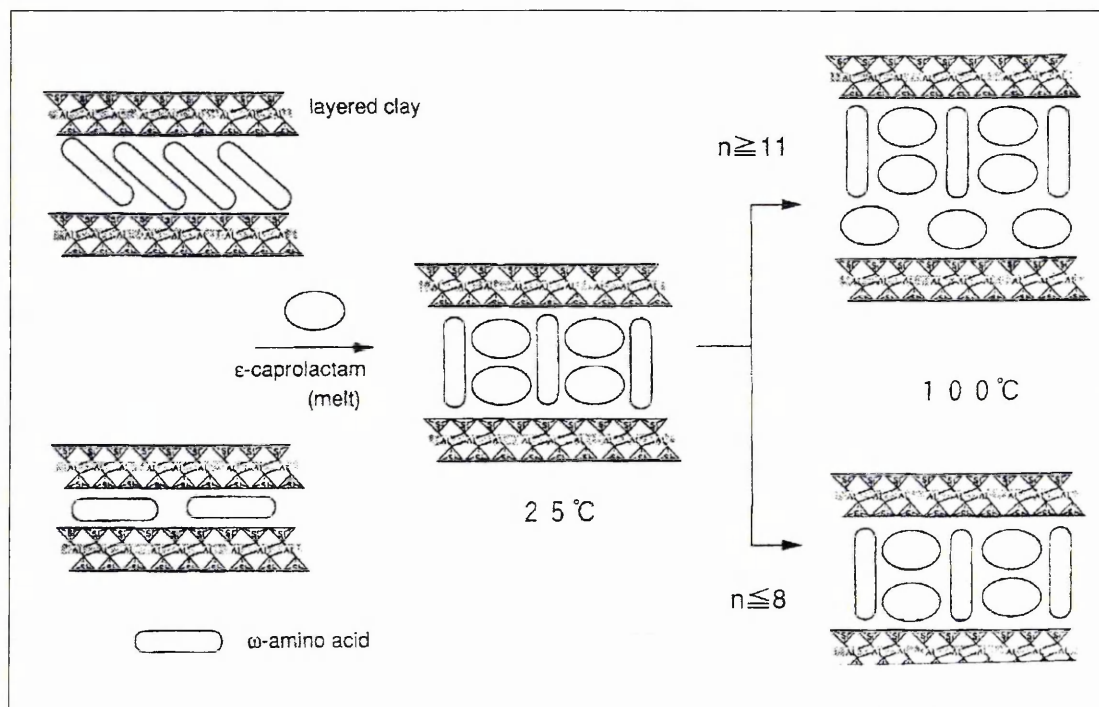
Figure 4.6 – Schematic diagram of the intercalation of ε-caprolactam

Comparison of the titrated amount of COOH and NH_2 end groups present in these nanocomposites with given values such as CEC of the clay (119 meq/100g) led to the conclusion that all of the "$NH_3^=$" end groups present should be interacting with the montmorillonite anions. Additionally the ratio of bonded to non – bonded polymer chains increases with the amount of incorporated montmorillonite (from 32.3% of bonded chains for 1.5% wt % montmorillonite to 92.3% of bonded chains for 59.6 wt % clay).

Further work with ε-caprolactam[132] has been performed without the need for oganophilic montmorillonite. The monomer was able to intercalate into montmorillonite in water in the presence of hydrochloric acid producing a product with a layer spacing of 15.1 Å. This clay can be swollen further at 200 °C with excess ε-caprolactam and polymerisation will proceed at 260 °C when 6-aminocaproic acid is used as an accelerator, to produce an exfoliated nanocomposite.

Nylon-12 nanocomposites may also be formed via in situ intercalative polymerisation as demonstrated by Reichert et al[133]. As in previous examples they used 12-aminolauric acid (ALA) to swell the clay (a fluorinated silicate), but they also used this as the monomer. The

monomer was intercalated in the presence of HCl, and the process was identified as being a cation – exchange of inorganic cations by protonated 12-aminolauric acid at low ALA concentrations (yielding a product of 17.0 Å) and a further diffusion of zwitterionic ALA into the interlayer space when the ALA concentration exceeds the amount of HCl in the medium (yielding an interlayer spacing of 20.0 Å). The ALA monomer was then polymerised at 280 °C and under 20 bar pressure using both types of clay. The product obtained was described as partially exfoliated and otherwise intercalated.

Messersmith and Giannelis[134] again used a protonated aminolauric acid to modify a Na montmorillonite for dispersion in liquid ε-capralactone prior to polymerisation at high temperature. In contrast to what is normally observed at this stage in such a reaction, there was no significant increase in layer spacing (13.6 Å). The authors assumed that the monomer intercalates in between the spaces of the aminolauric acid chains, or the intercalation may only proceed during the heating stage of the preparation. After polymerisation XRD traces showed that the structures obtained were exfoliated.

In addition Messersmith and Giannelis[135] also intercalated ε-capralactone into Cr^{3+} exchanged fluorhectorite at 100 °C. An increase in layer spacing was observed on this occasion (14.6 Å), but the nanocomposite obtained was an intercalated one (13.7 Å) due to the dimensional change accompanying the polymerisation of the cyclic monomer. The cyclic monomer is orientated with its ring structure standing vertically within the interlayer. After polymerisation this ring structure has been opened leaving the resulting polymer chain in a flatter orientation within the interlayer.

Closely related in properties to these nanocomposites are polyimide nanocomposites. These may be prepared in a similar manner for example, by using 12 – aminolauric acid to perform an ion exchange and then intercalating poly(amide acid)[136]. The product was an intercalated structure.

4.3.4.5 Nanocomposite formation without Organoclays

Clay nanocomposites have been used and made for a variety of other uses often employing different methods, some of which are discussed here. The constrained environment of the

clay interlayer in smecties has been used successfully by Wu et al[137] to study the polymerisation of aniline to form the highly conductive polyaniline (PAn). Aniline polymerisation is a complicated process as it is a precipitation polymerisation with a high reaction rate. These features make it difficult to capture and characterise the reaction intermediates and monitor the reaction rate. However, the manufacture of the nanocomposite was achieved without an organoclay as an intermediate. A Na montmorillonite (6.8 wt. %) was treated with aniline and HCl with stirring at 80 °C for 2 hours. After washing for 6 hours at the same temperature the reaction mixture was cooled to room temperature and adjusted to pH 2 before addition of ammonium persulphate to initiate the polymerisation. The resultant product was an intercalated nanocomposite with $d_{(001)} = 14.82$ Å which is consistent with a single extended chain of the polymer[138] and was further characterised by FTIR, bands at 1489.1, 1562.9 and 1311.5 cm^{-1} which are characteristic of an extended chain, and not a coiled structure.

Eastman et al[139] studied the formation of poly(methyl – methacrylate) on transition metal exchanged hectorite (Cu^{2+} and Fe^{3+}). These clays were then treated with the methyl methacrylate monomer via the vapour or the liquid phase and polymerisation induced by γ-ray irradiation or free radical catalysis. Subsequent analysis was by scanning force microscopy (SFM), electron spin resonance (ESR) and XRD, which combine to show that the method by which the monomer is delivered into the clay (liquid or vapour phase), has a marked effect both on the extent of polymerisation and polymer morphology. The polymer is found to form both on the surface and in the interlayer of the clay, and the liquid monomer delivery system works better to produce intercalated nanocomposites.

Polyvinylpyridine – clay nanocomposites have recently been studied by Fournaris et al[140,141]. These polyelectrolytes formed may be in the form of the 1,2 or 1,6 polymer. In this approach the monomer – a 4-vinylpyridinium salt – was added to a 2 wt. % aqueous suspension of the clay at 5 times the CEC, prior to polymerisation, with subsequent washing in water and methanol. The product was an intercalated nanocomposite (13.3 Å), producing only the 1,6 form of the polymer, as confirmed by FTIR measurement. Bands at 1645, 1525, and 1475 cm^{-1}, absent from the monomer are used as markers for polymerisation, and as the amount of

monomer is increased, so the intensity of these bands increases. Conversely a band at 1510 cm^{-1} characteristic of the monomer decreases.

An exfoliated nanocomposite may be prepared by increasing the amount of monomer to 90 wt.%. The important factor in this work is the amount of monomer added to the clay in what is essentially a cation exchange process. The authors have varied the amount of monomer added and found that it must be present to at least 3 times the CEC of the clay. This provides sufficient surface coverage in the interlayer to promote any subsequent polymerisation. At CECs below this value the monomers are in fixed positions (the exchange sites of the clay) and are not close enough to interact and polymerise. When the CEC of monomer is ≥ 4 times that of the clay it may occupy the spaces in between those at fixed positions facilitating further polymerisation.

4.4. Infrared Studies of Carbonyl bands in Montmorillonite and Related Materials.

This section deals with the study of carbonyl bands in montmorillonite, related materials such as silicates and carbonyl metal interactions. Although specifically aldehydes, in particular the dialdehyde glyoxal (Figure 4.7) was used in this thesis, of the reported literature that is relevant to work here has been performed with formaldehyde (Figure 4.7), which is similar in reaction chemistry and IR characteristics to glyoxal.
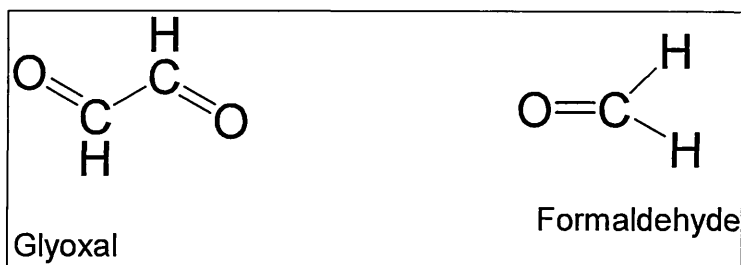

Figure 4.7 Structures of Glyoxal and Formaldehyde.

4.4.1. IR spectrum of Montmorillonite.

The IR spectrum of montmorillonite (Figure 4.8) is notably different to that of kaolin (Figure 4.0), and a basic understanding of this is required before any discussion of montmorillonite intercalates can proceed.
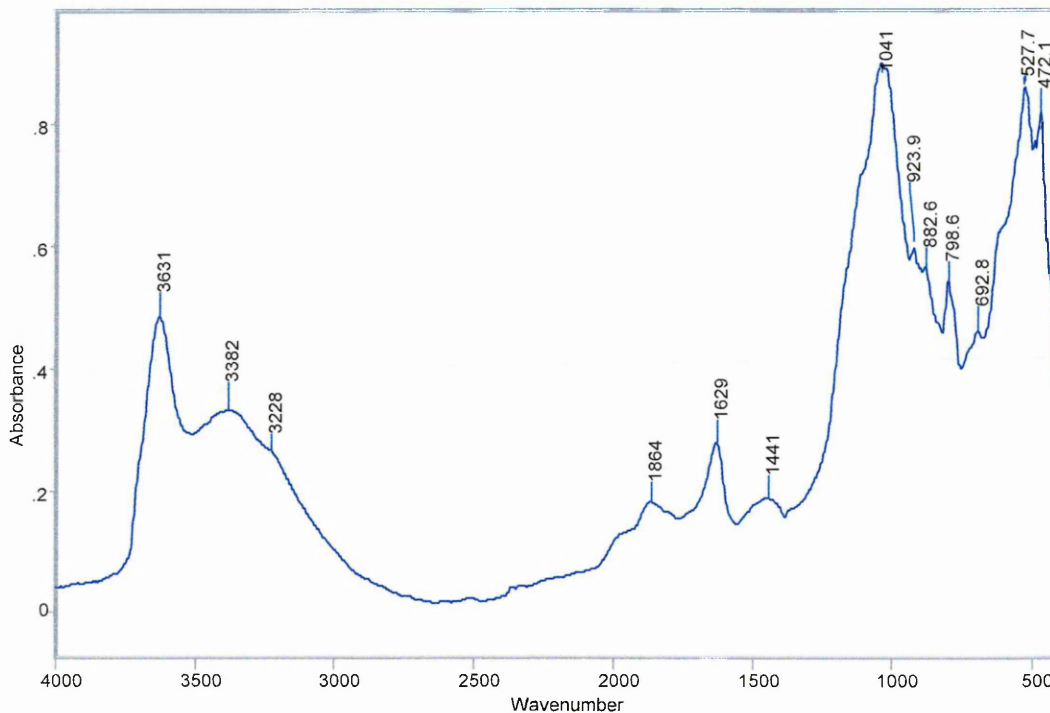

Figure 4.8 – DRIFTS spectrum of montmorillonite (SWy-2)

The most obvious difference between this spectrum and that of kaolin is in the hydroxyl stretching region. Whereas four bands are present in kaolin, which represent the inner and inner surface vibrations of the OH groups within the kaolin structure (Figure 6), in montmorillonite there is only the inner hydroxyl group present within the structure (Figure 8) and this seen by as an intense band at 3630 cm^{-1}. As montmorillonite contains an interlayer cation, water is sorbed into the clay via interaction with the interlayer cation, and this is reflected in the IR spectrum. Bands at 3382 cm^{-1} together with a shoulder at 3288 cm^{-1} are attributed to the OH stretching and 1630 cm^{-1} is the HOH bending of the interlayer water.

Unlike kaolin, where intercalation via hydrogen bonding can be observed through band shifts in the hydroxyl region, in montmorillonite this is not the case. The intercalated species may

exhibit band shifts relating to its own functional groups. It is the increase in interlayer distance observed via XRD which confirms intercalation.

Xu et al[143] studied by water sorption from the vapour phase, cation exchanged montmorillonites via infrared spectroscopy using an environmental infrared balance - EIRM). It was found that at water contents of < 6 molecules of water per exchange cation, the HOH bending mode shifts to a lower frequency and is characterised by an increase in molar absorptivity. In contrast the positions of the symmetric and asymmetric OH stretching modes of interlayer water shift to higher frequencies. This led to the conclusion that H_2O molecules sorbed to the clay surface at low water content are less hydrogen bonded than in bulk H_2O. In addition, the vibrational stretching and bending bands of the structural OH groups of the 2:1 layer structure are also strongly influenced by H_2O content and type of exchangeable cation. Structural OH bending bands of montmorillonite at 883 (decreased intensity) and 840 (increased intensity) cm^{-1} were found to be strongly influenced by H_2O content and type of exchangeable cation. These bands correspond to sites of isomorphic substitution within the 2:1 layer structure – AlFeOH (883 cm^{-1}) and AlMgOH (840 cm^{-1}). Because of the negative charge associated with these sites, exchangeable cations will reside near the ditrigonal cavities in the siloxane sheet. The change in frequency of these bands is assigned to perturbations by the exchangeable cation. Upon lowering the H_2O content, the interlayers collapse and the exchange cations enter the ditrigonal cavities which perturb the structural OH groups at the base of the cavity. The 920 cm^{-1} band (assigned to the AlAlOH group) decreased strongly at low H_2O content. Conversely, this band is assigned to neutral ditrigonal cavities where there is no isomorphous substitution near the cavity. The reduction in intensity may hence result from polarisation effects induced by the exchangeable cation or H_2O located near the ditrigonal cavity.

In general the Si-O stretch of montmorillonite at 1040 cm^{-1} does not change when dry, but Shewring et al[144] have found significant differences in this band and the evolution of two bands near this when evaluating surface hydration processes on bentonite (widely used as a source for montmorillonite). Structural bands of montmorillonite have also been further studied by Frost et al[145] using FT raman spectroscopy.

4.4.2. IR Characterisation of Glyoxal and Formaldehyde

In order to successfully characterise glyoxal or formaldehyde on mineral surfaces it is necessary to examine some of the products formed by these aldehydes when adsorbed onto such surfaces. This is described in the following section.

4.4.4.1. Formaldehyde

Much of the work carried out on formaldehyde characterisation involves the adsorption of formaldehyde on oxide surfaces and catalysts, mainly those used in the synthesis of methanol. These include copper supported on silica and zirconium oxide and other oxides – magnesia, titania alumina and iron oxide. Hence, the similarity with clay surfaces can be seen.

Formaldehyde is sold as formalin which is an aqueous solution containing 40% formaldehyde and 8% methanol, or as the more dangerous paraformaldehyde which is a white evaporated solid form, the vapour of which is extremely harmful. When in water it will form $CH_2(OH)_2$. It readily polymerises on surfaces such as silica to form polyoxymethylene (POM) – $(CH_2O)_n$ – and also a cyclic trimer trioxane[146].

When adsorbed onto surfaces, formaldehyde may form different species each of which has been extensively studied and include formate ions, methyl formate, methoxy ions, POM, and trioxane (Figure 4.9).
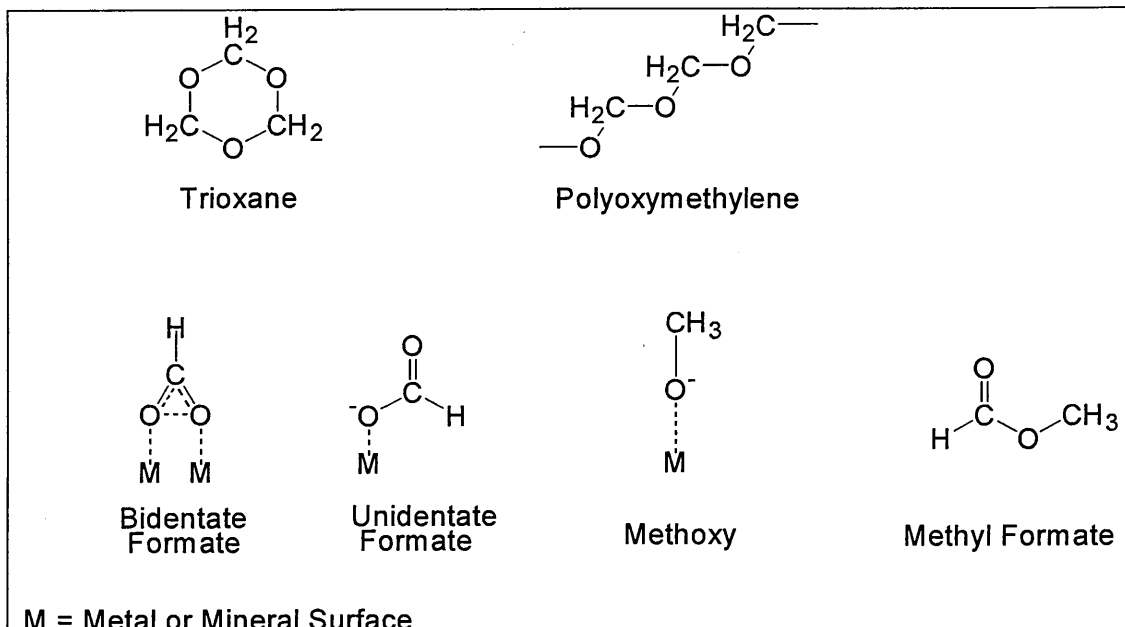
Figure 4.9 – Common forms of formaldehyde on mineral and metal surfaces

Formaldehyde itself has bands (derived from gas phase spectra) as follows[147 - 149], the carbonyl stretch is characteristically intense.

Wavenumber (cm^{-1})	Assignment
1167	CH_2 wag
1249	CH_2 rock
1500	CH_2 scissors
1689	CO stretch
2840	CH_2 symmetric stretch
2907	CH_2 antisymmetric stretch

Table 4.0 – Band Assignments for Formaldehyde Vapour[147-149].

On reduced and surface oxidised Cu/SiO_2 catalysts, formaldehyde has been reported to form both trioxane and polyoxymethylene (POM) [150]. Spectra were obtained via a time dependence study of formaldehyde adsorption on silica at 295K. Initially, the presence of formaldehyde on silica is characterised by the presence of a band at 1502 cm^{-1} (the CH_2 scissors mode). This peak gradually decreases with exposure time (as trioxane and POM are formed), whilst the

growth of bands at 1483, 1426 and 1392 cm^{-1} were observed. These bands are assigned to CH_2 bending vibrations of trioxane and polyoxymethylene [151,152].

An intense band at 1727 cm^{-1} is attributed to the carbonyl stretching vibration of formaldehyde molecules physisorbed on silica, which is a significant shift from the value given above but these carbonyl groups are physisorbed and not in the gaseous phase. The 1727 cm^{-1} band reduced in intensity with time suggesting that formaldehyde is reacting, possibly to form trioxane and other oxymethylene products as previously suggested. Indeed, this observation is further supported by the emergence of two bands at 2983 and 2916 cm^{-1} which are characteristic of trioxane and polyoxymethylene[151,152]. This reaction can be illustrated as follows (Figure 4.10):-
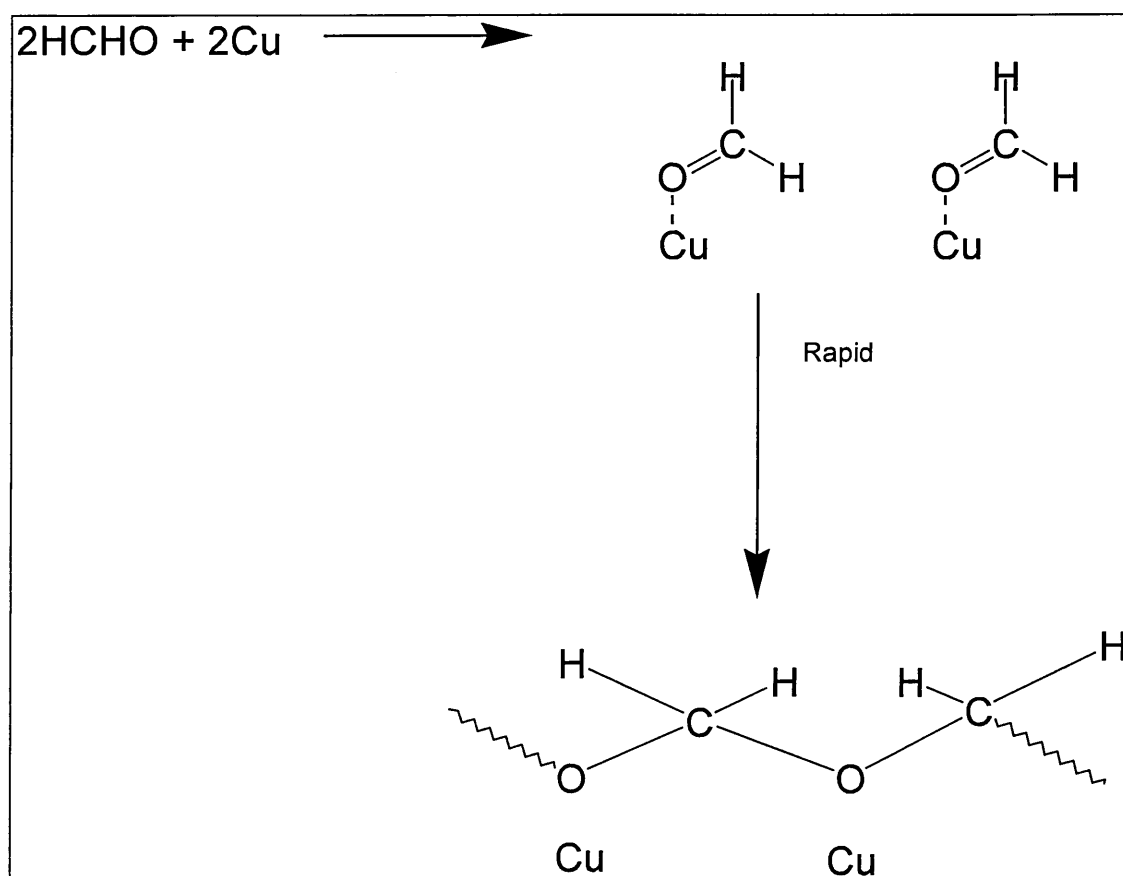

Figure 4.10 - Reaction of Formaldehyde on Silica[151,152].

Similar observations are made on a reduced Cu / SiO_2 catalyst, with the same products being formed but at a much quicker rate. In addition, bands were observed at 1353 and an envelope

of bands centred at 1555 cm^{-1}. These are characteristic of bidentate formate on copper. Evacuation of this sample at 295 K results in the loss of the characteristic formaldehyde bands followed by those for the trioxane and polyoxymethylene species to leave bands previously obscured at 2938 and 2857 cm^{-1} which again are characteristic of bidentate formate on copper which is formed as follows (Figure 4.11):-
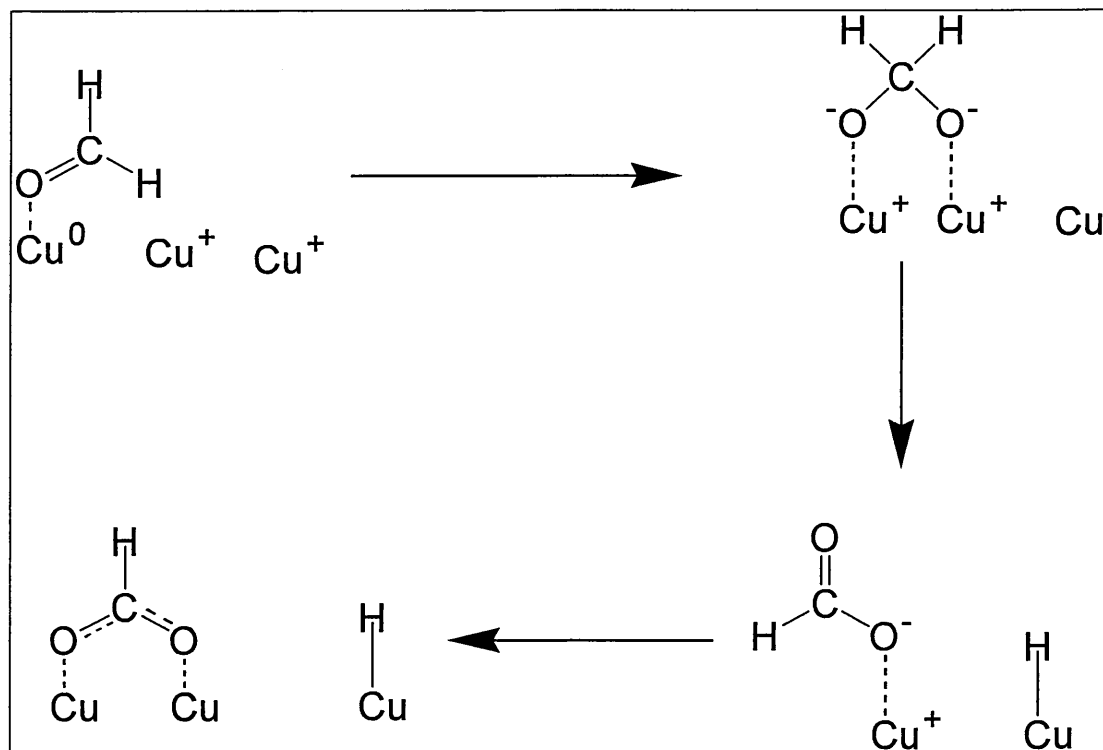

Figure 4.11 – Reaction of bidentate formate on copper

On the reoxidised catalyst, bands attributable to polymerised formaldehyde were seen at 2986, 2919, 1484, 1427 and 1395 cm^{-1}, but these were noticeably weaker in intensity than on the reduced catalyst. In addition a band for molecular water at 1630 cm^{-1} was observed, and also a band at 1573 cm^{-1} which is attributed to unidentate formate. This implies that the formation of bidentate formate is more favoured on the oxidised surface, and the reduced surface is promoting a mixture of the two forms. The production of bidentate formate on the reduced catalyst suggests that adsorbed formaldehyde reacts with the residual oxygen on the catalyst.

Similar observations have made been made by several other authors. Schrader et al[153] investigated the adsorption of formaldehyde on Cu / ZnO and the subsequent formation of a bidentate formate species. At 200 °C and 1 atm bands for formate species (2970, 2875, 2739, 1578, 1379, and 1364 cm^{-1}) and methoxy species (2935 and 2820 cm^{-1}) were observed on the catalyst with no evidence of formaldehyde at this temperature and pressure. At 100 °C and 1 atm chemisorbed formaldehyde (2935, 2860, 2739 and 1609 cm^{-1}) and formate were in evidence. Additionally a band at 1700 cm^{-1} was assigned to physically adsorbed formaldehyde. The authors offerered the following assignment for adsorbed bidentate formate (Table 4.1):-

Wavenumber (cm^{-1})	Assignment
2875 ± 5	Asymmetric CH Stretch
1575 ± 5	Asymmetric OCO stretch
1380 ± 2	CH bend
1365 ± 5	Symmetric OCO bend
2966 ± 4	CH Scissoring overtone
2740 ± 4	Symmetric CH stretch

Table 4.1 – Bands Assignments for adsorbed bidentate formate on Cu/SiO$_2$[153].

Bands for adsorbed formaldehyde are assigned as follows (Table 4.2):-

Wavenumber (cm^{-1})	Assignment
2935 ± 5	CH$_2$ Scissoring overtone
2850 ± 10	Asymmetric CH$_2$ stretch
2740 ± 5	Symmetric CH$_2$ stretch
1610 ± 10	C=O stretch

Table 4.2 – Band Assignments for adsorbed formaldehyde on Cu/SiO$_2$[153].

The assignment for the carbonyl group of formaldehyde represents a significant shift for such a vibration and no comment or explanation is given for this.

Methoxy assignments[153] are given as 2935 ± 2 cm^{-1} - asymmetric CH$_3$ stretching and 2820 cm^{-1} for symmetric CH$_3$ stretching.

Busca et al[154], studied the adsorption of formaldehyde on surfaces including silica, magnesia alumina and iron oxide. On these surfaces the transformation of formaldehyde was observed

spectroscopically to form physisorbed HCHO, polyoxymethylene, formate ions and methoxy groups.

A more detailed assignment of the adsorbed formate is given by these authors (Table 4.3):-

Assignment	Al_2O_3	MgO	Fe_2O_3
Asymmetric CO_2^- stretch + CH bend	2970	2930	2960
CH Stretch	2905	2860, 2810	2880
Symmetric CO_2^- stretch + CH bend	2750	2770, 2735	2730
Asymmetric CO_2^- Stretch	1595	1630, 1605	1565
CH bend	1395	1395, 1383	1378
Symmetric CO_2^- Stretch	1380	1370, 1340	1350

Table 4.3 – Band Positions (cm^{-1}) of Adsorbed Formate Ions on different oxides[154].

In all cases there is a significant shift of the carbonyl band indicating that it is likely that there is some interaction between the lone pairs of electrons on the formaldehyde oxygen and the sample in question, which is to expected. Additionally a band at 1720 cm^{-1} is assigned to formamdehyde interacting with surface hydroxy on alumina. Bands for physisorbed formaldehyde on silica and alumina were observed as follows (Table 4.3):-

Assignment	SiO_2 (180K)	Al_2O_3 (170K)
Asymmetric CH_2 Stretch	2894	2885
Symmetric CH_2 Stretch	2830	2818
CO Stretch	1725, 1717	1718
CH_2 bend	1501	1498, 1485
CH_2 wag		1252

Table 4.3 – Band positions (cm^{-1}) for physisorbed formaldehyde on silica and alumina[154].

Upon heating to room temperature, the spectra of these silica bound species changed dramatically. The sharp CO stretch and CH_2 bend both completely disappear, while in the CH stretching region two intense bands at 2980 and 2915 cm^{-1} are now seen together with a weaker band at 2805 cm^{-1}. Very weak bands are also observed at 1480, 1425 and 1385 cm^{-1}.

Similar changes were also noted in the alumina sample when the concentration of formaldehyde was increased. This evidence suggests that polymerisation has occurred, which the authors attribute to polyoxymethylene (Table 4.4).

Assignment	Hexagonal POM	MgO (230K)	SiO$_2$ (R.T.)	Al$_2$O$_3$ (170K)
CH$_2$ Stretch	2984, 2920	2980, 2918	2980, 2915	2980, 2910
CH$_2$ bend	1471	1485	1480	
CH$_2$ wag	1434, 1384	1430, 1395	1425, 1385	
T CH$_2$	1290	1325, 1290		
CH$_2$ rock	1238, 1098	1235, 1115, 1105		1230, 1210, 1110
CO stretch	936, 897	940, 910		

Table 4.4 – Band positions (cm^{-1}) for POM on MgO, SiO$_2$ and Al$_2$O$_3$[154].

Extensive work on adsorbed formate has also been carried out by Bell *et al.,*[155 – 158] in the study of methanol synthesis and decomposotion over Cu / SiO$_2$ and Cu / ZrO$_2$ / SiO$_2$. In such reactions formate, methyl formate and formaldehyde are often formed as intermediates and these have been characterised spectroscopically. Bands for formaldehyde correlate well with previous studies discussed here and a more comprehensive study of both unidentate and bidentate formate is given on Cu / SiO$_2$, which may be summarised as follows (Table 4.5):-

Species	Mode	Wavenumber (cm^{-1})
Formaldehyde	CO Stretch	1713, 1722
m-HCOO	CH stretch	2902
m-HCOO	COO Stretch	1564
m-HCOO	COO stretch	1366
b-HCOO	COO$^+$ stretch	2935
b-HCOO	CH stretch	2851
b-HCOO	COO stretch	1553
b-HCOO	COO Stretch	1351

M = monodentate formate b= bidentate formate.

Table 4.5 – Band Assignments for unidentate and bidentate formate[155-159].

Bands for methyl formate were in good agreement between both Bell[155-158] and Rochester[150], and both these authors studied methyl formate on Cu/ SiO$_2$ catalysts (Table 4.6).

Assignment	SiO$_2$	Reduced Cu/ SiO$_2$	Oxidised Cu/ SiO$_2$
	3044	3045	3042
CH$_3$-CO	3017	3017	3017
Asymmetric CH stretch	2964	2964	2964
asymmetric CH$_3$ stretch	2952	2952	2949
Symmetric CH stretch	2900	2900	
Symmetric CH$_3$ stretch	2850		2849
C=O stretch (gaseous methyl formate)	1765	1765	1765
C=O stretch	1718	1718	1718
C=O stretch		1664	
CH$_3$ bend	1457	1456	1456
CH$_3$ bend	1428	1438	1438
CH bend	1383	1382	1383

Table 4.6 – Band positions (cm^{-1}) for methyl formate on Cu/SiO$_2$ catalyst[150, 155-158].

It should be noted that the 1718 cm^{-1} band is assigned to methyl formate via carbonyl – SiO$_2$ and is in a similar position to formaldehyde on alumina[154].

4.4.2.2 Glyoxal

Commercially, glyoxal is available as a 40% aqueous solution due to its instability toward rapid polymerisation in pure forms. An anhydrous form of this polymer changes back to the monomer upon heating. It is prepared by the oxidation of actaldehyde by nitric acid or the dehyrdogenation of ethylene glycol and is soluble in anhydrous solvents and exists predominantly as trans planar molecule. The greatest merits of glyoxal are that is an odourless and non – hazardous chemical. While the largest quantity of glyoxal is used in the production of well known products like metrinidazole drug and dihydroxy ethylene urea resins, lesser amounts have found use in a variety of applications, the more important of which are in the fields of cement, paper, leather, rubber, adhesives, photography, food to name but a few[159].

In aqueous solutions however, glyoxal is not stable and may form the following structures including coordination with any metal cations present (Figure 4.12). On drying these hydrated forms revert to their corresponding dry structures.
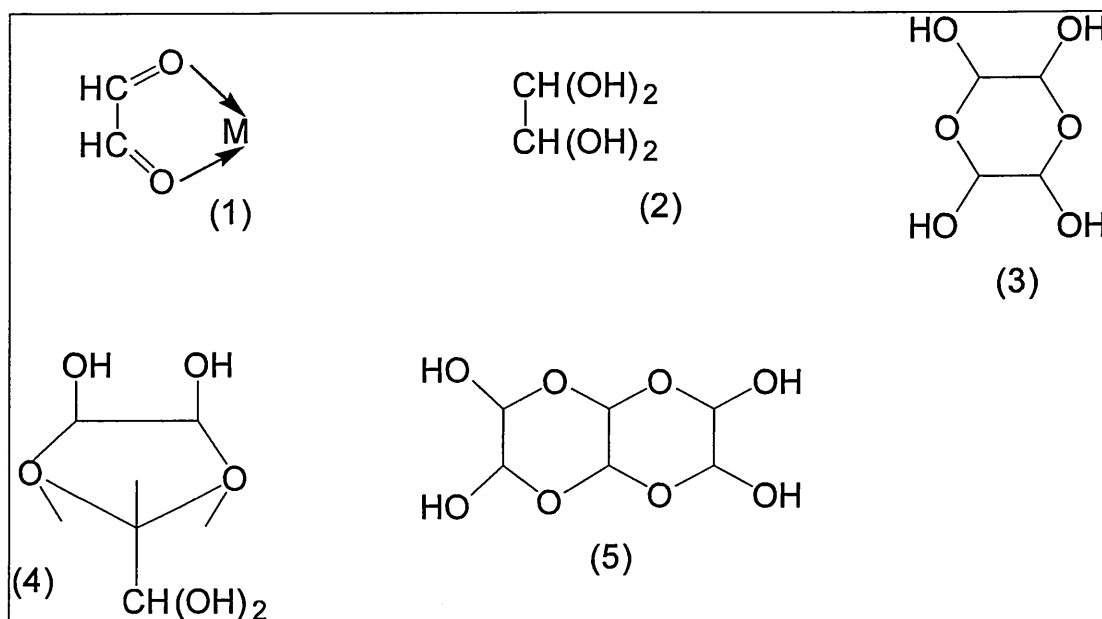

Figure 4.12 – Possible structures of glyoxal in aqueous solution.

Characteristic FTIR spectrum for normal aldehydes consist of a carbonyl stretch in the region of 1725 cm^{-1} and sometimes a pair of weak aldehydes C-H stretching bands at 2850 and 2750 cm^{-1} [160]. Indeed, these bands have been used in FTIR – MS detection as indication of evolved glyoxal[161] (not illustrated). In a 40% aqueous solution of glyoxal all that may be observed are the stretching and bending vibrations of water, which may suggest that glyoxal molecules remain in their hydrated forms. However, one should account for the intensity of these stretching bands which may cause the glyoxal bands, which are relatively weaker (than the water bands), not to be observed.

Due to the instability of glyoxal liquid, which rapidly polymerises at room temperature and below the vibrational spectrum of glyoxal has been studied as a gas, authors taking care to measure the spectrum of the gas cell after evacuation of glyoxal to identify any glyoxal which may have polymerised onto the window of the gas cell. One of the earliest, and unambiguous assignments was made by Harris[162] in 1964 and later by Cole[163]. The fundamental bands for

gaseous glyoxal (trans conformation) are identified here at 2836 cm^{-1} (CH stretch) 1730 cm^{-1} (C=O stretch) 1312 cm^{-1} (CH bend) and 802 cm^{-1} (CH wag). However, more recent studies have identified the carbonyl stretching frequency to be at 1745 cm^{-1} as observed by Pebay Peyroula[164] and Oelichmann[165], both who used more advanced optics. The cis isomer of glyoxal[166] is almost identical having the carbonyl frequency at 1746 cm^{-1}.

In cotton fibres treated with glyoxal[167] a band at approximately 1640 cm^{-1} is observed and found to remain to 125 ° C. This led the authors to conclude that glyoxal in their spectrum displayed "no free aldehyde" and it is implied that glyoxal easily forms five membered rings with metal ions, which may account for this. No assignment for this band, however, was given. Presumably this is a shifted C=O stretch. Further evidence for hydrated forms of glyoxal were examined by Knaul et al.,[168] who used ^{13}C NMR to study the 40% aqueous solutions of glyoxal. They proposed that structure 5 above (Figure 4.12) was the correct form for glyoxal stating that the NMR signal of glyoxal displays many carbons adjacent to two oxygens, and that the existence of these numerous signals can be explained by the formation of many isomers. However, it also has been proposed by others[169] that it exists as mixture of the hydrated monomer, dimer and trimer.

Examination of other dicarbonyl molecules and their interaction with metal ion may enable some identification of the IR bands, particularly the carbonyl stretch (bidentate binding of both carbonyl groups to the metal ion) observed upon such interaction, but such research has not been plentiful. Kraft and Rode[170] studied the chelate complexes of Li, Na, Mg and Ca with diacetyl, acetylacetone and acetonylacetone. They found that there was only a small shift (1 – 5 cm^{-1}) in the carbonyl band in these dicarbonyl ligands when compared to the original spectra of the dicarbonyls. More promising is the work of Para[171] et al in the study of semicarbazone of starch dialdehyde and its complexes with metal ions. The IR spectrum for this ligand displays the carbonyl stretching frequency at 1680 cm^{-1}, which after complexation via both carbonyl groups shifts by 12 – 20 cm^{-1} (a maximum of 1660 cm^{-1}). This is a large ligand and smaller dicarbonyl ligands may such as 2-furaldehyde semicarbazone and 5-methyl –(2-furaldehyde) semicarbazone[172-173] (both which interact with the metal ion through both carbonyl groups) can cause shifts up to 30 cm^{-1} more – as low as 1630 cm^{-1}. It should be

noted, however, that these molecules also interact through other functional groups within the molecules as well as the carbonyl groups.

One of the few specific examples of carbonyl interaction with clay minerals is illustrated by Sohn et al[174], who examined the interaction of alkyl ketones with various cation exchanged montmorillonites. The clay samples were air dried as self – supporting films and exposed to the ketone vapour after evacuation of these films at various temperatures. The main observation of interest was the shift of the carbonyl stretching band in these samples. The carbonyl stretching band is usually observed at approximately 1740 cm^{-1}, yet two bands were consistently observed in the region of 1703 – 1640 cm^{-1} for each different cation exchanged clay used. Both these bands were attributed to carbonyl interaction with the clay and the shift was in good correlation with the polarising power of the interlayer cation. The higher frequency band was thought to be carbonyl interaction with surface hydroxyl, whilst the lower frequency was thought to be carbonyl interaction via interlayer cations. The lower frequency band always appears as broad and intense and shows more variation depending on the cationic species and evacuation temperature. Additionally, they observed a band at 1715 cm^{-1} which was attributed to the carbonyl groups of ketones adsorbed by surface hydroxyl of the clay. No indication of the thermal stability of these samples were given however.

4.4.3. Osmotic Swelling of Montmorillonite

Another example of carbonyl interaction with montmorillonite is that of propylene carbonate (PC) as investigated by Onikata et al[175]. This work and a discussion of osmotic swelling is of particular relevance to the work in this thesis.

The $d_{(001)}$ expands depending on the size, orientation and number of solvent molecules. This is referred to as crystalline swelling. Norrish and Quirk[176] used electrolyte solutions to control the swelling of montmorillonite with water. They found that Na – rich montmorillonite swelled to $d_{(001)}$ values of 19.0 Å in aqueous NaCl solutions with concentrations of > 0.3 M but increased sharply to 40. 0 Å fro montmorillonite in 0.3M NaCl. In more dilute solutions, the spacing increased with decreasing concentration of the electrolyte. At high spacings - ~ 40.0 Å – the interactions between the 2:1 layers of montmorillonite by way of the interlayer cations

97

is much weakened, and a repulsive (osmotic) force between the electrical double layers on the surface of the 2:1 layers is balanced with attractive Van der Waals forces. Since the thickness of the electrical double layers, or the Debye length, increases with decreasing concentration of the elcectrolyte solution, the $d_{(001)}$ increases with decreasing concentration.

Onikata et al[175] investigated the interactions between cation – exchanged montmorillonites and PC to better understand the mechanism of osmotic swelling. Osmotic swelling was confirmed to occur when the $d_{(001)}$ spacing of intercalated montmorillonite in solution exceeds 20.0 Å. The complexes were prepared by mixing the cation – exchanged montmorillonites with different amounts of PC. The mixing ratios were in the range of 15 – 45% by weight for cation – exchanged montmorillonite PC : montmorillonite.

XRD results showed that the $d_{(001)}$ spacing in all complexes increased with increasing amount of PC to 25%. Montmorillonite saturated with monovalent cations such as NH_4^+ and K^+ formed complexes with a $d_{(001)}$ spacings of 14 Å, suggesting the formation of a monolayer. Complexes with monovalent cations of greater polarising power such as Na^+ and Li^+ formed two types of complexes with $d_{(001)}$ spacings of 14 and 19 Å for samples containing small and large amounts of PC respectively. These correspond to a monolayer and bilayer of PC molecules intercalated respectively. Divalent cation complexes followed the same trend described as for monolayer cation – exchanged complexes.

The swelling power of the complexes was investigated by measuring the apparent expanded volume of 2.0g of complex in 100ml of a 0.5M NaCl aqueous solution. The swelling power of the montmorillonite complex with 45 wt % of PC follows the order : Ba > Na > NH_4 > Mg > Li > Ca > K > Ni. It is postulated that the $d_{(001)}$ value of 20.0 Å is probably a critical value where the electrostatic attractive forces between the 2:1 layers exerted by the interlayer cations are sufficiently weak that the crystalline swelling is transformed to osmotic swelling with spacings of > 40.0 Å

FTIR was used to observe the shift in the C=O stretch. In liquid PC this band is observed at 1792 cm^{-1}. Upon intercalation this shifts as anticipated to lower frequency, but the extent of the band shift is dependant on the interlayer cation and the preheating and drying of the complex to 105 °C prior to examination. Addition of water however causes a band shift to

higher frequencies, though the magnitude of this shift is smaller relative to that due to the cation. The magnitude of the shift increased with an increase in the polarising power of the interlayer cation, and also via the heat treatment of the samples. Furthermore, complexes prepared with montmorillonite dehydrated using propanol showed an even larger shift (up to 40 cm^{-1}).

These results correlate well with previous studies of carbonyl compounds intercalated into montmorillonite[177 – 180]. According to these studies, carbonyl compounds coordinate to the interlayer cations via bridging H_2O molecules and the shift to lower frequency of the carbonyl stretching band is $20 - 30 \text{ cm}^{-1}$. However, the band shows a greater shift of $40 - 50 \text{ cm}^{-1}$ if the C=O group coordinates to the interlayer cation directly (as in the propanol dehydrated montmorillonite samples described above). The relatively small shifts of the C=O frequency observed for the PC – montmorillonite complexes with different interlayer cations suggest that the PC molecules are bound to the interlayer cation via water molecules. The water molecules are so strongly bound to the interlayer cations in the complexes that heating to 105 °C does not remove them. A proposed model for this interaction is shown in Figure 4.13, outlining the arrangement of water and PC molecules around the interlayer cation for different degrees of hydration.
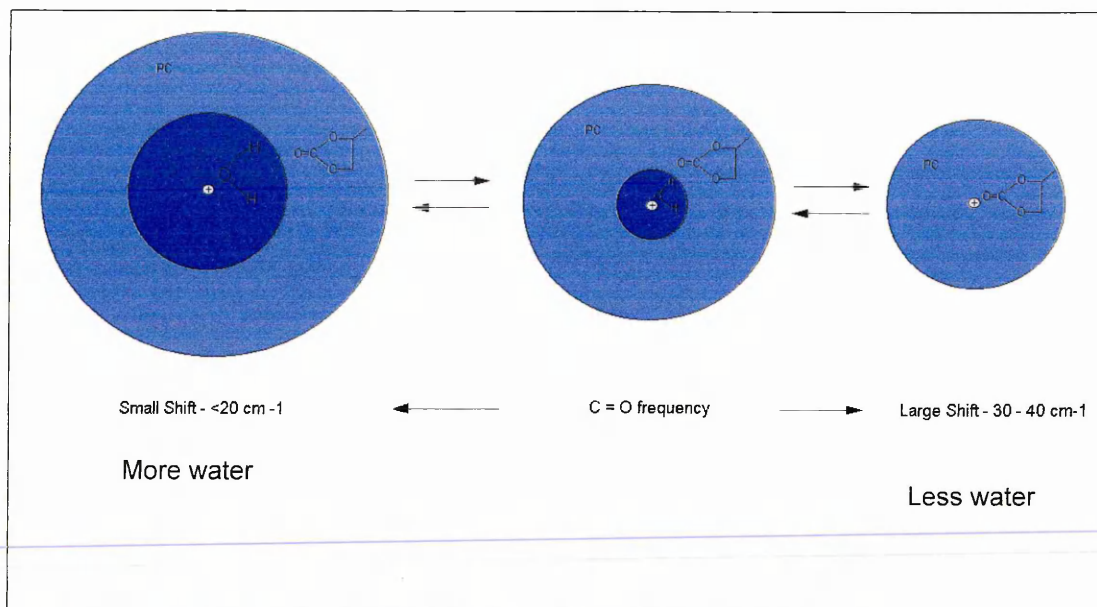

Figure 4.13 – Band shift of C=O stretch with increasing and decreasing amounts of water.

The PC molecules coordinate to the interlayer cations through the cation hydration shell. The shift of the C=O frequency increases as the thickness of the hydration shell decreases upon dehydration.

The bonding forces between the 2:1 layers of montmorillonite are primarily electrostatic through the interlayer cations. The attractive forces are balanced by repulsive forces resulting from the solvation of the interlayer cations. The $d_{(001)}$ spacing expands, depending on the size, number and orientation of solvent molecules. This is known as crystalline swelling. In solutions of NaCl > 0.3M the authors found that the $d_{(001)}$ spacing for a Na exchanged montmorillonite with PC was 20.0 Å. Any subsequent decrease in the concentration of NaCl led to spacings of 45.0 Å. It is postulated that at high spacings of 45.0 Å, the interaction between the 2 : 1 layers by way of the interlayer cations are much weakened, and a repulsive – osmotic – force between the electrical double layers on the surface of the 2 : 1 layers is balanced with attractive van der Waals forces. 20.0 Å is thought to be the critical value where the electrostatic forces are sufficiently weak to allow osmotic swelling to occur. Such an observation has also been made by Olejnik et al[181], who studied the osmotic swelling of montmorillonite in polar organic liquids such as formamide and N – methylformamide. The critical point for osmotic swelling was also determined to be similar at 20.0 Å.

The driving force for the intercalation of solvent molecules into the interlayer of montmorillonite is primarily the solvation of the interlayer cations. The interactions become stronger when cations with larger polarising power are combined with a solvent which has a large electron donor ability, or as defined by Gutman[172] a large donor number (DN). The DN is a measure of the basicity of a solvent and is defined as the negative enthalpy of reaction of a base with the Lewis acid, antimony pentachloride ($SbCl_5$). Donor numbers provide an interesting comparison of the relative donor abilities of various solvents, and this concept was extended by Gutman to include an acceptor number (AN), that measures the electrophilic behaviour of a solvent.

In the PC – montmorillonite system water molecules with a DN of 18.0 strongly coordinate with the interlayer cations, forming a primary hydration shell. The PC molecules are weaker

electron donors (DN = 15.1) and therefore tend to coordinate to the cations through a hydration shell. N – propyl alcohol has a donor number of 18.0 which is comparable to that of water, and thus able to replace the water molecules around the cations. Water molecules are bifunctional and can act as electron donors and acceptors. Therefore, in montmorillonite, the water molecules bound to interlayer cations can act as electron acceptors to water as well as PC. The $d_{(001)}$ spacing of the PC – montmorillonite complex is already large at 19.0 Å and near the critical value for osmotic swelling. In an aqueous solution water molecules will be further coordinated around the cations, thereby forming a larger hydration shell within the PC coordination shell (Figure 4.13).

Further study into this concept was performed by Onikata et al[183], who used as a starting point a montmorillonite – formamide (FA) complex. The post swelling behaviour of this complex was then studied with a variety of polar liquids. The $d_{(001)}$ spacing of this complex was determined to be 37.0 Å. Some of these results are shown below (Table 4.7).

Polar Liquid	Donor Number	$d_{(001)}$ in polar liquid (Å)	
		Na - Montmorillonite	FA – Montmorillonite
Triethylamine	61	14.0	16.7
Pyridine	33.1	20.6	23.9
N,N – Diethylacetamide	32.3	21.6	23.3
Ethanol	32	17.3	18.8
Methanol	30	17.3	18.4
N,N-Dimethylformamide	26.6	20.6	19.2
Ethylene Glycol	20	17.7	17.3
Formamide	24	Osmotic	Osmotic
Tetrahydrofuran	20	15.0	Osmotic
Water	18	Osmotic	Osmotic
Acetone	17	18.8	Osmotic
Propylene Carbonate	15.1	20.1	Osmotic
Sulphalone	14.8	15.2	Osmotic
Acetonitrile	14.1	20.1	Osmotic

Table 4.7 – DNs and $d_{(001)}$ spacings of solvents with Montmorillonite and Formamide – montmorillonite. FA = formamide[183].

With the exception of ethylene glycol, polar liquids with DNs smaller than that of formamide (DN = 24) show osmotic swelling when treated with the FA – montmorillonite complex. Therefore, for any given polar liquid which will intercalate into montmorillonite, subsequent treatment of this new complex with a polar liquid of a smaller DN should result in osmotic swelling.

In this study of formamide intercalated montmorillonite, formamide acts as a bi – functional molecule with an electron donor group –NH_2 at one end, and an electron acceptor group – CHO, at the other. FA has a donor number of 24 which is mid – range in the above table. If the FA – montmorillonite complex is treated using polar liquids with larger donor numbers, the polar liquids can penetrate into the coordination shell of FA to directly coordinate with the interlayer cations and thus FA is expelled from the interlayer (Figure 4.14). In contrast, if the FA – montmorillonite complex swells with polar liquids with a smaller donor number than FA, the FA molecules remain coordinated to the interlayer cations. The bi – functional FA molecule now acts as an acceptor for polar liquids expanding the interlayer to an osmotic swelling range.
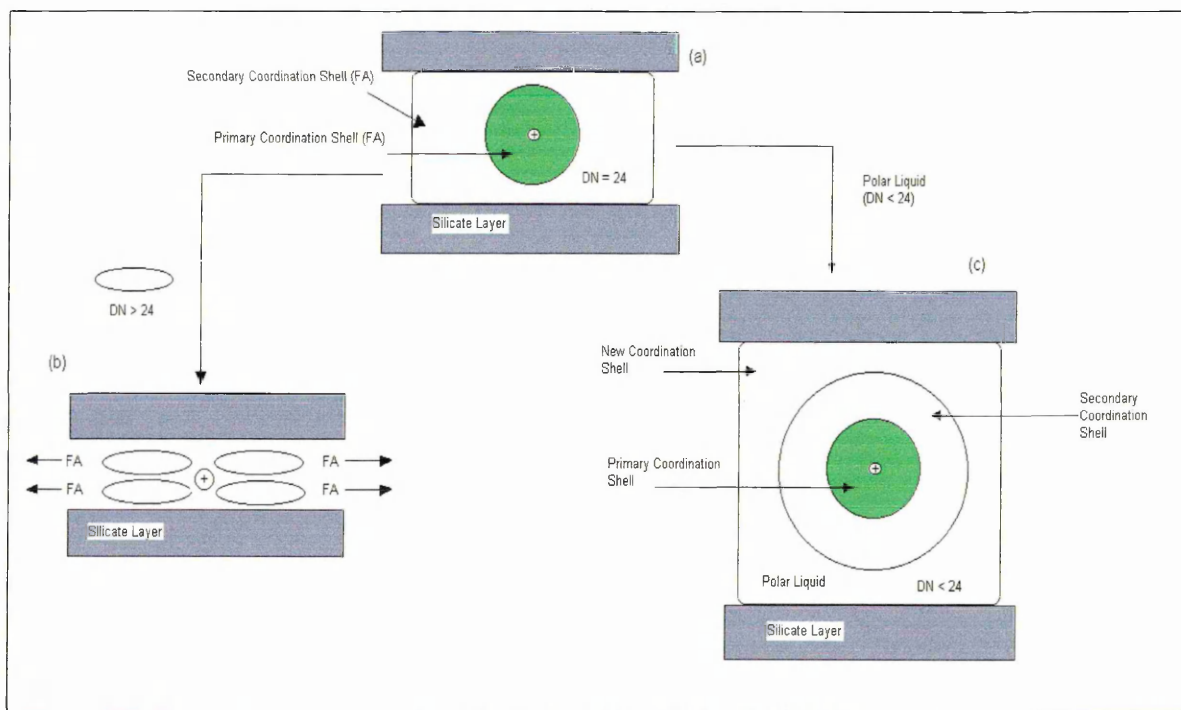
Figure 4.14 – Swelling behaviour of Formamide - montmorilonite complex illustrating the effect of donor numbers of solvents.

4.4.4. Amine and Amide Interactions with Mineral and Clay Surfaces.

Amine and amide interactions are another type of interaction studied in this thesis. The important amine group frequencies used in studies here are those associated with the N-H stretching, N-H bending, and C-N stretching vibrations. In dilute solution of non – polar organic solvents, primary amines show two adsorption bands in the $3300 - 3500$ cm^{-1} region that are attributable to asymmetric and symmetric stretching vibrations of the NH_2 group. The frequency and intensity of both bands depend on the nature and size of the organic compound. Secondary amines show a single band in the region $3300 - 3500$ cm^{-1} that is attributable to the stretching vibration of the NH group. The intensity and frequency of this band are very sensitive to structural changes. The band is located at $3310 - 3350$ cm^{-1} in aliphatic secondary amines, $3440 - 3460$ cm^{-1} in alkaryl amines, and higher frequencies ($3480 - 3500$ cm^{-1}) in heterocyclic compounds. The N-H stretching band of the imino group =N-H is located in the $3300 - 3400$ cm^{-1} region. Tertiary amines do not contain an N-H group and consequently do not absorb in this region.

Primary and secondary amines take part in hydrogen bonding either as proton acceptors (bases) or donors (acids). Tertiary amines may act only as proton acceptors. The basicity of amines results from the presence of lone pair electrons on the nitrogen atoms. Their acidity results from the polarity of the N-H bond, the σ electrons being pushed from hydrogen towards nitrogen. Hydrogen bonding through either proton donation or acceptance is identified by a shift of the N-H frequency to lower values. The stronger the bond, the higher the shift. Both intermolecular and intramolecular hydrogen bond also cause marked effects on the IR spectra of amines. Additional low – frequency bands (often weak) also appear in neat liquid or concentrated solutions. These frequencies are regarded as those of free amine with no hydrogen bonds.

Theoretically there should be at least four NH_2 deformation bands in the spectra of primary amines. In practice only one band has been unequivocally attributed to a scissoring vibration. This deformation vibration is located at $1590 - 1650$ cm^{-1}. Because this band appears in the region of the water deformation band ($1620 - 1650$ cm^{-1}), its use in the interpreation of IR spectra of amino – clay complexes should be carried out with great caution. Secondary

aliphatic amines show an extremely weak band in the range 1510 – 1650 cm^{-1} due to an N-H deformation vibration.

The C-N stretching vibrations generally give rise to bands in the 1000 – 1400 cm^{-1} region. The number of these bands, their intensity and frequency are very sensitive to the type of the amine group – whether it is primary secondary or tertiary – and to whether it is bound to an aliphatic or aromatic group. In the spectra of primary amines, only one band can be attributed to this vibration. In the spectra of secondary amines, two vibrations are sometimes assigned to C-N stretching. In the spectra of tertiary amines, at least two bands are sometimes assigned to C-N stretching. The band is located in the 1000 – 1120 cm^{-1} range in aliphatic primary amines, when the NH_2 group is bound to a CH_2 group e.g., in $R-CH_2-NH_2$, where R is an alkyl group. It is shifted to 1100 - 1200 cm^{-1} when the NH_2 group is bound to a CH group, e.g., in $R_1R_2CH-NH_2$. This band is shifted to higher frequencies (1250 – 1350 cm^{-1}) when the NH_2 group is bound to an aromatic group. Similar effects on the location of the C-N stretching frequency are observed with the secondary and tertiary amines.

Ethylenediamine (EDA) was extensively used by Laura and Cloos[184 – 186], to study its intercalation in montmorillonite exchanged with various cations. In these studies EDA (0.1M) was intercalated into the relevant cation exchanged clay suspensions via shaking overnight. Half of this mixture was air dried to form a self – supporting film whereas the other was washed with water prior to film formation. In some cases the clay was simply exposed to the vapour.

For the washed samples IR analysis revealed three broad bands near 3200, 1617 and 1518 cm^{-1} arising respectively from N-H stretching, asymmetric and symmetric deformation vibrations of the NH_3^+ group. At 200 °C they are replaced by two bands at 3300 and 1429 cm^{-1} indicating the formation of NH_4^+ ions. There is no evidence of NH_2 groups, which would be observed at 3362 cm^{-1} (asymmetric NH stretching) and 1600 cm^{-1} (NH_2 scissoring). Hence, this would suggest that from aqueous solution EDA is adsorbed in the form of EDAH$^+$ which is protonated to EDAH$_2^{2+}$ on washing.

However, it is equally as important to consider the unwashed system by comparison as EDA may be adsorbed differently here. Up to 80 °C a well resolved doublet at 3362 and 3289 cm^{-1}

is observed due to NH_2 stretching and a broad adsorption from $3600 - 2200$ cm^{-1} is also observed. The presence of residual water is seen as a shoulder at 1636 cm^{-1} on a very strong NH_2 scissoring band at 1595 cm^{-1}. Solid EDA shows a weak band at 1552 cm^{-1} which has been attributed to a combination band of CH_2 rocking, and is reported here. In addition, a band at 1340 cm^{-1} is assigned to NH_2 wagging or twisting. Conversely, therefore, it can be concluded that EDA in the unwashed sample is mainly present in the unprotonated form. As this sample is heated to 120 °C the broad adsorption near 2500 cm^{-1} almost disappears and the prominent band at 1595 cm^{-1} is greatly reduced and any indication of water present is now lost. If an outgassed clay film is exposed to EDA vapour, however, the NH_2 scissoring band is observed at 1606 cm^{-1} with a distinct shoulder at 1595 cm^{-1}. If this film is exposed to air or water vapour the NH_2 scissor vibration shifts to 1592 cm^{-1} with a well pronounced shoulder at 1640 cm^{-1}. The position of this band is important when coordination of EDA in this system is considered (Figure 4.15)
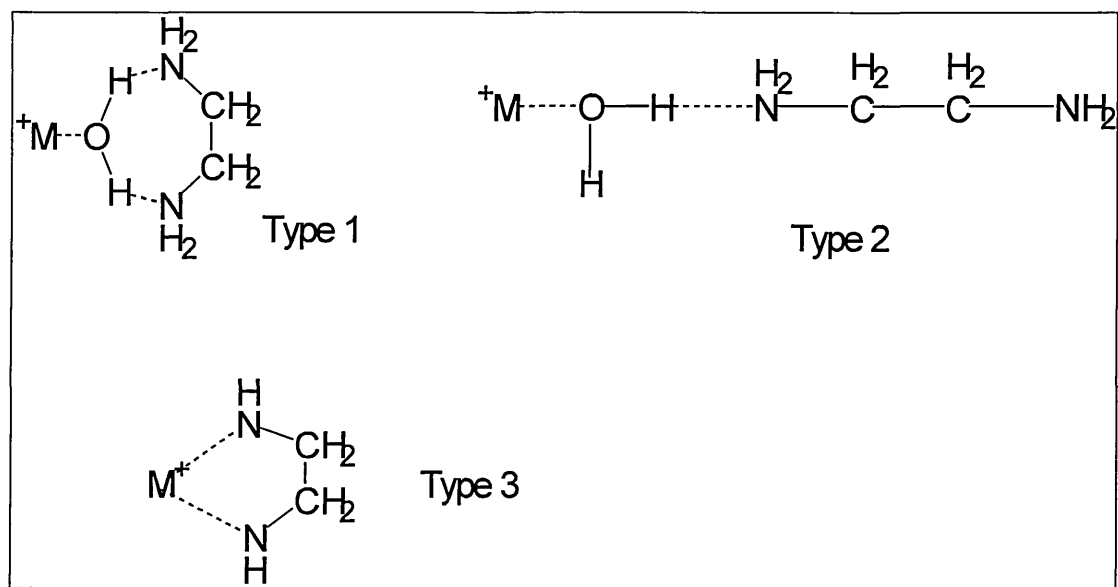
Figure 4.15 – Possible coordination of EDA to interlayer cations.

The fact that two scissoring bands are observed depending on the experimental conditions in which the spectra are recorded is an indication for the presence of two kinds of NH_2 groups, one belonging to EDA loosely bound (1606 cm^{-1}) and the other to EDA more tightly bound (1592 cm^{-1}). The lower frequency associated with the presence of strongly retained water is

attributed to NH_2 linked to the exchangeable cation by hydrogen bonding through a coordinated water molecule. The broad NH_2 scissoring band and the prominent absorption presenting a diffuse maximum near 2500 cm^{-1} suggest that besides freely vibrating NH_2 (3362 and 3289 cm^{-1}) hydrogen bonded N-H groups are also present. Such bonding with water or neighbouring amine molecules is likely to occur if type 2 (Figure 4.15) occurs.

Additionally, it should be noted that if the exchange cations with valency higher than one (e.g. Al^{3+}, Ca^{2+} and Mg^{2+}) occupy the exchange sites, then EDA is present in the protonated form These cations are more polarising than their alkali counterparts (Na^+, Li^+ and K^+), and their hydroxides less basic. Protonation of the amine through dissociation of residual water can therefore be stimulated by the presence of Ca^{2+} and Mg^{2+}.

Morishige et al[187] studied the effect of the methyl substituent on the interaction between the exchangeable cations in alkaline earth metal X zeolites and methyl – substituted amines. Dimethylamine (Me_2NH) adsorbed on dehydrated NaX exhibited IR bands at 3280 cm^{-1} (N-H stretching), bands at 3000 – 2800 cm^{-1} due to the CH stretching of the CH_3 group and bands at 1480 – 1460 cm^{-1}. NH_3 adsorbed onto these zeolites gives two bands near 1640 and 1560 cm^{-1} which are attributed to the NH_3 asymmetric bending mode. SrX gives the NH stretch at 3500 cm^{-1}. Overall, there is a general tendency for the NH stretching frequency for a given N-H bond to increase with increasing negative charge on the nitrogen atom.

Cyclic amines such as cyclohexylamine also provides valuable data in a study of amine IR bands and the behaviour in clay minerals[188,189]. When intercalated into montmorillonite these produce bands dependant on the interlayer cation, but generally in the region of 3300 – 3200 cm^{-1} for NH_2 and NH_3^+ stretching 1610 – 1520 cm^{-1} for NH_3^+ bending and around 1590 cm^{-1} for NH_2 bending. CH_2 stretches are generally seen at 1450 cm^{-1} and a band at 1510 cm^{-1} is considered as diagnostic for a hydrated ammonium ion.

Of particular interest to work carried out in this study is the position of imine bands or more precisely it is the C=N stretch of the imine that is observed. When synthesised as a pure form this band has been reported[190] at frequencies in the range of 1668 – 1630 cm^{-1}, but more importantly imines have been reported to form from cyclohexylamine and isopropylamine on oxides such as SiO_2, Al_2O_3, Fe_2O_3, MgO and CaO[191]. The imine forms on these oxides

surfaces via dehydrogenation and is characterised by a band at 1656 cm^{-1} on CaO, 1652 cm^{-1} on MgO and 1654 cm^{-1} on Al_2O_3.

The interactions of amides with clay minerals has been investigated in a large number of publications, but perhaps the most relevant here is the interaction of N-methylformamide[192] (NMF), and dimethylformamide[193] (DMF) with Ca, Mg and Na exchanged montmorillonites. Both NMF and DMF give large $d_{(001)}$ spacings when intercalated into montmorillonite – for Ca and Mg montmorillonite and NMF these values are 18.4 and 18.2 Å, respectively, whereas the corresponding intercalates with DMF produce a value of 19.3 Å for both Ca and Mg and 19.8 Å for the Na exchanged clay. NMF is also present in two layers when the complex is fully loaded.

For the NMF intercalates, the derivative thermograms (DTG) from TGA measurements exhibit three maxima at temperatures which depend upon the exchange cation (e.g. for Mg these occur at 120, 180 and 400 °C whereas in Na these are at 100, 120 and 230 °C). These maxima also coincide with decreases in interlayer spacing determined by VT – XRD studies.

VT – DRIFTS data for both the NMF and DMF intercalates was also used to show that both of these amides were directly coordinated to the exchange cation via the carbonyl group. However the position of the carbonyl band in the Na exchanged - NMF complex was at higher frequency (1678 cm^{-1} than in the respective spectra in the Mg and Ca exchanged complexes (both at 1664 cm^{-1}), indicating that the NMF molecules were interacting less strongly with the Na$^+$ cation. Another interesting observation in this study is the shift observed in the carbonyl frequency during VT-DRIFTS analysis. Below 50 °C this is observed at 1664 cm^{-1} (Ca^{2+} cation), but at 150 °C has shifted to 1671 cm^{-1} at which temperature the liquid – like NMF had been removed. This indicted that the NMF molecules were interacting less strongly through their carbonyl group and infers that the formation of a hydrogen bond between NMF molecules was stronger than the bond formed between the NMF carbonyl group and a cation. Also given in these studies are the useful band assignments for liquid NMF and DMF (Table 4.8).

NMF		DMF	
Band Position (cm^{-1})	Assignment	Band Position (cm^{-1})	Assignment
3300	NH stretch	3552 / 3334	OH stretch – water
3066	Fermi Resonance Band	2993	Asymmetric CH$_3$ stretch
2944	Asymmetric CH$_3$ stretch	2929	Symmetric CH$_3$ stretch
2879	Symmetric CH stretch	2859	Symmetric CH stretch
2807 (shoulder)	Symmetric CH$_3$ stretch	2809	Symmetric CH$_3$ stretch
2756 (shoulder)	Symmetric CH$_3$ stretch	2779	Symmetric CH$_3$ stretch
1667	Amide I (mostly C=O stretch)	1723 (shoulder)	Amide I (C=O stretch)
1543	Amide II (NH bend + CN stretch)	1675	Amide I (C=O stretch)
1453	Asymmetric CH$_3$ bend	1503	CN stretch
1412	Symmetric CH$_3$ bend	1457 (shoulder)	Asymmetric CH$_3$ bend.
1384	CH bend	1439	Asymmetric CH$_3$ bend
1321 (shoulder)	CH bend	1406	Symmetric CH$_3$ bend
1242	Amide III (CN stretch + NH bend)	1388	Symmetric CH$_3$ bend & NCH bend
1148	CH$_3$ rock	1253	Asymmetric (CH$_3$)$_2$N stretch

Table 4.8 – Band assignments for NMF and DMF[192,193].

In the NMF intercalates, VT-DRIFTS revealed that at low temperatures NMF was removed from NMF clusters similar to those in liquid NMF (with good correlation to TG weight losses and decrease in interlayer spacing seen in VT-XRD) and at high temperatures the NMF molecules are firmly bound to the exchangeable cations (band shifts remain). Of note is the N-H stretching region that was studied. A band at 3420 cm^{-1} was assigned to an NH stretch which was significantly asymmetric on the low wavenumber side of this band. As the temperature was increased (to 250 °C) this asymmetry was reduced and assigned to the removal of NMF molecules involved in interactions of varying strengths via the N-H bond. Furthermore, this NMF removed is described as a species coordinated to external exchangeable cations found at broken edges and surfaces (which account for 20% of the CEC) or to directly coordinated NMF molecules. Unusually a shift to higher wavenumber was observed for the CH stretch to 2923 cm^{-1} a shift of 44 cm^{-1} and this (as is also seen for DMF

intercalates) is attributed to the close proximity and so called "keying in" of the H to hexagonal cavities in the clay structure and interaction with the layers themselves.

In the DMF intercalates the DTG trace maxima were at 420, 330 and 220 °C for the Ca^{2+}, Mg^{2+} and Na^+ cation exchanged clay complexes respectively, which enables distinction between the cation simply by the temperature at which the most strongly held molecules were desorbed. VT-DRIFTS analysis has shown that the DMF was coordinated, via its carbonyl group, to the exchangeable cations and was also likely to be present as DMF clusters and DMF-water clusters within the interlayer space and on external surfaces. This is in good agreement with DTG data, which exhibit maxima at lower temperatures. These maxima are low temperatures (90 and 130 °C) and reflect the desorption of water from different binding sites, and are seen in the VT-DRIFTS as bands in the $3500 - 3100$ cm^{-1} region, which lose intensity as the temperature is raised. Shifts in the IR band assigned to the $v_3(CH_3)$ bond to a higher frequency, also indicate that the DMF molecules are in a more perturbed environment caused by the reduction in interlayer spacing observed via VT-XRD as the complexes were heated.

Of interest also is the number of components attributed to the main carbonyl stretching frequency observed. The first a shoulder at 1720 cm^{-1} and is related to DMF vapour (similar band position) and indicates that there were very weakly coordinated DMF molecules in the clay. A second at 1658 cm^{-1} which was strong and the major component was the carbonyl group present to high temperatures and directly coordinated to the exchange cations. The third component was seen as asymmetry on the high wavenumber side of the 1658 cm^{-1} band and indicated liquid like DMF molecules present in the complex. Present until 250 °C these DMF molecules were described as small clusters on clay surfaces, between stacks or in the interlayer region. The last component was a shoulder on the low wavenumber side of the 1658 cm^{-1} band at 1627 cm^{-1} and is attributed to weakly bound water molecules that were found in clusters between clay stacks, on external surfaces and possibly in the interlayer.

Unusual shifts of the C-H and N-H bands were observed – to a higher frequency – and these were attributed to a unique orientation of these groups which was thought to reflect their

keying into the hexagonal cavities of the tetrahedral sheet of the aluminosilicate layer. This was seen as a consequence of the bulky nature of the CH_3 groups of the molecule.

4.5. N-vinylformamide

4.5.1. Structure and Properties.

N-vinylformamide (VFA) is the simplest member of the enamide group, and has begun attracting interest in its polymerisation due to some of the favourable properties of not only the polymer (polyvinylformamide), but also the monomer itself.

$$
\begin{array}{c}
H \qquad\qquad O \\
\diagdown \qquad\qquad \diagup\diagup \\
N\!\!-\!\!C \\
\diagup \qquad\qquad \diagdown \\
CH_2\!\!=\!\!CH \qquad H
\end{array}
$$
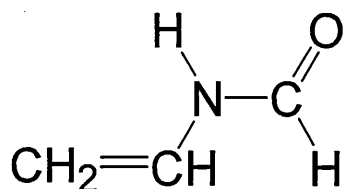
VFA has the following properties:-

Molecular Weight   71.0 g / mol

Boiling Point   210 °C

Density @25 °C   1.014 g / ml

Miscibility   All common solvents (limited with alkanes).

Appearance   Clear liquid

VFA is the key compound in the synthesis of linear cationic polymers with reactive primary amino groups. Such polymers have been the subject of intense research to find economic and ecological routes in manufacture, due to their large number of technical properties they are expected to display[194]:-

- The very high possible charge density of maximum 23 meq / g because of the low molar mass of vinylamine of 43 g/mol more than 50% of which is retained at pH 7.

110

- The high availability of H-atoms in the primary amino groups, which, according to Linhart and Auhorn are available for hydrogen bonding to suitable substrates[195].

- Favourable environmental aspects because the polymer solutions are completely free of residual monomer after hydrolysis to polyvinylamines.

VFA has three different nucleophilic sites: the carbon − carbon double bond (addition and polymerisation reactions), the carbonyl oxygen (O attack) and the amide nitrogen (N attack). Principally, all three nucleophilic sites can interact with an electrophilic component during cationic polymerisation.

Addition of water can be achieved using, for example formic acid and gives N-(α-hydroxyethyl)formamide (Figure 4.16).
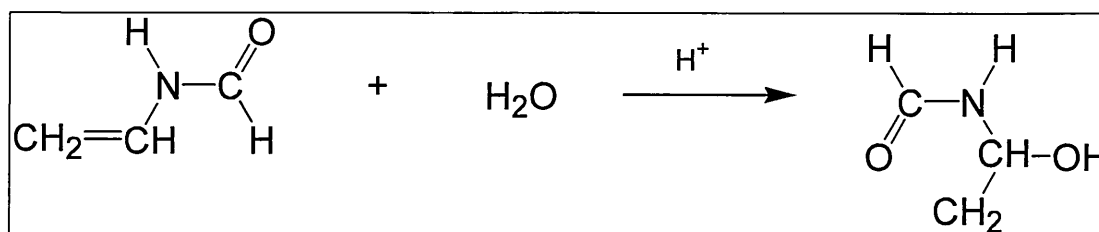
Figure 4.16 – Addition of water to VFA.

Polyvinylformamide and its copolymers find uses in a large number of applications. These include water treatment, papermaking, personal care, dye fixation, ion exchangers, UV − curable coatings and oilfield chemicals.

4.5.2. Polymerisation Reactions

VFA may be polymerised by radical cationic and acid based initiation. Although radical polymerisation is the method used in this thesis, cationic is also possible when interacting with clay mineral surfaces.

VFA radical polymerisation yields homopolymers with molecular weights from $10^4 > 10^6$ [196]. Such radical polymerisation by solution, precipitation, suspension or inverse techniques is facile using most common initiators: redox, thermal or radiation triggered. VFA may serve as a solvent as well as a monomer. The high polarity of VFA of solvent does not disturb the

formation of oligomers or polymers, but the similar DMF however will completely inhibit polymerisation.

Whilst VFA is soluble in water and all common organic solvents except saturated hydrocarbons polyvinylformamide is very soluble in water, but insoluble in most other common solvents except formamide, ethylene glycol and DMSO. Once polymerised the formyl group can be completely or partially cleaved by hydrolysis from the water soluble polymer to from the strongly basic polyvinylamines (Figure 4.17).
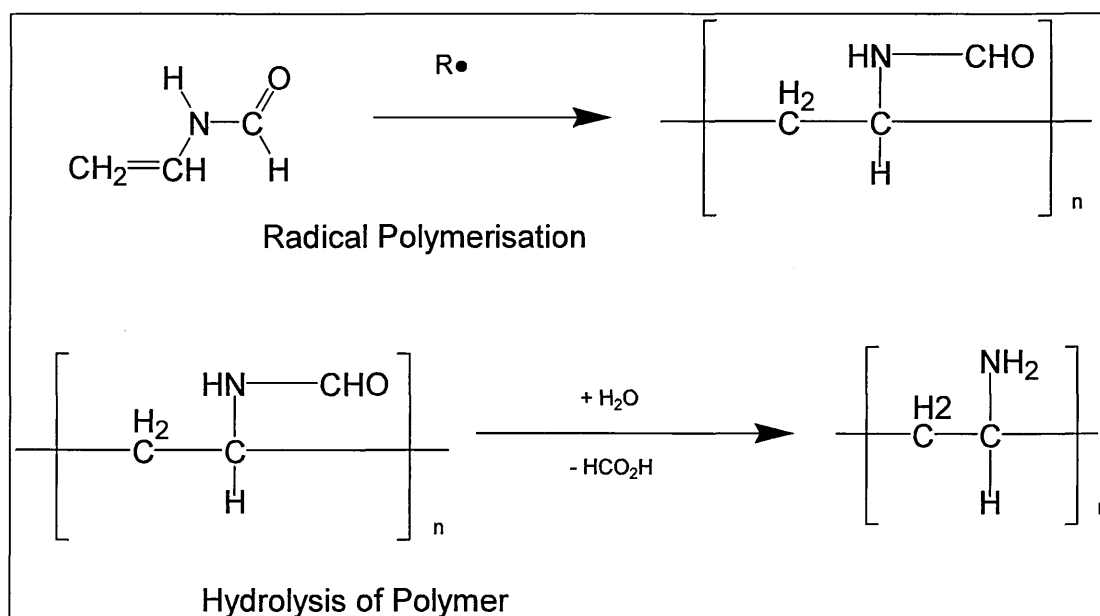
Figure 4.17 – Polymerisation of VFA and Hydrolysis of VFA and its polymer.

The work of Gu et al[197] examined the effects of temperature, monomer and initiator concentrations on the effect of polymerisation kinetics and molecular weight development, using the initiator 2,2'-azoisobutyronitrile (AIBN). The reaction was carried out at 50, 60 and 70°C, and at initiator concentrations of 0.006, 0.012 and 0.030 mol l^{-1}. In terms of conversion to polymer, the initiator concentration showed little difference. The rate of reaction, however, was fastest at 70 °C, with a time of 1.17 min reported with an initiator concentration of 0.03 mol l^{-1}; the higher the initiator concentration, the quicker the reaction. The molecular weight of the final product was found to be highest at 50 °C and with an initiator concentration of 0.006

mol l^{-1}. With these conditions however, the reaction can take as long as 49 minutes. The product is reported as a glassy, colourless, transparent monomer – polymer mixture.

Cationic polymerisation is a way to synthesise low molecular weight polymers and oligomers. Oligovinylamines are of interest to synthesise for use as polyelectrolyte building blocks and for other applications including components in hybrid materials and copolymers. Cationic polymerisation of VFA is difficult to control because a lot of undesired side effects side reactions take place and the yield of oligovinylformamide is low[198]. Branching of the polymer chain is via cationic polymerisation is thought by Pinschimdt[199] to be possible due to the basicity of both heteroatoms, the carbonyl oxygen and the amide nitrogen atom of the VFA monomer[200] (Figure 4.18). Evidence of this is via ^{1}H NMR and GPC of the oligomrs. No direct evidence was reported.
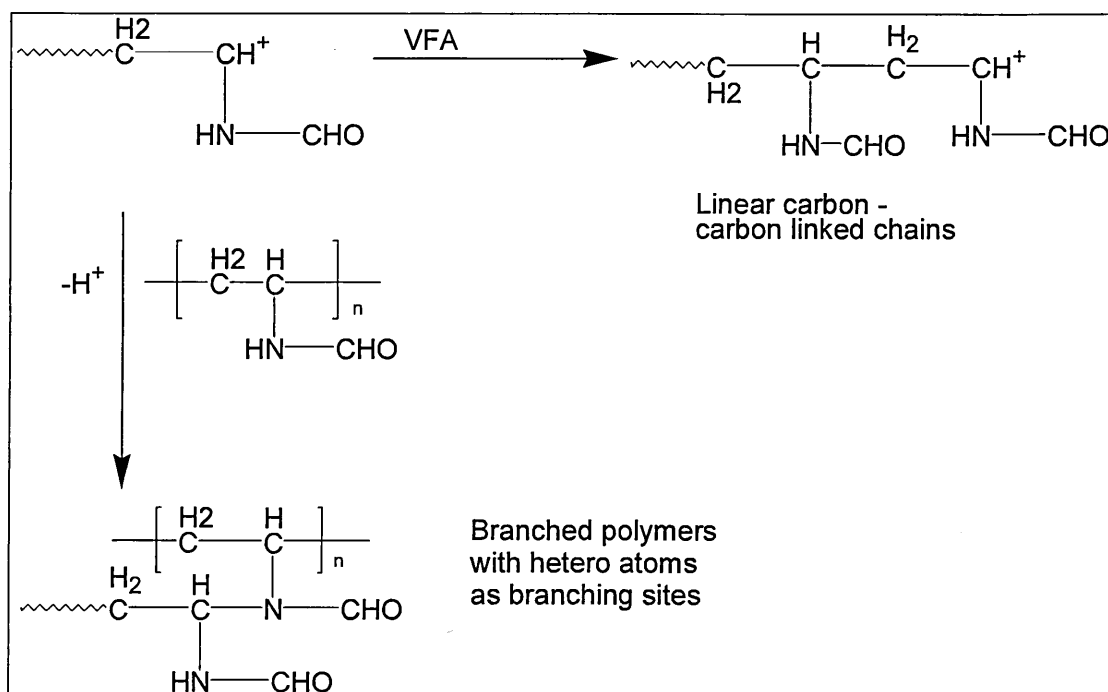
Figure 4.18 – Proposed branching of chain during cationic polymerisation of VFA.

Uyama *et al*[200] have reported the dispersion polymerisation of VFA where the monomer is polymerised in a polar medium using a stabiliser to produce micron sized monodisperse

113

particles of a highly hydrophilic polymer. Particle size can be controlled via the stabiliser concentration.

Some IR data is given for the polymerisation product of VFA[200] as DRFITS with assignments given as 3300 (-NH stretch), 3050 (C=C stretch presumably the authors are implying that there is some monomer left, though this band is often weak and could quite easily be obscured by NH stretching), 2870 (CH stretch) and 1712 cm^{-1} (carbonyl stretch). Bands for oligovinylformamide are reported at[201] 3265, 3046, 2866, 2795, 1665, 1533, 1387, 1252 and 1134 cm^{-1} but no assignments are given.

Recently reported was also a mechanism for the proton catalysed dimerisation of VFA by Spange et al[198], but further propagation to higher oligomers could not be achieved. In this review however, it is suggested that chain branching during cationic polymerisation does not take place. It is suggested that GPC measurements by Pinschmidt et al[196] do not take into account the interactions of poly and oligo vinylformamide with the column and not only separation by size exclusion occurs. This gives the impression of higher molecular weights as would be expected if there is any branching of the polymer chain. In order to find direct proof of branching, Spange et al[198] looked to examine the thermal decomposition of oligovinylformamide. The bisamidate function on the branching point should act as a predetermined breaking – point in the oligomer, and, if examined TG then this should appear in DTG analysis as an additional decomposition product when compared to the DTG of a linear chain. This was found not to be evident, and hence they concluded that no branching took place.

It is suggested that cationic polymerisation proceeds as the en-reaction via a non – ionic cyclic transition state (Figure 4.19), incorporating a chain end with a N-formyline structure and a second VFA molecule with an orbital interaction between the HOMO of VFA and the LUMO of the N-formyline species. During the reaction the amide bonded hydrogen is transferred to the penultimate unit and the N-formyline structure as the active centre is restored (Figure4.19).
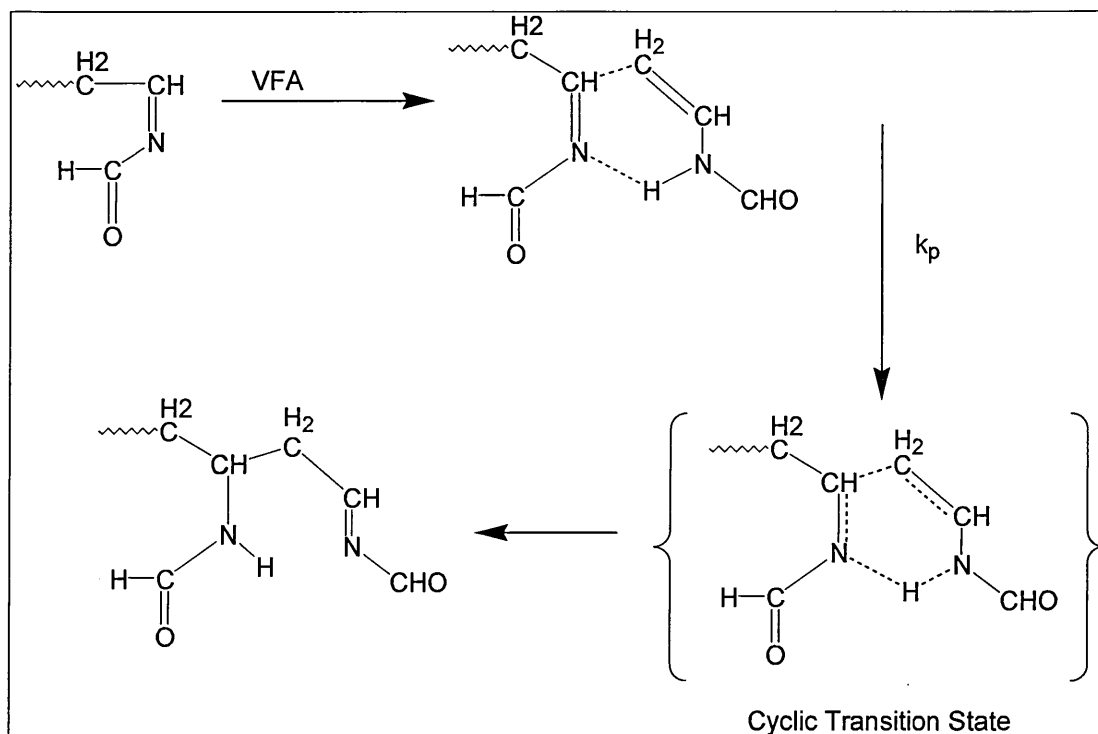
Figure 4.19 – Cationic polymerisation / oligomerisation of VFA via cyclic transition state.

Further to this work Spange[199,201] has also reported that the VFA polymer chains may also end in cyclic end groups when cationic initiation is used (Figure 4.20).
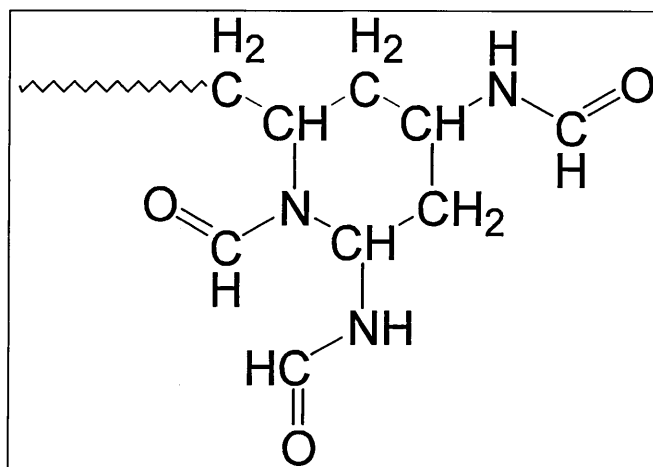
Figure 4.20 – Cyclic chain end group of VFA polymer

Also studied and of interest in this review is the polymerisation of VFA in two phase systems

115

with a second solvent. With n-hexane an improved yield was obtained (no figures given), but with polar donor solvents such as acetonitrile DMF and diethyl ether no oligomers or a very low yield was obtained.

Copolymers of VFA have been the subject of research due to their water soluble and water dispersible properties. The work of Kathmann et al[202,203] has specifically looked at copolymers of VFA with sodium 3-acrylamido-3-methylbutanoate, sodium 2-acrylamido-2-methylpropanesulphonate and sodium acylate to study their microsturcture and solution behaviour. These copolymers were found to have excellent applications in water treatment, remediation, coatings, personal care formulations and frictional drag reduction, but are only characterised to give their molecular weights. Water soluble copolymers of VFA have also been prepared to produce a VFA – vinylamine copolymer. The aim of this study was to investigate this copolymers structure and surface polarity when adsorbed onto silica particles in water – this in effect functionalises the silica surface. It was found that the higher the degree of conversion of the formamide of the polyvinylformamide part of the copolymer into amino groups (as this adsorption takes place in water) the higher the amount of this copolymer can be adsorbed onto silica. Atomic force microscopy (AFM)[203] revealed that the silica surface was completely covered by the copolymer and has a layer thickness of 0.5 and 2 nm depending of the polyvinylamine content of the copolymer. Adsorption of the copolymer on the silica surface also significantly decreases the hydrogen bond donating capacity and therefore the surface polarity decreases with increasing amounts of the polyvinylamine component of the copolymer.

Chapter Five – The Thermal Stability of Mixed Phenylphosphonic Acid / Water Intercalates of Kaolin and Halloysite.

5.0 Introduction

The aim of this study was to complement and extend the work of Wypych and co-workers[86] in their study of a kaolin – phenylphosphonic acid intercalate. By using two different clay minerals in kaolin and halloysite we hoped to determine whether the nature of the clay mineral used has any influence on the ease and extent of intercalation and the thermal stability of the resulting product. Additionally this study contributes to the ongoing debate concerning the role of water in kaolin organic intercalates and the effect of infrared (and Raman) spectra of the hydroxyl stretching and deformation modes.

The work of Wypych has previously been discussed (section 4.2.2) but is examined again here. The reaction occurring between kaolin and halloysite (using a 1:1 (v/v) acetone : water entraining agent) can be represented by the equation:-

$$Al_2Si_2O_5(OH)_4 + 3H_2O_3PPh \rightarrow Al_2Si_2O_5(OH)(HO_3PPh)_3.2H_2O + 3H_2O$$

Note that the product formed implies that it is hydrated. The $d_{(001)}$ spacing of this product was found to be 15.02 Å.

The TGA results show a 5% weight loss by 164°C which was attributed to loss of water of crystallisation and an overall weight loss of 15%. The authors also state that the decomposition of the complex shows that the organic (PPA) part of the structure is only eliminated at temperatures as high as the dehydroxylation temperature of 500°C, suggesting that this complex displays extremely high thermal stability. PPA itself has a melting point of 250 °C.

The FTIR results showed a decrease in the intensity of the OH stretching bands of kaolin, as well as new bands at 3537, 3056, 3015, 1199, 883, 850 669 and 580 cm^{-1} for which no assignment was given. A band at 1642 cm^{-1} was observed to be an O-H bend but a band at 1595 cm^{-1} was incorrectly assigned to a vibration arising from PPA. This could be free spacing filling water trapped within the interlayer. Furthermore the hydroxyl deformation

113

region shows an intensification of the peaks attributed to inner hydroxyl groups in comparison to the outer surface hydroxyl groups (915 and 942 cm^{-1}). A significant background contribution in the OH stretching region was also observed (though not commented on by the authors), which is indicative of a significant degree of hydrogen bonding.

5.1 Experimental

5.1.1 Materials

Kaolin – English China Clays International

Halloysite – Provided by Dr. Stephen Hillier of the Macauley Land Use Reasearch Institute

Phenylphosphonic acid (PPA) (98%) – Aldrich.
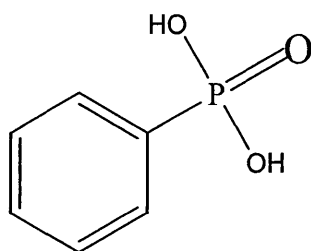
5.2 Instrumental Techniques.

VT-DRIFTS was performed using a Graseby Selector™ DRIFTS accessory and an environmental chamber controlled by an automatic temperature controller (20 – 500 °C) in which all the compartments were continuously purged with dry air. All the samples were prepared by mixing with finely ground dried KBr as a 5% clay mixture. The sample was then transferred to the diffuse reflectance cup positioned in the heating chamber, the surface levelled and a DRIFTS spectrum collected prior to any heating or purging treatment at 25 °C. The sample was then purged with dry air for 15 minutes before collecting a second spectrum. The sample was then raised at 25 °C increments to 500 °C allowing equilibration for 15 minutes at each temperature before each spectrum was recorded.

X- Ray diffraction traces were collected using a Philips PW 1830 diffractometer operating at 35 kV and 45 mA with a copper target (λ = 1.418 Å). A simple heating stage was used to collect diffraction profiles at different (increasing) temperatures up to a maximum of 300 °C (VT-XRD).

114

Thermogravimetric analysis (TGA) was performed using a Mettler TA3000 thermogravimetric analyser. The samples were preconditioned in a nitrogen gas flow for 15 minutes at 35 °C. The sample was then heated to 800 °C at a rate of 20 °C min^{-1}. The traces were recorded as weight loss versus temperature but are presented as the negative of the first derivative (*i.e. –* dw/dt).

Evolved gas analysis was carried out using a synergic chemical analysis system supplied by Thermo Unicam. This system consists of a thermobalance (TG 131, Cahn) fitted with two outlets which are connected to heated transfer lines. One transfer line was connected to an infrared gas cell (10 cm path length) contained in an infrared (FTIR) spectrometer (Infinity Series Mattson). The second transfer line was connected directly to a mass spectrometer (Automass System 2, Unicam). Thus real time TG – MS and TG – FTIR information was available.

X – ray fluorescence samples were prepared by pressing powdered samples into cellulose before analysing the samples on a Philips PW2400 XRF spectrometer using calibration software prepared from standard reference materials.

5.3 Preparation of Intercalates.

1.5g of a kaolin sample was dispersed in 300 cm^3 of a 1:1 (v/v) distilled water : acetone mixture to which was added 2.75g of phenylphosphonic acid. The reaction was carried out at 68 °C in a 500 cm^3 round – bottom flask fitted with a reflux condenser. The kaolin – PPA sample (KPPA) was treated for a period of five weeks and the halloysite – PPA sample (HPPA) for one week. At the end of the reaction time the samples were subjected to five consecutive processes of centrifugation (at 4000 rpm) and washing with acetone. Finally the solid white residue was allowed to dry in air at room temperature for 24 hours. Phosphorous contents of digested samples were determined using ICP – AES by Medac Brunel University, UK.

5.4 Phosphorous Contents

According to the work of Wypych et al[86] the topotactic reaction between kaolin and phenylphosphonic acid is illustrated as :-

$$Al_2Si_2O_5(OH)_4 + 3H_2O_3PPh \rightarrow Al_2Si_2O_5(OH)(HO_3PPh)_3.2H_2O + 3H_2O$$

This equation can be used in conjunction with the determined P contents of the intercalates to provide an insight to the interaction between PPA and the kaolin interlayer.

In such a complex as shown in the above equation the PPA would interact with all of the inner surface hydroxyls of kaolin leaving the only remaining OH group, as the relatively inaccessible inner sheet hydroxyl. From the above equation the phosphorous content can be calculated 13% in the dihydrate. This is based on determining the RMM of the dihydrate (717 g mol^{-1}) and hence using the calculated total of the RMM for phosphorous in the dihydrate. The determined phosphorous content of HPPA was 12.2%, whereas for KPPA it was only 6.5%. Hence there is twice as much PPA in HPPA than KPPA.

5.5 XRD Analysis.

For both kaolin and halloysite (Figures 5.1 and 5.2 respectively) the XRD traces show that both kaolin and halloysite have expanded to 15.4 Å after reaction with phenylphosphonic acid. This is a considerable increase in interlayer spacing as the dehydrated form of both of these minerals displays interlayer spacing of 7.2 Å. This value is in good agreement with that obtained by Wypych (15.02 Å).
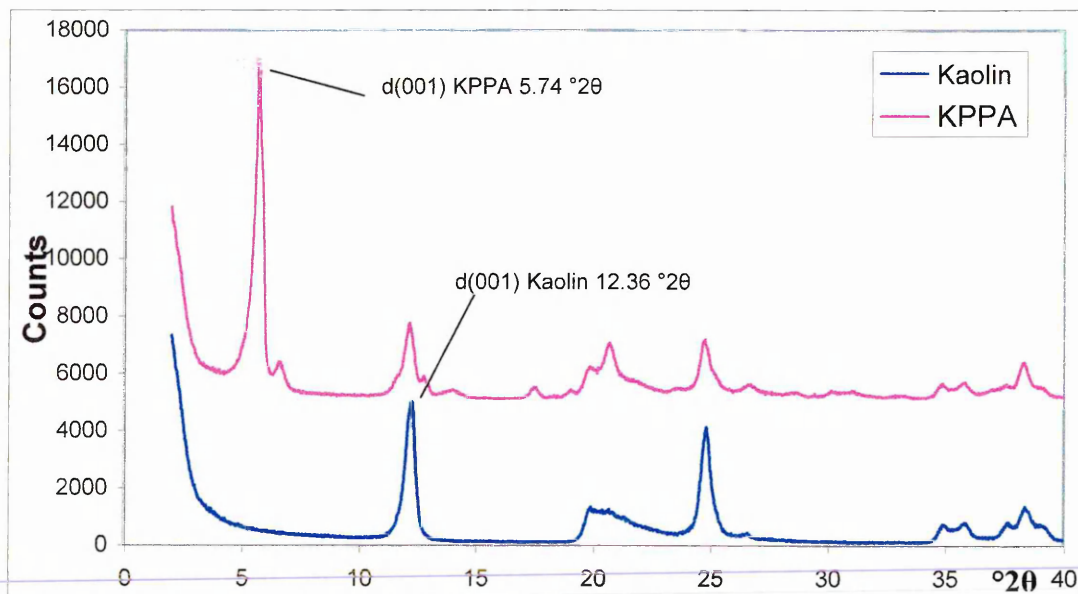
Figure 5.1 - XRD traces of Kaolin and KPPA.

116

The $d_{(001)}$ peak for kaolin is seen at 12.36 °2θ whereas for the KPA complex, this is seen at 5.74 °2θ. In HPPA the $d_{(001)}$ peak is the seen at the same position (5.68 °2θ) but in halloysite the $d_{(001)}$ is seen at 8.86 °2θ, reflecting the interlayer water of this mineral.

The intercalation ratio may be calculated for both of these intercalates which is effectively a measure of the percentage of the layers of the sample which had been expanded – it is the number of expanded versus non – expanded layers. This value is determined by the ratio between the intensity of the first basal reflection of the new phase and the sum of this signal plus the signal of the non – reacted kaolin i.e.

$$d_{(001)} \text{ (KPPA)} \times 100 \div d_{(001)} \text{ (KPPA)} + d_{(001)} \text{ Kaolin}$$

For the HPPA intercalate this value is 100% indicating that the halloysite has been completely expanded, whereas for the KPPA intercalate this is 82%. This is illustrated by the presence of the $d_{(001)}$ of both the expanded intercalate, and the low intensity kaolin 001 peak at 12.3 °2θ (Figure 5.1). The intercalation ratio was not reported by Wypych and co. workers in their study of this intercalate.
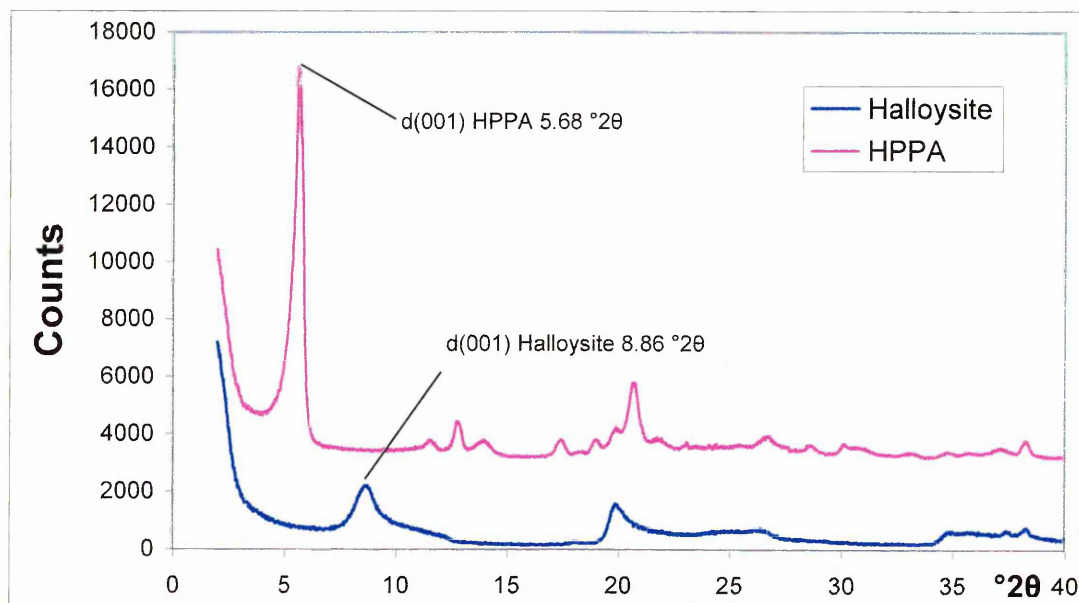
Figure 5.2 - XRD traces of Halloysite and HPPA

Note also that the value of the $d_{(001)}$ spacing for HPPA and KPPA are consistent with other intercalates of PPA as well as Wypych's kaolin intercalate – MG, Al and Zn LDHs[94] all have interlayer spacings of 15.8 Å. Cd/Al LDHs[93] (with NO_3 and CO_3 anions) have interlayer spacings of 14.59 Å. Although smaller than that obtained here with KPPA and HPPA the

117

amount that these LDHs expanded by was 6.35 Å (NO$_3$) and 7.05 Å (CO$_3$), which is approaching that observed here of 7.2 Å. Similarly, γ zirconium phosphate[95] expands from 8.55 Å to 15.3 Å (an increase of 6.75 Å) whilst layered AlH$_3$(PO$_4$)$_2$[96] and bayerite, Al(OH)$_3$[97] both expand to 15.2 Å.

The VT-XRD results (Figure 5.3 and 5.4) shows that the intensity of the 001 intercalate varies little as the temperature is raised. After heating to 500 °C in air for 2 hours the KPPA intercalation ratio was 70% indicating that the phenylphosphonic acid is strongly bound to the kaolin interlayer as demonstrated by Wypych. Semi – quantitative XRF of the pressed powder samples of the KPPA heated to 500 °C for 2 hours confirms that at least 75% of the original phosphorous content was present. As with other results from the recent literature, this displays an improvement in the thermal stability of phenylphosphonic acid which normally decomposes above 250 °C.
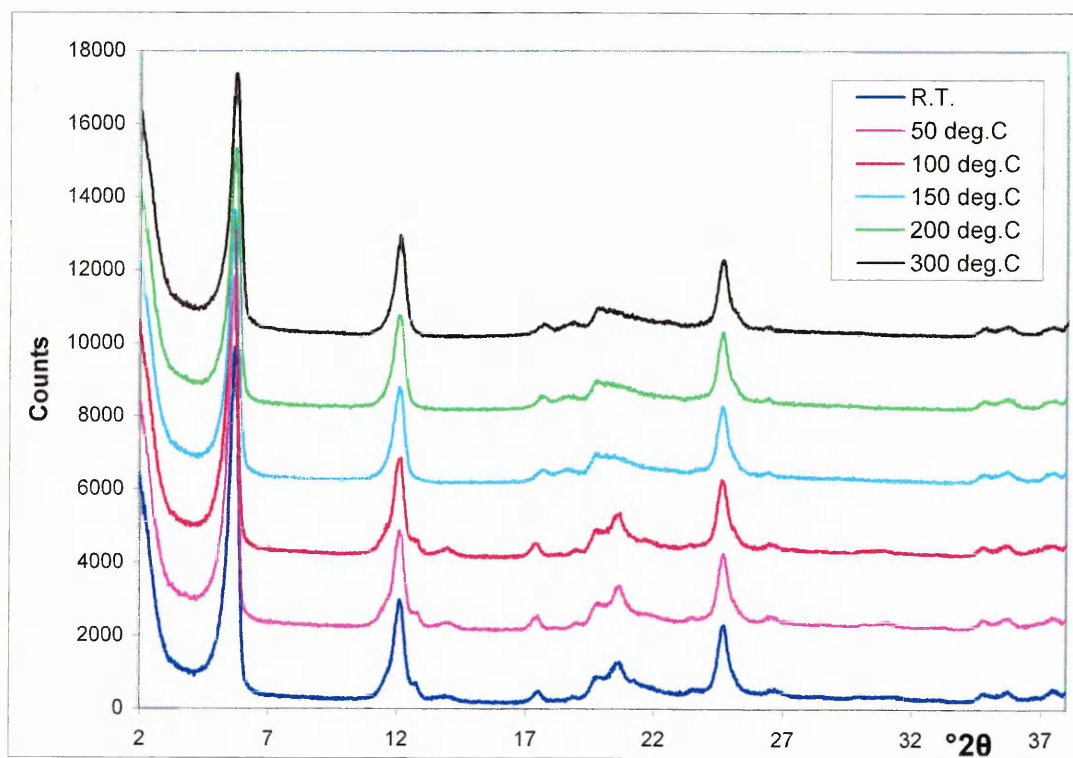
Figure 5.3 - VT-XRD results of KPPA
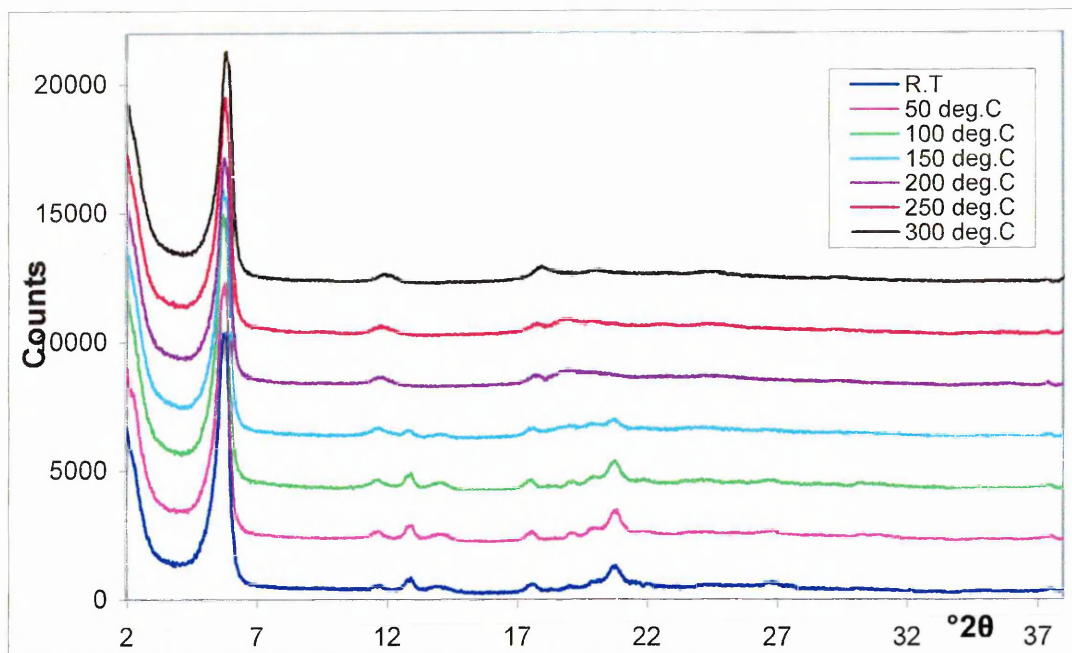
Figure 5.4 - VT-XRD results of HPPA

5.6 Thermogravimetric Analysis

TGA results reflect the thermal stability of the PPA intercalates (Figure 5.5). The derivative thermograms for halloysite and kaolin show that both minerals underwent dehydroxylation in the same temperature regime and reached a maximum, T_{max} near 500 °C (Fig 5.5). Halloysite is distinguished from kaolin by the loss of interlayer water (12 wt%) with T_{max} at 75 °C.

The intercalates of both minerals exhibited two additional features. The KPPA intercalate has a sharp maximum at 140 °C (2.5 wt%), which is also observed in the HPPA at 10 °C higher (5 wt%). These temperatures are similar to those reported by Wypych at 164 °C, who reported this as loss of adsorbed water but provided no experimental evidence[86]. A second discriminating feature occurred, after dehydroxylation at 585 °C in KPPA and at 610 °C in HPPA (Fig 5.5). The intensity of the maximum occurring in the dehydroxylation region was very much less for HPPA than KPPA. Wypych and co-workers observed two endothermic peaks for the decomposition of their KPPA intercalates at 551 and 569 °C [86]. As can be seen by results reported here these values are in good agreement. The temperature at which the PPA decomposes depends on the mineral used, provided that the two events are indeed separate processes of dehydroxylation and PPA decomposition.
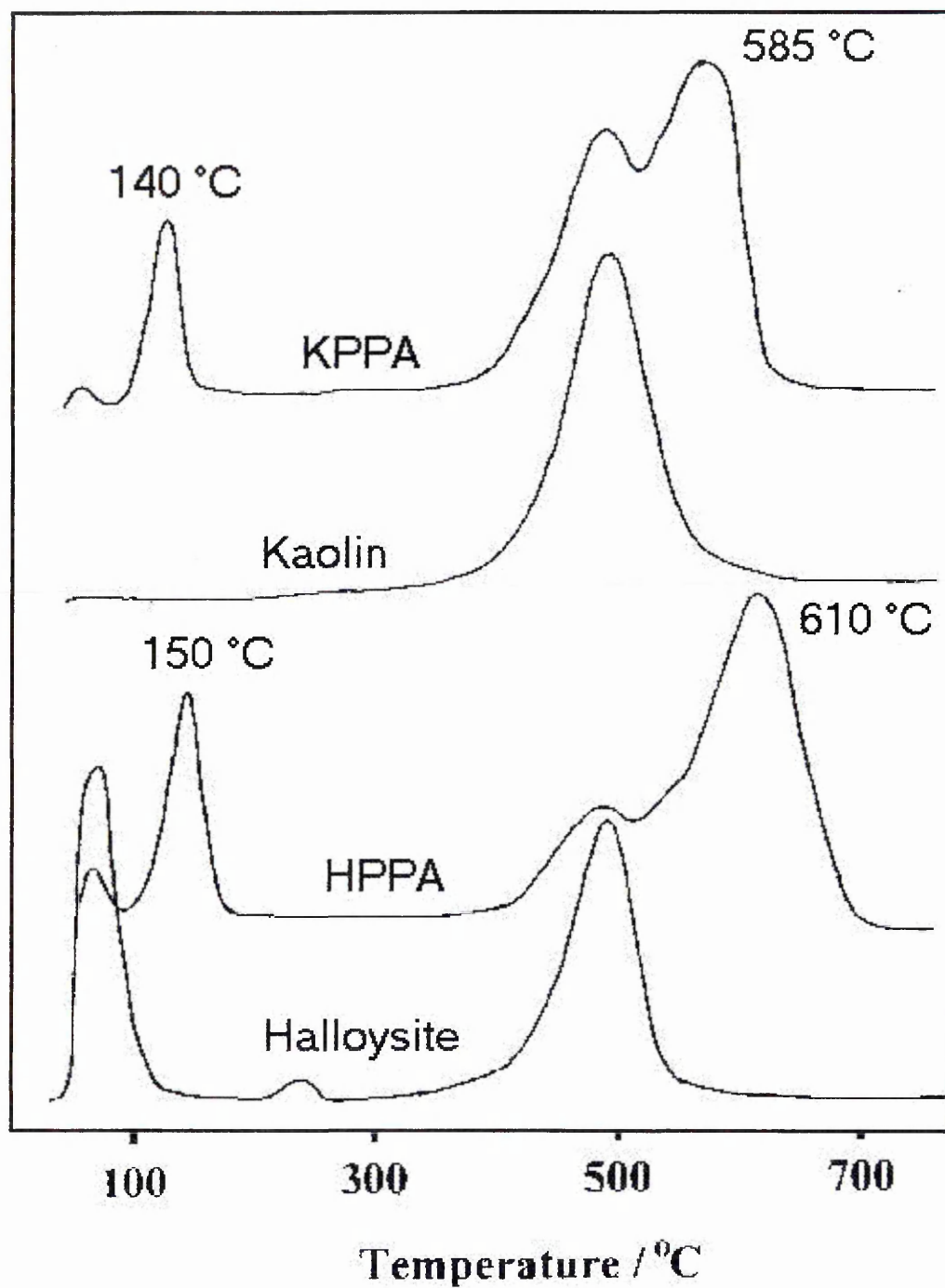
Figure 5.5 – DTGs of Pure Minerals and their Intercalates

Comparing the thermal stability of HPPA and KPPA to other intercalates of PPA, results compare favourably. Mg, Al, and Zn LDHs[94] have been reported as thermally stable up to 500 °C. In layered $AlH_3(PO_4)_2$[96] the stability is again 500 °C. Even higher stability has been reported with bayerite $(Al(OH)_3 - 600$ °C and also with zinc and cobalt phenylphosphonates[96].

120

Recalling that the determined phosphorous contents of the HPPA and KPPA complexes are 12.2 % and 6.5 % respectively. This enables determination of the formulae for the complexes to be:-

$$HPPA - Al_2Si_2O_5(OH)(HO_3PPh)_3.5H_2O$$

$$KPPA - Al_2Si_2O_5(OH)_3(HO_3PPh).3H_2O$$

This is well within the accuracy of determining the water content of the samples from thermogravimetry. Hence the stoichiometry of the HPPA complex suggests that three of the four available hydroxyls can be removed. Examination of the TG data (Figure 5.5) qualitatively supports this observation, as there is a marked reduction in the weight loss attributed to dehydroxylation of HPPA when compared with halloysite alone. Conversely, in the KPPA complex, only one of the four hydroxyls should be removed which appears to be the case given that a substantial weight loss occurs in the dehydroxylation region of kaolin (Figure 5.5). As the weight loss due to dehydroxylation is known to be 3.5%, the 26% weight loss in HPPA above 420 °C can therefore be assigned to 3.5% due to dehydroxylation and 22.5% due to loss of the organic intercalate. For the KPPA the weight loss above 420 °C is 21%. In a similar manner this may be also be assigned to 10.5% due to dehydroxylation and 10.5% due to loss of the organic species. This approach is considered to be qualitatively correct because the weight loss attributed to loss of organic matter is in line with the phosphorous contents of the two intercalates. The difference in these values illustrates the ease in which halloysite is able to accommodate intercalates compared with kaolin. In this particular case more PPA molecules occupy the gallery in halloysite than kaolin.

The expansion of the interlayer spacing by 8 Å is consistent with the phenyl ring of PPA being orientated at a high angle to the kaolin basal surface. In addition, this result is consistent with spacing reported by others [93 - 98]. Observations as to the rate of reaction in reaction media have also be noted. Alberti et al[98] reported that the rate of reaction of the topotactic reaction between γ- zirconium phosphate and PPA was much faster in a water – acetone mixture than in water alone. This was attributed by the authors to the presence of exfoliated layers in the mixed solvent system which permitted PPA easy access to the reaction sites, whereas in water (where no exfoliation occurred) the progress of the topotactic reaction was diffusion

limited. Hence, the expanded halloysite layers provide a logical explanation for differences in the speeds of reaction observed.

5.7 EGA Analysis

Decomposition of KPPA and subsequent analysis of the gases evolved (Figure 5.6.1) provides confirmation that the dehydroxylation process precedes the decomposition of PPA in both intercalates. Elucidation of the loss of water was also provided by the specific ion for water (m/z = 18), which displays maxima at 150 and 500 °C, thus confirming that the desorption event near 150 °C was due to the loss of adsorbed water and that layer dehydroxylation preceded the major decomposition of PPA. Nonetheless, the specific ion chromatogram for benzene (m/z = 78), which was attributed to the loss of the phenyl ring from PPA, began at the same temperature as dehydroxylation but did not reach a maximum until over 100 °C later. Although the HPPA intercalate decomposed in a similar manner the signal from the m/z = 18 ion near 150 °C was more intense (Figure 5.6.2), as anticipated due to the large amount of adsorbed water (Figure 5.5) and significantly weaker in the dehydroxylation region.
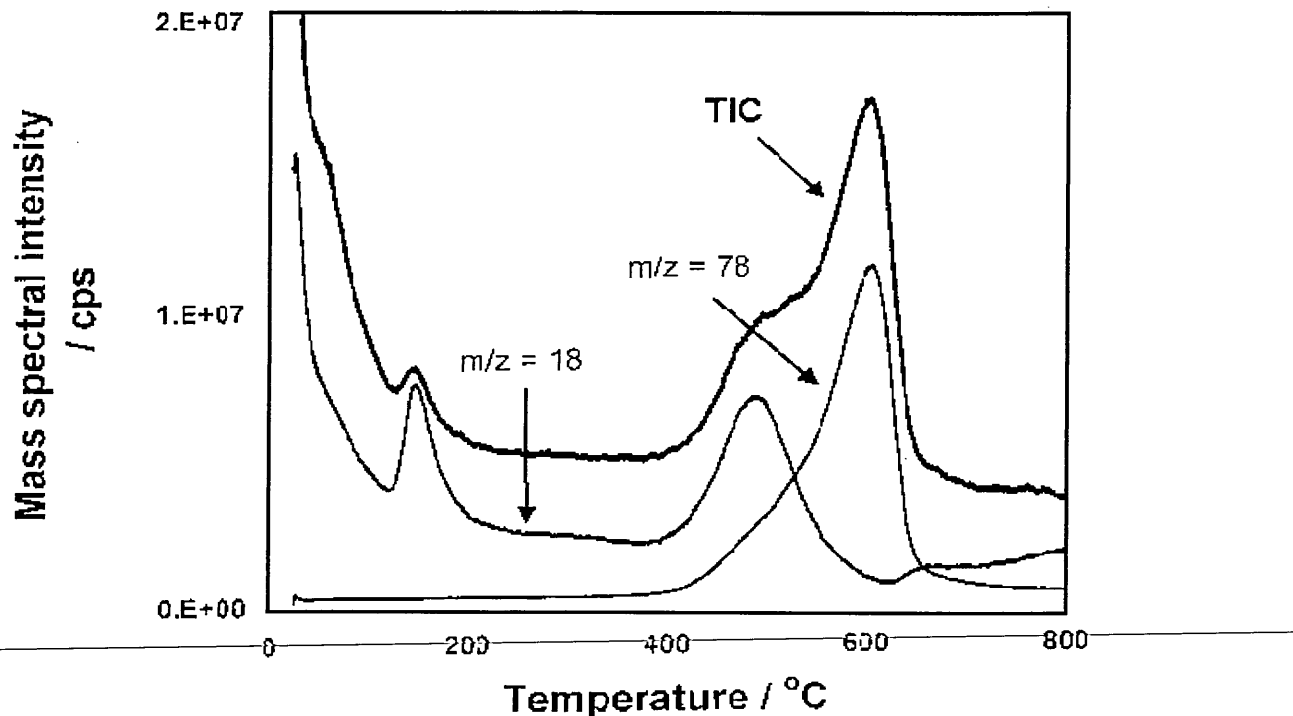
Figure 5.6.1 – TG – MS traces for desorption of water (m/z=18) and benzene (m/z=78) from Kaolin - PPA

122
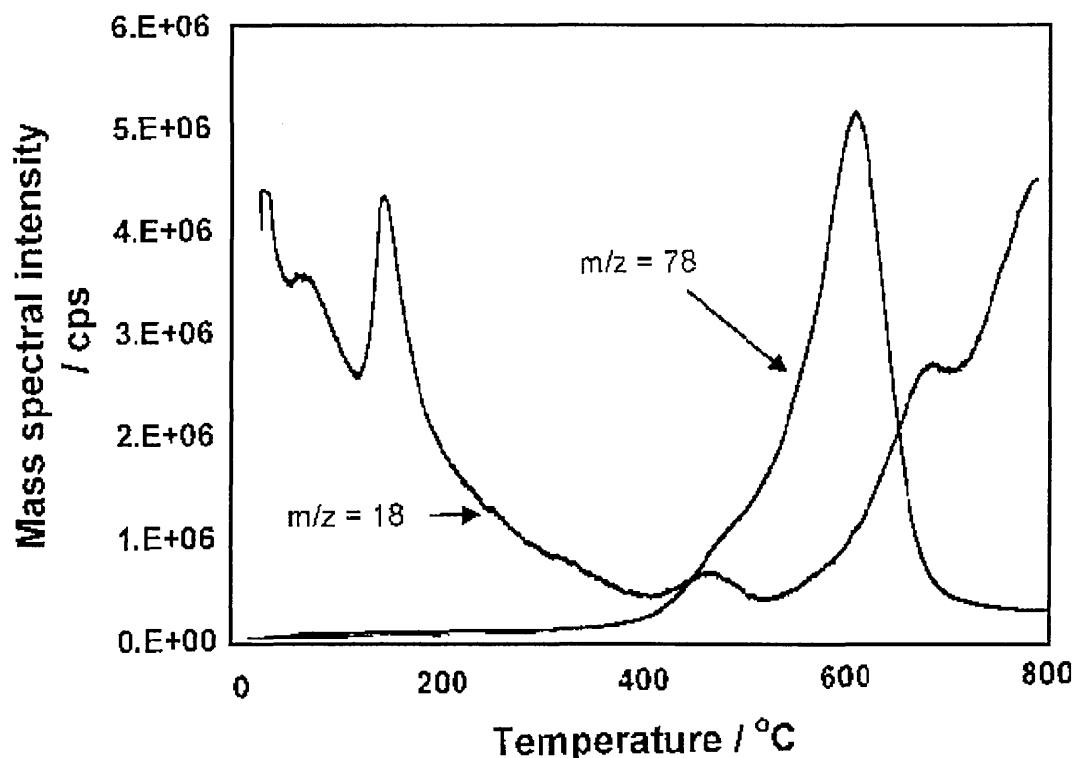
Figure 5.6.2 – TG – MS traces for desorption of water (m/z=18) and benzene (m/z=78) from Halloysite – PPA

5.8 DRIFTS Analysis

The DRIFTS spectrum of HPPA (Figures 5.7 & 5.8) revealed the bands attributable to either the halloysite or the PPA species. The bands at 3698 and 3625 cm^{-1} (Figure 5.6) are assigned to the inner surface and inner sheet hydroxyls respectively. New, broad bands at 3539 and 3332 cm^{-1} are attributed to hydrogen bonded hydroxyls arising from either the interaction of water or PPA with the inner surface hydroxyls on the gibbsite sheet.

These observations are similar to those previously discussed (Chapter 4) with kaolin and halloysite intercalates. Halloysite – urea intercalates[78] display a significant decrease in the intensity of the hydroxyl stretching bands with new bands at 3387,3410, and 3497 cm^{-1} all attributed to hydrogen bonds between urea and halloysite (N-H stretching bands). Frosts work with aqueous hydrazine[85] also results in IR bands observed at 3413, 3469 and 3599 cm^{-1} all of which are assigned as water OH stretching bands. It is interesting to note that Wypych[86] also observed a new band at 3537 cm^{-1} in his Kaolin – PPA intercalate (the band was unassigned).

123
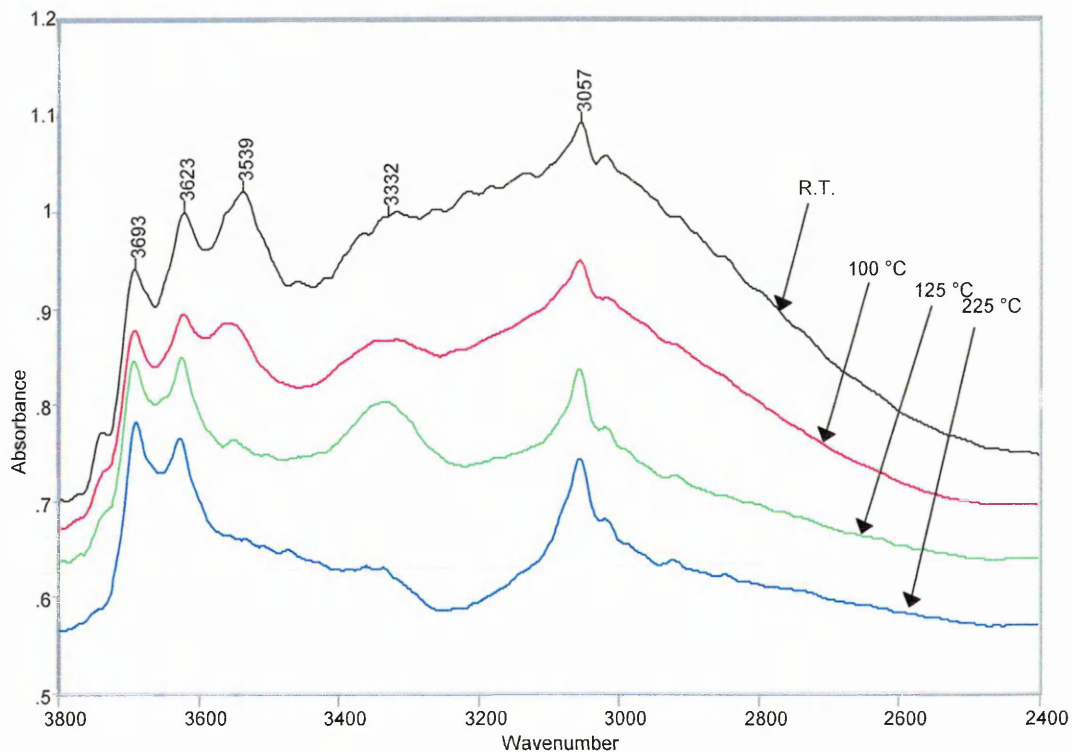
Figure 5.7 – VT-DRIFTS spectra of intercalates 3800 – 2400 cm^{-1}.

Complementing these assignments is the broad contribution from hydrogen bonded OH in the region 2500 – 3700 cm^{-1}, which diminished in intensity as the temperature was raised.

As previously discussed new bands are often observed upon intercalation. Frost *et al*[70] have used DRIFTS to study the interaction of DMSO with the inner surface hydroxyls of kaolin and reported the loss of bands at 3695, 3668 and 3652 cm^{-1} together with the appearance of new bands at 3660, 3538 and 3502 cm^{-1}. These new bands are assigned to hydrogen bonding between the S=O of DMSO and the inner surface hydroxyls (3660 cm^{-1}), water involved in bonding to the inner surface hydroxyls (3538 cm^{-1}) – thus confirming the assignment above – and water hydrogen bonded to the lone pair of electrons on the sulphur atom in DMSO (3502 cm^{-1}). The authors did not report VT-DRIFTS data but associated TG-MS results confirmed that water was occluded in the kaolin – DMSO complex and that it was desorbed at 70 ˚C. Tunney and Detellier[88] reported bands at 3575 and 3394 cm^{-1} when they grafted ethylene glycol on to the inner surface OH groups of kaolin. These two bands were assigned to the stretching of the surface OH groups and the OH group of ethylene glycol respectively. All of

124

these bands are at a higher wavenumber than the thermally stable, prominent 3330 cm^{-1} band in HPPA and to a lesser extent KPPA.

The 3332 cm^{-1} band gradually decreases in intensity as the temperature is raised. TGA data for both these samples shows that weight loss over the temperature range 200 – 400 °C is 3% with TG – MS only identifying the ion m/z = 18, water. Therefore, given that the 3332 cm^{-1} band was more intense in HPPA than in KPPA and that the former contains twice the amount of PPA, the 3320 cm^{-1} band was assigned to water hydrogen bonded to the phosphonic acid moiety of PPA.

It is important to retain a clear distinction between the number of molecules present in the gallery and the intercalation ratio reported earlier in this chapter. This is an observation well illustrated by Frost[77] as discussed in Section 4.2.1. To reinforce this observation, the intensity of the OH stretching modes of the inner surface hydroxyls are a more quantitative measure of the number of interlayer OH groups which are involved in interactions with adsorbed molecules in the gallery. It may take merely one molecule of an intercalate to expand a layer and if this happens in all the layers of a sample the intercalation ratio will be 100%. There will be, however, residual intensity in the IR data indicating that not all the OH are interacting with the intercalate. In both KPPA and HPPA the residual intensity at 3695 cm^{-1} confirms that some inner surface hydroxyls have not been replaced and are not interacting with the PPA. The OH stretching band should increase in intensity as the PPA is lost, but due to the remarkable thermal stability of the PPA within the mineral this exceeded the operating temperature of the VT-DRIFTS accessory.

Phenyl ring vibrations were observed at 3076 and 3056 cm^{-1} (C-H stretch, observed in Wypych's work at 3056 and 3015 cm^{-1}), and 1598 and 1436 cm^{-1} (ring breathing modes) (Figure 5.7). Phenyl ring bands at 749 and 693 cm^{-1} overlapped with the structural bands of kaolin and halloysite.

Further confirmation of the increased thermal stability of the PPA is seen via the P-C stretch which is a sharp band at 1436 cm^{-1} and remains virtually unaltered up to 500 °C as the temperature is raised together with the other phenyl ring modes, which are not significantly affected.
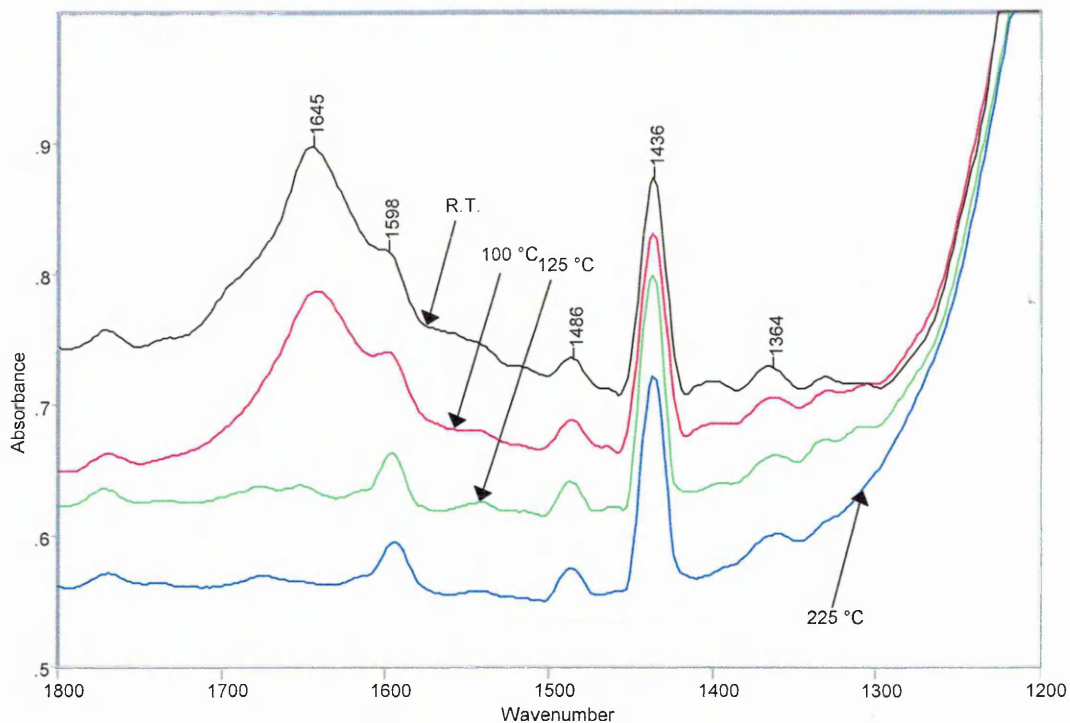
Figure 5.8 – VT-DRIFTS spectra of intercalates 1800 – 1200 cm^{-1}.

The broad band at 1645 cm^{-1} is attributed to hydrogen bonded water and is confirmed by its poor thermal stability. The presence of water in the two intercalates accounts for various changes seen in the DRIFTS spectra of both clay minerals. Frost has also stated that as the OH stretching frequency decreases, the HOH bending frequency increases thus providing a measure of the strength of the bonding of water molecules either physically or chemically bonded to a surface. Bending frequencies below 1630 cm^{-1} indicate weak hydrogen bonding whereas frequencies above 1650 cm^{-1} indicate coordinated and chemically bound water. Thus the loss of the bands at 3550 and 1640 cm^{-1} (Figure 5.8) together with the loss of water confirmed by TG-MS indicate the loss of water which is weakly hydrogen bonded to the surface aluminols or any OH groups remaining on PPA. The band at 3332 cm^{-1} suggests a more strongly bonded species which agrees with its greater thermal stability.

Further examples of study of the water OH deformation band have also been reported which reinforce these observations. Frosts work with formamide intercalates with kaolin[75] reports "space filling" water via a band at 1595 cm^{-1} whereas adsorbed water in the same complex is observed at 1630 cm^{-1}. Similarly in hydrazine intercalates of kaolin[85] a series of bands

126

attributed water in different environments was reported. These include bands at 1578, 1598, 1612, and 1627 cm^{-1} which were assigned to free or non-hydrogen bonded water in the interlayer space of kaolin (1578 and 1598 cm^{-1}), water in the hydration sphere of hydrazine (1612 cm^{-1}) and adsorbed water on the kaolin surface (1627 cm^{-1}). Additionally bands at 1650 and 1679 cm^{-1} were assigned to water coordinated to the siloxane surface or strongly hydrogen bonded due to their appearance at high wavenumber.

Some uncertainty remains as regards to the band at 1207 cm^{-1} as the P=O band occurs at 1220 cm^{-1} in PPA. The same is true of the 1140 cm^{-1} P-O stretch, which is also downshifted by 26 cm^{-1} and appears at 1164 cm^{-1}. Other P-O bands at 1068, 1040 and 990 cm^{-1} are obscured by the prominent and intense Si-O stretching bands.

The inner sheet and inner surface hydroxyls of halloysite are seen as the two OH deformation bands (Figure 5.8) at 916 and 934 cm^{-1} respectively. However, there is clearly a third contribution in this region near 885 cm^{-1} (Figure 5.9). The inner sheet hydroxyl is considered to be relatively inaccessible although its perturbation via interaction with sorbed hydrazine has been reported[73] which suggests that the 885 cm^{-1} band may represent a significant blue shift in the 934 cm^{-1} band.
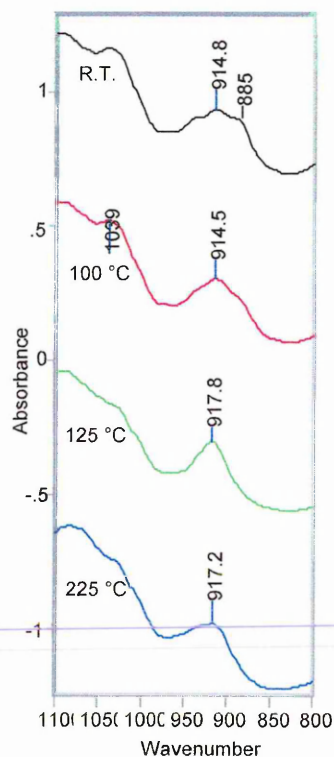
Figure 5.9 – VT-DRIFTS of intercalates showing loss of 885 cm^{-1} shoulder.

127

Analysis of the VT-DRIFTS data in the 1800 – 1200 cm^{-1} region (Figure 5.8) shows that at 100 ˚C a small quantity of adsorbed water has been removed in that the relative intensity of the 1645 cm^{-1} band has been reduced in comparison to the 1439 cm^{-1} band causing the shoulder at 1598 cm^{-1} to become better resolved. The three bands in the 880 – 950 cm^{-1} region are also less distinct from one another. At 125 ˚C the bands at 3547 and 1642 cm^{-1} are no longer observed and the 1205 cm^{-1} has completely merged with the SiO vibration. The 885 cm^{-1} has essentially disappeared and the broad band in the 2500 – 3700 cm^{-1} region has been significantly reduced whilst the 3332 cm^{-1} band has become very prominent and remains so as the temperature is increased, but then gradually diminishes in intensity. In addition, at 125 ˚C a new band appears at 645 cm^{-1}. This band has not been assigned, and is still present at 200 ˚C but not at 225 ˚C.

Recalling Frost's work on intercalated Formamide[75] and Johnstons work on kaolin – hydrazine intercalates[73] both authors observed a band at 904 and 905 cm^{-1}, respectively. In both studies this band is assigned to perturbation of the inner sheet hydroxyl by hydrogen bonding. In fact, perturbation to as much as 885 cm^{-1} have been reported in hydrazine intercalates. Therefore, the 885 cm^{-1} band observed herein was lost at the same temperature as the bands at 1643 and 3547 cm^{-1} (in both HPPA and KPPA) favours the interpretation that it arises from water weakly hydrogen bonded to the inner sheet hydroxyl.

The KPPA VT-DRIFTS data (Figure 5.10) is similar to the HPPA data (Figure 5.8) but exhibits differences in detail. The P-C stretch and ring vibrations were thermally stable but no 645 cm^{-1} band was observed when the 724 cm^{-1} band disappeared. The 1204 cm^{-1} band (Figure 5.10.2) merged with the main SiO vibration between 125 and 150 ˚C when the bands at 3544 and 1642 cm^{-1}, attributed to sorbed water, were reduced to zero. The band near 3332 cm^{-1} (Figure 5.10.1) was present up to 225 ˚C but was not as prominent as in the corresponding spectra for HPPA. Lastly, the band at 885 cm^{-1} was less intense than in the HPPA spectra and was removed by 150 ˚C. Note also the residual intensity of the hydroxyl stretching bands at 3697, 3652 and 3621 cm^{-1}.

128
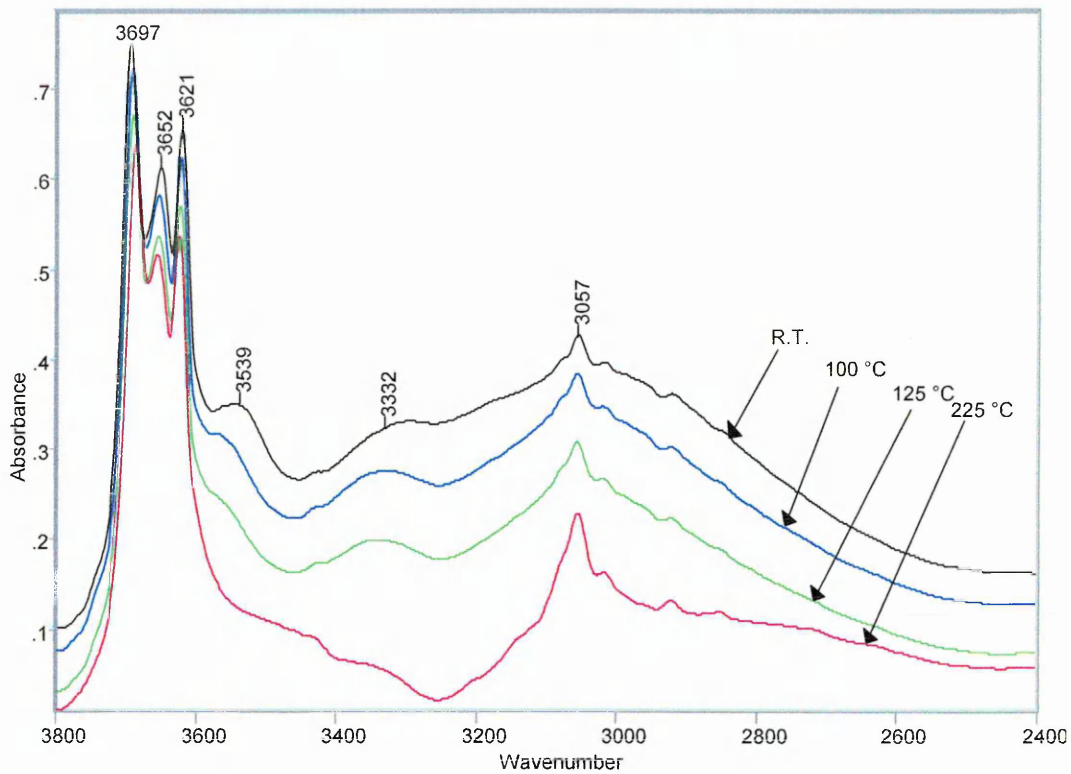
Figure 5.10.1 – VT-DRFITS of KPPA 3800 – 2400 cm^{-1}
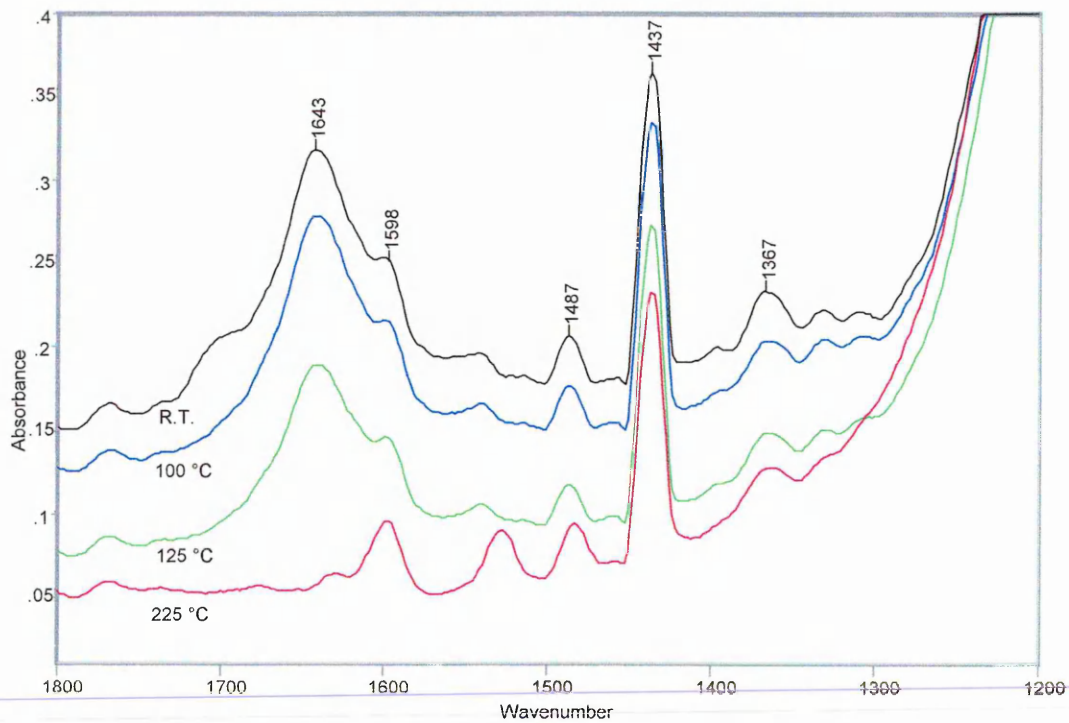
Figure 5.10.2 – VT-DRIFTS of KPPA 1800 – 1200 cm^{-1}

129

5.9 Summary of HPPA and KPPA Intercalates

Results reported here offer a more complete picture of the KPPA (and HPPA) thermal stability then Wypych's results, which do not illustrate this property.

A model for the structure of this intercalate is presented here (Figure 5.11) and there are several points of interest to note.
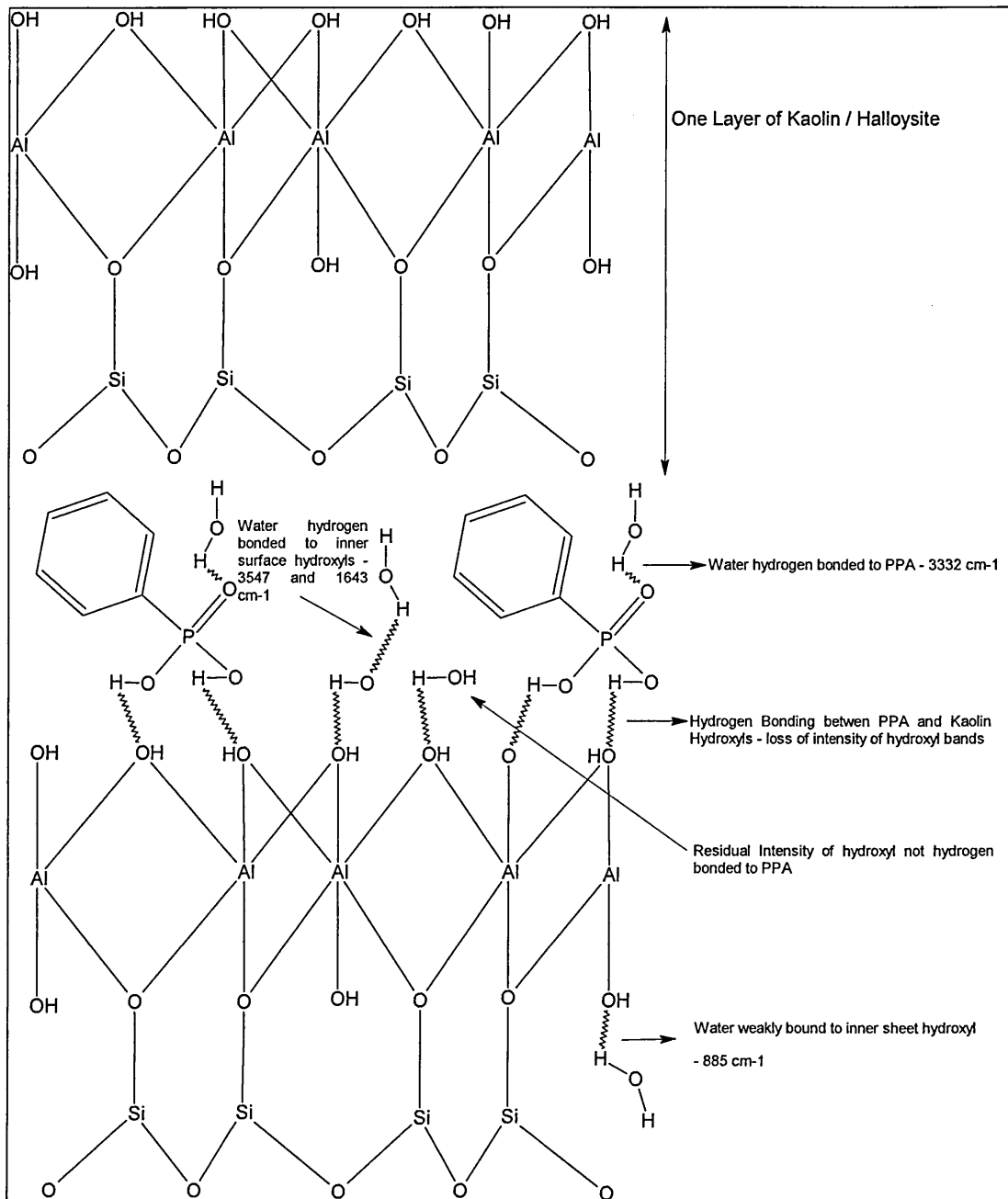
Figure 5.11 – Proposed Model for the Structure of the KPPA and HPPA Intercalate.

1. Water can be seen in the structure of the intercalate in three positions. Although the presence of water is indeed acknowledged by Wypych, the position of this water is not detailed. The water in the intercalate is present as follows

- Hydrogen bonded to the phsphonic moiety of PPA. This water is characterised by a new band at 3332 cm^{-1}. The 3332 cm^{-1} band is seen at room temperature in the VT-DRIFTS and becomes more prominent as the temperature is raised, but by 225 °C has diminished in intensity.

- Weakly bound to the inner surface hydroxyls as seen by the bands at 3547 and 1643 cm^{-1}. The loss of these bands after 125 °C correlates well with the peak at 140 °C in the TG-MS when the ion m/z = 18 (water) is examined.

- Weakly bound to the inner sheet hydroxyls. Much debate as to the assignment of OH deformation bands (as previously discussed) has ensued. Johnston[73] has reported a band at 885 cm^{-1} in the presence of hydrazine, whilst Frost[72,75] using formamide or DMSO has attributed a band at 905 cm^{-1} to either C=O or S=O hydrogen bonded to inner surface hydroxyls. However, the fact remains that the 885 cm^{-1} band (In HPPA and KPPA) was lost at the same temperature regime as the bands at 3547 and 1643 cm^{-1} favours the interpretation that it arises from water weakly hydrogen bonded to the inner sheet hydroxyls.

2. Both these intercalates formed an expanded phase with remarkable thermal stability.

- The 1439 cm^{-1} band (P-C, aromatic) remains virtually unaltered up to 500 °C.
- Heating of both the intercalates to 500 °C does not alter the $d_{(001)}$ spacing.
- TG – MS analysis shows that layer dehydroxylation began at the same temperature as PPA decomposition, but PPA decomposition did not peak until 100 °C later than dehydroxylation. In KPPA this is shown by the maxima at 490 °C (dehydroxylation m/z =18 in TG-MS) and 585 °C (m/z = 78 in TG-MS). Similarly the same observation is made in HPPA, with loss of PPA however at 610 °C.

3. Halloysite absorbed twice as much PPA, and, in a shorter time.

- The time of reaction was five weeks for kaolin and one week for Halloysite. This is not unexpected however given the relative ease with Halloysite may be intercalated.
- The phosphorous content of HPPA is 12.2% whereas KPPA is 6.5%

- More PPA molecules occupy the gallery in HPPA then in KPPA.

Possible avenues for further work include replacing the water bound to the PPA moiety with a suitable monomer with aim of subsequent polymerisation and nanocomposite formation. This should be relatively easy to facilitate as the layers of the clay are already pushed apart by the PPA.

It would also be interesting to compare and contrast the intercalation of PPA in montmorillonite and investigate the thermal in this clay – the interaction between the clay and PPA should be markedly different.

Chapter Six – N – vinylformamide – Smectite Composites.

6.0 Introduction

As previously discussed, the vast majority of nanocomposite synthesis proceeds via the use of an organoclay. As such the clay is organophilic and it is possible to swell the organoclay with the monomer prior to initiation which encourages, where appropriate, the desirable formation of an exfoliated nanocomposite. It was the aim in this work to carry out an in – situ intercalative approach to nanocomposite formation without the use of an organoclay. As previous studies have illustrated (Breen [192,193]) the amides NMF and DMF have been found to swell montmorillonite to as much as 18.4 and 19.3 Å respectively. Hence it was envisaged that N-vinylformamide (VFA) would swell montmorillonite to similar values.

In addition, as an aid to exfoliation, in this novel approach (therefore encouraging intercalation of as much monomer as possible in the clay interlayer) the osmotic swelling of montmorillonite as studied by Onikata et al. [175,183], was employed. Recalling that the authors had used propylene carbonate to swell cation exchanged montmorillonites to more than 20.0 Å (the point at which osmotic swelling is considered to occur), propylene carbonate was added to solutions containing the clay and the monomer VFA with the aim of swelling the clay to such values (Figure 6.0).

The distance (a) (Figure 6.0) represents the primary coordination sphere of VFA around an interlayer cation, whilst the distance (b) is the secondary coordination sphere caused by the addition of PC and its interaction with VFA. Both these coordination spheres are within the interlayer of the clay, thus causing the clay to osmotically swell. The structures of these molecules are :-

VFA   PC
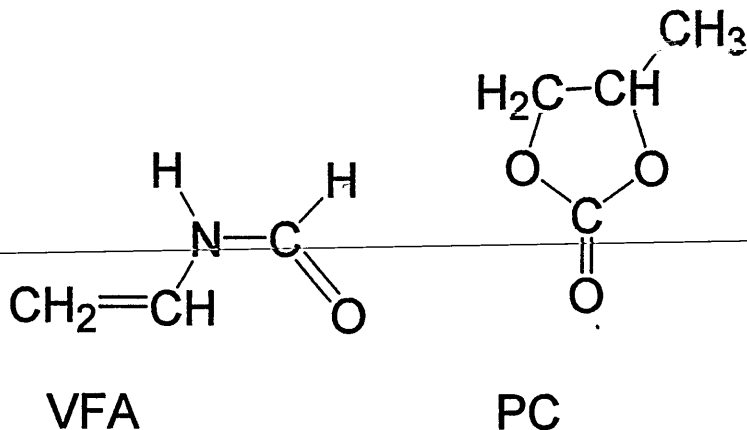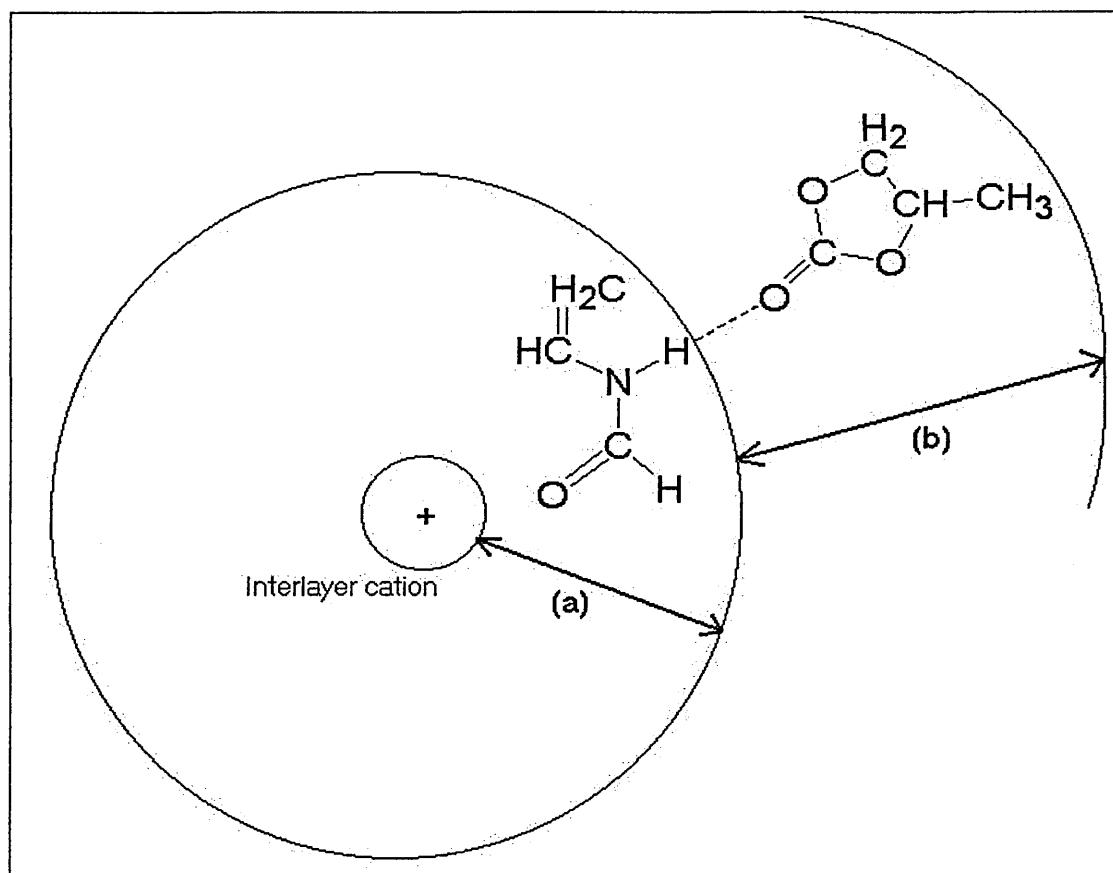
Figure 6.0 – Schematic illustrating proposed osmotic swelling caused by the addition of PC to MCBP and VFA.

The Gutman donor numbers[182] of selected, relevant molecules are presented in Table 6.0.

Polar Liquid	Donor Number	$d_{(001)}$ in polar liquid (Å)	
		Na - Montmorillonite	FA – Montmorillonite
Triethylamine	61	14.0	16.7
Pyridine	33.1	20.6	23.9
N,N – Diethylacetamide	32.3	21.6	23.3
Ethanol	32	17.3	18.8
Methanol	30	17.3	18.4
N,N-Dimethylformamide	26.6	20.6	19.2
Ethylene Glycol	20	17.7	17.3
Formamide	24	Osmotic	Osmotic
Tetrahydrofuran	20	15.0	Osmotic
Water	18	Osmotic	Osmotic
Acetone	17	18.8	Osmotic
Propylene Carbonate	15.1	20.1	Osmotic
Sulphalone	14.8	15.2	Osmotic
Acetonitrile	14.1	20.1	Osmotic

138

Table 6.0 – Gutman Donor Numbers

Taking formamide which has a Gutman Donor number of 24, as an example, when a formamide treated clay is immersed in PC,(donor number = 15.1), the bi – functional nature of formamide enables it to act as an acceptor for polar liquids such as PC expanding the interlayer region of the clay even further, or osmotically. Similarly, VFA may act in the same manner.

The strategy was to use clay layers separated in this way would encourage the rate of polymerisation of VGFA to be equal to that of the bulk outside the clay and therefore encourage exfoliation of the clay.

6.1. Experimental

6.1.1. Materials.

Mineral Colloid BP (MCBP) – English China Clays. CEC = 81 meq $(100g\ clay)^{-1}$. Contains quartz impurity and has mixed interlayer cations of Na, Mg and Ca.

N – vinylformamide (VFA) – Aldrich 99%

Propylene carbonate (PC) – Aldrich 99%

Azo – isobutyronitrile (AIBN) – BDH.

6.1.2. Sample Preparation.

VFA Intercalated Clay – To prepare VFA intercalated clays the clay was simply immersed in an excess of VFA solution and left in a sealed container overnight. The excess VFA liquid was then drained off and the treated clay sample – now green in colour - left to dry on filter paper in air. Adsorption of VFA from the vapour phase was unsuccessful.

VFA / Clay composites – These composites were prepared such that the weight of the clay in the final reaction mixture was 5% by weight. This weight was constant whether or not the reaction mixture contained a mixture of the solvents VFA and PC. The reaction mixture was also fixed to a final volume of 10 ml. To the final reaction mixture containing clay and solvent, AIBN was added to give a concentration of 0.01 mol dm^{-3}. The whole reaction mixture was then stirred for one hour after degassing with nitrogen to ensure that oxidation reactions could

139

not take place. This mixture was then heated under nitrogen, whilst stirring with a magnetic stirrer, and maintained at 70 °C until polymerisation was complete. This was judged to be when a solid had formed, and there was little or no liquid left. This temperature was considered to be the lowest at which polymerisation could be initiated, and reaction did not occur below this temperature. A slow polymerisation rate is desirable so as to enable the rate of polymerisation to be equal within the interlayer and in the bulk monomer. At 70 °C the reaction would proceed to completion in 20 minutes, and this rate increases with increasing temperature.

The resultant composite was then washed with methanol and dried in air. The samples of VFA polymerised without the addition of clay or propylene carbonate were colourless and glassy in appearance – on addition of clay the composite formed is glassy in appearance and brown. A composite of VFA, PC and clay is a white solid.

The following table illustrates the composition of composites made and the ratio of initiator to VFA which may have some bearing on the results.

Volume VFA (cm^3)	Volume PC (cm^3)	Initiator Conc. (mol dm^3)	Ratio Initiator : VFA (mol)
10	0	0.01	0.007:1
5.40	4.60 (50%)	0.01	0.013:1
2.70	7.30 (75%)	0.01	0.026:1
2.16	7.84 (80%)	0.01	0.033:1

Table 6.1 – Composition of Composites made.

6.1.3. Instrumental Techniques.

As in section 5.2.

6.2. MCBP – N-vinylformamide Intercalate

In order to fully understand the following results an appreciation of the XRD trace of MCBP is first required (Figure 6.1). As in all smectites the $d_{(001)}$ is strong at 6.6 °2θ which arises from an interlayer spacing of 12.5 Å. This value encompasses the thickness of one layer of this 2:1 clay mineral (an octahedral sheet and two tetrahedral sheets) and also the water bound to the interlayer cation.
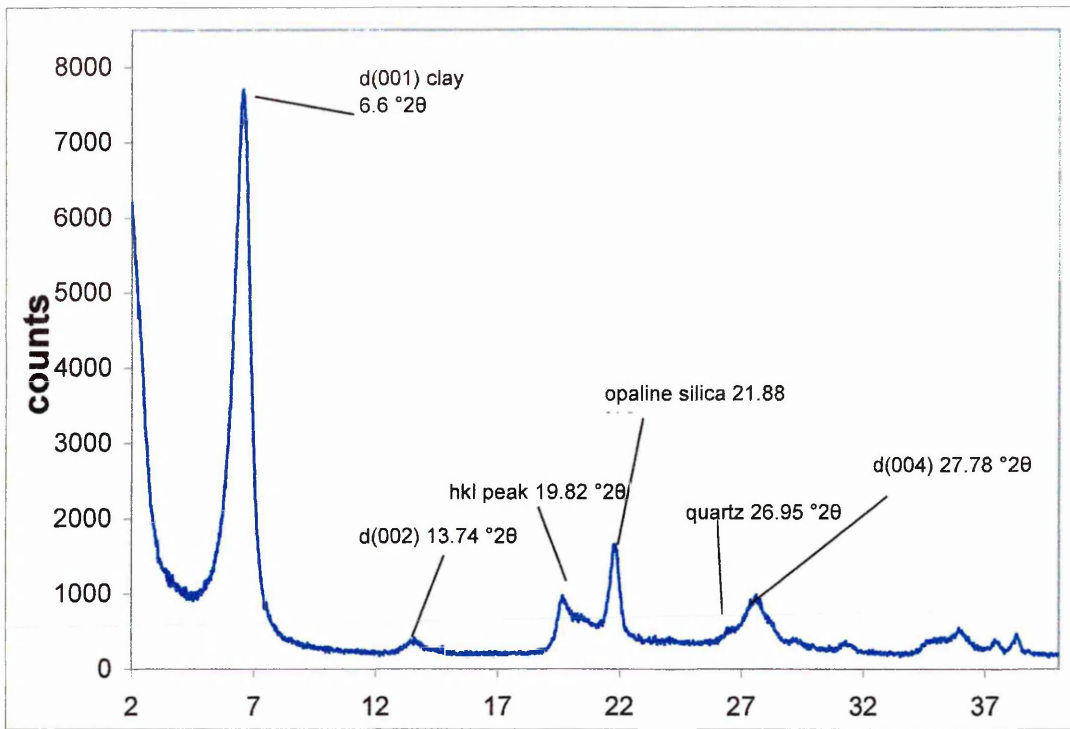
Figure 6.1 – XRD trace of Montmorillonite (MCBP).

The $d_{(002)}$ is characteristically weak and this is indeed the case as shown by the peak at 13.74 °2θ.

Other important features of note in this XRD trace are the 110, 020 or hkl peak at 19.82 °2θ and the impurity opaline silica at 21.88 °2θ. Quartz may also be observed at 26.95 °2θ, and in this trace the quartz peak is seen as a shoulder on the $d_{(004)}$ of the clay. The hkl and opaline silica peaks are orientation independent and will remain of constant intensity regardless of their orientation. Conversely, the $d_{(001)}$ of a clay mineral is orientation dependent, and depends upon the layer structure remaining intact. Therefore as the layers of a clay are forced further apart (by intercalation for example) then the $d_{(001)}$ will move to lower angles (intensity is still dependent on packing) until no $d_{(001)}$ is observed and exfoliation has therefore taken place. The $d_{(003)}$ of the clay is almost present at the same angle as the hkl peak and is not marked on the diagram above.

The XRD results for the VFA intercalate show that the $d_{(001)}$ spacing is 21.0 Å, indicating that the layers of the clay have been expanded (Figure 6.2). This result is not unexpected given the increase in d – spacing observed for NMF and DMF intercalates[192,193] (18.4 and 19.3 Å respectively).

141
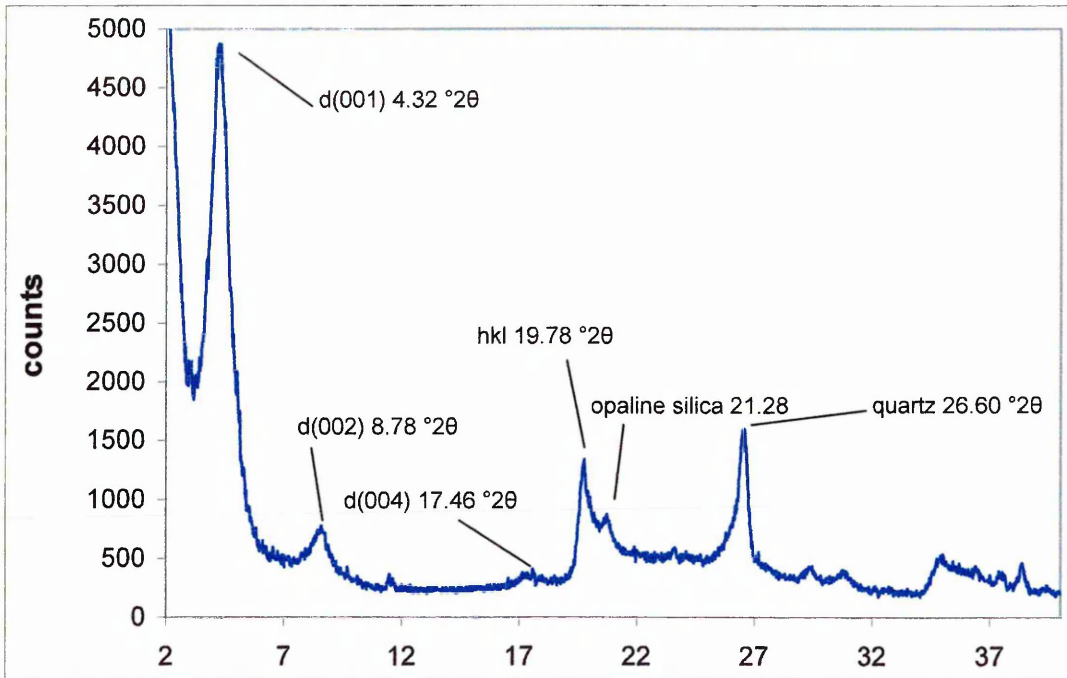
Figure 6.2 – XRD trace of VFA intercalated clay.

Note that the hkl and opaline silica peaks are still observed as they still detected as impurities in the now VFA intercalated clay.

If the variable temperature XRD (VT-XRD) is examined (Figure 6.3), it indicates that the d – spacing of 21.0 Å ($d_{(001)}$ at 4.32 °2θ) in the VFA intercalated clay is stable to 200 °C. At 250 °C this value is reduced to 15.0 Å, and finally at 300 °C to 14.4 Å, as seen by the movement of the d $_{(001)}$ to higher values of °2θ. The 001 (4.32 °2θ), 002 (8.78 °2θ) and 004 (17.46 °2θ) in this sample are observed up to 250 °C indicating the sample is well ordered. Note that the hkl and opaline silica peaks (19.78 and 21.28 °2θ respectively) are still observed at the same positions at high temperature, despite desorption of some of the intercalate.

142
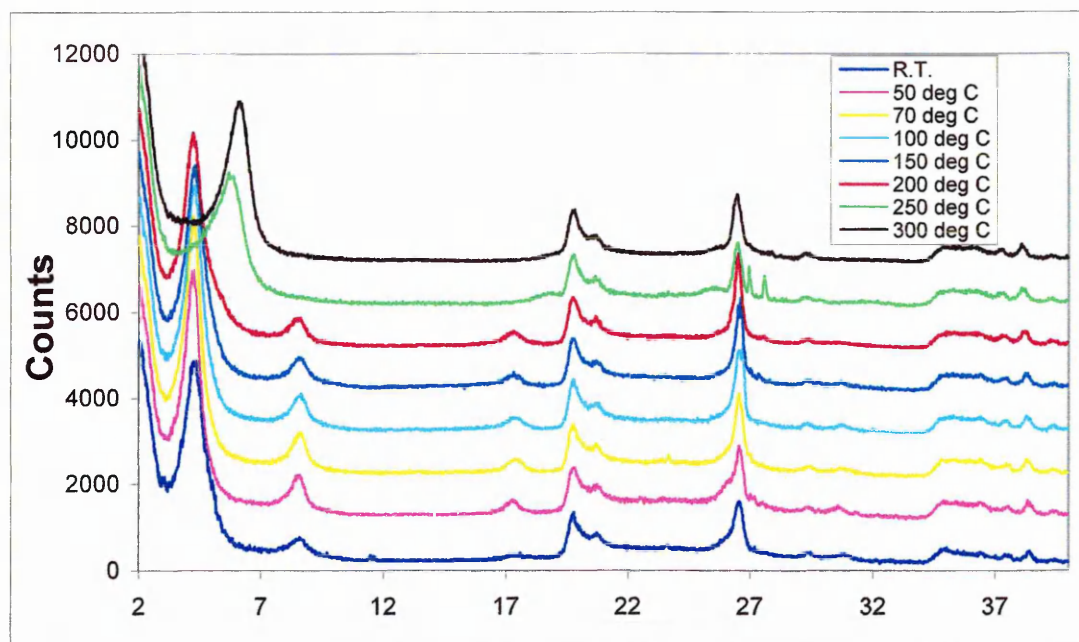
Figure 6.3 – VT-XRD of Montmorillonite – VFA Intercalate.

The DTG (Figure 6.4) shows peaks at 110, 120, 155, 160, 280, 290, 300, 320 and 620 °C. The sample loses 24% wt overall and 11% of this is lost over the DTG peaks at 280, 290, 300 and 320 °C, which are four closely occurring processes. This is the region at which, as indicated by VT-XRD there is a decrease in d – spacing. The DTG peak at 620 °C is most likely to be dehydroxylation of the clay.

Other than the dehydroxylation of the clay the intercalates the NMF and DMF intercalates[192,193] both show three peaks. In NMF these are at 100, 120 and 230 °C (for the Na SWy-2). In the DMF intercalates the highest temperature maxima in the DTG trace were at 420, 330 and 220 °C for the Ca, Mg and Na cation exchanged clay complexes respectively. However the clay used in these studies is of mixed interlayer cation – Ca^{2+}, Na^+ and Mg^{2+}, and this may be reflected in the DTG trace, for the desorption of VFA. Note, however, that there may be other explanations.
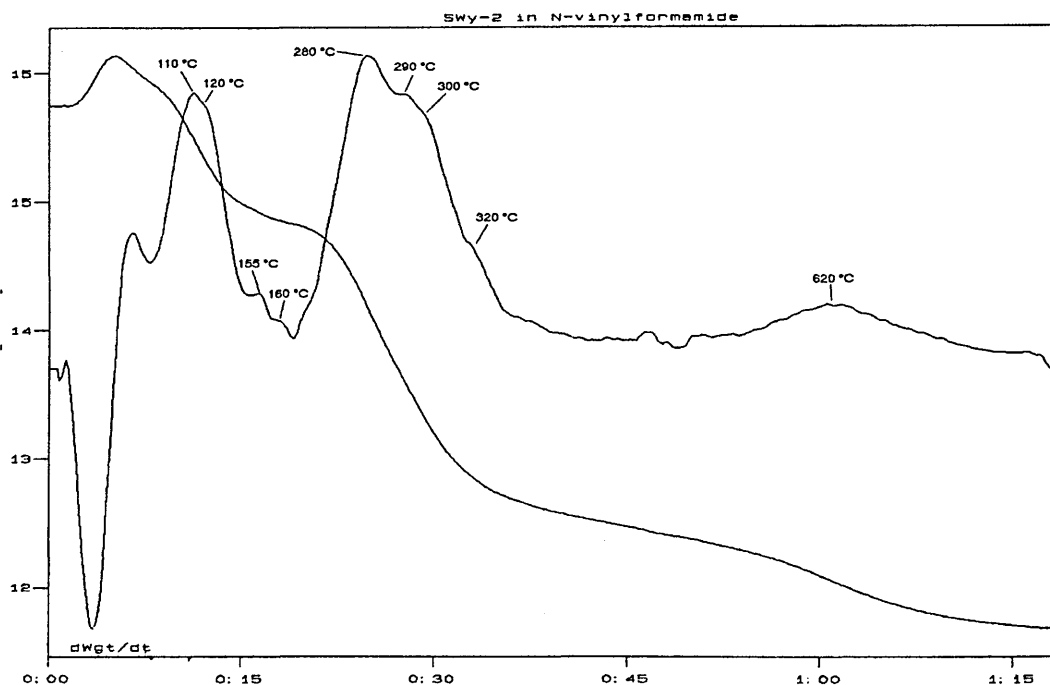
Figure 6.4 – TGA and DTG data for Montmorillonite – VFA Intercalate.

6.2.1 DRIFTS Analysis

N-vinylformamide liquid (spectrum not shown) has bands at the following positions:-

Wavenumber (cm^{-1})	Assignment
3280	N-H Stretch NH$_3^+$ stretch
3150	CH$_2$ stretch (H$_2$C=C-)
3030	CH Stretch (HC=C-)
2890	Symmetric CH stretch
2780	N-C-H stretch
1680	Amide I (C=O stretch)
1650 (shoulder)	C=O stretch. / NH$_3^+$ deformation
1510	Amide II N-H deformation
1400	C=C (CH$_2$ deformation)
1390	CH bend
1300	C=C (CH deformation)
1250	Amide III (CN stretch and NH bend)
1210	
990	C=C (CH bend)

Table 6.2 – Band Assignments for VFA liquid.

The single temperature DRIFTS spectrum of the VFA-MCBP intercalate is shown in Figure 6.5.

144
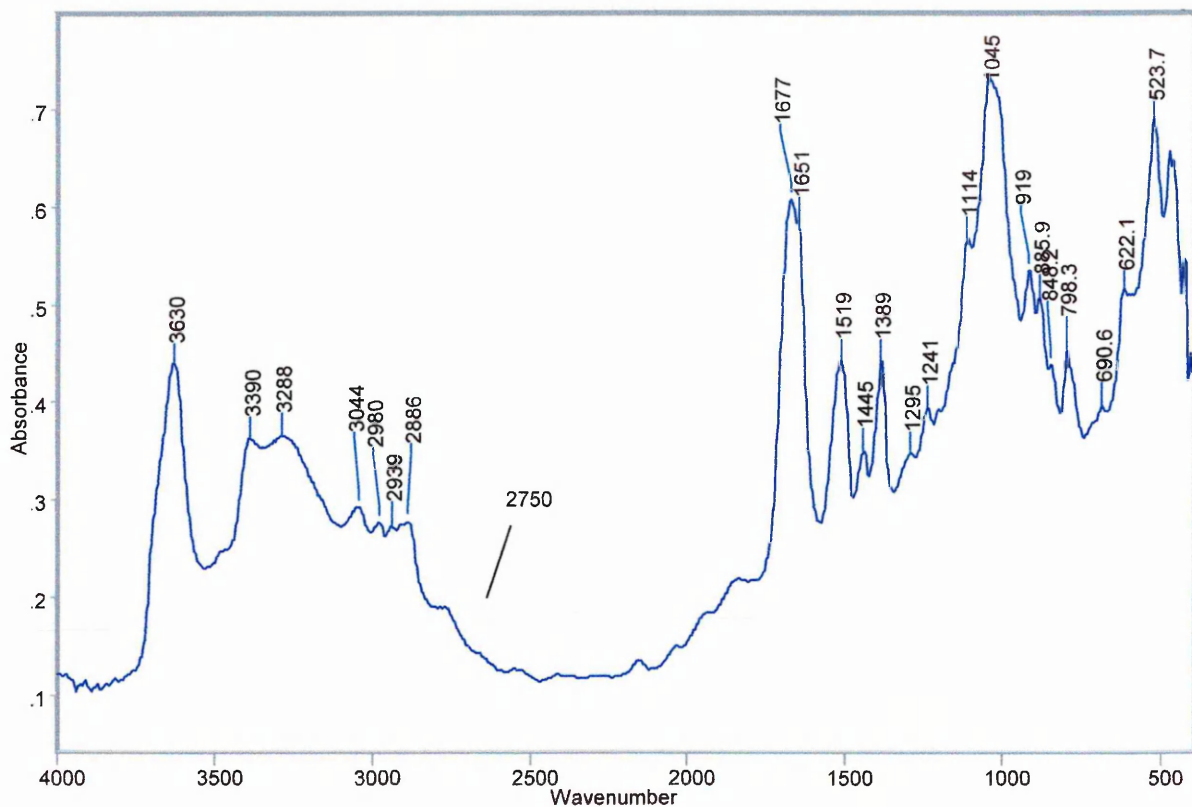
Figure 6.5 – DRIFTS spectrum of Montmorillonite – VFA intercalate

The intense band at 3630 cm^{-1} is the OH stretching band arising from the AlOH and MgOH in the clay structure. The band at 3390 cm^{-1} is an NH stretch arising from VFA molecules which are not significantly involved in hydrogen bonding as this band is at higher frequency than in liquid VFA – in liquid VFA this band would be involved in hydrogen bonding. This band is discussed in more detail in the VT-DRIFTS data. The broader band at 3288 cm^{-1} is attributed the NH stretch of N-H groups that are involved in hydrogen bonding. The band at 3044 cm^{-1} is the unsaturated CH stretch from the C=C within VFA. Weak bands are also seen at 2980, 2839 and 2866 cm^{-1} which are all in the correct region for CH stretches and again discussed further in the VT-DRIFTS.

The next prominent band of interest is the intense band at 1677 cm^{-1} with a shoulder at 1651 cm^{-1}. These are assigned to carbonyl stretching bands. It is possible that the latter could also be attributed to the unsaturated CH stretch, but these bands are not always intense and would more likely be dominated by the more intense carbonyl band. The 1677 cm^{-1} band in the intercalate is in the same position as in the liquid VFA and this may indicate that the interaction with the interlayer cation (expected via the carbonyl group) is of the same strength

as the hydrogen bond in VFA liquid (which boils at 210 °C). Note that Breen[192] *et al* did not observe any significant shifts in the amide I band for NMF and DMF intercalates. The band at 1519 cm^{-1} is a CN stretch. Bands at 1389 and 1295 cm^{-1} are attributed to an unsaturated CH_2 deformation or a CH bend and an unsaturated CH deformation respectively (Table 6.2). The amide III band is seen at 1241 cm^{-1}.
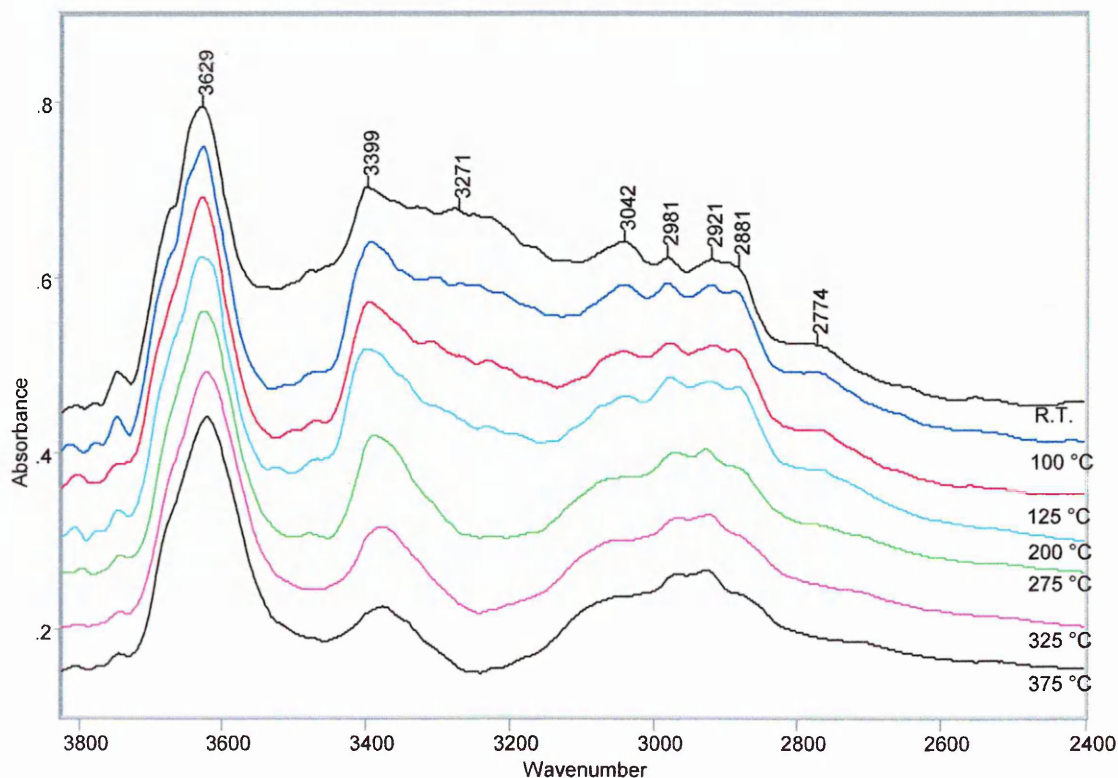
Figure 6.6.1 – VT-DRIFTS 3800 – 2300 cm^{-1} region of VFA – MCBP intercalate.

The VT-DRIFTS data shows various changes in these bands in the 2400 – 3800 cm^{-1} region (Figure 6.6.1). A broad band or indeed a series of bands centred at 3271 cm^{-1} are gradually lost with increasing temperature and no longer observed by 275 °C. This observation is similar to that of Breen[192] *et al* (Chapter 4 section 4.4.4) where asymmetry on the low wavenumber side of a band at 3420 cm^{-1} was seen to reduce by 250 °C. Therefore, this loss may be due – by comparison – to removal of VFA molecules involved in interactions of varying strength via the N-H bond. This removed VFA may originate from species coordinated to external exchangeable cations found at broken edges and surfaces (recalling that these account for 20% of the CEC) or to directly coordinated VFA molecules (those that are bound

to interlayer cations). Moreover the position of this band indicates that, relative to the NH stretching band at 3399 cm^{-1}, this band is indicative of hydrogen bonded NH (c.f. 3280 cm^{-1} in liquid VFA). In NMF intercalates this loss is correlated to a maximum at 200 °C in DTG data, but DTG data for the VFA intercalate (Figure 6.4) has a series of peaks over this range (peaks at 110, 120, 155, 160, 280, 290, 300 °C), none however are centred at 200 °C. It is likely that the DTG peak at 280 °C is related to the loss of the bands near 3271 cm^{-1} since they are removed by 275 °C.

The NH stretching band (non – hydrogen bonded) at 3399 cm^{-1} is lost by 400 °C which is 50 °C lower than its NMF intercalate counterpart. Since this band is retained to high temperature however it must indicate the presence of VFA to a high temperature. This correlates with the presence of the amide I band at 1678 cm^{-1} (Figure 6.6.2) – mostly due to the stretching frequency of the C=O bond - which is also present at 375 but lost by 400 °C. Given that the interaction between the clay and VFA by analogy with NMF and DMF it is most likely that interaction is via the carbonyl group and exchangeable cations.

The unsaturated CH stretch (3042 cm^{-1}) is present as a characteristically weak band and is lost by 275 °C and correlates well with the loss of the unsaturated CH$_2$ deformation band at 885 cm^{-1} (Figure 6.6.2). However, amides are also known to be protonated in the interlayer of montmorillonites and the extent of protonation depends on the acid strength of the exchangeable cation and the polarisation of the adsorbed water by the cation. Hence the band at 3045 cm^{-1} could also be an NH$_3^+$ stretching band if protonation of the amide has taken place. The saturated CH and CH$_2$ stretches in the region 3000 – 2900 cm^{-1} begin to decrease in intensity from 200 °C and are lost by 400 °C. Similarly the 3399 cm^{-1} band is lost also over the same temperature range. Thus far the majority of changes in the VT-DRFITS occur in the temperature range R.T. – 400 °C. Although the maximum temperature available via VT-XRD is 300 °C there is a large change in the interlayer spacing from the original value of 21.0 Å to 14.4 Å at 300 °C.
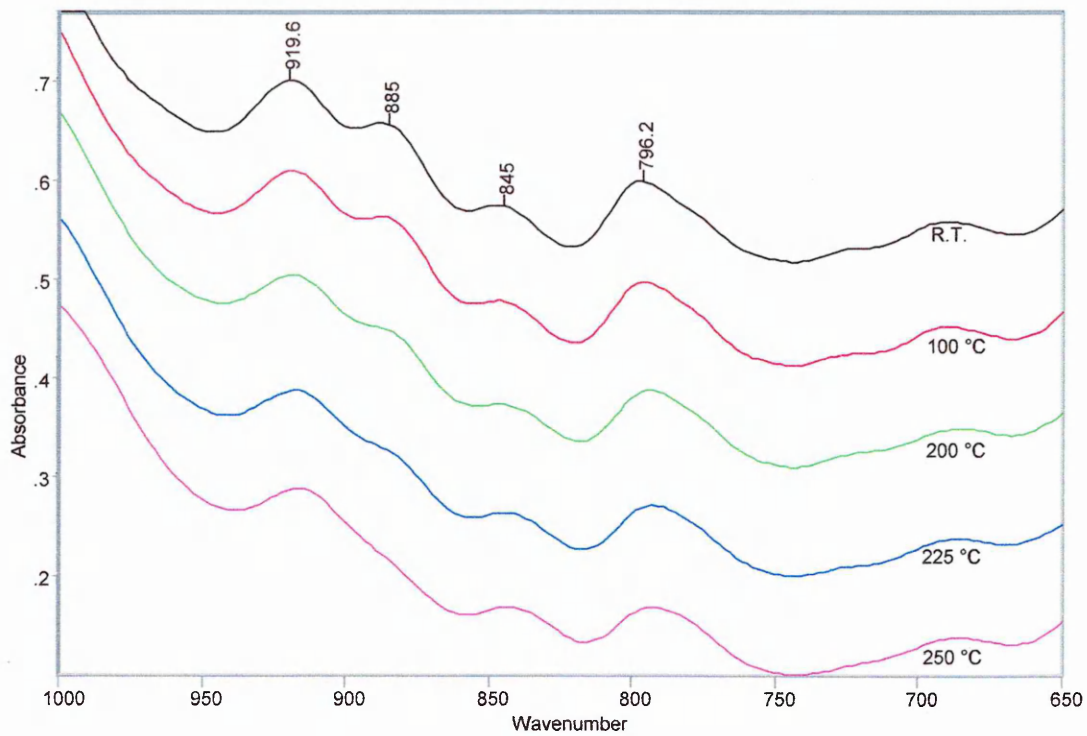
Figure 6.6.2 – VT-DRIFTS Swy-2 – VFA intercalate 1000 – 650 cm^{-1} showing loss of 885 cm^{-1} band.
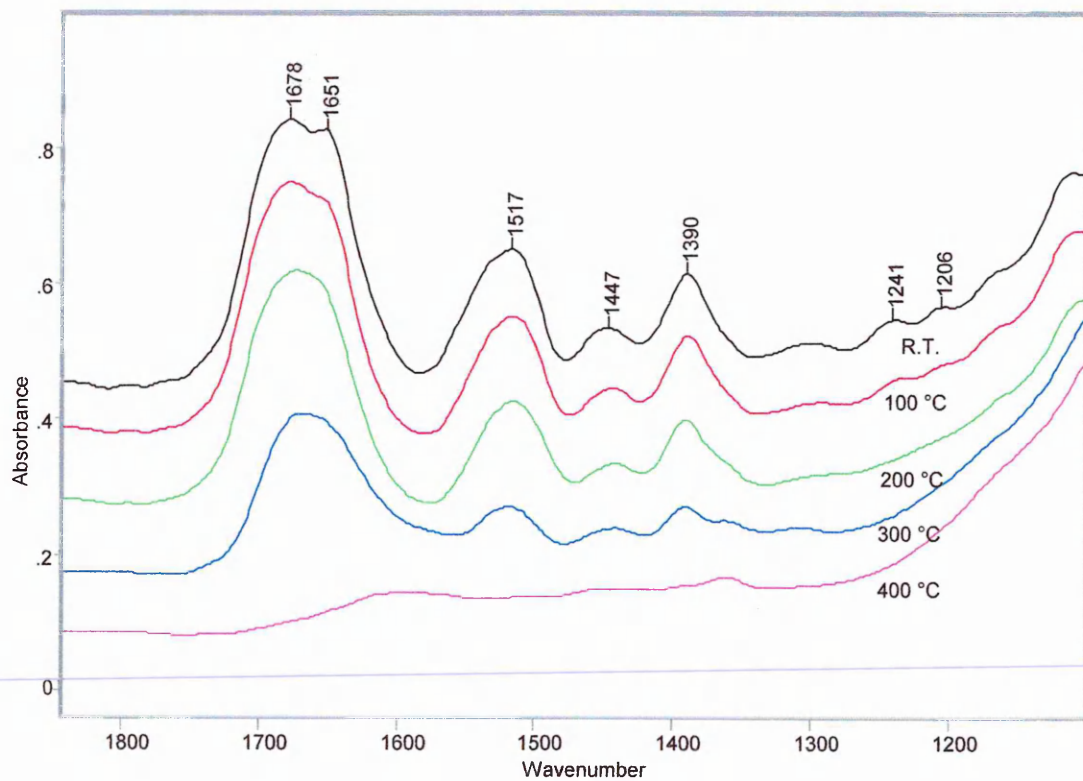
Figure 6.6.3 – VT-DRIFTS of SWy-2 VFA intercalate, 1900 – 1100 cm^{-1}.

The carbonyl stretching (amide I) band observed at 1678 cm^{-1} (Figure 6.6.3) decreases in frequency to 1666 cm^{-1} before it is lost at 400 °C. This comprises a shift to 1674 cm^{-1} by 125 °C, 1672 cm^{-1} by 150 °C, 1668 by 250 °C and finally 1666 cm^{-1} by 275 °C. This may be loss of interlayer water coordinated to the interlayer cations in the clay, bridging water, (hence the move to lower frequency) or very strongly hydrogen bonded water. Indeed the series of bands centred at 3271 cm^{-1} may also comprise an OH stretching band from water as there is some loss in intensity by 125 °C.

The shift indicates that the carbonyl group is now interacting more strongly with the exchange cation. Note that this shift is not as large as would normally be expected for carbonyl interaction. This observation has also be reported by Breen et al[192] where it is attributed to the fact that intermolecular hydrogen bonding may be as strong as the carbonyl – clay interaction. In liquid NMF for example the carbonyl stretch is seen at 1667 cm^{-1} and in the NMF – clay intercalate at 1664 cm^{-1}. As the latter is not as high as the liquid NMF wavenumber, this means that the carbonyl groups are interacting very strongly with the clay (interlayer cation). This is because NMF molecules in the liquid phase form very strong intermolecular bonds which is reflected in NMF's high boiling point of 180 – 185 °C. Similarly in the spectrum of liquid VFA (Table 6.2) the main carbonyl stretching band is at 1680 cm^{-1} (VFA liquid has a boiling point of 210 °C) and is seen in the VFA – clay intercalates at lower frequencies.

A shoulder on the 1678 cm^{-1} band is presnet at 1651 cm^{-1}. This is dissimilar to the observation of the DMF intercalates seen by Breen et al[193] where the carbonyl band was seen as three components relating to water (1627 cm^{-1}), weakly bound amide (1720 cm^{-1}) and asymmetry on the high wavenumber side of the main carbonyl band at 1658 cm^{-1}. It is difficult to say when this band decreases with increasing temperature as the 1678 cm^{-1} band decreases in intensity considerably by 100 °C where the 1651 cm^{-1} shoulder is still clearly visible. However if the intercalates of NMF with Na, Mg and Ca exchanged clay are examined the DRIFTS spectra show that the position of the carbonyl bands in these clays are 1678, 1664 and 1665 cm^{-1} respectively. Hence the two bands observed here at 1678 and 1651 cm^{-1} in the VFA intercalate may reflect the mixed interlayer cations present within the clay. Alternatively, given the prior discussion on amide protonation this band could be the NH$_3^+$ deformation band.

The amide II band at 1517 cm^{-1} (NH deformation) decreased in intensity over the same temperature regime as the 3399 cm^{-1} NH stretching band, and hence correlates well.

The amide III band at 1241 cm^{-1} together with a band at 1206 is lost by 175 °C, though both these bands are weak.

The TIC for the evolved gas analysis (EGA) (Figure 6.7) shows the temperatures of the main peaks detected during the analysis and these results are tabulated (Table 6.1), which also shows the time and hence subsequent order in which the ions are detected. The peaks shown in the TIC at 120, 160, 280 and 300 °C all of which coincide with temperatures at which there are peaks in the DTG trace for this sample. Also shown are the reconstructed ion chromatograms of the most intense ions observed during the analysis (Figure 6.8).

Swy-2 in N-vinylformamide
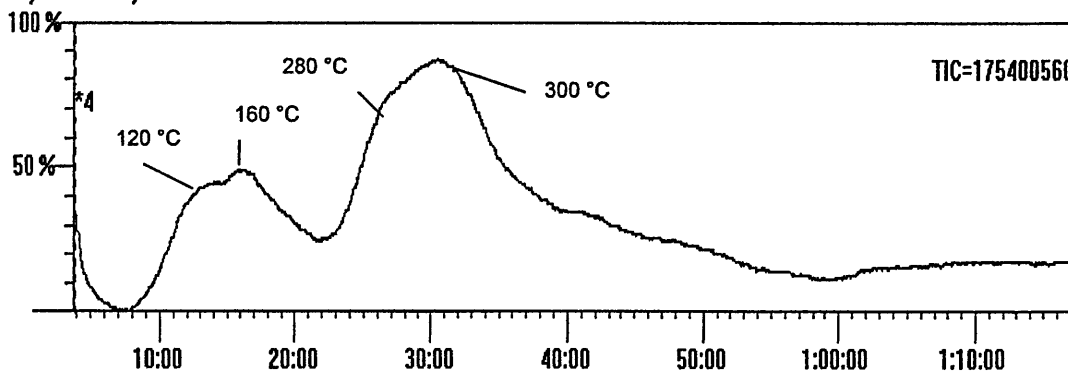
Figure 6.7 – TIC of SWy-2 – VFA intercalate
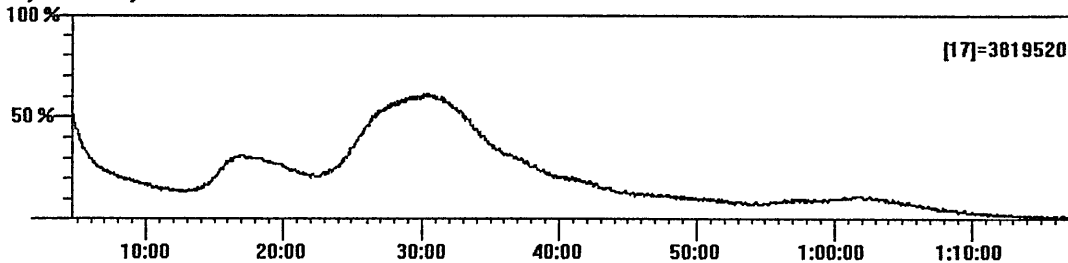
M / z = 18 (water) saturates and is not shown.

[45]=4567040

[43]=4665344

[41]=3670016

10:00   20:00   30:00   40:00   50:00   1:00:00   1:10:00
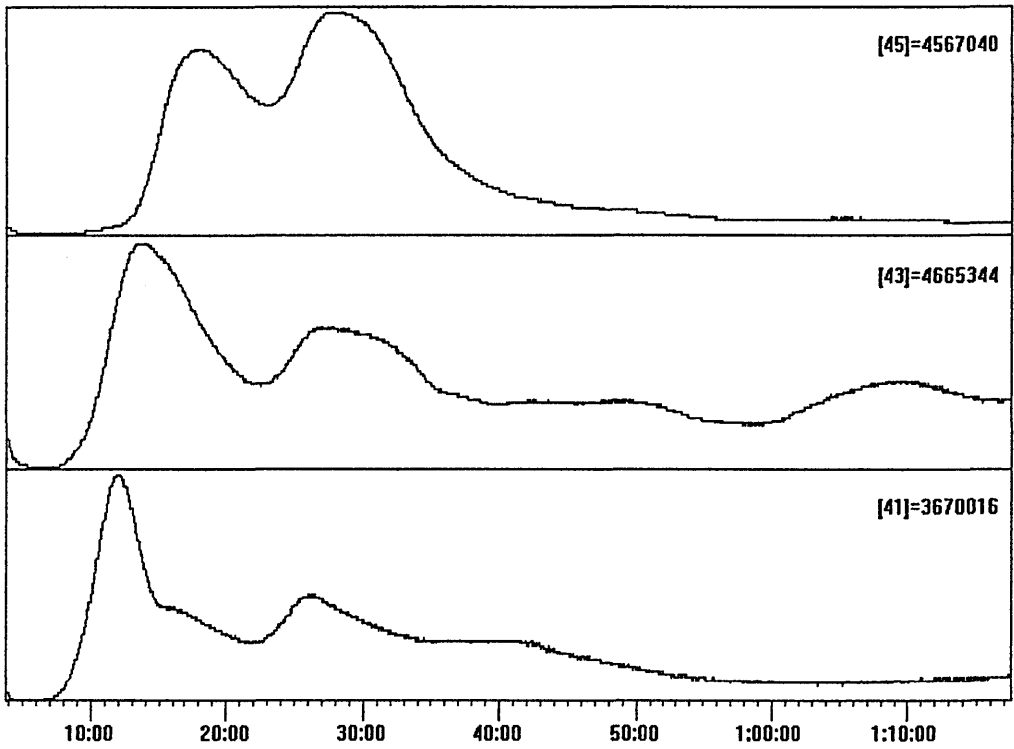
Figure 6.8.1 Reconstructed Ion Chromatograms from Swy-2 – VFA intercalate

Swy-2 in N-vinylformamide

[53]=1116160

[52]=1713152

[51]=1581056

[50]=1111040

10:00   20:00   30:00   40:00   50:00   1:00:00   1:10:00
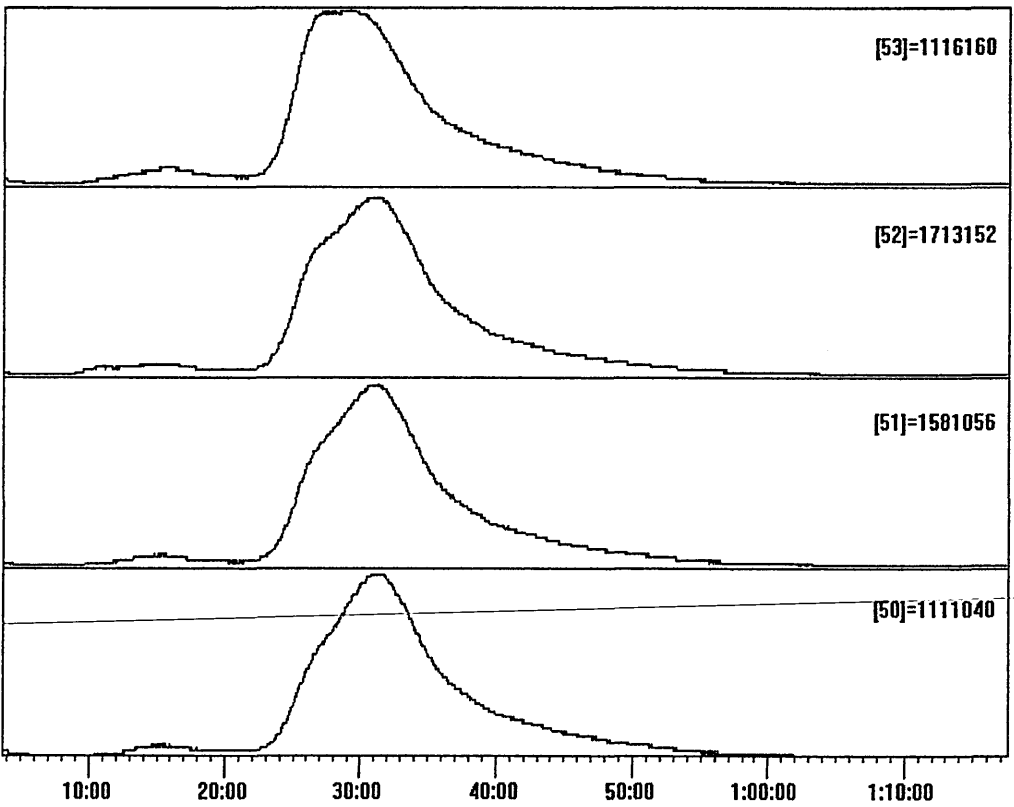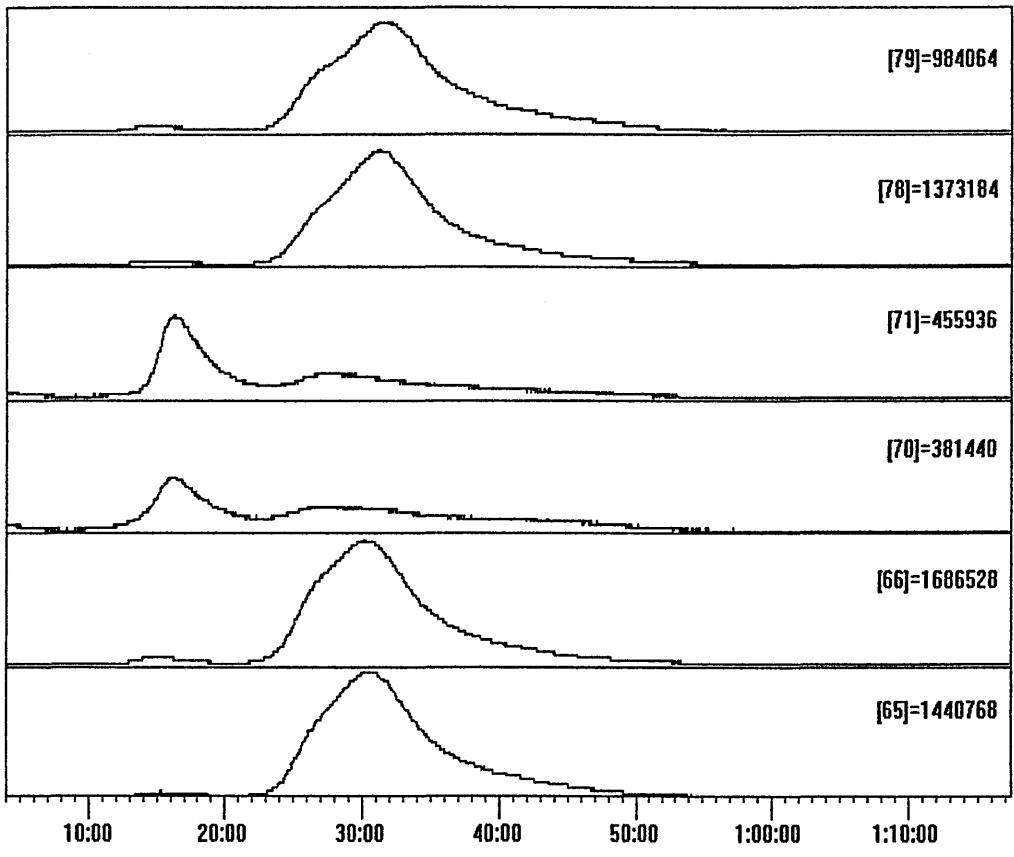
Figure 6.8.2 Reconstructed Ion Chromatograms from Swy-2 – VFA intercalate

Swy-2 in N-vinylformamide
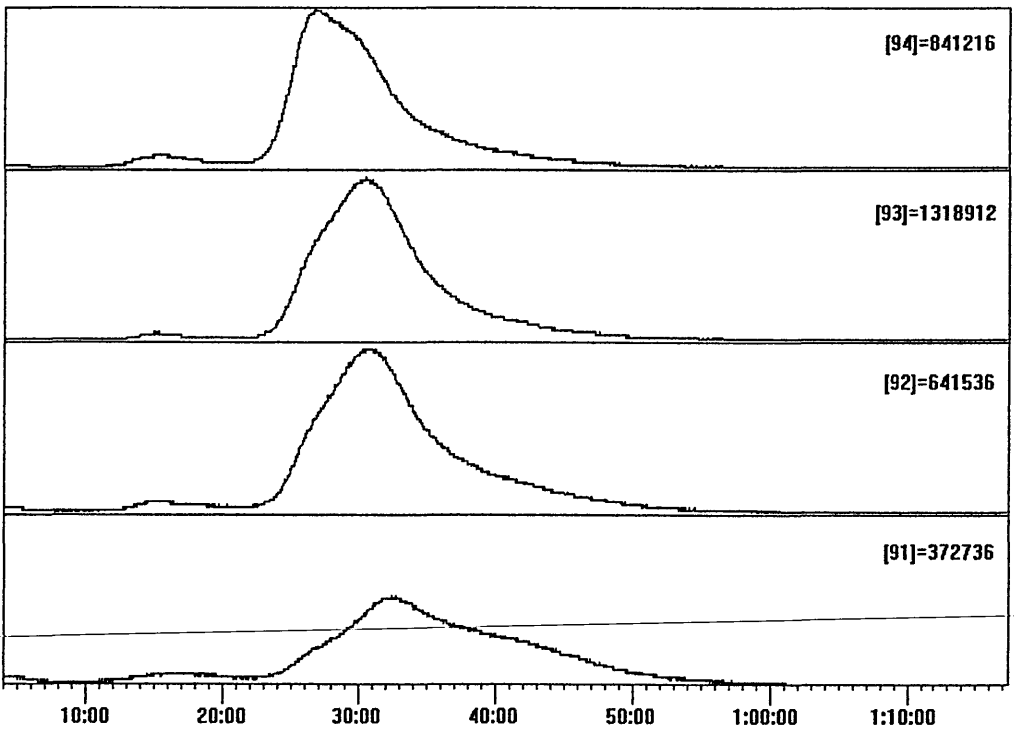
Figure 6.8.3 Reconstructed Ion Chromatograms from Swy-2 – VFA intercalate

Time (Mins)	Temperature (°C)	Ions Detected
11	110	
12	120	41
15	150	43,66,71,78,79
16	160	17,45,70
28	280	17,43,45,50,51,52,53,65,66,70,71,78,79,92,93,94
29	290	52,53
30	300	50,51,52,65,66,78,79
32	320	17,20,51,52,91
62	620	

Table 6.1 – Ions detected from SWy-2 – VFA intercalate

The MS results are complex and allowing for possible thermal (or cationic) polymerisation it was still not possible to assign these ions to meaningful fragments. Some of the ions that have been assigned are shown in Figure 6.9. $M / z = 71$ is a VFA molecule and it is interesting to note that this (and $m/z = 70$ which is the same species minus a proton) are detected up to 280 °C which correlates well with the observations in the VT-DRIFTS that indicate that VFA is being lost from surface, edge sites and VFA that is hydrogen bonded to directly coordinated VFA up to 275 °C. Some water ($m/z = 17$ as $m/z=18$ was saturated) is also lost up to 320 °C and this also correlates well with the shift in the carbonyl stretching band at 1678 cm^{-1} which moves to lower frequency (1666 cm^{-1}) as this water is lost. It is possible that the remaining ions detected are breakdown products of VFA as it boils at 210 °C.
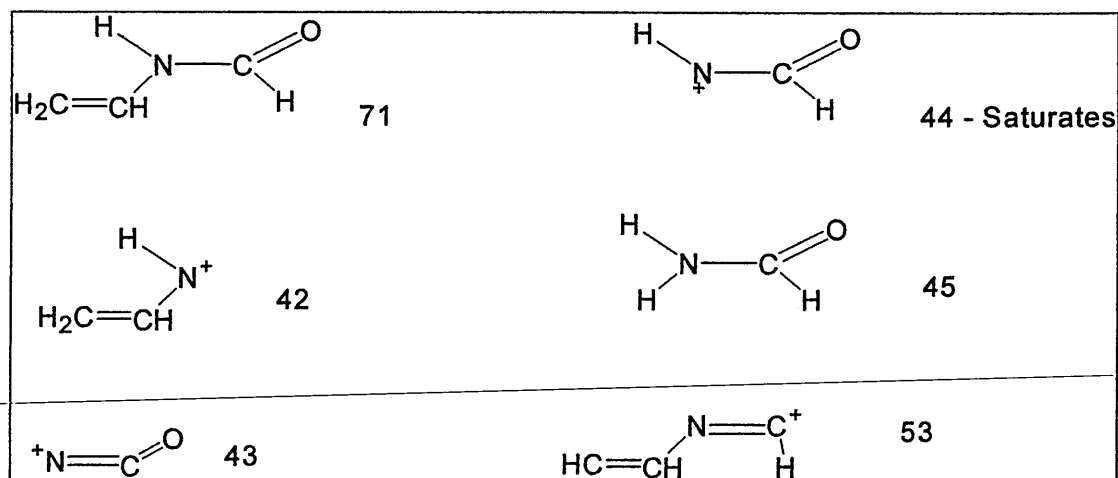
Figure 6.9.1 - Possible ion fragments from EGA of SWy-2 – VFA Intercalate

It should also be noted that the possibility of polymerisation occurring makes this process more complex. If VFA polymerises via thermal initiation[198] the following products may be detected by MS (Figure 6.9.2).
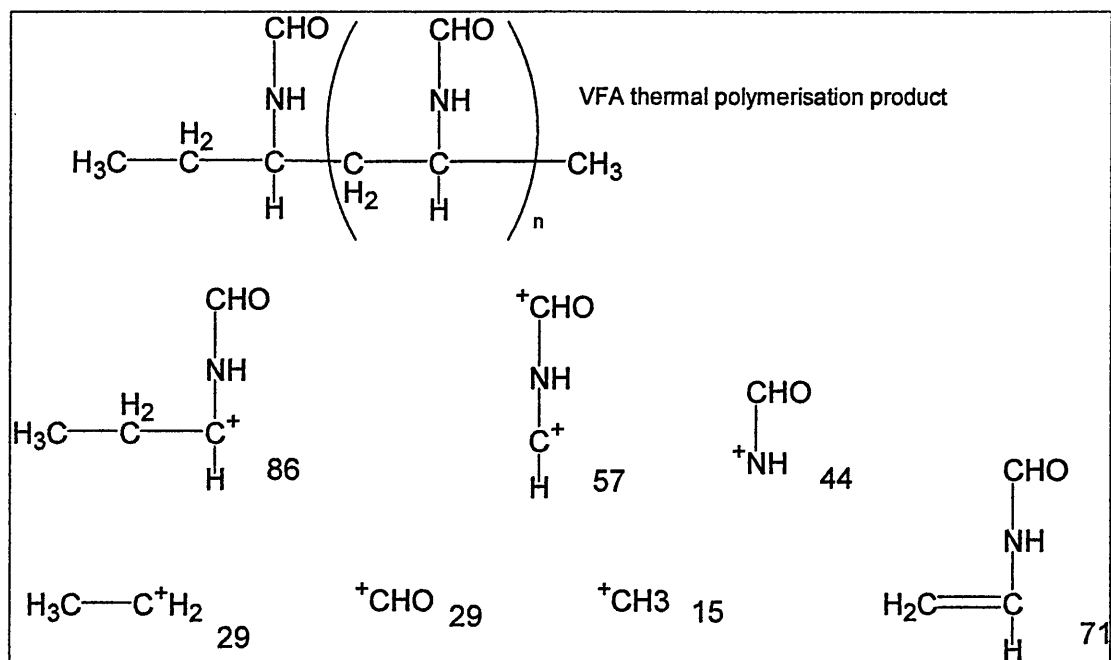
Figure 6.9.2 – Possible ion fragments from thermal polymerisation of VFA – SWy-2 intercalate.

Indeed the situation is further complicated by examination of the cationic polymerisation product[198] (Figure 6.9.3).
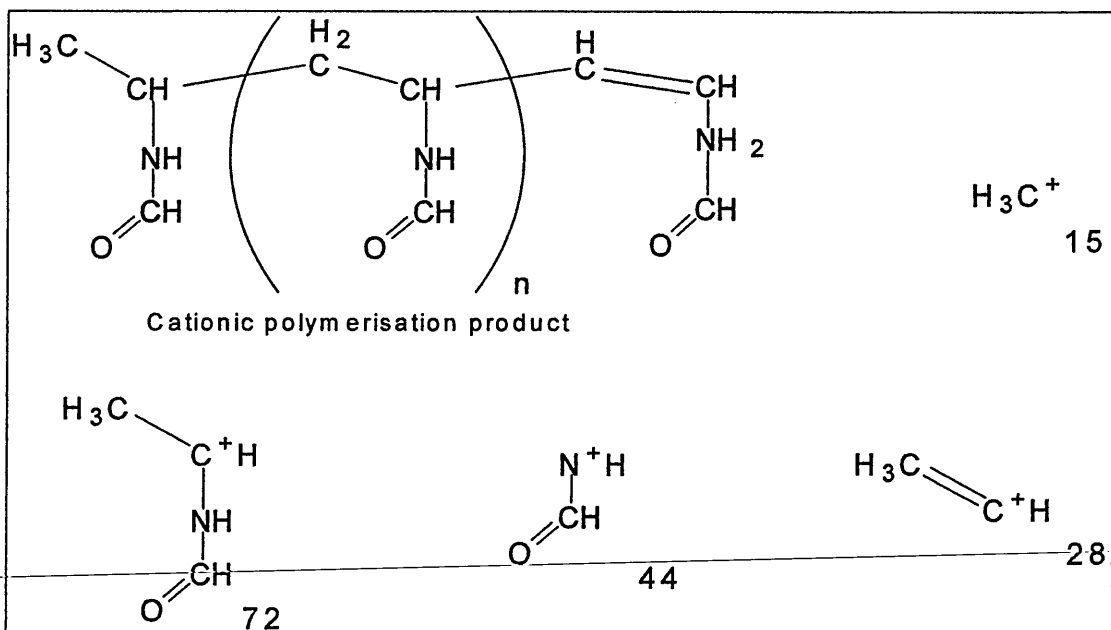
Figure 6.9.3 – Possible ion fragment from cation polymerisation product of VFA in VFA – SWy-2 intercalate.

Furthermore, as illustrated by Spange[199] the cationic polymerisation of VFA may also result in cyclic end groups when chain termination of the growing polymer chain occurs (Figure 6.9.4)
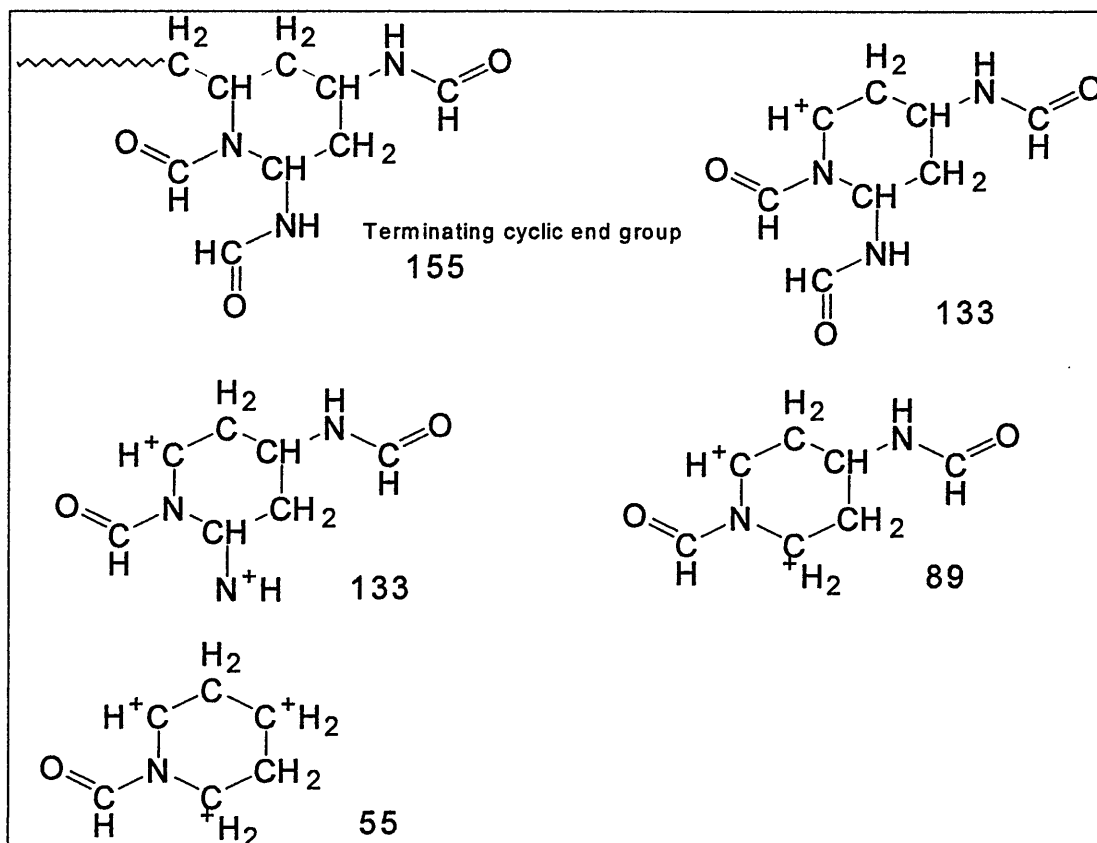
Figure 6.9.5 – Possible ion fragments from the cyclic end group resulting from cationic polymerisation of VFA.

Additionally, it should be remembered that water is present within the interlayer of the clay and this may facilitate addition of water across the carbon – carbon double bond in VFA, as described by Kroner[183] (Figure 6.9.6).
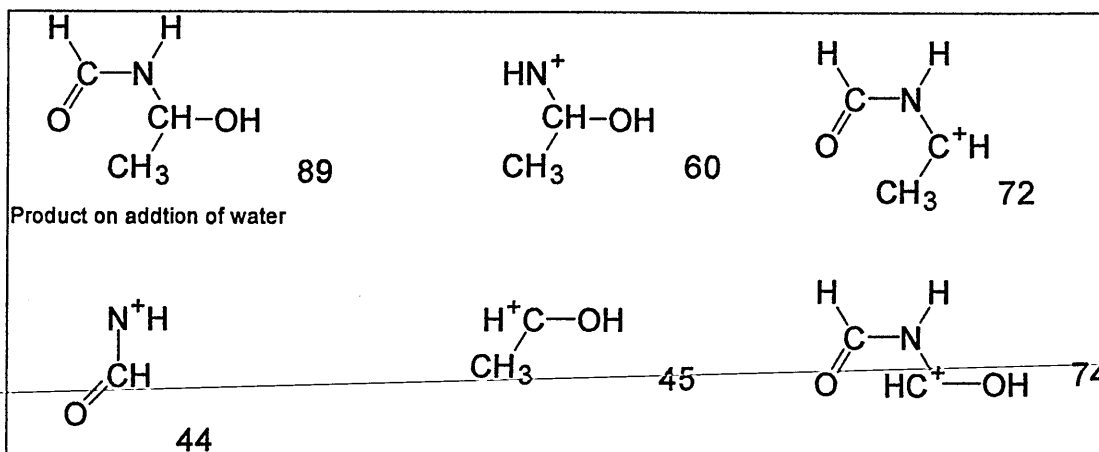
Figure 6.9.6 – Ion fragments from product obtain on reaction of VFA with water in VFA – SWy-2 intercalate

6.2.1 Summary of VFA – Clay Intercalate

VFA successfully intercalates MCBP (Figure 6.9.7) as characterised by the DRIFTS and XRD data

- The XRD shows that the $d_{(001)}$ spacing of the clay has now increased to 21.0 Å. This is in good agreement with NMF and DMF intercalated montmorillonites[192,193].

- The VT – XRD shows that the $d_{(001)}$ spacing decreases to 14.4 Å by 300 °C.

- The frequency of the carbonyl stretching bands at 1677 and 1651 cm^{-1} indicate that there is interaction of the carbonyl group of VFA with most likely the interlayer cation of the clay. As this frequency does not differ greatly from that of liquid VFA – where the position of this band is related to the high degree of hydrogen – bonding – the strength of this interaction is therefore of similar magnitude.

- Similarly, like NMF and DMF intercalates[192,193], VFA is also bound to surface and edge sites. This is reflected in the VT-DRIFTS by the broad band, or series of bands centred at 3271 cm^{-1}, which represent interactions of varying strength via the N-H bond.
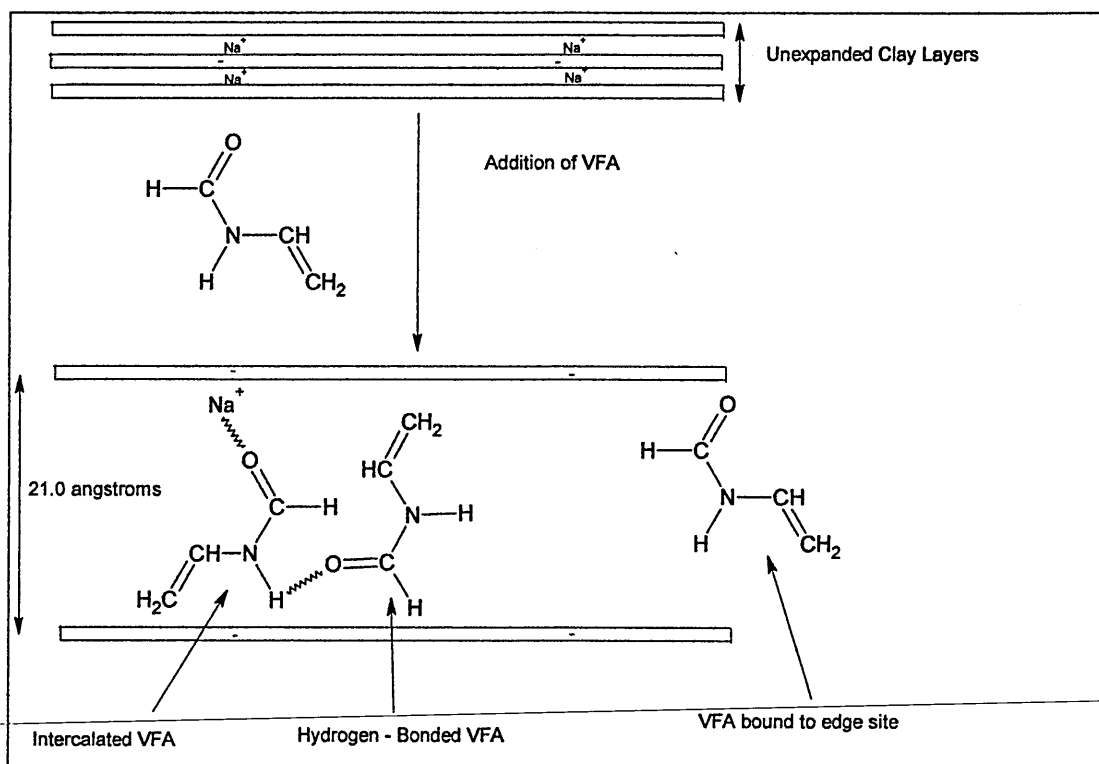
Figure 6.9.7 – Schematic Showing VFA intercalated within Clay

156

- EGA results are complex and illustrate the complexity that may occur if polymerisations occurs on heating. It was not possible. However, to assign all the mass fragments. The use of DSC may indicate if a polymerisation reaction does indeed take place upon heating.

6.3 N-vinylformamide – Montmorillonite Composites.

In this section the polymerisation of VFA was attempted between the layers of the clay using the initiator AIBN. Prior to any characterisation of such composites, VFA liquid alone was polymerised and characterised. The DRIFTS analysis of the product (Figure 6.10) shows some similarities with work by Spange[198,199,201] and other authors[197,200] who reported bands with the following assignments for polyvinylformamide – 3300 (NH stretch), 3050 (unsaturated CH stretch, presumably implying that there is some monomer left) 2870 (CH stretch) and 1712 cm^{-1} (C=O stretch). Bands for oligovinylformamide were reported at 3265, 3046, 2866, 1665, 1533, 1387, 1252 and 1134 cm^{-1} but without assignments. Note the significant difference of the carbonyl frequency for polymeric (1712 cm^{-1}) and oligomeric (1665 cm^{-1}) VFA. Based on these band positions alone for the carbonyl stretch they indicate that the carbonyl group is relatively freer in the polymeric VFA. This may be an indication that no hydrogen bonding can now place in the polymeric form as long (amorphous) chains stearically hinder this, whilst it is still possible in the oligomeric form of VFA.
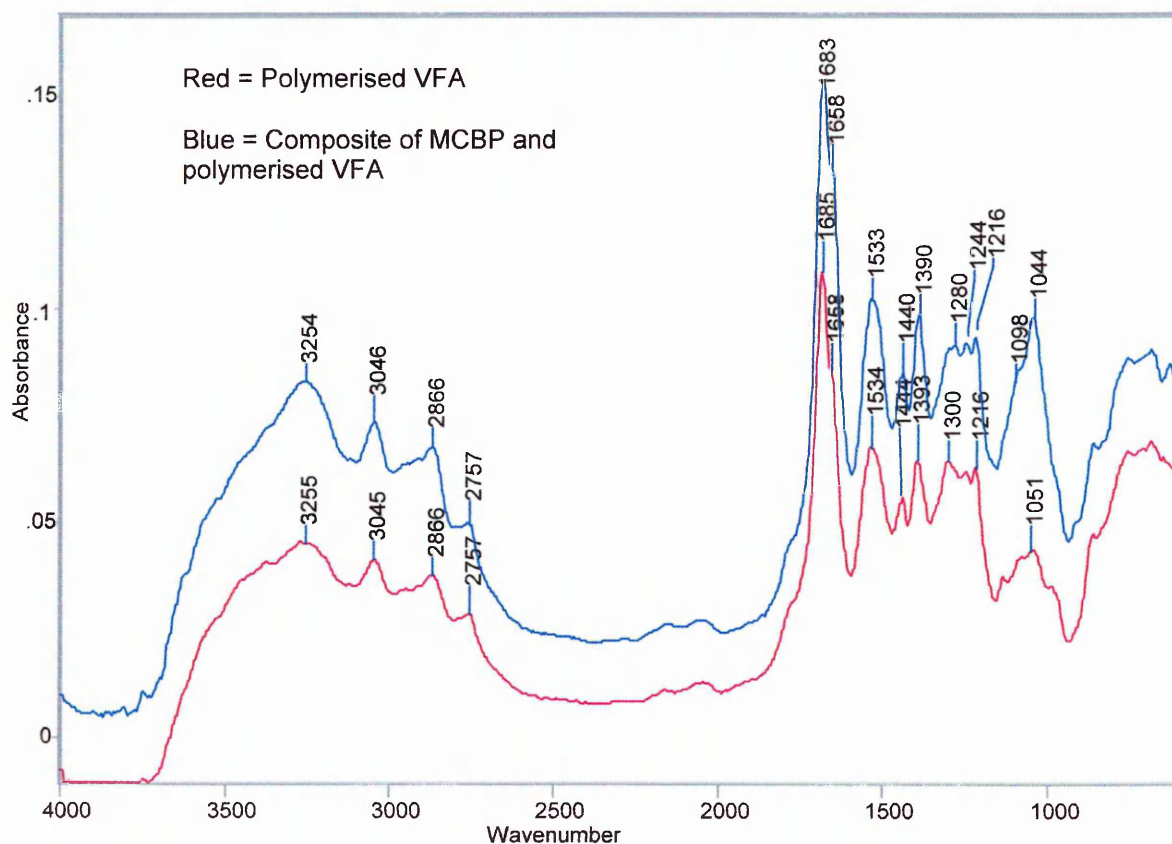
Figure 6.10 - DRIFTS spectra of Polymerised VFA and its clay composite.

The DRIFTS data obtained from the polymerised VFA product (no clay) in Figure 6.10 has bands at 3255, 3045, 2868, 2757, 1685, 1658 (shoulder), 1534, 1444, 1393, 1300, and 1216 cm^{-1}. This data when compared to that for polymeric VFA above shows additional bands at 2757, 1444 and 1216 cm^{-1}. The carbonyl band (for both the polymerised VFA and the clay + polymerised VFA composite) is at a frequency intermediate between the data reported for poly and oligovinylformamide. The unsaturated CH stretch at 3045 cm^{-1} indicates that there may be some unreacted monomer present. Assignment of these bands is given below:-

Band (cm^{-1})	Assignment
3267	N-H Stretch
3045	CH Stretch (C=C)
2868	CH Stretch
2754	CH_2 Stretch

1683	C=O stretch
1657 (shoulder)	C=O stretch
1537	C-N Stretch
1440	CH_2 deformation
1392	CH_2 deformation (C=C)
1296	CH deformation (C=C)
1246	Amide III
1215	
1132	

Table 6.2 – Band assignments for DRIFTS analysis of polymerised VFA

The presence of the CH_2 stretch at 2754 cm^{-1} indicates that some polymerisation has taken place as this band is not in VFA but is not observed by other authors as discussed above. Structures of the possible polymerisation products are shown below for convenience (left = straight chain product, right = branched product):-
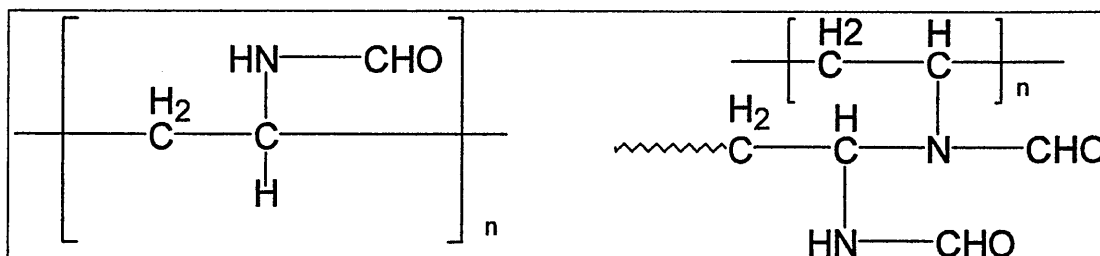
The DTG for this sample (Figure 6.11) shows maxima at 70, 135, 210, 250, 310 and 410 °C. The peak at 250 °C is near the boiling point of VFA (210 °C) and is most likely loss of unpolymerised VFA. The sample loses 80% of its weight by 500 °C, which is expected given the high organic content.

159
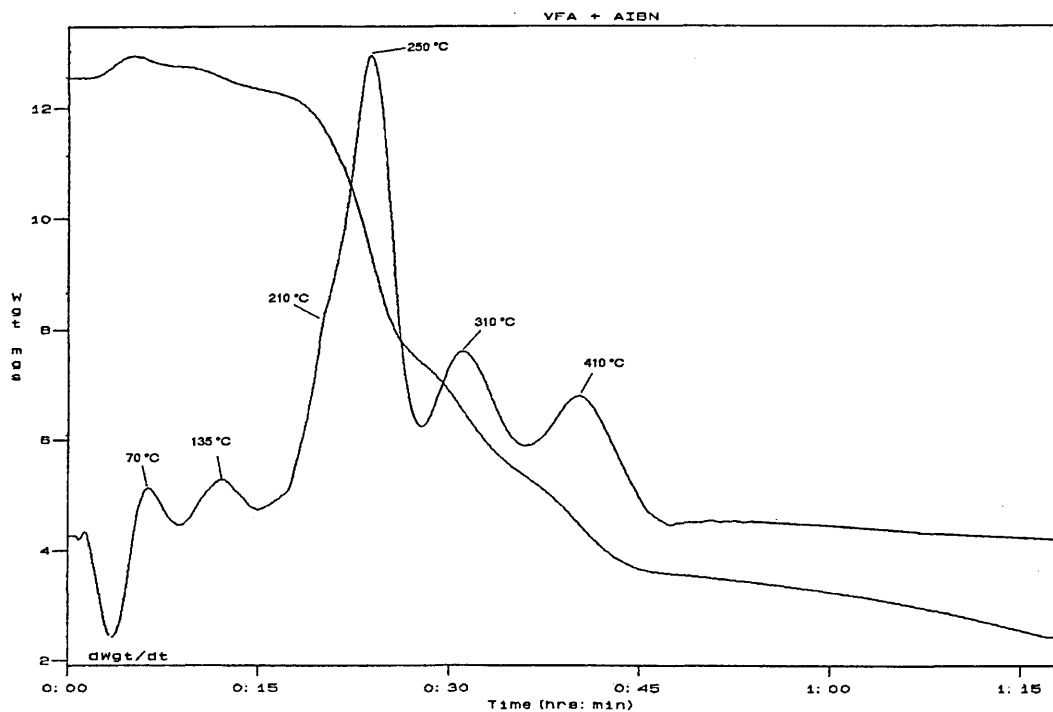
Figure 6.11 – TGA and DTG for polymerised VFA

The TIC from the TG-MS results (Figure 6.12) is shown with temperatures of the major peaks detected and these are also the temperatures for the most abundant ions detected in this sample by MS (Figure 6.13).
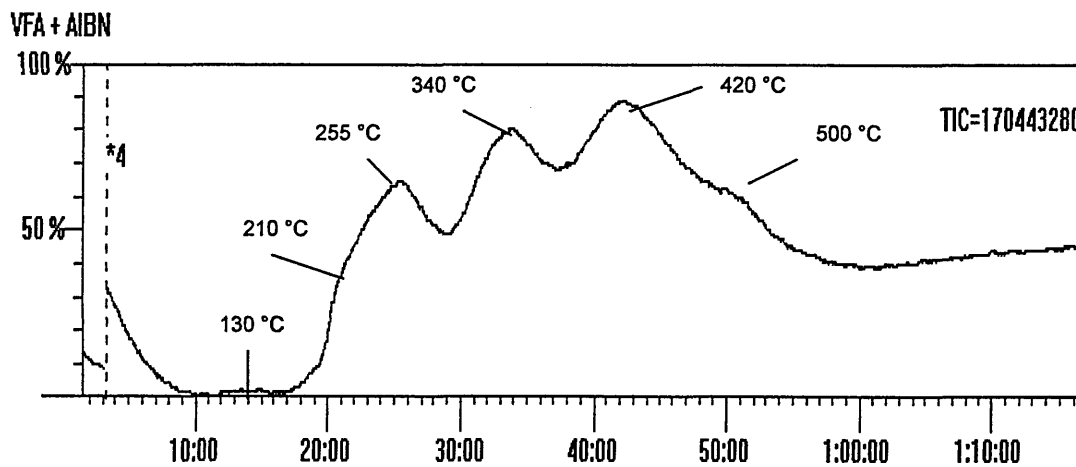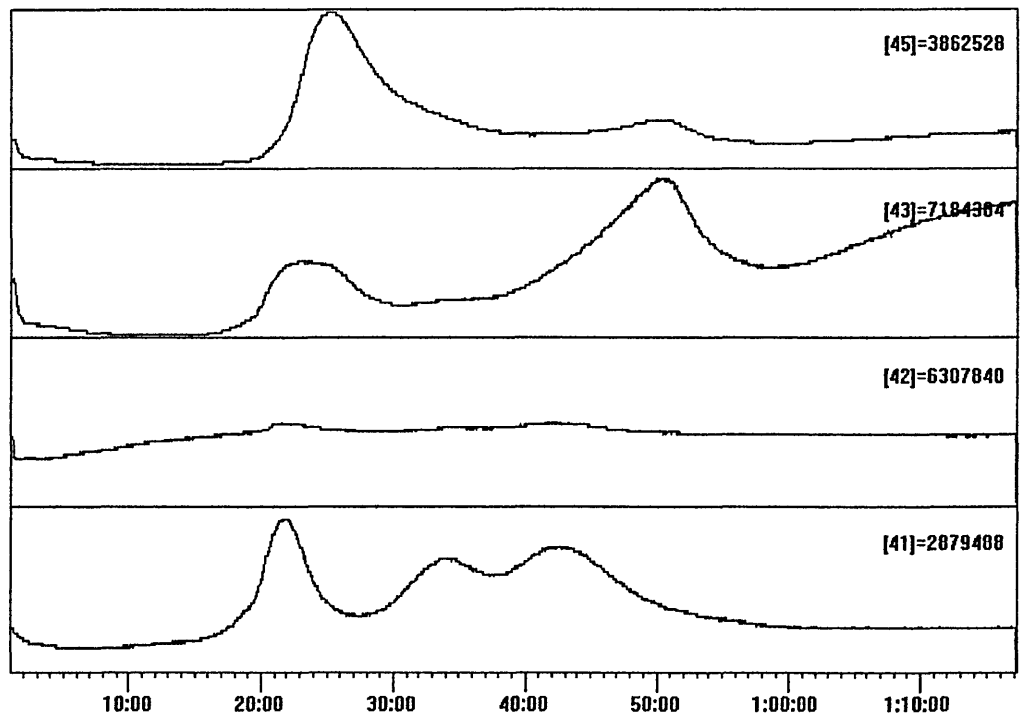

Figure 6.12 – TIC of polymerised VFA

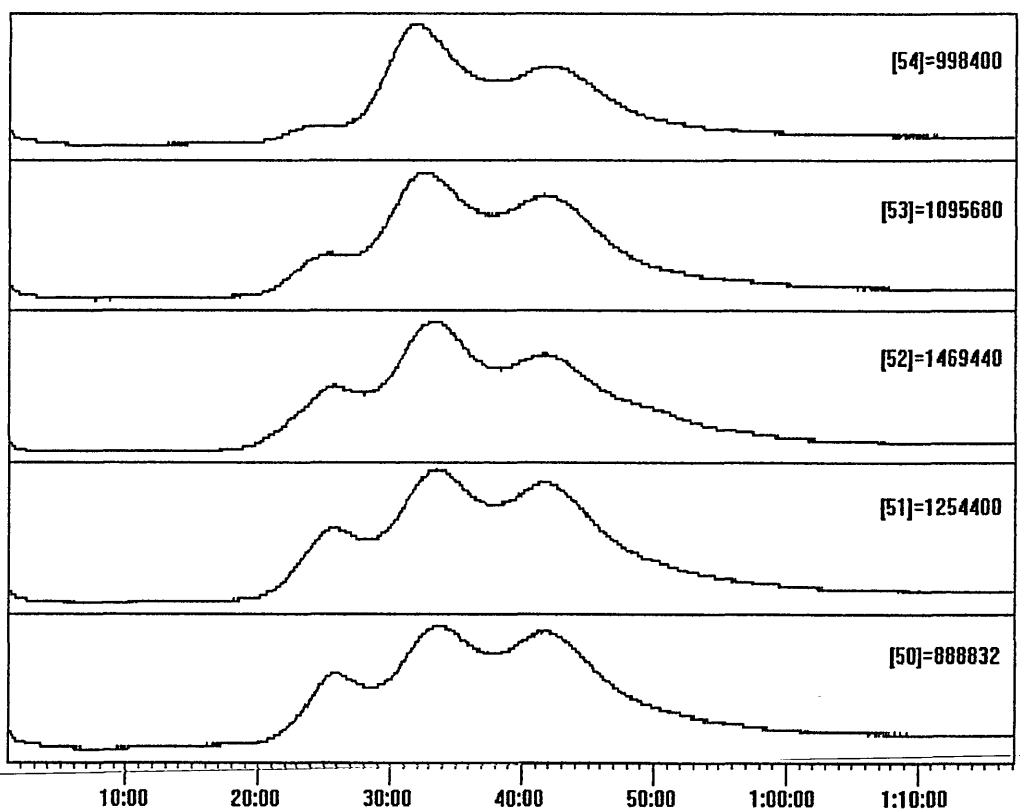Figure 6.13.1 – Reconstructed ion Chromatograms for EGA of polymerised VFA

[79]=929792

[78]=1133568

[77]=882688

[67]=903168

[66]=1304576

[65]=1267712

10:00   20:00   30:00   40:00   50:00   1:00:00   1:10:00

VFA + AIBN

[120]=365056

[107]=619008

[94]=423168

[93]=614400

[91]=684032

[80]=613888

[80]=613888

10:00   20:00   30:00   40:00   50:00   1:00:00   1:10:00
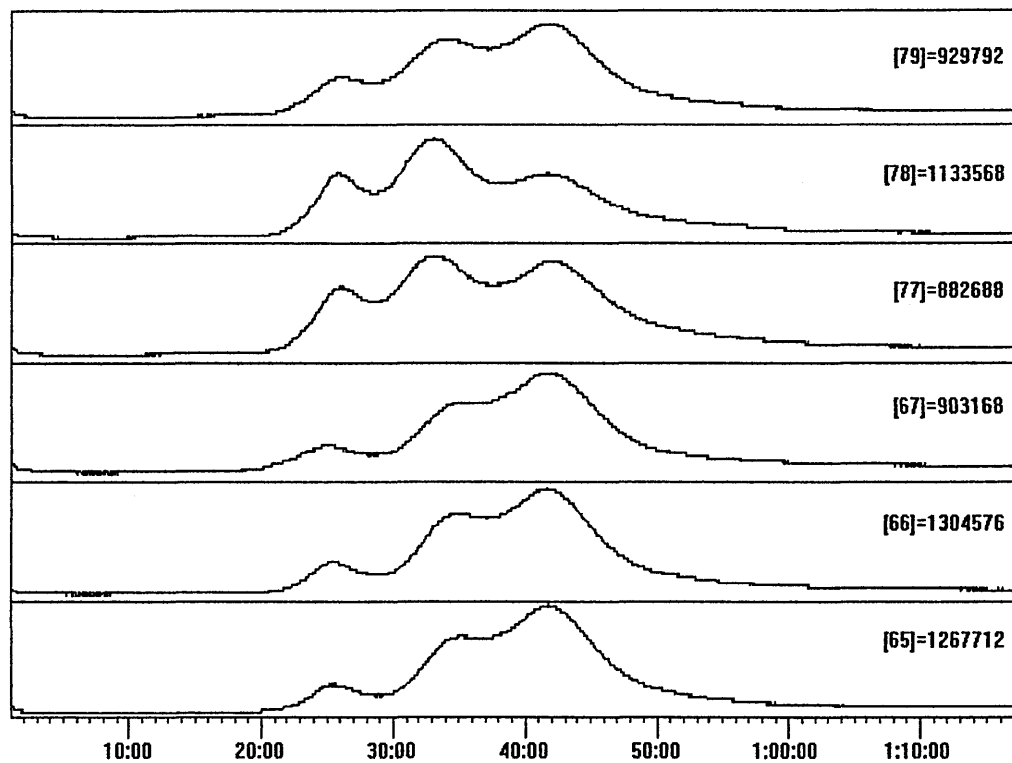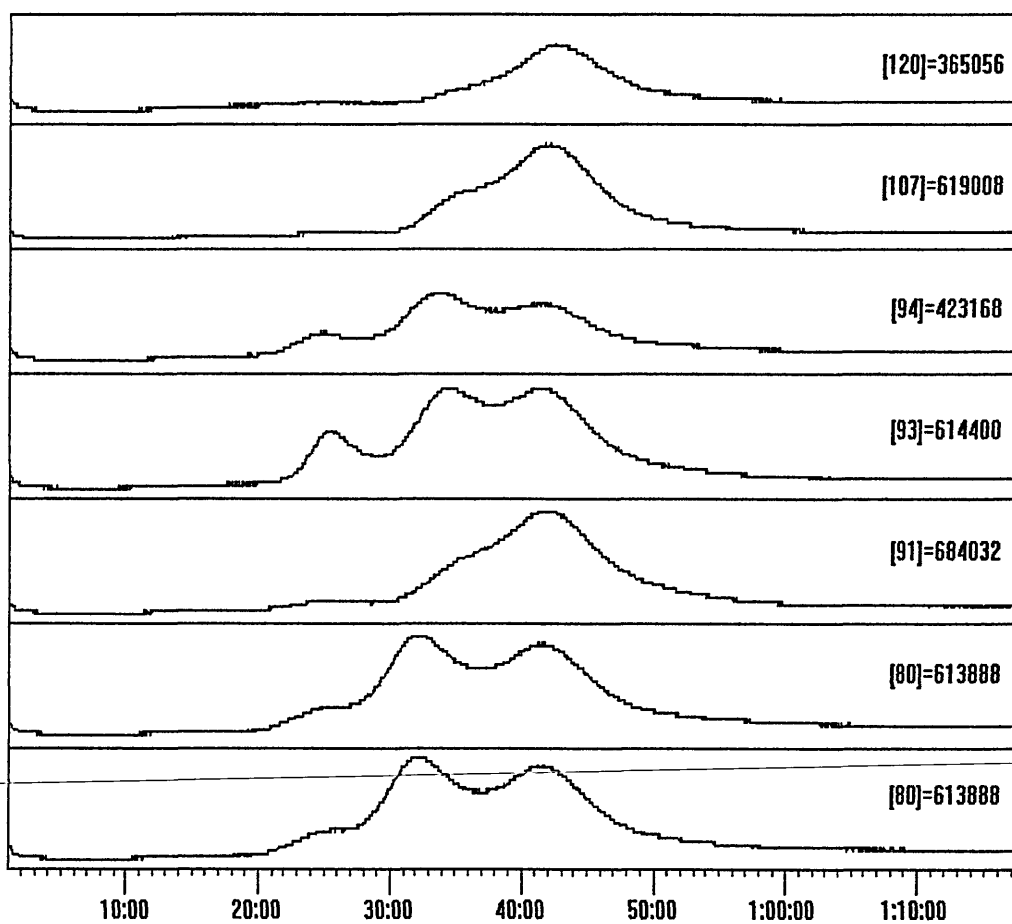
Figure 6.13.2 – Reconstructed ion Chromatograms for EGA of polymerised VFA

162

Temperature °C	Time (Mins)	Ions Detected
130	13	
210	21	41,43
255	25	43,45,50,51,52,53,54,65,66,67,77,78,79,80,91,93,94
340	34	50,51,52,53,54,65,66,67,77,78,79,80,91,93,94,107
420	42	50,51,52,53,54,65,66,67,77,78,79,80,91,93,94,107,120
500	50	43,45

Table 6.3 – Ion detected from EGA of polymerised VFA

This data shows the complex nature of the ions evolved in this analysis. The ions detected do not, once again correspond to any meaningful ions that may be anticipated upon degradation of polymerised or oligomerised VFA (Figure 6.9 illustrates some of these). Some of the ions may correspond to those observed in Figure 6.9 and be the unreacted monomer. These include m/z = 43, 66, 78, 79, 93 and 94.

As the method of manufacture for these composites involved mixing all the reactants together for one hour prior to polymerisation the XRD trace of MCBP stirred with VFA for one hour was recorded and this (not shown), shows that intercalation of the monomer into the clay has taken place, during this time.
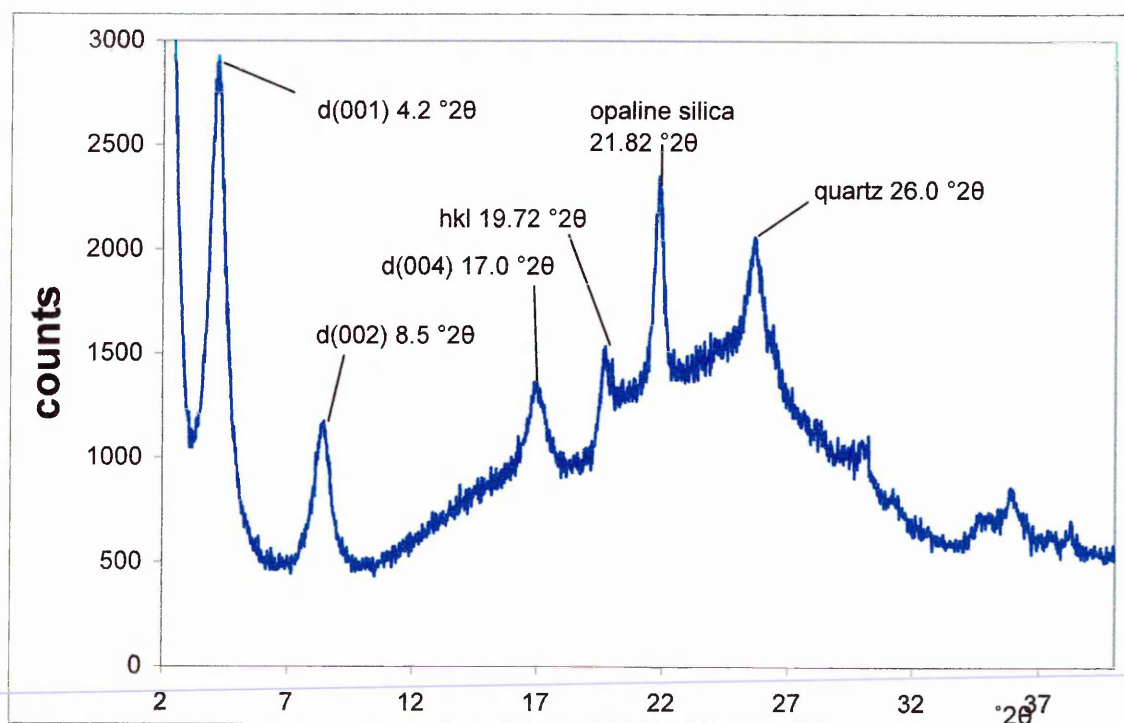

Figure 6.14 XRD trace of MCBP - VFA polymer

Figure 6.14 shows the XRD trace corresponding to the composite of MCBP and VFA where polymerisation has been initiated. The d – spacing remains at 21.0 Å, but the $d_{(001)}$ peak has decreased in intensity relative to the intercalate of VFA + clay (Figure 6.2). This decrease may be the result of the uneven surface presented for XRD analysis or it could indicate that there is some exfoliation and some intercalated nanocomposite formed. Note once again the presence and position of the hkl and opaline silica peaks at 19.72 and 21.28 °2θ respectively. The DTG for this sample (Figure 6.15) shows maxima at 130, 210, 250, 320 and 410 °C as compared to peaks at 70, 135, 210, 250, 310 and 410 °C for polymerised VFA without the clay. Thus the DTG traces for these samples are similar, which, given the large organic content (95%) of the sample containing clay is not unexpected. The dehydroxylation is not observed in the DTG as this is relatively small compared to the decomposition arising from the polymer.
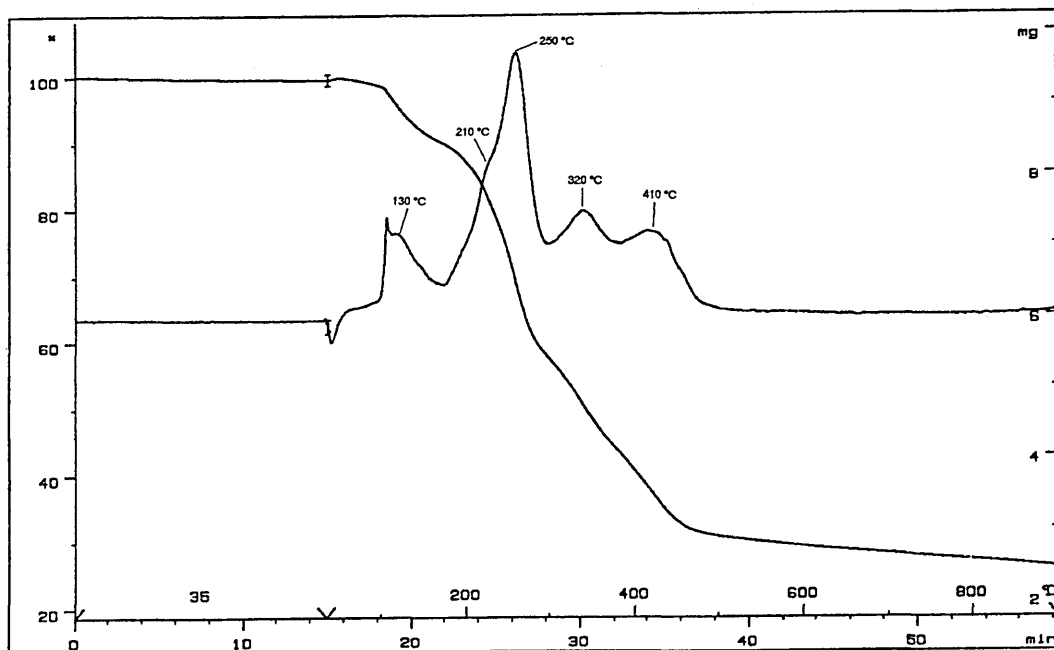

Figure 6.15 – TGA and DTG for MCBP + VFA Polymer

The DRIFTS spectrum for this composite (Figure 6.10) shows identical bands to the polymerised sample of VFA above with an additional band at 1046 cm^{-1}. This is clearly the Si-O stretch from the silica tetrahedra of the clay, which at 5% by weight in this sample is still detected by both DRIFTS and XRD. The band at 3254 cm^{-1} is also more intense, indicating that there is more NH in this sample.

6.3.1 Summary of Clay – Polymerised VFA Composites.

A schematic depicting the polymerisation of VFA within the interlamellar space of MCBP is shown below (Figure 6.15.1)
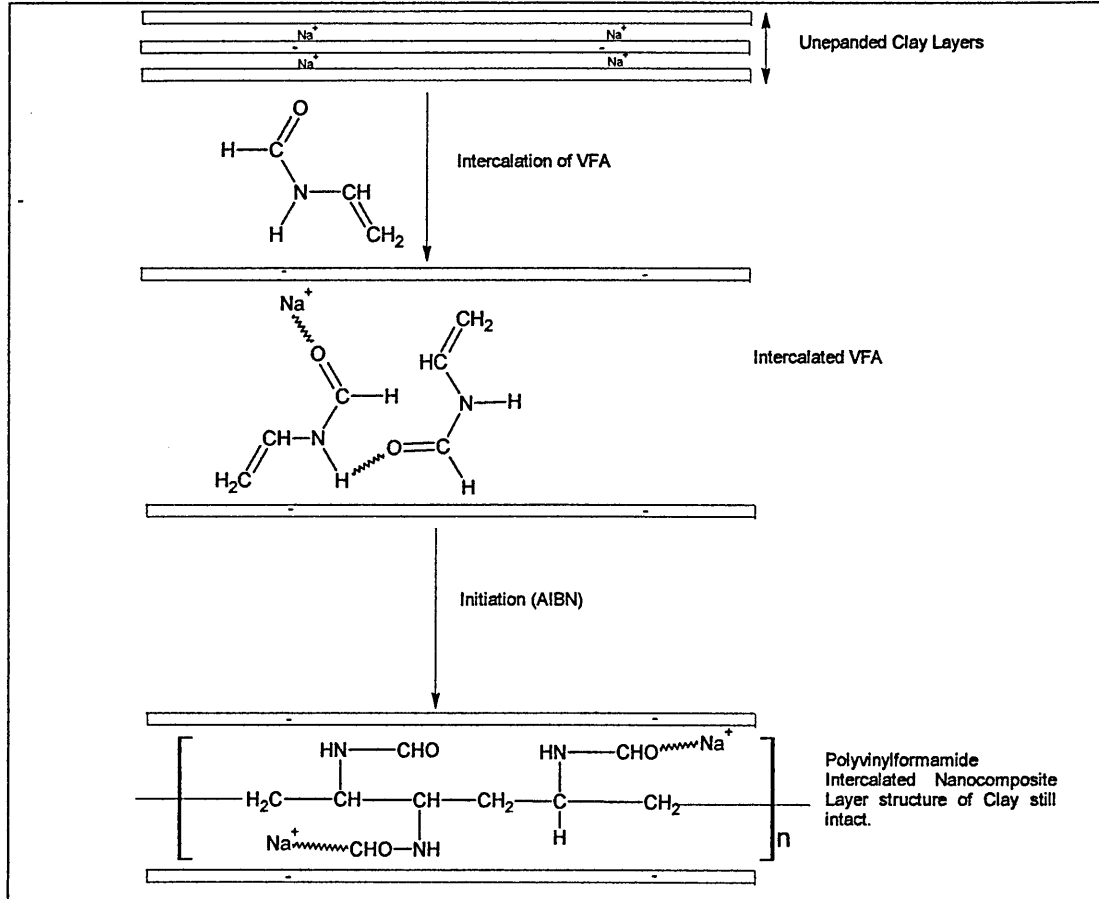
Figure 6.15.1 – Schematic of MCBP – Polymerised VGFA Composite

The following conclusions can be drawn from this data to illustrate the interpretation of this model.

* The $d_{(001)}$ spacing in this composite is 21.0 Å, which would appear to indicate that there has been no increase in the interlayer spacing of MCBP.

* However the $d_{(001)}$ peak has reduced intensity which may be an indication that some of the clay layers are being exfoliated thus causing a decrease in intensity of this peak (no peak being observed for exfoliated composite).

* DTG traces for both the polymerised VFA liquid and the polymerised VFA – clay composite were very similar as were the DRIFTS spectra, though the latter spectrum indicates some presence of the clay in the sample. Both spectra however exhibited similar band positions to those reported in literature. The position of the carbonyl

band (1683 cm^{-1}) was midway between the values reported for polymeric VFA (1712 cm^{-1}) and oligomeric VFA (1665 cm^{-1}).

* No meaningful results could be obtained from the complex EGA data.

6.4 The Use of a Polar Activator.

As seen in previous chapters the addition of a second organic molecule to a clay already expanded by solvent may cause further expansion and even in some cases, osmotic swelling. As discussed earlier (Chapter 4, Table 4.7) this relies on the second molecule added having a smaller donor number than the first (Table 6.0). It is also postulated here that if the MCBP – VFA system can be encouraged to swell as much as possible prior to polymerisation, then this would encourage exfoliation. Hence it was decided to use propylene carbonate to act as the polar activator, and encourage the expansion of the interlamellar space of MCBP (Figure 6.0).

It is already known that propylene carbonate (PC) when intercalated into a Na – montmorillonite results in a d – spacing of 20.1 Å. If the clay is treated with formamide prior to treatment with PC then osmotic swelling occurs. Hence it was decided to add PC to the reaction mixture replacing half of the VFA so that the final reaction mixture contained equal amounts by weight of VFA and PC, which is equivalent to a molar ratio of 1:1.4, VFA to PC. The weight of clay used remained constant at 5%. This reaction mixture was again stirred for one hour prior to polymerisation. The resultant polymerised product was a brittle particulate powder. It was noted that this product also did not dry overnight and was left for three days in air before it was considered to have dried. The XRD trace (Figure 6.16) shows once again that the d-spacing of this product is 21.0 Å, but the $d_{(001)}$ peak has this time decreased even more in intensity, with the trace overall showing more signs of an amorphous phase with the large background.
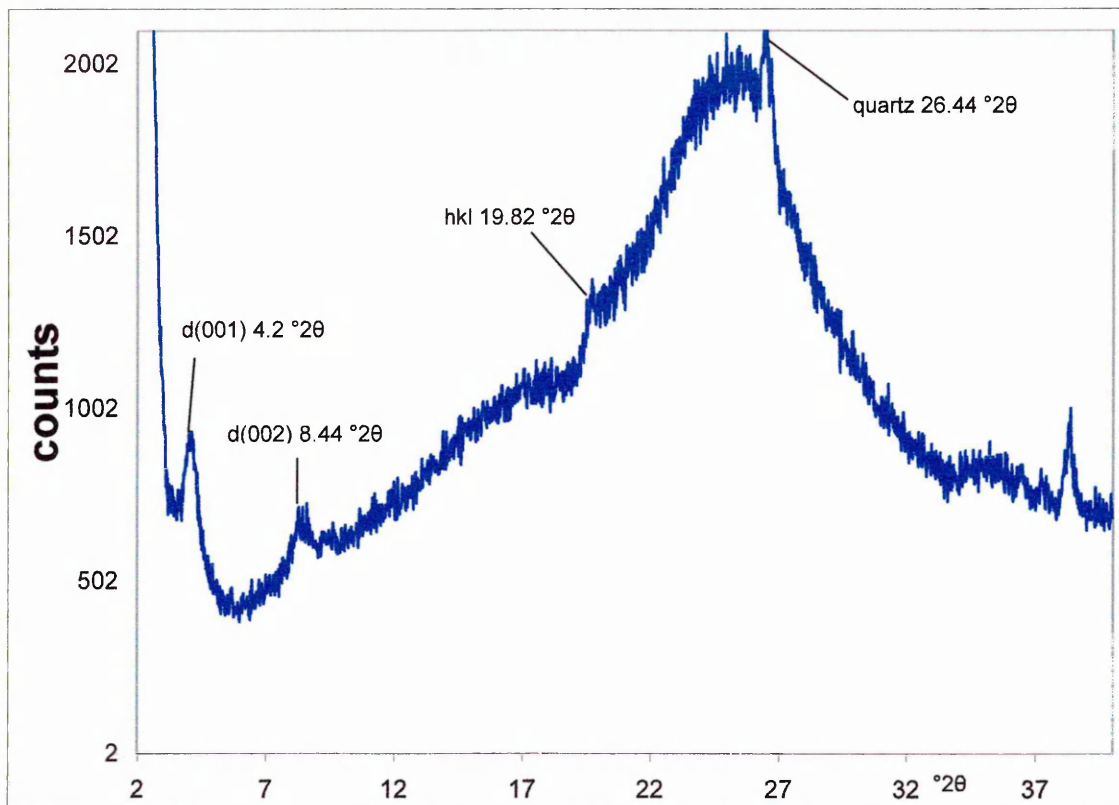
Figure 6.16 – XRD trace for MCBP – polyvinylformamide composite

Although the opaline silica peak at 21.28 °2θ is not seen due to the large amorphous background the hkl peak is still observed at 19.82 °2θ, as is the quartz at 26.44 °2θ.

The DTG for this polymerised VFA / PC mixture with and without the clay present (Figure 6.17.1 and 6.17.2 respectively) are identical with peaks at 70, 150, 210, 250, 330, and 410 °C. Compared with polymerised VFA alone (DTG peaks at 70, 135, 210, 250, 310 and 410 °C) these traces are very similar (peaks in both at 70, 210, 250 and 410 °C) apart from the peaks at 150 and 330 °C in the samples containing 50% PC. Assuming that most of the VFA is polymerised the peak at 150 °C may be occluded PC within the sample or PC loosely interacting with the clay surface.
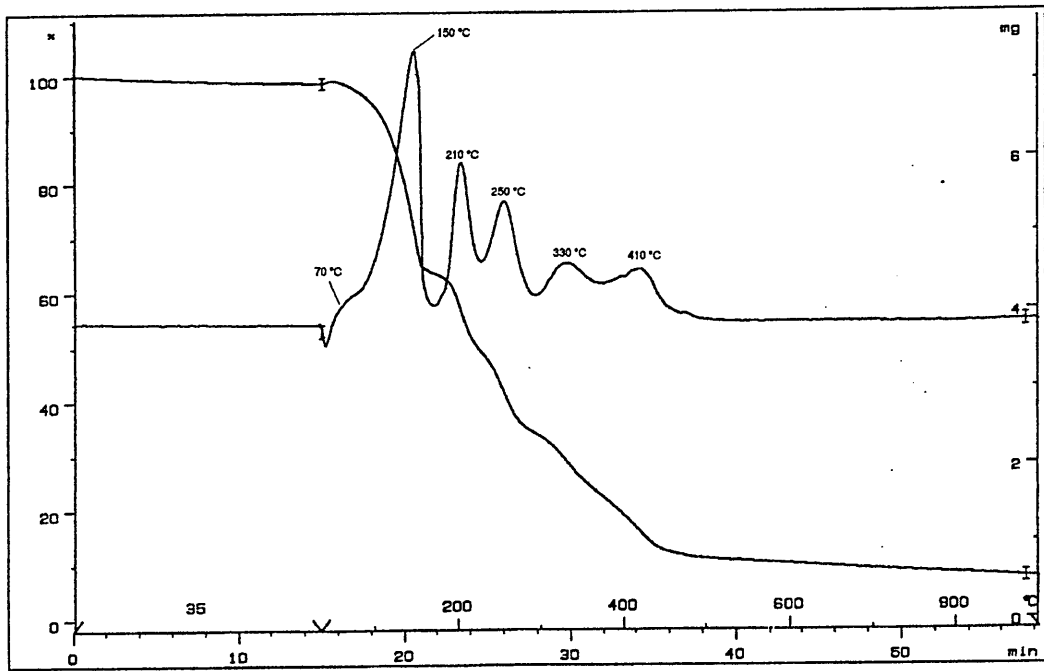
167

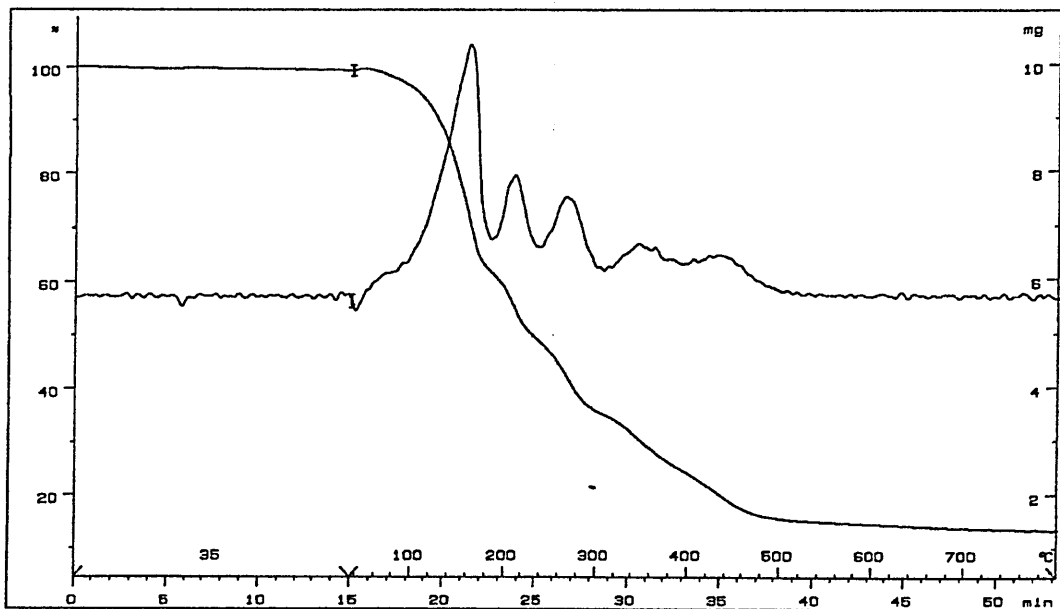Figure 6.17.1 TGA and DTG for Polymerised VFA +PC (No Clay)

Figure 6.17.2 TGA and DTG for Polymerised VFA + PC + Clay

The DRIFTS spectrum for this sample (Figure 6.18) reveals very little about this sample except for the carbonyl stretching band of PC. In liquid PC this is observed at 1792 cm^{-1} and as shown by the work of Onikata et al[175] (Chapter 4 Section 4.4.3) this band shifts by 20 – 30

cm^{-1} when intercalated via a water bridge and 40 – 50 cm^{-1} when coordinated directly to the interlayer cation.
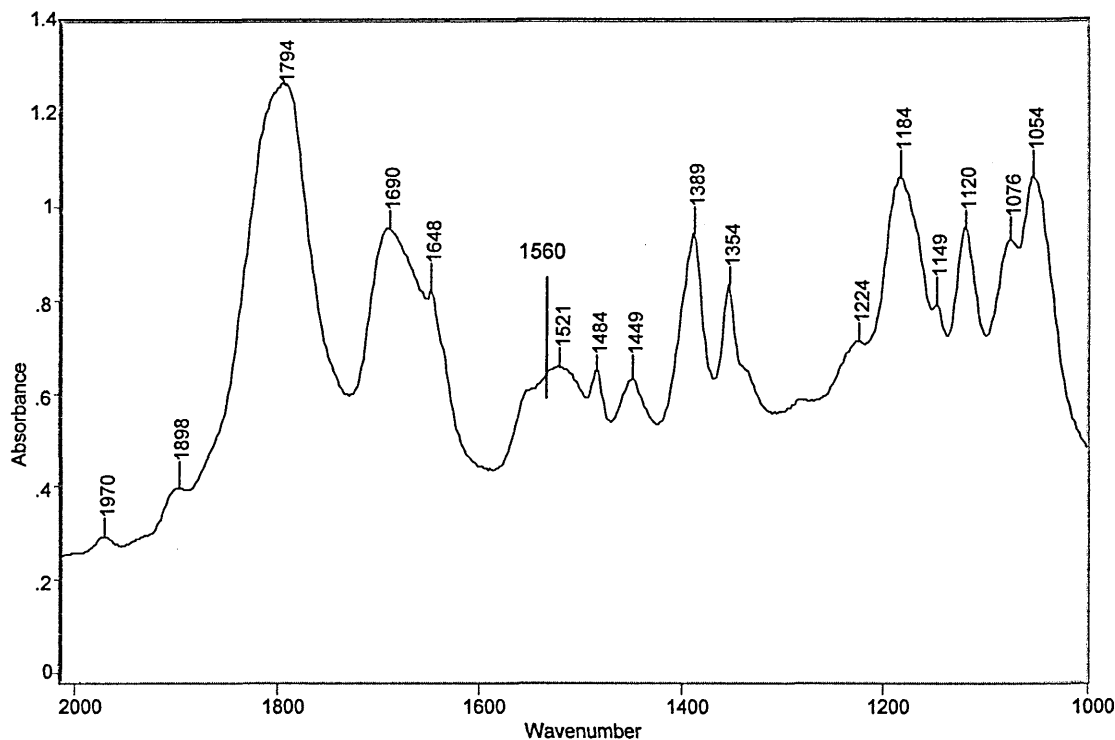

Figure 6.18 – DRIFTS spectrum of composite of 50% PC polymerised VFA and clay.

In this sample the carbonyl stretching band for PC is seen at 1794 cm^{-1} which would indicate that there is no interaction with the interlayer cations of the clay (though this is not unexpected given the relatively small amount of clay present), possibly weakly with the polymerised VFA (via NH group on polymer). This band at 1794 cm^{-1} is in an identical position to that of liquid PC and may indicate the presence of PC as liquid like clusters and hence account for the extra time required for this sample to dry. These clusters may be trapped with the polymerised VFA / clay structure or interacting weakly on the surface.

Comparing the DRIFTS spectra of the polymerised VFA and clay (Figure 6.10) and the DRIFTS spectrum of composite of 50% PC polymerised VFA and clay there also appears to some difference in the band positions. The former has bands at 1683, 1658, 1533, 1440 and 1390 cm^{-1} whereas the latter has bands at 1690, 1648, 1560, 1521, 1484, 1449, 1389 and 1354 cm^{-1}. The bands at 1690 and 1648 cm^{-1} are carbonyl stretching bands (amide I) but have moved to higher and lower wavenumber respectively. This may indicate some interaction with PC. Both the 1560 and 1521 cm^{-1} bands can be assigned to amide II bands.

The band at 1484 cm^{-1} is the CH_3 deformation arising from this group in PC. It is also interesting to note that the 1389 cm^{-i} band is seen in both oligomeric VFA and the clay – VFA composite. The 1354 cm^{-1} band is seen in polymerised VFA. These bands (1389 and 1354 cm^{-1} indicate that polymerisation has still taken place in this sample.

The presence of two amide I and II bands (1690, 1648 and 1560 and 1521 cm^{-1} respectively may also indicate that there is some interaction between PC and the polymerised VFA in the sample, but this is not supported by the position of the carbonyl band in PC (1754 cm^{-1}).

6.5 Changing the Ratio of the Polar Activator

6.5.1 Using 75% PC and 25% VFA

As the above results showed encouraging signs of a trend towards exfoliation due to the decrease in the $d_{(001)}$ peak in the XRD results it was decided to increase the concentration of the polar activator in the reaction mixture in the an attempt to push the clay towards exfoliation. Hence the amount of polar activator was increased from 50% PC to 75% PC, and polymerisation initiated under the same conditions described above, keeping the clay concentration fixed at 5%. The product this time however was a smooth flowing white powder, with none of the brittleness of the product obtained using 50% PC.

The resultant XRD trace (Figure 6.19a) shows a very weak $d_{(001)}$ peak corresponding to a d-spacing of 21.0 Å, and also a weak $d_{(002)}$ corresponding to a spacing of 10.5 Å. If this sample is repacked and presented once again for XRD analysis(Figure 6.19b) then there remains no trace of either of these peaks. However the hkl and opaline silica peaks remain at 19.74 and 21.48 °2θ respectively and are clearly still observed, indicating that although there is very little evidence for peaks relating to the presence of the clay via the $d_{(001)}$ and $d_{(002)}$ which relate to the layer structure (interlayer spacing) of the clay, the clay is still present in this sample and can still be detected efficiently as the presence of the hkl peak. The opaline silica peak also remains.

This indicates the possibility again of some exfoliated and some non – exfoliated (though possibly intercalated) nanocomposite formation. The fact that the $d_{(001)}$ has decreased steadily as the concentration of PC is increased is key to this observation, as this may indicate increasing exfoliation.
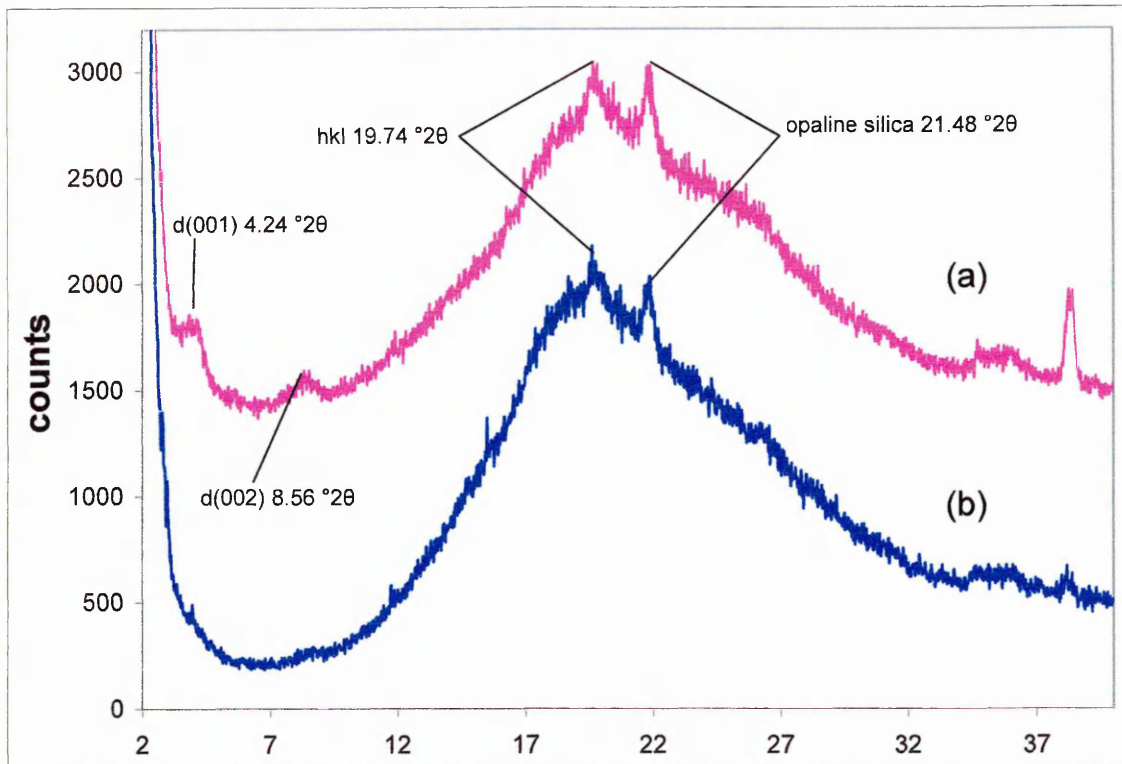
Figure 6.19 – XRD trace of composite prepared using 75% PC

It should be noted that in all of the composites the clay concentration is constant at 5%, as is the organic content at 95%, yet the clay is still detectable. In order to ascertain the ability of the polar activator (PC) to osmotically swell this system the $d_{(001)}$ spacing was measured prior to initiation of polymerisation (but after stirring for one hour). This shows (Figure 6.20) that the clay has swollen to 26.0 Å.
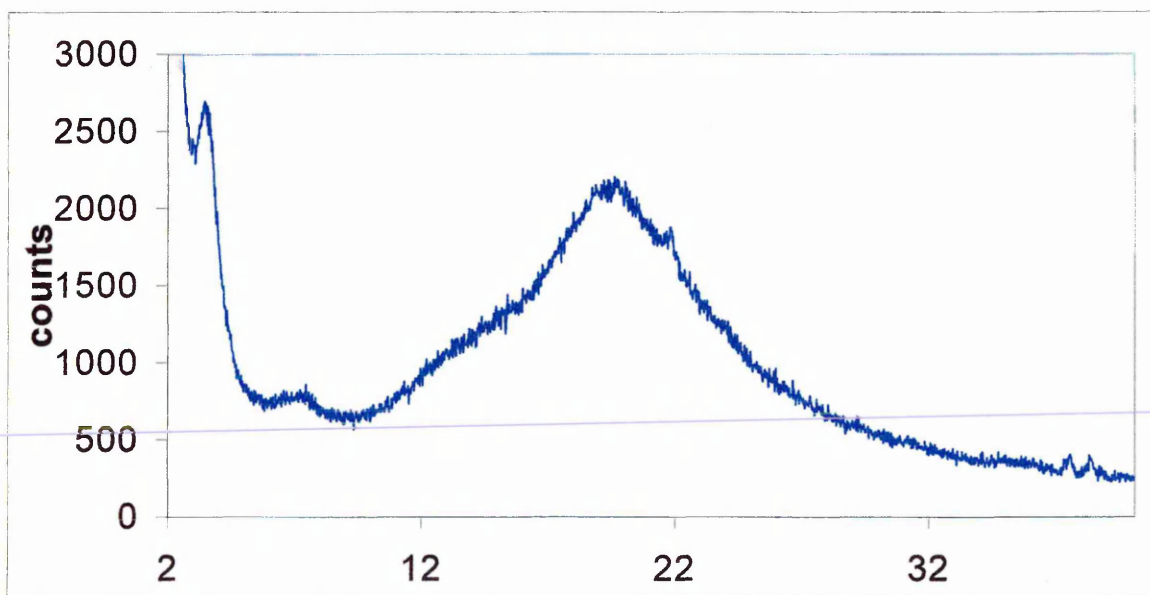

Figure 6.20 – Reaction mixture prior to initiation

The DTG for this sample (Figure 6.21.1) shows maxima at differing temperatures than those for the composites with 50% of PC at 150, 200 and 250, 320 and 410 °C. If the DTG results are examined for the sample without any clay present (Figure 6.21.2) then the maxima observed are at the same positions. The peak at 250 °C is also more intense when there is clay present. Compared to the sample containing 50% PC (DTG peaks at the 70, 150, 210, 250, 330, and 410 °C for the 50% sample), then these samples are very similar except for the peak at 70 °C in the sample containing 50% PC (Figure 6.17).
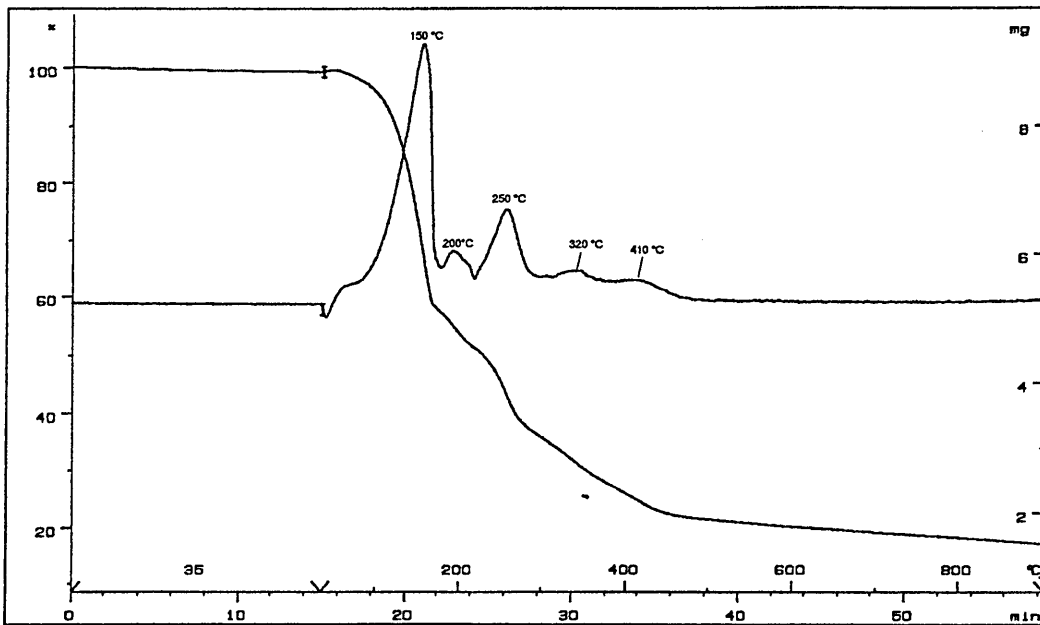

Figure 6.21.1 – TG and DTG for composite containing 75% PC, VFA and clay after polymerisation

In the samples here containing 75% PC the intense peak at 150 °C has an associated weight loss of 40% when clay is present and 70% it the absence of clay. This is a significant difference and may indicate that the sample was thoroughly dry. The corresponding weight losses for the 150 °C peaks in the samples containing 50% PC are both 38%, so there is a slight increase in the weight loss associated with peak as the amount of PC is increased but only in the absence of clay.

The peaks at 210 and 250 °C are discussed in more detail in the next section.
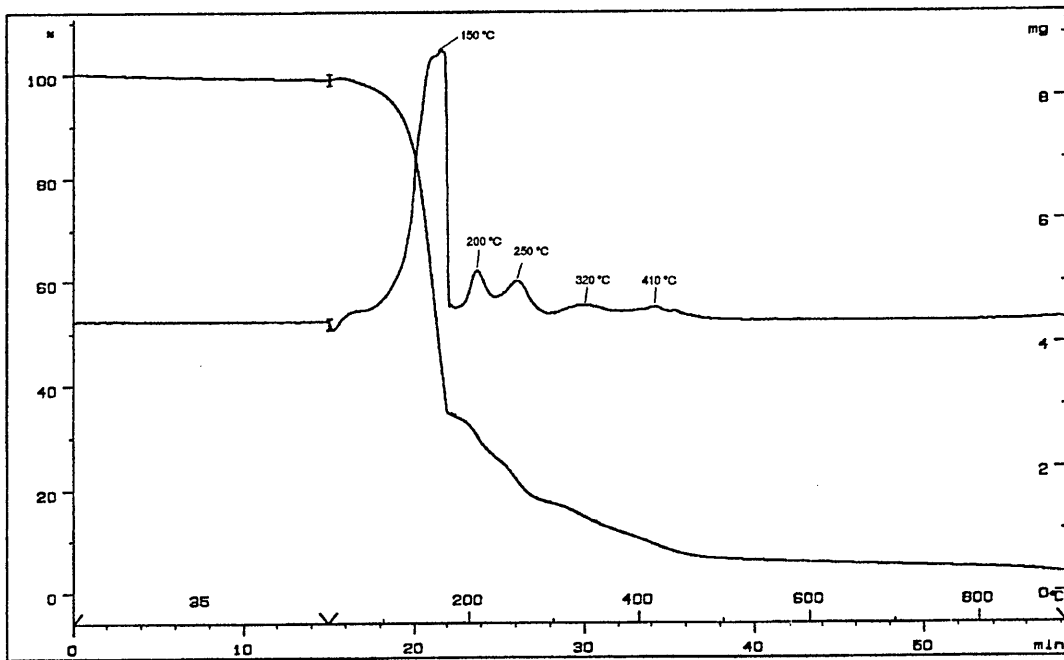
Figure 6.21.2 – TGA and DTG for 75% PC, VFA composite without clay, after polymerisation.

The DRIFTS spectrum for this sample (Figure 6.22) is almost identical to the sample containing 50% PC (Figure 6.18) with the carbonyl stretching band at the same frequency of $1794\ cm^{-1}$. Differences are apparent in the width of the $1671\ cm^{-1}$ band that may encompass the 1690 and $1648\ cm^{-1}$ band seen in the 50% sample, and also the $1535\ cm^{-1}$ that, in the 50% sample is seen as two bands at 1560 and $1521\ cm^{-1}$. The increased amount of PC in this sample may account for the differences in these band positions as there may now be more interactions between PC and the polymerised VFA of varying strength, hence the broadening of these bands. Note however that there is no data presented here as to the morphology of the VFA polymer / Oligomer produced and this may affect the ability of PC to interact with it.
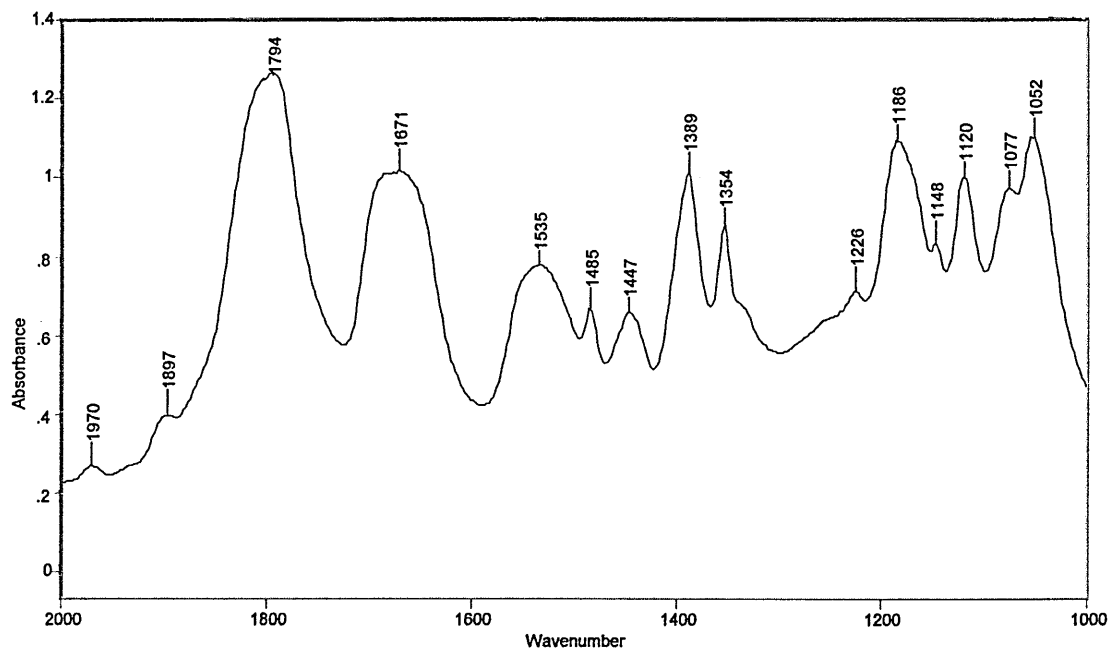
173

Figure 6.22 – DRIFTS spectrum of composite containing 75%PC polymerised VFA and clay

6.5.2 Increasing to 80% PC

The XRD trace for this sample prior to polymerisation gives a $d_{(001)}$ spacing of 24.3 Å and a $d_{(002)}$ at 12.15 Å. When polymerised this sample yields a product which is again a free flowing white powder. The determined d- spacing of this product (Figure 6.22) was found to display a $d_{(001)}$ spacing of 21.0 Å at an angle of 4.1 °2θ, though, like the sample containing 75% PC, this peak is an extremely weak feature. However, once again the hkl peak (19.78 °2θ) and the opaline silica peak (21.48 °2θ) are still observed indicating that the clay is still present in the sample, but the most of the clay layers are now too far apart, too disordered or far from the surface to be detected.
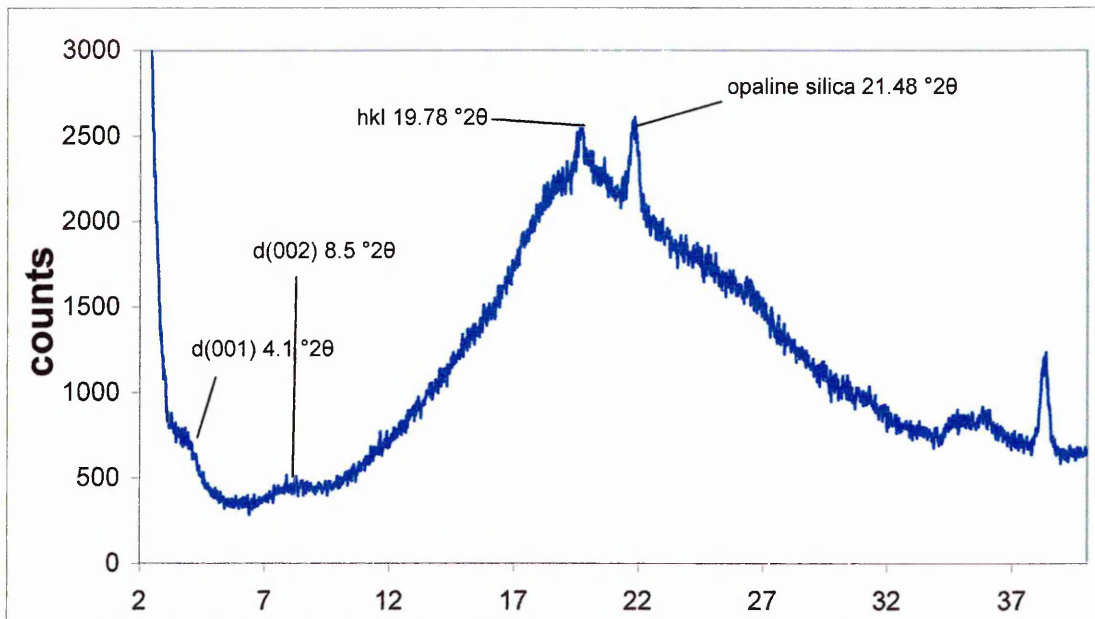
Figure 6.22 – XRD trace of composite containing 80% PC, VFA and clay after polymerisation.

The DTG for this sample exhibits maxima at 150, 200, 250 320 and 410 °C, both with and without the clay present (Figure 6.23). Thus these samples are similar to those containing 75% PC.
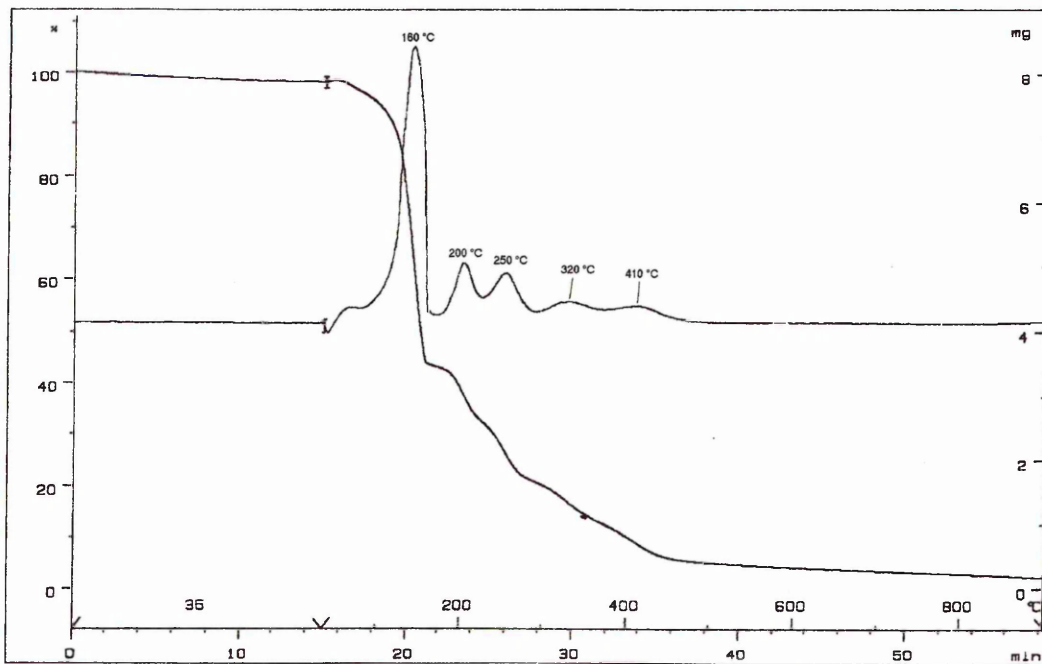

Figure 6.23.1 TGA and DTG for 80% PC, VFA composite without clay, after polymerisation
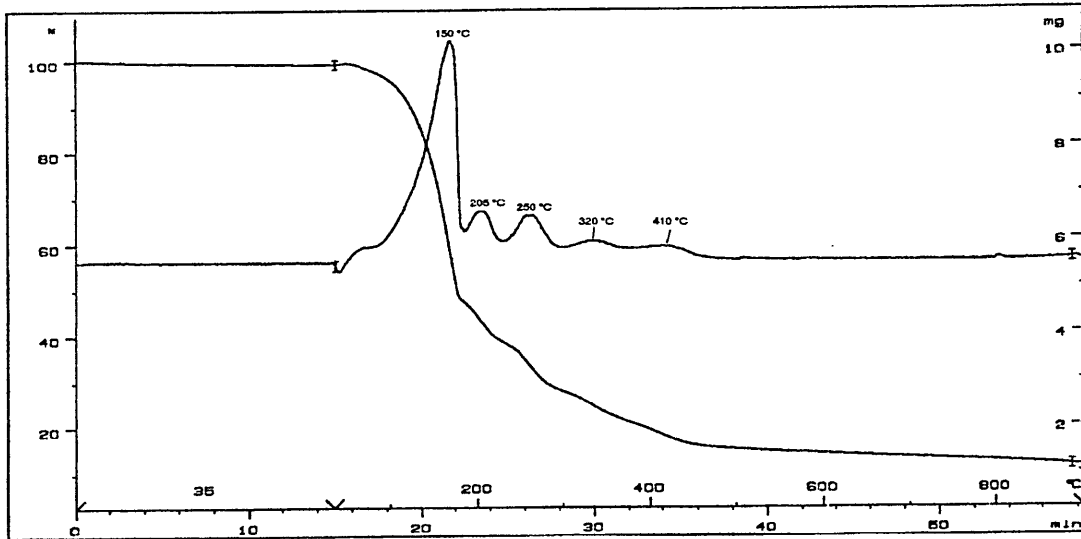
Figure 6.23.2 – TGA and DTG for 75% PC, VFA composite + clay, after polymerisation

A summary of the findings from the TG traces of the composites prepared thus far is given

Tables 6.4.1 and Table 6.4.2.

Sample	% Weight Loss for Individual DTG Peak				
	Up to 175-180 °C (PC)	200 / 210 °C	250 °C	320 °C	410 °C
Polymerised VFA Alone	0	Shoulder	36	16	17
Polymerised VFA + 50 % PC	35	11	12	4	12
Polymerised VFA + 75% PC	70	5	6	-	-
Polymerised VFA + 80% PC	55	8	6	-	-

Table 6.4.1 – DTG weight losses for major peaks in composites without clay present

Sample	% Weight Loss for Individual DTG Peak				
	Up to 175-180 °C (PC)	200 / 210 °C	250 °C	320 °C	410 °C
Polymerised VFA Alone	0	Shoulder	31	12	13
Polymerised VFA + 50 % PC	35	12	11	7	13
Polymerised VFA + 75% PC	40	5	5	-	-
Polymerised VFA + 80% PC	50	5	5	-	-

Table 6.4.1 – DTG weight losses for major peaks in composites with clay present

176

As indicated, the weight loss up to 175 – 180 °C is assigned to loss of PC from these samples. Note that the sample containing 70% PC VFA and no clay may not have been entirely dry due to the amount PC in this sample, 70% as determined. There is a reasonable agreement otherwise in the amount of PC in these samples (with and without clay).

The figures in table 6.4.1 and 6.4.2 show that the weight losses for the individual peaks are greater for the samples where the clay is not present. The peaks at 320 and 410 °C are too small at 75 and 80% PC to calculate the weight losses. With the exception of that at 200 °C, which appears at 210 °C in some samples the peaks in the above tables (at 200 / 210, 250, 320 and 410 °C), are present when polymerisation of VFA has been initiated. Thus as the amount of PC added increases the weight losses associated with these peaks which are characteristic of polymerised VFA decrease. This is not wholly unexpected given that the amount of VFA in these composites has decreased. Adding PC introduces a DTG peak at 150 °C in the samples, the weight loss of which increases when the amount of PC present increases from 50 to 75%.

6.5.3 Increasing to 90%PC

Increasing the amount of PC to 90% prevented polymerisation from occurring in this system. This is most likely due to the small amounts of VFA now left in the reaction mixture. Nevertheless, the XRD trace (Figure 6.25) obtained shows that the layers of the clay have expanded to 22.0 Å, with the $d_{(001)}$ peak appearing very distinct.
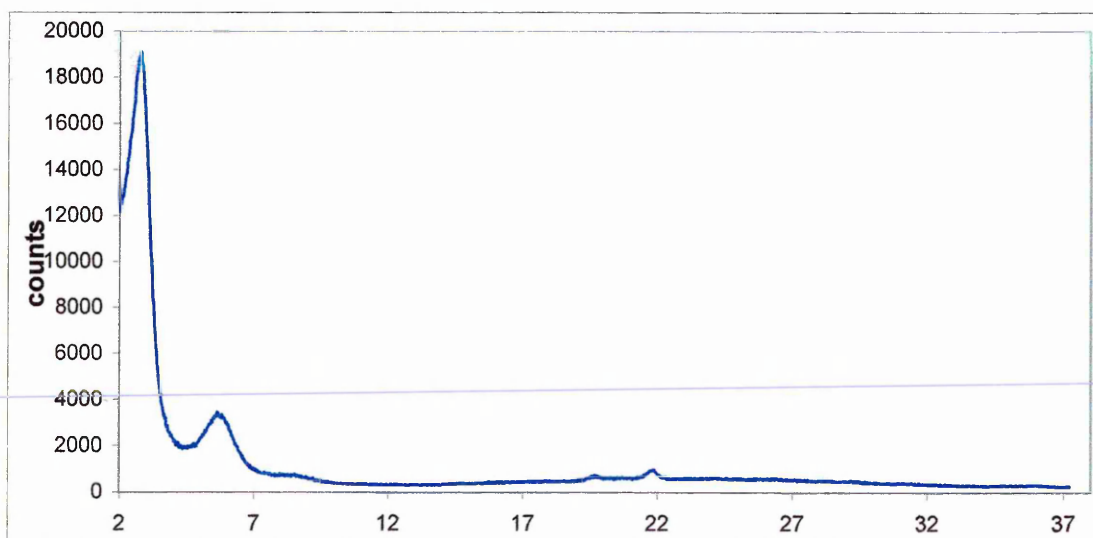

Figure 6.25 – Composite of MCBP 90% PC and 10 % VFA.

6.6 Summary of MCBP VFA Composites made using Polar Activator

Attempts to make composites using VFA alone result in composites with a $d_{(001)}$ spacing of 21.0 Å, hence a polar activator was employed for reasons previously discussed. The composites made using the polar activator (PC) to swell the clay prior to polymerisation show that as the amount of PC added increased there is a steady decrease in the intensity of the $d_{(001)}$ peak, until it is barely detectable. Note that the clay itself is still present in these samples as the hkl peak, which do not decrease in intensity, are still detected via XRD (Figure 6.26.1). The amount of clay in all composites prepared is constant at 5% by weight.
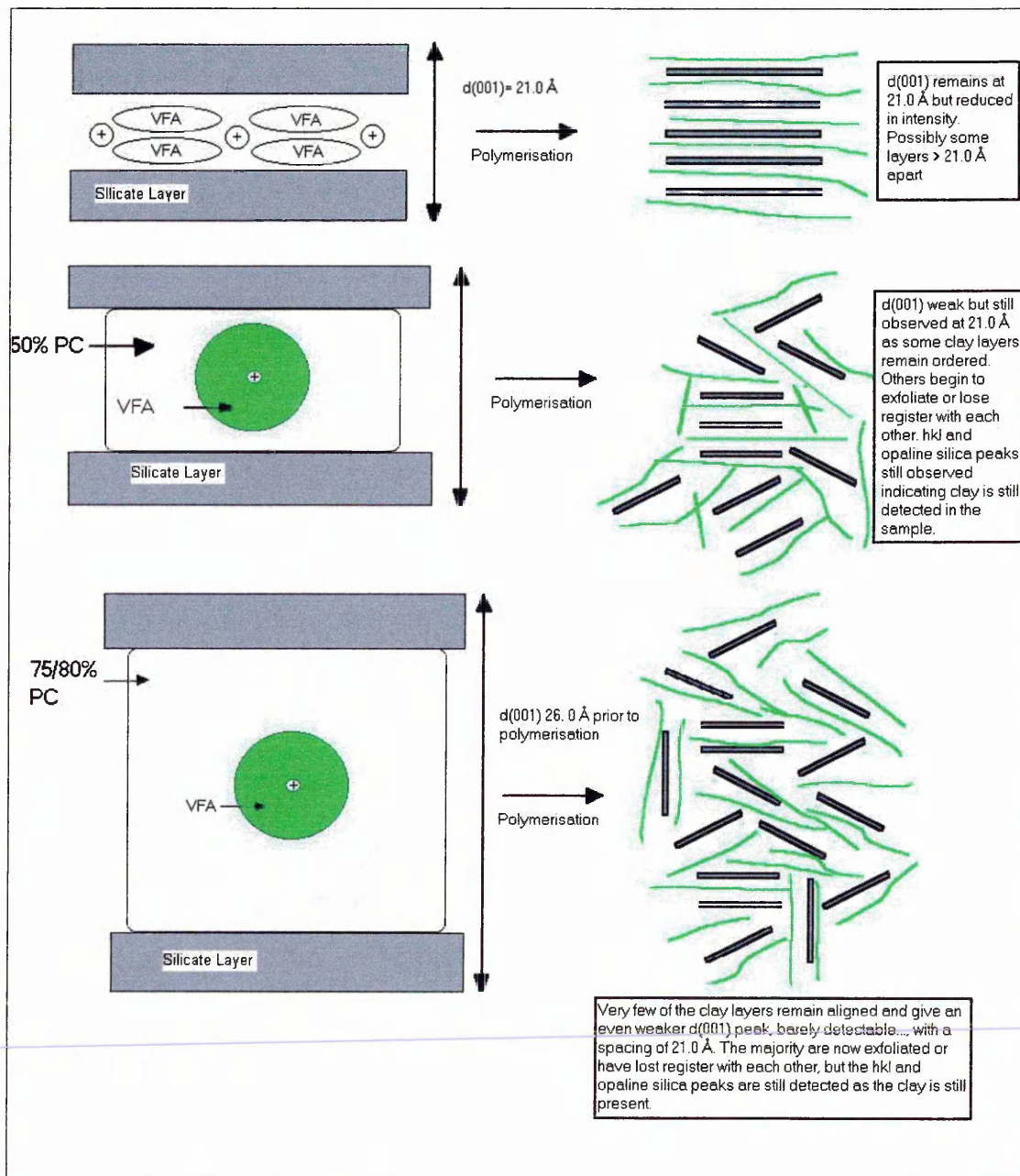

Figure 6.26.1 – Summary of Composites made with and without polar activator (PC).

178

There is evidence to suggest that the $d_{(001)}$ spacing of the clay and solvents (monomer and polar activator) prior to polymerisation is, as anticipated, greater than the spacing of the clay plus the monomer alone (21 and 26 Å respectively).

As the amount of PC is increased the amount of VFA decreases. This may mean that at lower VFA contents it is possible to direct the reaction of VFA into the clay interlayer where the relative concentration of VFA is considerably higher than in the bulk phase (outside the clay layers). As the amount of PC is increased to 90% there appears to be a distribution problem of getting the VFA into the interlayer or alternatively the concentration of VFA is now too dilute to promote polymerisation within the interlayer of the clay.

The PC added to these reaction mixtures may become occluded (this may be apparent from the DTG peaks 150 °C but TGA alone cannot provide evidence for this) and trapped within the composite structure, which could account for the long drying times required. There is no evidence from DRIFTS spectra that the carbonyl group on PC is interacting with any of the sites in the clay (a shift to lower wavenumber). There are however differences in the band positions for the amide I and amide II bands as the amount of PC added is increased.

DTG peaks for composites where VFA has been polymerised show peaks at 200/210, 250, 320 and 410 °C, with IR bands in good agreement with published data for both polymeric and oligomeric VFA.

The process by which this occurs is best illustrated in Figure 6.26.2.

- When the clay is treated with the monomer (VFA) and polar activator (PC), prior to polymerisation the $d_{(001)}$ spacing is 26.0 Å (Figure 6.26.2).

- After polymerisation the absence of the $d_{(001)}$ peak indicates that exfoliation of the clay within the VFA – polymer matrix has occurred.

- The presence of the band at 1794 cm^{-1} in the DRIFTS spectrum indicates that some PC remains, most likely trapped within the exfoliated composite.

- The peak in the DTG trace at 150 °C also supports this, given that this peak only appears when PC is added and that there is more PC present than VFA (which may account for the intense peak observed). PC also does not react with VFA or participate in the polymerisation reaction.
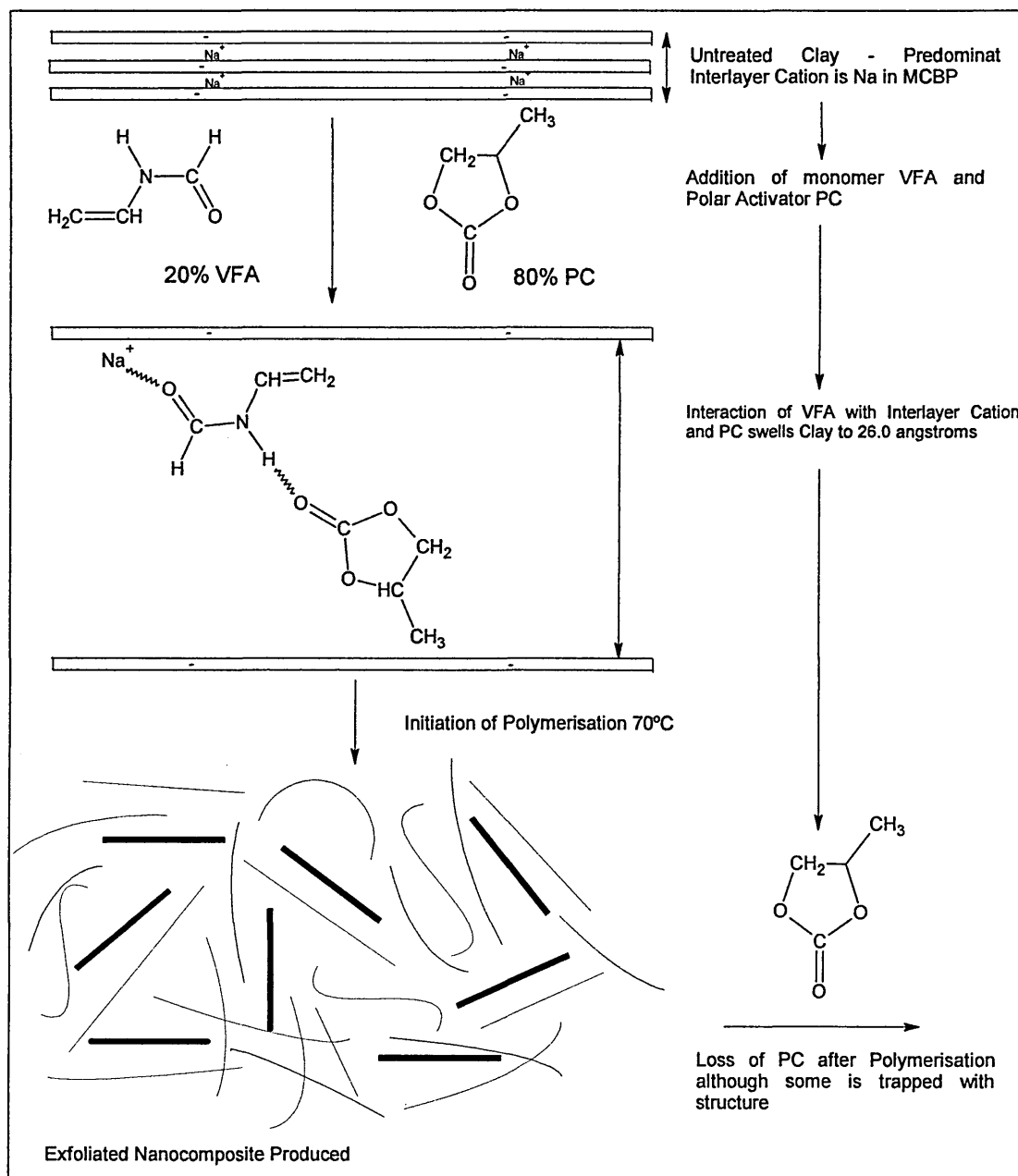
179

Figure 6.26.2 - Schematic depicting the exfoliation of MCBP when treated with VFA and PC.

6.7 Intercalates of VFA with Kaolin and Halloysite.

An attempt was made to intercalate VFA into both kaolin and halloysite by stirring them for a period of 3 days at room temperature. The excess VFA was decanted off the clay and the clay itself was left to dry on filter paper in air at room temperature. Each sample (VFA treated kaolin and halloysite) took 1 week to dry and the XRD patterns were measured as a wet paste of the sample (Figure 6.27). No initiation of the VFA monomer was attempted at this stage.
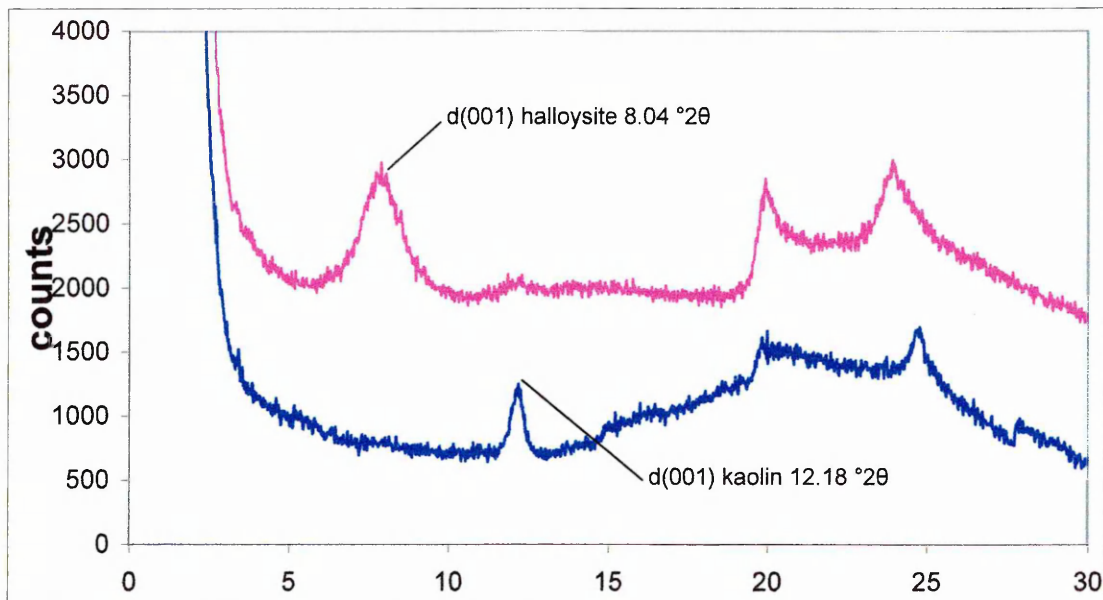
Figure 6.27 – XRD traces of Composites of VFA with kaolin and Halloysite

The results show that the kaolin still exhibits a weak $d_{(001)}$ at 12.18 °2θ corresponding to unexpanded kaolin at 7.2 Å, which implies that there is either no expansion or this sample is largely exfoliated and there still remains some unexpanded kaolin. Examination of the DRIFTS spectrum (recorded with the now dry sample) of the VFA treated kaolin sample may be advantageous via study of the kaolin hydroxyls (Figure 6.28).
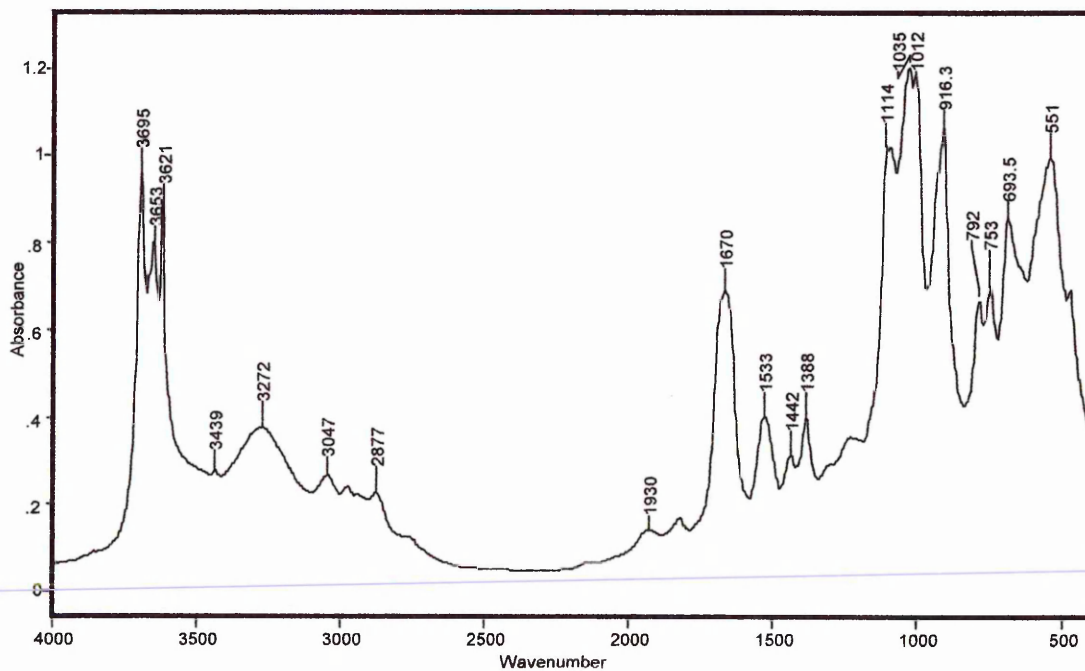

Figure 6.28 – DRIFTS spectrum of VFA treated kaolin, dried.

181

Reduction in intensity or the evolution of new bands near to the hydroxyl stretching bands of kaolin (seen here at 3695, 3663 and 3621 cm^{-1}) are indicative of intercalation into kaolin taking place (by means of hydrogen bonding within the interlayer space of kaolin with the kaolin hydroxyl as seen in Chapter 5), but since neither of these are observed then it is unlikely that intercalation has taken place. If exfoliation to a large extent had taken place then there would be gross changes in the 3695, and 3653 cm^{-1} bands observed in this sample as these are represent the hydroxyl groups in the octahedral sheet which hydrogen bond to hold the layers of kaolin together (recalling that exfoliation involves the layers of clay to be far enough apart that interaction by whatever means cannot take place). No change would observed in the 3620 cm^{-1} band as this is not involved in interlayer hydrogen bonding. However, bands remain at 3272, 3047, 2877, 1670, 1533, 1442 and 1388 cm^{-1} in sample. As this sample was dry there remains the possibility that the VFA is interacting with the surface of kaolin and is loosely bound, but no VT-DRIFTS was performed which would indicate how strong the interaction is (these bands may be lost at low temperatures). Assignments for these bands, which are indicative of VFA are given earlier in this chapter (3280, 3150, 3030, 2890, 2780, 1680, 1650, 1510, 1400, 1390 and 1250 cm^{-1}), but note that the 1670 cm^{-1} band, which is the carbonyl stretching band, now does not have a shoulder on the low wavenumber side. This may be an indication of there being only one type of C=O interaction with kaolin and not a second band due to interaction with more than one type of interlayer cation as seen in smectites. The position of this band is also 10 cm^{-1} lower than that in liquid VFA, indicating interaction of the carbonyl group with the surface of kaolin.

The DTG results (Figure 6.29) show two large peaks centred at 210 and 490 °C and a small peak at 110 °C .The 490 °C peak is the dehydroxylation of kaolin and the 210 °C corresponds to the boiling point of VFA, suggesting that this is VFA being lost from the sample. This itself may indicate that VFA is lost from the surface of kaolin, and this is a loss of 13%, which is large for a non – expanded kaolin. This observation is in good agreement with the DRIFTS data (no evidence of intercalation by examination of kaolin hydroxyl bands) but not the XRD (reduced intensity of $d_{(001)}$). Therefore due the long drying time involved with this sample – one week – the sample may not be totally dry.
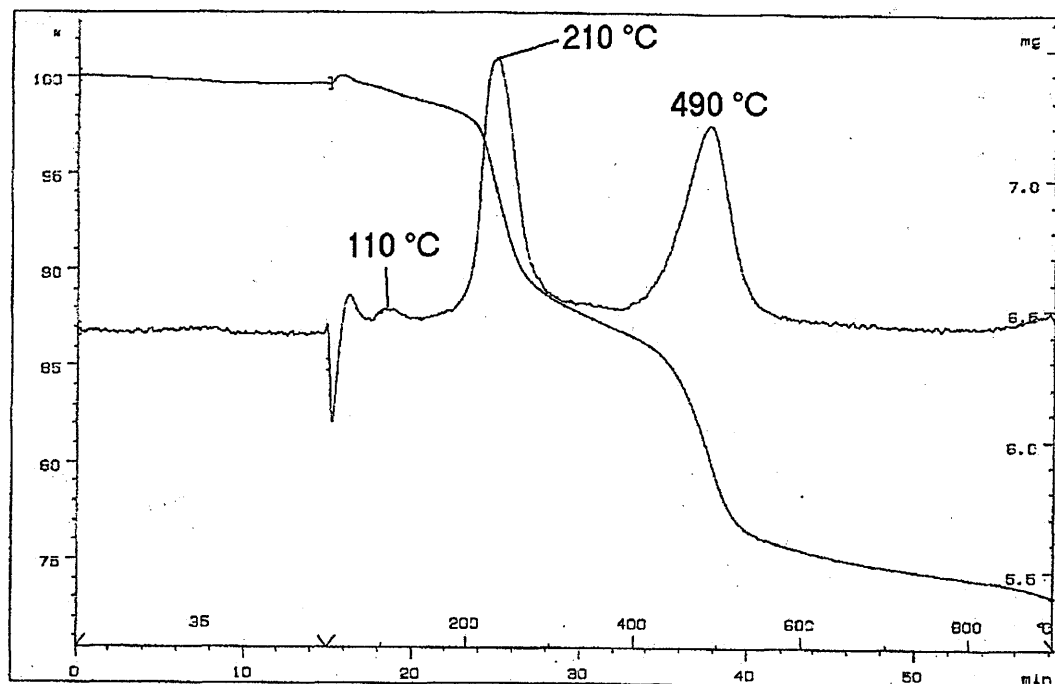
Figure 6.29 TGA and DTG trace for VFA treated kaolin sample.

No other information as to the interaction (if any) of VFA with kaolin can be drawn from these results.

The results for halloysite are somewhat different. The XRD trace (Figure 6.27) shows that a peak present at 8.04 °2θ corresponds to a d – spacing of 11.1 Å, which implies that there has been some expansion in this sample (halloysite itself – 10.2 Å in its naturally occurring hydrated form). This may be a significant increase in layer expansion as the VFA may have replaced the interlayer water of halloysite and expanded the halloysite by 4 Å. The VT – XRD results (Figure 6.30) show that this peak is present at 300 °C though reduced in intensity with another phase present with a $d_{(001)}$ spacing of 7.2 Å – clearly this is halloysite which has desorbed the intercalate at elevated temperatures.
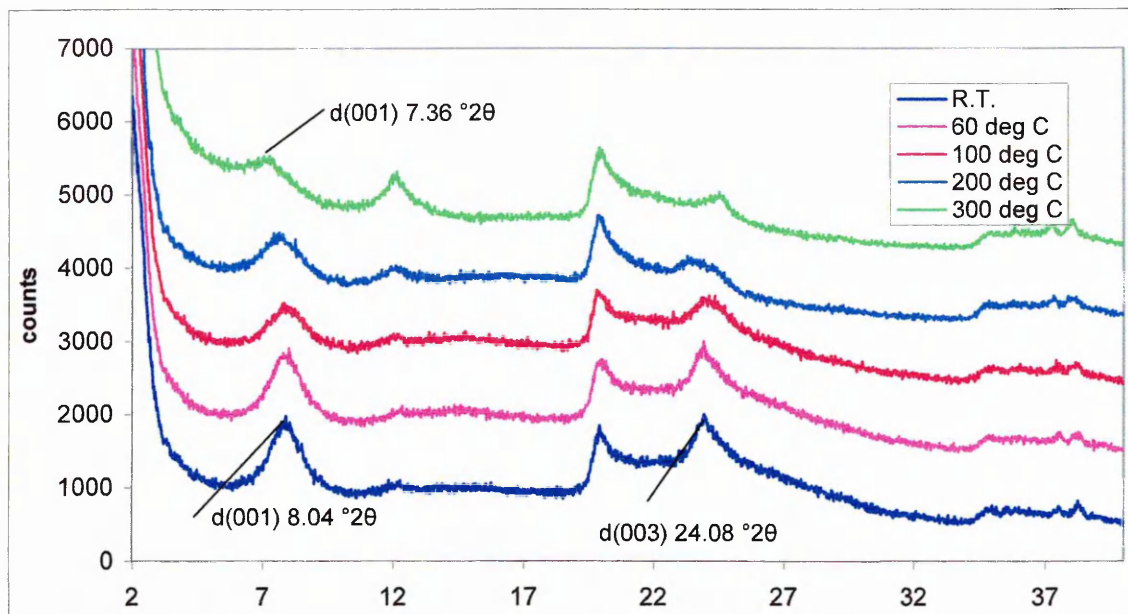
Figure 6.30 – VT – XRD of halloysite – VFA

Also observed is the movement of the $d_{(001)}$ of the 11.1 Å phase – as the temperature is increased this moves to a higher angle which corresponds to an increase in the d – spacing of the halloysite i.e. the layers of halloysite are moving further apart. This may imply that thermal polymerisation is taking place, but no such increase to a higher angle was observed in the $d_{(001)}$ peak in the VT-XRD results of the VFA – montmorillonite intercalate (Figure 6.3), and no initiator has been added to this sample of VFA treated halloysite. This change may be a change in orientation of the intercalated VFA upon heating. Nevertheless, there remains a $d_{(001)}$ present to 300 °C (the maximum for VT-XRD measurements), which is intercalated VFA. The DTG of the halloysite – VFA sample (Figure 6.31) shows peaks at 115, 140, 210, 310, 430 and 460 °C and has an overall weight loss of 43%. This weight loss is very large for halloysite and it is unlikely that this will all be intercalated VFA. The two peaks at 430 and 460 °C are also very broad and, as subsequent TG-MS will reveal that are many ions detected at these temperatures.
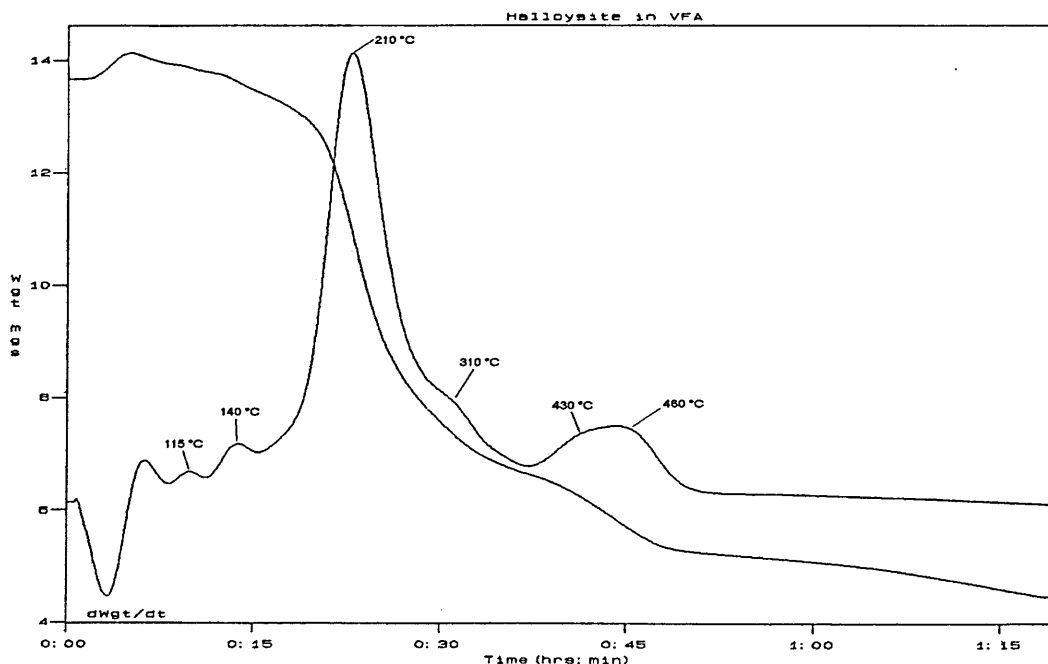
184

Figure 6.31 – TGA and DTG trace for VFA treated Halloysite

It is not possible to compare this DTG trace to that of its intercalated montmorillonite counterpart (which has DTG peaks at 110, 120, 155, 160, 280, 290, 300, 320 and 620 °C) as the interaction between the clay and VFA is different for each clay. However for the halloysite – VFA sample the peaks at 115 and 140 °C may be loss of the hydrogen bonded water from the hydrated halloysite structure. The peak at 460 °C is the dehydroxylation of halloysite. The peak at 210 °C is at the boiling point of VFA and may therefore be loss of this. This TG analysis is also not comparable with the kaolin – VFA sample due to its large weight loss.

The DRIFTS spectrum of this intercalate (taken with the dried sample) also indicates that there may be intercalation (Figure 6.32). Bands are observed at 3386, 3289, 3049, 2883, 1672, 1530, 1442, 1390, 1313 and 1233 cm^{-1}. There is a significant loss in intensity of the halloysite hydroxyls, as compared to the untreated halloysite. The carbonyl stretching frequency has also moved to 1672 cm^{-1} (amide I) and there is no shoulder on this band as previously seen in the montmorillonite intercalates. Compared with the VFA treated kaolin (bands at 3272, 3047, 2877, 1670, 1533, 1442 and 1388 cm^{-1}) there is a difference in the band position of the N-H stretch – 3272 cm^{-1} in kaolin (also broad) and 3386 and 3289 cm^{-1} in halloysite (3280 cm^{-1} in liquid VFA and 3390 and 3288 cm^{-1} in VFA-MCBP intercalate). If the VFA is intercalated in halloysite then the position of the NH stretch indicates its inability to

hydrogen bond whilst intercalated, whilst if VFA is surface bound in kaolin, it may still be able to do so. However the 3289 cm^{-1} band in the VFA treated halloysite is a broad band and may encompass bands at a lower frequency (possibly revealed by the required VT-DRIFTS analysis, though this band is seen in MCBP-VFA and stable to 275 °C). This may indicate hydrogen bonding between the VFA and halloysite interlayer (and therefore intercalation).
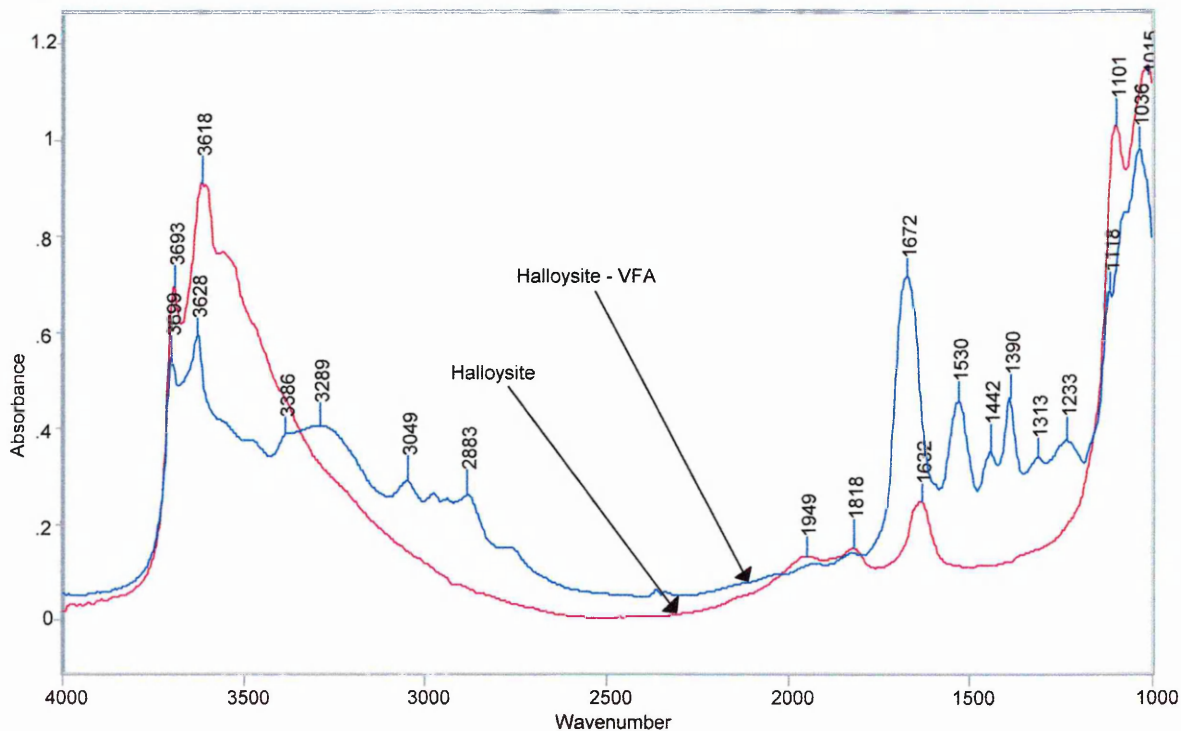
Figure 6.32 – DRIFTS spectrum of Halloysite and Halloysite – VFA

The TIC from the EGA analysis (Figure 6.33) shows peaks at 160, 265, 330 and 450 °C, and the reconstructed Ion Chromatograms subsequently follow (Figure 6.34).
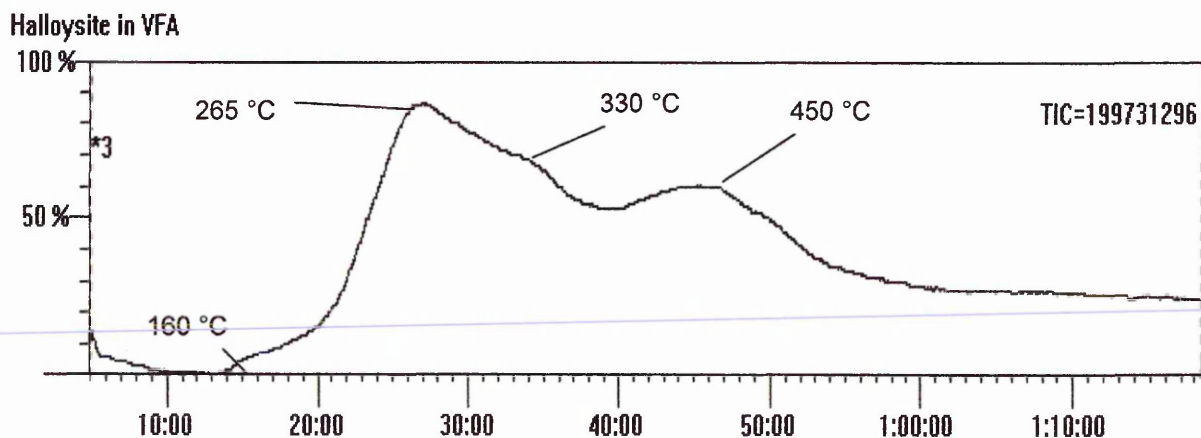
Figure 6.33 – TIC from EGA of Halloysite – VFA

186

[43]=7208960

[41]=3028992

[17]=8310784

10:00   20:00   30:00   40:00   50:00   1:00:00   1:10:00

[57]=768512

[55]=731648

[54]=660992

[53]=1203200

[52]=1732608

10:00   20:00   30:00   40:00   50:00   1:00:00   1:10:00
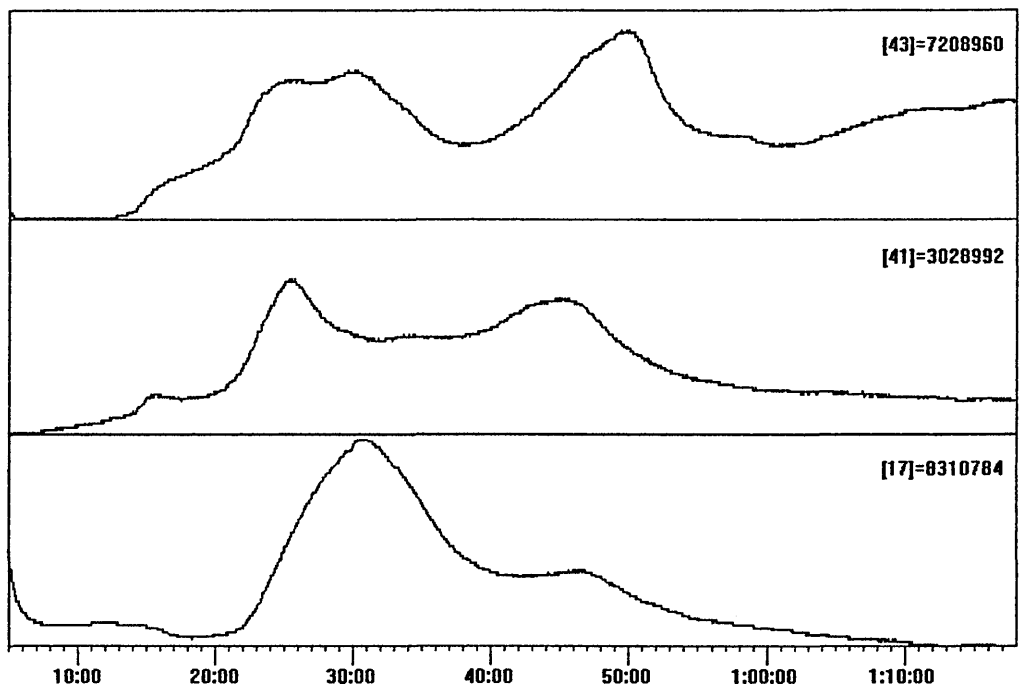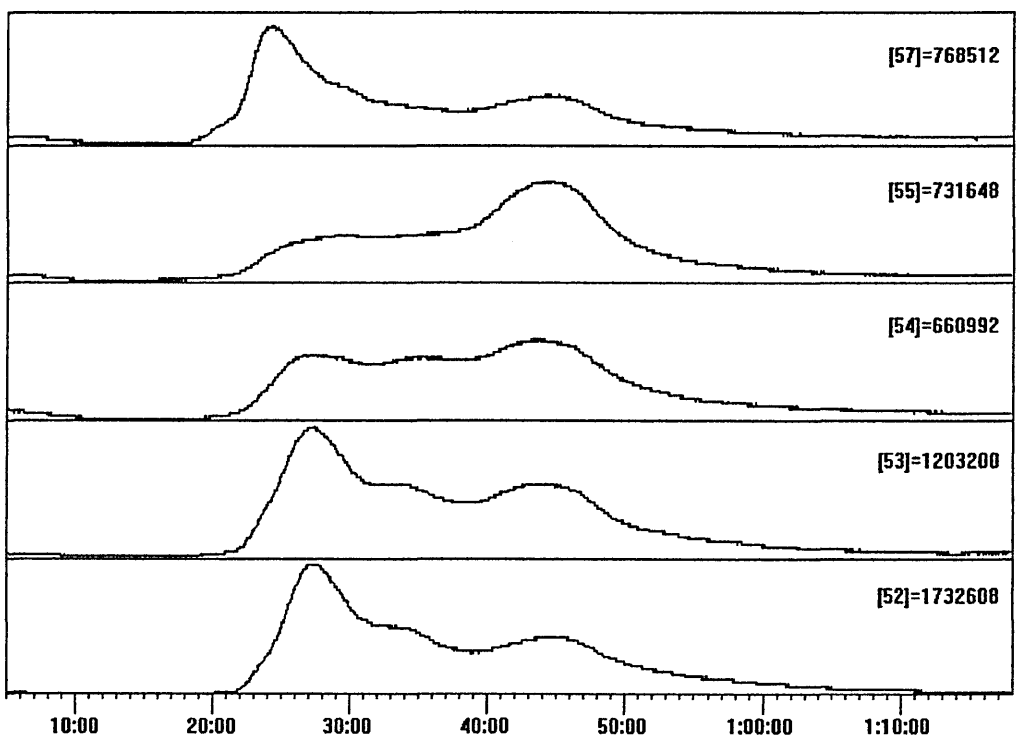
Figure 6.34.1 Reconstructed Ion Chromatograms from Halloysite - VFA
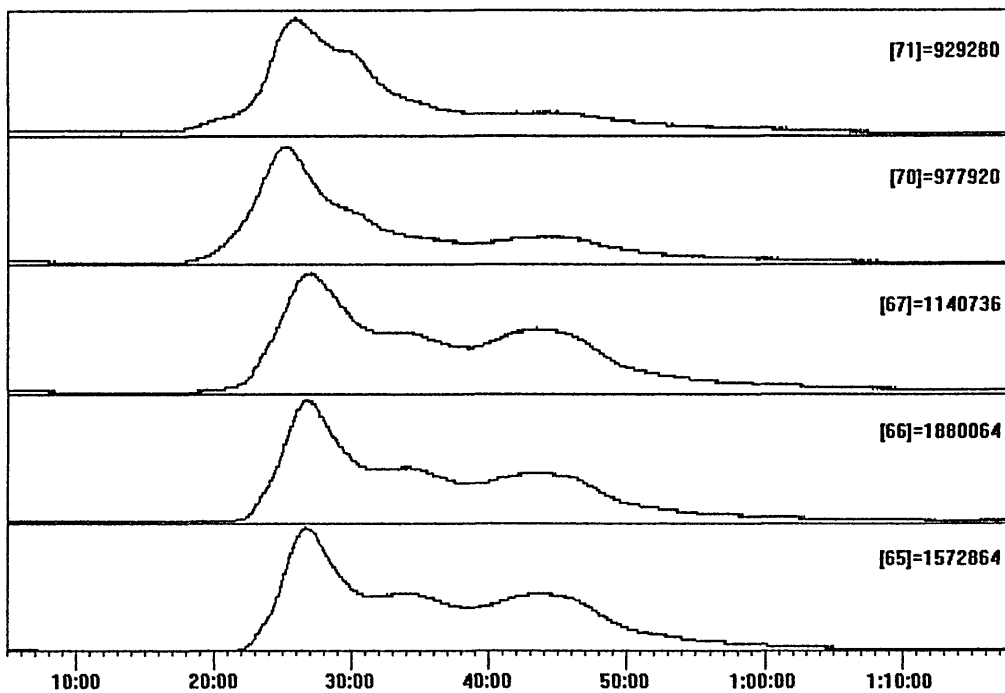
Figure 6.34.2 Reconstructed Ion Chromatograms from Halloysite - VFA
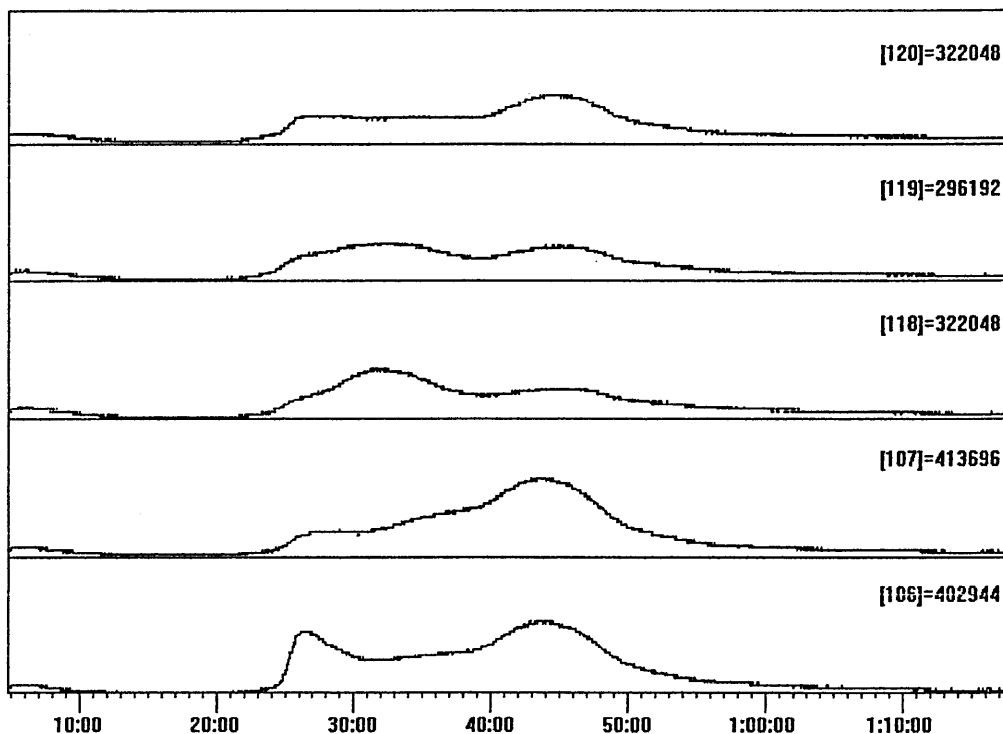
Figure 6.34.3 Reconstructed Ion Chromatograms from Halloysite – VFA

Temperature °C	Time (Mins)	Ions Detected
160	15	41,43
265	27	41,43,52,53,54,55,57,65,66,67,71,77,78,79,92,93,94,106,107,118,119,120
330	32	17,43,52,53,71,65,66,67,118,119
450	45	17,41,43,52,53,54,55,57,65,66,67,71,77,78,79,92,93,94,106,107,118,119,120

Table 6.5 – Ions Detected from EGA of Halloysite – VFA

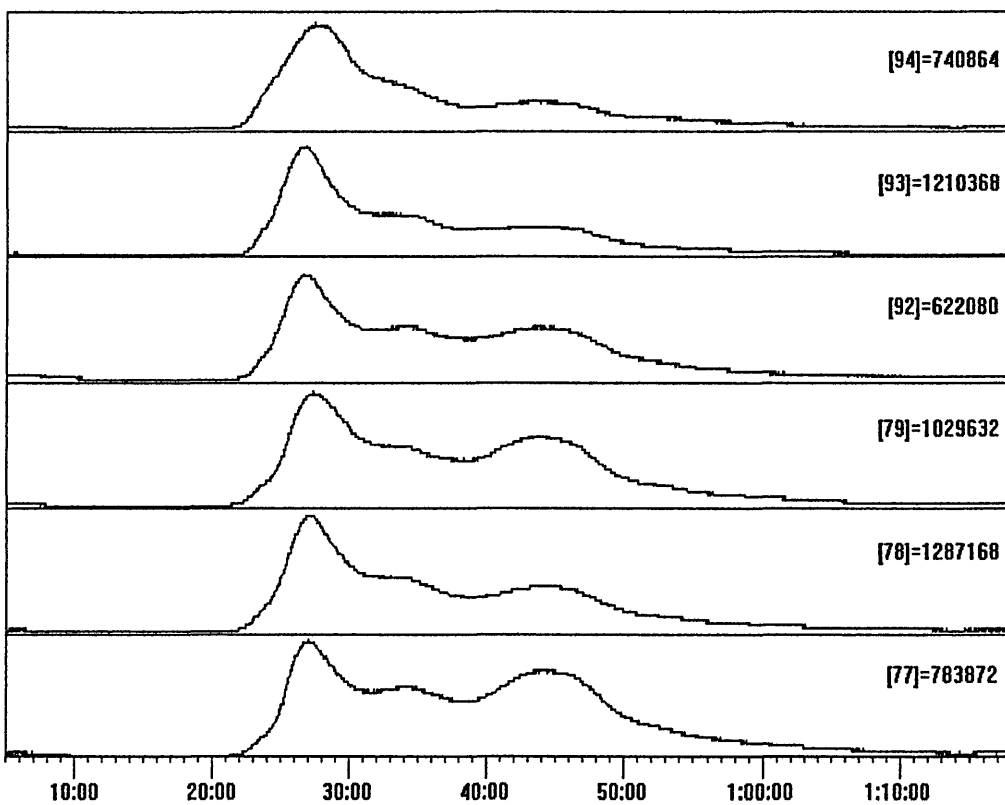Table 6.5 displays the ions detected vs. time and temperature. The DTG of this sample has peaks at 115, 140, 210, 310, 430 and 460 °C, and does therefore not correlate well with the peaks observed in the TIC. Compared to the TIC of the sample of VFA treated montmorillonite, (TIC peaks at 120, 160, 280 and 300 °C) the ions are detected at different temperatures, which given the differing interactions upon intercalation in these two clays is not unexpected. Similarly the MS data is also complex and does allow meaningful assignment of the ions detected. However, m/z = 71 which corresponds to molecular VFA is still detected in small amounts by 450 °C, though this ion peaks most strongly at 265 and 330 °C. Ions that are detected in both the halloysite and montmorillonite treated VFA samples include 41, 43, 52, 53, 66, 71 and 78. The structures of some of these ions are shown in Figure 6.9.

189

6.7.1 Treating halloysite with VFA and a Polar Activator (PC).

In an attempt to treat halloysite in a similar manner to the montmorillonite samples where exfoliation largely occurred with the addition of PC and VFA, halloysite (5%) was treated in the same manner (80% PC and 20% VFA) and polymerisation initiated (using AIBN). The resultant XRD trace (Figure 6.35) shows that the $d_{(001)}$ peak for halloysite was absent.
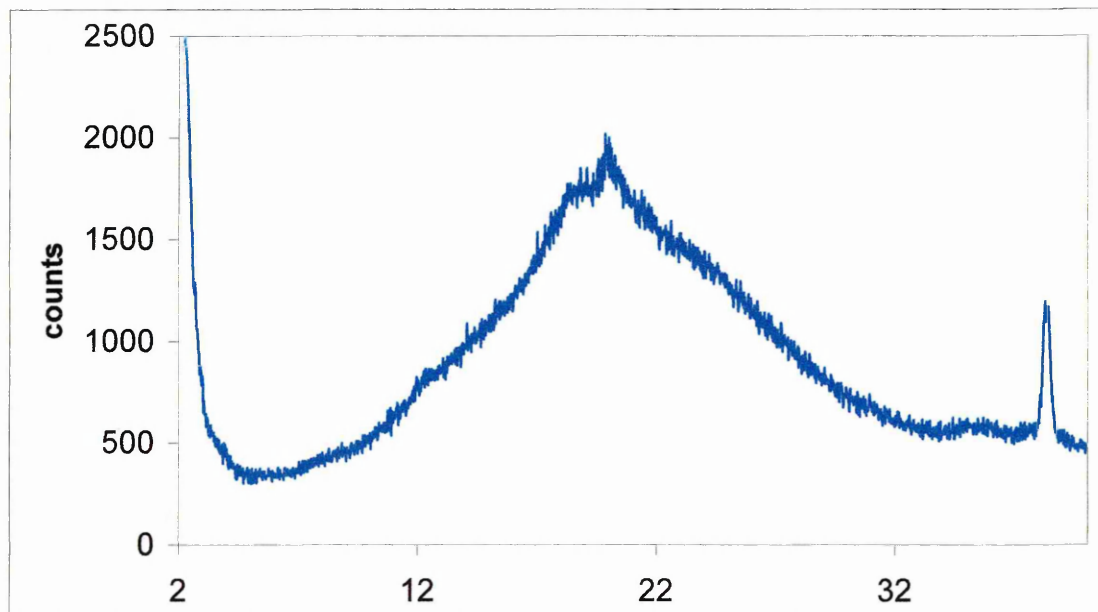

Figure 6.35 – XRD trace of Halloysite with 80% PC 20% VFA after polymerisation
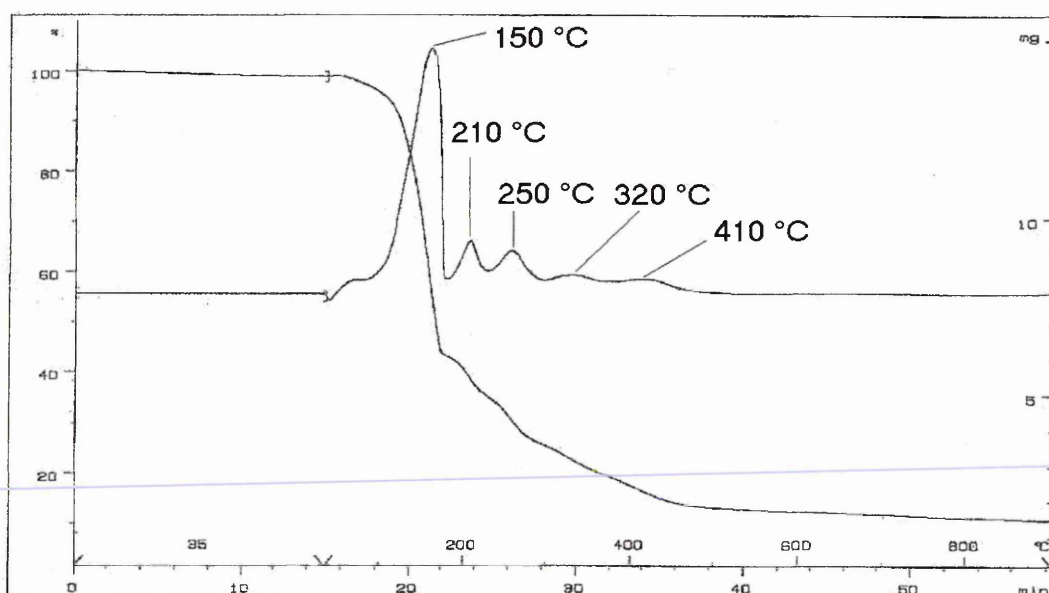

Figure 6.36 – TGA and DTG trace for Halloysite treated with 80% PC and VFA after polymerisation.

The DTG for this sample (Figure 6.36) shows that there are peaks in identical positions to that of the montmorillonite sample using the same reactants – 150, 210, 250, 320 and 410 °C, and that 55% of this sample is lost by 180 °C (50% in MCBP-VFA sample).

6.8 Composites of VFA with Kaolin and Halloysite PPA Intercalates

As previously seen the kaolin and halloysite intercalates with phenylphosphonic acid (PPA) – termed KPPA and HPPA respectively (Chapter 5) - each contain water coordinated to the PPA moiety within the intercalate. This water presents an opportunity for displacement of the water by VFA. Additionally the lone pairs of electrons on the oxygens of the PPA also provide scope for further coordination. Furthermore, the kaolin and halloysite layer structure has been extensively expanded, leaving the layer structure in these two clays held together by the PPA intercalate rather than by the hydrogen bonding network between the octahedral and tetrahedral sheets. This should facilitate relatively easy intercalation / displacement reactions. The approach adopted here is similar to that of Wypych[87] and co - workers (Chapter 4 section 4.2.2) in that they used their KPPA intercalate and replaced the water present in the complex by stirring with hexylamine. The interlayer spacing was found to increase to 16.36 Å (from 15.02 Å for their kaolin – PPA intercalate), but the intercalate was lost on heating at 230 °C. Hence, both intercalates were reacted with VFA by stirring with VFA for a period of three days, after which time the solid phase was allowed to settle, the supernatant decanted and the solid phase allowed to dry at room temperature in air on filter paper. No initiator was added to these samples.

6.8.1 KPPA and VFA

The XRD trace for this sample is identical to that of KPPA and shows no sign of a decrease in intensity of the $d_{(001)}$ (interlayer spacing remains 15.4 Å). DTG peaks (Figure 6.37) are observed at 140, 220, 320, 480 and 550 °C. This is much different from the DTG of KPPA alone (Figure 5.5). From the DTG of KPPA it is known that the peak at 140 °C is water and the corresponding weight loss for this peak is 2.5 wt%, which correlates well with the peak observed here for the VFA treated KPPA sample. However KPPA also has peaks at 480 and

585 °C, the former being the dehydroxylation of kaolin and the latter the decomposition of PPA and is observed as a larger peak than the dehydroxylation peak.
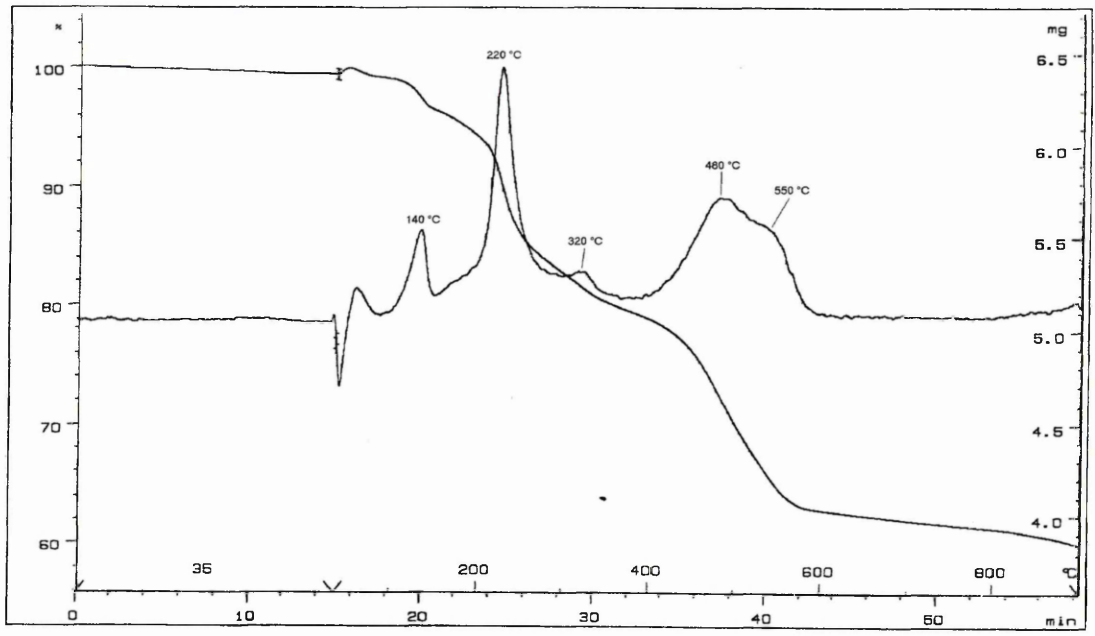

Figure 6.37 -TGA and DTG trace for KPPA - VFA

Certainly in the VFA treated KPPA sample the 480 °C peak is observed, but the PPA decomposition is seen at 35 °C lower. The peak at 210 °C may be loss of VFA, but there is also a new peak at 320 °C. 20% of this sample is lost by 180 °C.
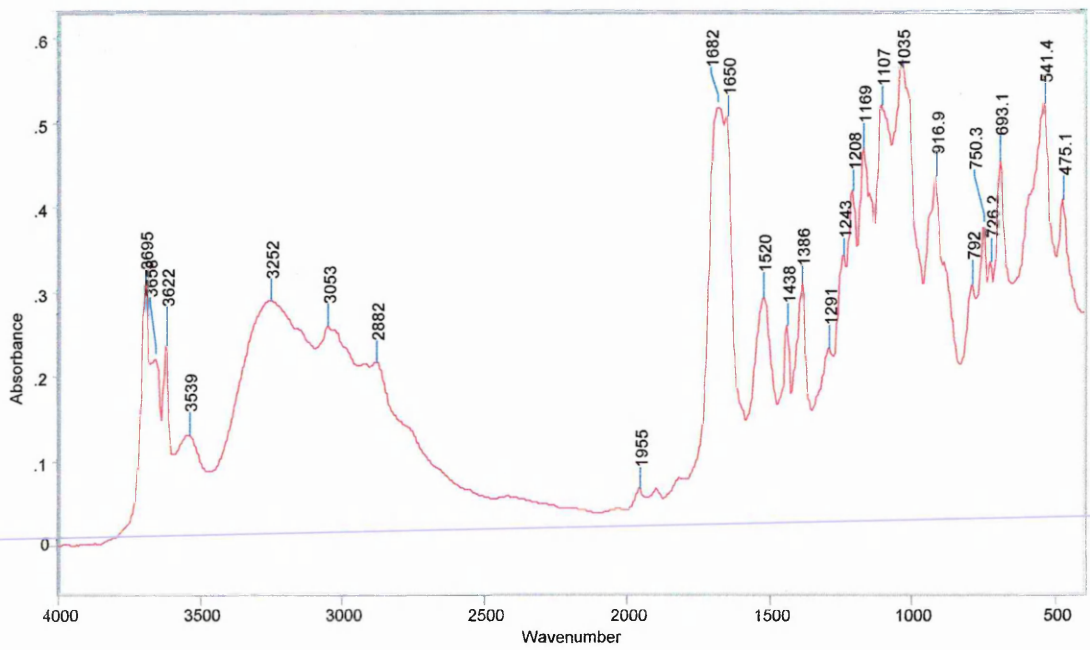

Figure 6.38 – DRIFTS of KPPA – VFA

THE DRIFTS spectrum for this sample (Figure 6.38) shows that the kaolin hydroxyl stretching bands (3695, 3665 and 3622 cm^{-1}) have reduced in intensity, but the band attributed to water in this complex (which interacts with surface aluminols and PPA) remains as intense suggesting that VFA has not interacted with PPA by displacing such water from the KPPA complex. Two carbonyl stretching bands are observed in this sample at 1682 and 1650 cm^{-1}, both lower than observed in liquid VFA, suggesting some interaction of the carbonyl groups most likely with the surface of kaolin. It is interesting to note that the position of the NH stretching and deformation bands in this sample are at 3262 and 1520 cm^{-1} respectively, as compared to 3272 and 1533 cm^{-1} in the VFA treated kaolin sample. This indicates that the NH groups are either interacting more within this sample (KPPA – VFA.

6.8.2 HPPA and VFA

This sample was allowed to settle for three days after which on further examination it was found that the supernatant was still cloudy, underneath which there was, a thick viscous (sediment) layer, reminiscent of the initial stages of the polymerisation reaction of VFA. Hence the supernatant layer was separated from the viscous bottom layer. This sample differed in appearance to the kaolin after being stirred for three days - upon drying both phases dried to a very hard glassy solid very similar in appearance to polymerised VFA (recall however that no initiator was added to these samples). These samples were in fact harder than these obtained from polyvinylformamide ones as DRIFTS could not be attempted on these (grinding in a mortar and pestle was not possible).

The sediment XRD trace (Figure 6.39, unwashed trace) displayed the HPPA spacing (15.50 Å), and this sample was washed with de – ionised water to remove any excess VFA or loosely bound VFA. This resulted in a increase in intensity of the $d_{(001)}$ peak (Figure 6.39 washed trace). Such a difference could be due to the fact that in the unwashed state, this sample does have VFA interacting as hypothesised with the PPA creating a new intercalate (which is subsequently washed out with water) with a $d_{(001)}$ of higher angle which is not seen here, but there remains no sign of a $d_{(002)}$ peak. Alternatively, this may be due to difficulties in sampling handling when presenting such a hard glassy substance for analysis.
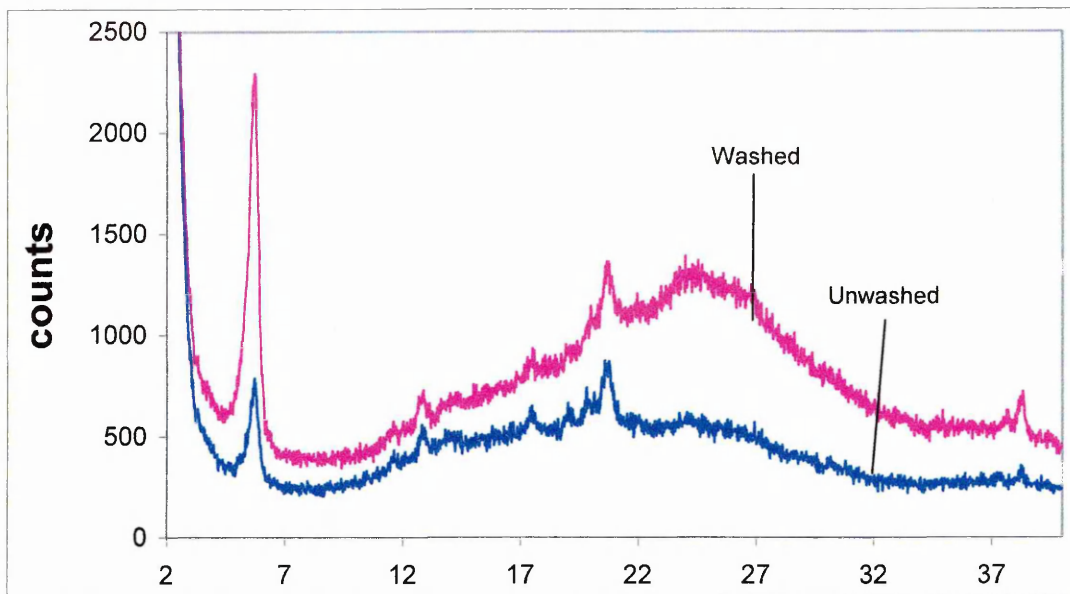
Figure 6.39 XRD trace of HPPA – VFA Sediment

The DTG (Figure 6.40) shows the water peak for HPPA at 140 °C (10 °C lower) and an overall weight loss of 80%. An intense broad peak centred at 210 °C is present together with a peak at 170 and 390 °C. It is possible that the dehydroxylation and loss of PPA from HPPA are not observed due to the relatively large loss associated with the 210 °C peak. DTG peaks associated with VFA polymerisation however are not observed (210, 250, 320 and 410 °C).
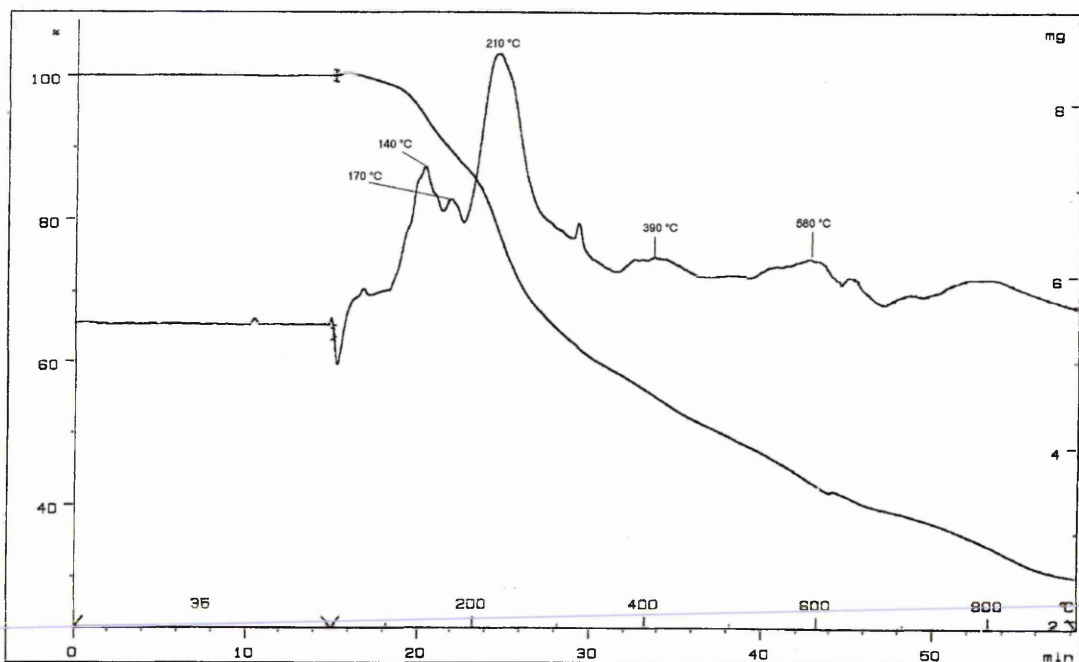
Figure 6.40 – TGA and DTG for HPPA – VFA Sediment

194
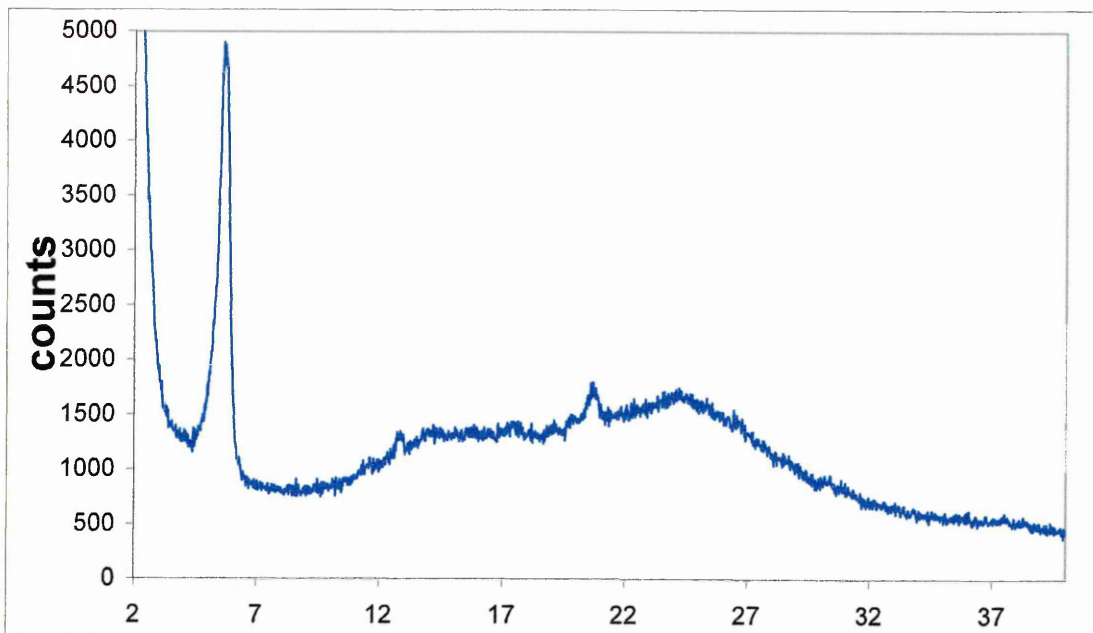
Figure 6.41 – XRD trace for HPPA – VFA Supernatant

The HPPA – VFA treated supernatant XRD trace again gives a $d_{(001)}$ spacing of 15.5 Å
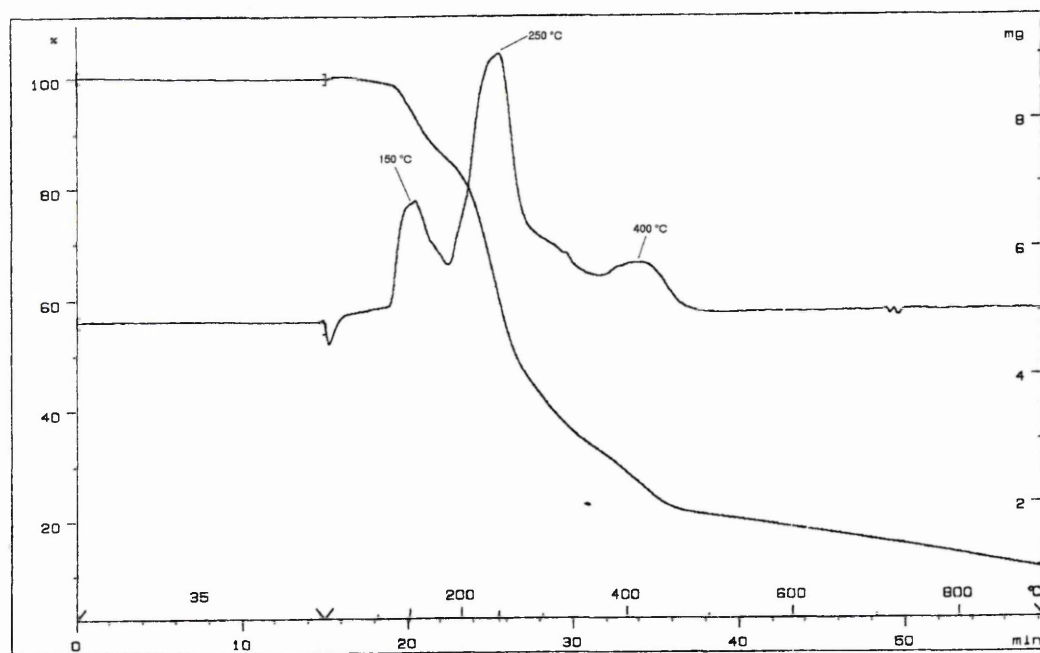
Figure 6.42 – TGA and DTG for HPPA- VFA supernatant

The DTG trace for the supernatant however, (Figure 6.42) displays peaks at 150, 250 and 400 °C with again no signs of halloysite dehydroxylation or loss of the intercalated PPA (at 490 and 610 °C respectively).

6.9 Summary of VFA - Kaolin and Halloysite Composites.

The results obtained from this section are promising but clearly need more study in order to obtain more conclusive results.

The VFA treated kaolin sample requires VT-XRD to be performed on a dry sample, in order to ascertain the nature of the interaction of VFA with kaolin, which would also benefit from VT-DRIFTS here. Studies on the wet paste show that the $d_{(001)}$ peak for this sample is weak and much reduced and new bands are observed in the DRIFTS spectrum. A knowledge of the temperature stability of this complex may indicate indeed whether the interaction is strong or not.

Similarly the VFA treated halloysite would benefit from a VT-DRFITS study. The VT-XRD shows the $d_{(001)}$ peak move to higher angle as the temperature is increased ($d_{(001)}$ spacing of 11.1 Å), and VT-DRIFTS may shed some light on this particularly as the maximum temperature of VT-DRIFTS (500 °C) exceeds that of VT-XRD (300 °C). The room temperature DRIFTS spectrum for this sample also shows some indication of an interaction between VFA and halloysite (reduced intensity of hydroxyl stretching bands and shift to 1672 cm^{-1} carbonyl stretching band in VFA).

Both these samples (VFA treated kaolin and halloysite) should also be treated with initiator and polymerised as were the MCBP – VFA samples and then subsequently treated with increasing amounts of the polar activator PC. It would be interesting to see if there is a progressive decrease in the $d_{(001)}$ as observed in the MCBP samples. The results obtained from the halloysite sample which was treated with 80% VFA 20% VFA and polymerised shows no $d_{(001)}$.

The VFA treated KPPA and HPPA samples also show promising signs of some interaction with VFA. Both show marked differences in DTG data, particularly at high temperature where dehydroxylation and loss of PPA occur. VT-DRIFTS and TG-MS would be required here as previous TG-MS data (Chapter 5) shows what is happening at these temperatures (400 – 600 °C). Most intriguing is the VFA treated halloysite sample which behaves differently when treated with VFA - in appearance of the resultant product at least this shows signs of polymerisation, possibly acid activated by the PPA of the intercalate.

Chapter 7 – Aldehyde and Amine Clay Composites

7.0 Introduction

This work was undertaken as an exploratory study for Schlumberger Cambridge Research (SCR) in the field of shale stabilisation. Preliminary studies (performed elsewhere) in this work indicate that the use of a water based drilling mud capable of forming a clay mineral – composite / polymer may achieve this end. The most promising composite in terms of barrier properties and resistance to water treatment was found to be one made from the aldehyde glyoxal and the amine 3,3 – diamino - N – methyldipropylamine, the product being either a (poly) imine or an amino resin. Therefore it was necessary to study the interaction between this mixed solution and the clay. Consequently studies here are mainly based on these reactants. Preliminary studies with simpler amines had identified the presence of a band near 1660 cm^{-1} after immersion of the clay in a solution of 1% diaminopropane and 1% glyoxal (both weight %). This region of the mid- IR spectrum is a complicated one to study when using these reagents due to overlapping bands.

7.1 Experimental

7.1.1 Materials.

SWy-2 – A Wyoming montmorillonite obtained from the Source Clay Repository. Contains Na, Ca and Mg ions.

Glyoxal – BDH Chemicals available only as 40% aq. Solution

Formaldehyde - BDH Chemicals available only as 40% aq. Solution

3,3 – diamino - N – methyldipropylamine (3NH2) – Aldrich 99%

1,3 – Diaminopropane (DAP) – Aldrich 98%

Ethylenediamine (EDA) – Aldrich 98%

1,7 – Diaminoheptane (DAH) – Aldrich 98%

Solutions of the above aldehydes and amines were prepared in concentrations of 2, 5 and 10 weight % in water for preparation of composites with the clay. These concentrations used stem from earlier studies which investigated the hardness and water permeability of the composites using the aldehyde and amine solutions in this weight % range (see chapter 1).

From these studies the most favourable combinations were found to be glyoxal and 3NH2. Due to the huge excess of water in these solutions it may be expected that the clay will intercalate water, but this has proven not to be the case, though some water still remains. The melting point for glyoxal is 15 °C and the boiling point is 51 °C.

7.1.2 Preparation of Composites

For preparation of single reactant systems where either a single aldehyde or amine was interacted with the clay, 0.1g of clay was added to 6ml of the required aqueous solution of organic. When a binary solution of an aldehyde and an amine was required, in order to form an imine polymer, 3ml of a 2 wt. % solution of each reactant was used and added to the reaction vessel prior to immediate addition of 0.1g of clay. This was then left for the required amount of time after which the supernatant solution was removed and the treated clay sample left to dry in air on filter paper. It was observed that on mixing the two reactants the resultant solution immediately turned cloudy and white. In time this solution eventually adopted a brown colouration. If washing of the sample was required then this was achieved by treating the sample with 3ml of deionised water and shaking gently. Upon settling the water was then decanted or centrifuged to remove.

7.1.3 Instrumental Techniques

As in section 5.2.

7.2 Results

7.2.1 Clay – Aldehyde Intercalates.

An immediate observation on preparation of these intercalates is the visible swelling that occurs of the clay sample – quite often these samples would require centrifugation in order to separate the supernatant from the treated clay. All the following results have been obtained using a 2% solution of either glyoxal or formaldehyde.

The XRD trace for the glyoxal intercalate (2% solution) with SWy-2 with and without washing the sample (Figure 7.1) shows that the $d_{(001)}$ spacing has expanded to 14.70 Å (recalling that SWy-2 has a layer spacing of 12.0 Å). The intercalate with formaldehyde (2% solution), (Figure 7.1.1) after washing shows a slightly higher interlayer spacing of 15.10 Å. As the

formaldehyde molecule is smaller than glyoxal it would appear that the packing of formaldehyde would initially imply that there may be a double layered structure for this intercalate, or perhaps osmotic swelling caused by water. It is also interesting to note the shape of the $d_{(001)}$ of the unwashed glyoxal intercalate(Figure 7.1.2 and 7.1.3). This peak is broader than the others (Figure 7.1.3) and has a shoulder at 5.36 °2θ ($d_{(001)}$ = 16.48 Å) The XRD trace of the washed glyoxal sample also appears more ordered than the unwashed counterpart.
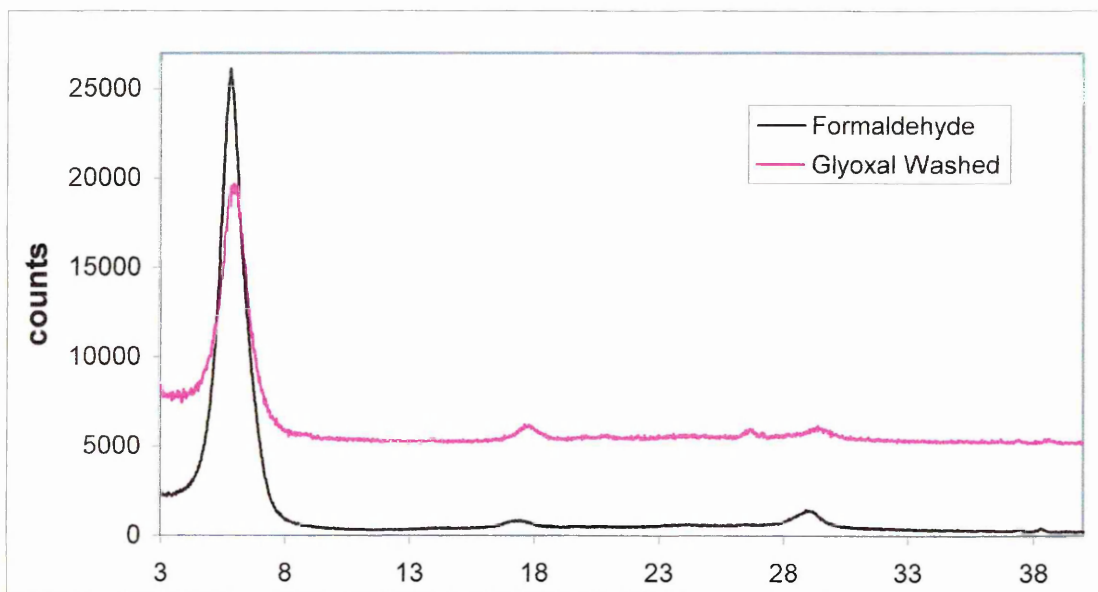
Figure 7.1.1 – XRD traces of SWy-2 – aldehyde intercalates.
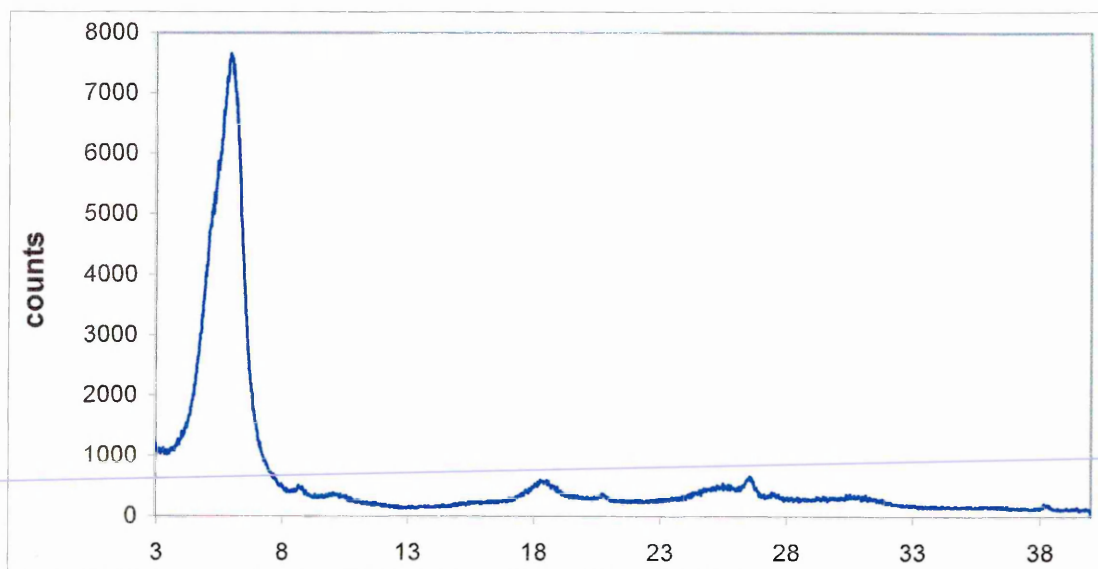
Figure 7.1.2 – XRD trace of SWy-2 – glyoxal intercalate unwashed
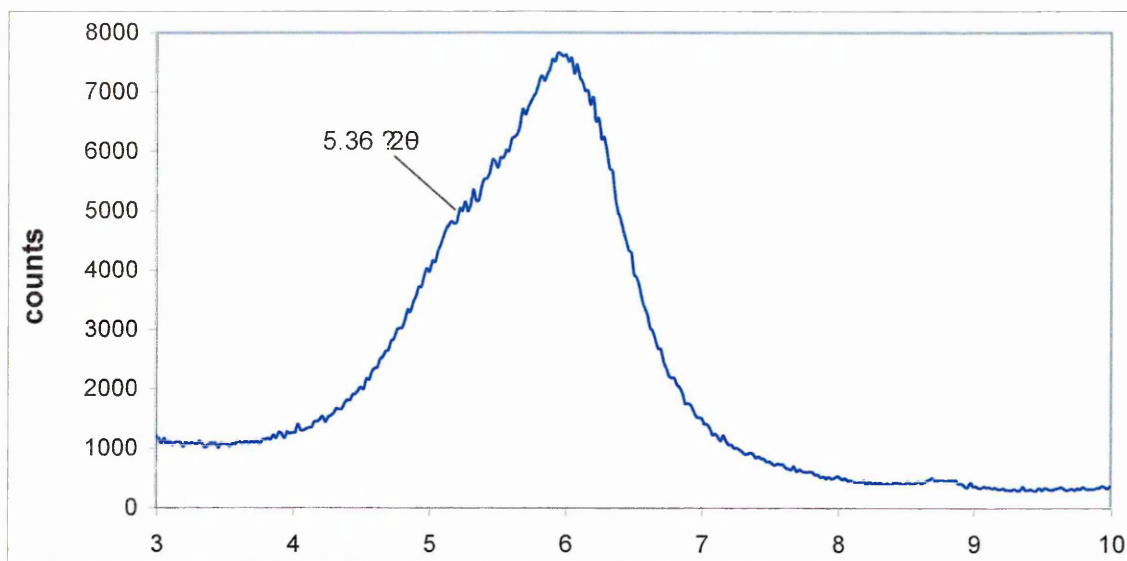
Figure 7.1.3 – XRD trace of SWy-2 glyoxal intercalate 3 – 10 °2θ

Studying the unwashed glyoxal intercalate further, the VT – XRD (Figure 7.2) shows the following changes:-

Temperature °C	Interlayer Spacing Å
R.T	14.70
70	14.50
140	14.30
160	13.60
190	13.00
280	12.60
300	12.00

Table 7.1 Interlayer spacings from VT-XRD analysis of Glyoxal – SWy-2 intercalate

The $d_{(001)}$ peak for this sample moves to a higher angle and also becomes broader upon heating. The shoulder at 5.36 °2θ is lost by 140 °C. The $d_{(003)}$ at 18 °2θ reduces in intensity and is no longer observed at 190 °C. This may be indicative of loss of ordering in the intercalate which gives the 14.70 Å spacing.

By 300 °C the interlayer spacing has decreased to 12.00 Å . This is not however, a return to the original 12.00 Å spacing of SWy-2 as this distance includes the water around the interlayer cation between the clay layers and, at such an elevated temperature, water is highly unlikely to be present. This would indicate that glyoxal in some form or another is present – a polymerised or hydrated form, being the most likely.
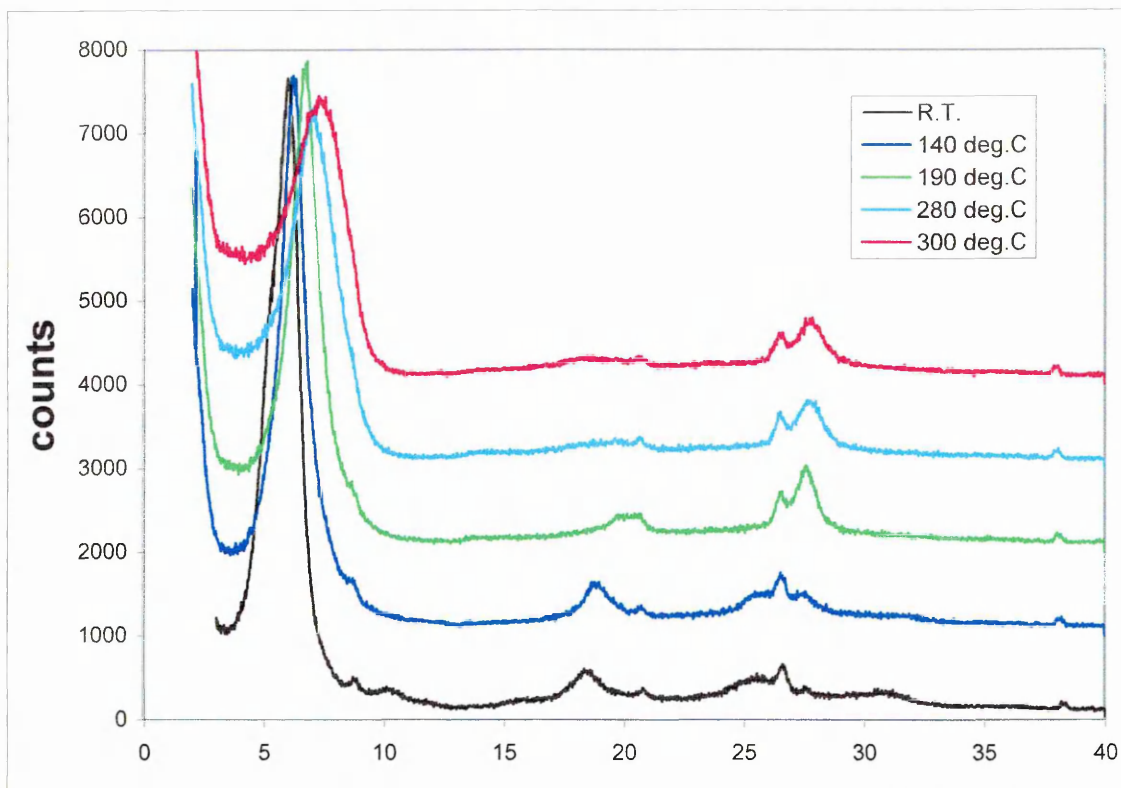
Figure 7.3 – VT-XRD of the Unwashed SWy-2 – Glyoxal Intercalate

Examining the TGA data for the glyoxal – SWy-2 intercalate, (Figure7.4) intercalates were prepared for samples left in the 2% aqueous glyoxal solution for 18, hours, 1,2, and 3 days.

The DTG peaks for these samples are in identical positions. The overall weight losses for these samples however are different:- 18 hours – 28%, 1 day – 34%, 2 days – 32% and 3 days – 34%. Eight major peaks are identified in the DTG of these samples at 100 140, 170, 230, 263, 300, 490 and 620 °C (390 °C is shown for comparison with TG-MS data and is very weak if present at all). The peak at 620 °C is most likely due to the dehydroxylation of the clay, and it would appear from the TG data that the most of the intercalate is lost from the clay by 400 °C (beyond the highest temperature obtainable by VT – XRD measurement).
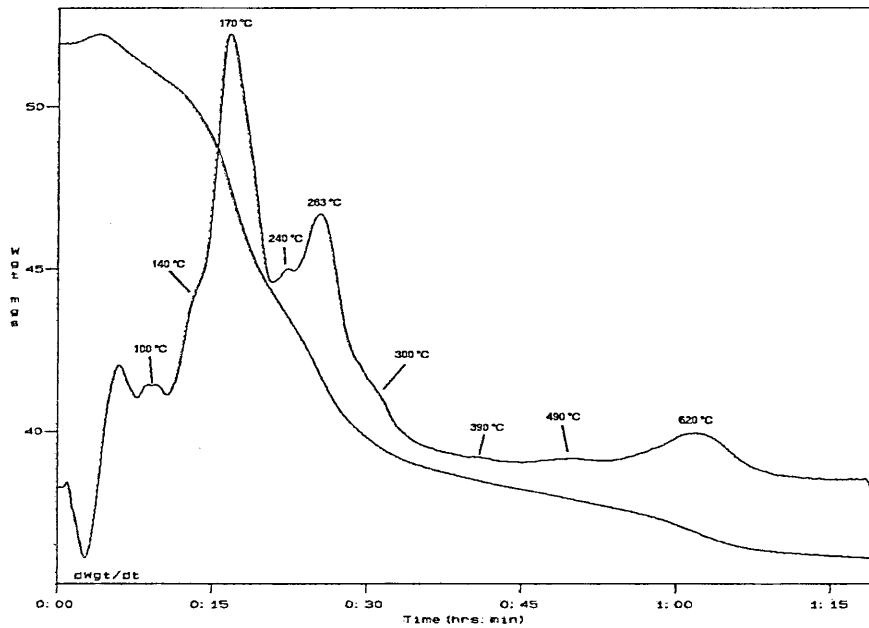
Figure 7.4 – TGA and DTG trace for SWy-2 – Glyoxal Intercalate

The intercalate of SWy-2 and formaldehyde solution shows a much different DTG (Figure 7.5.1). For the SWy-2 treated with 2% formaldehyde solution, there is only a 15% weight loss overall and a large peak at 100 °C with a large shoulder at 150 °C with corresponding weight losses of 8 and 2% respectively.
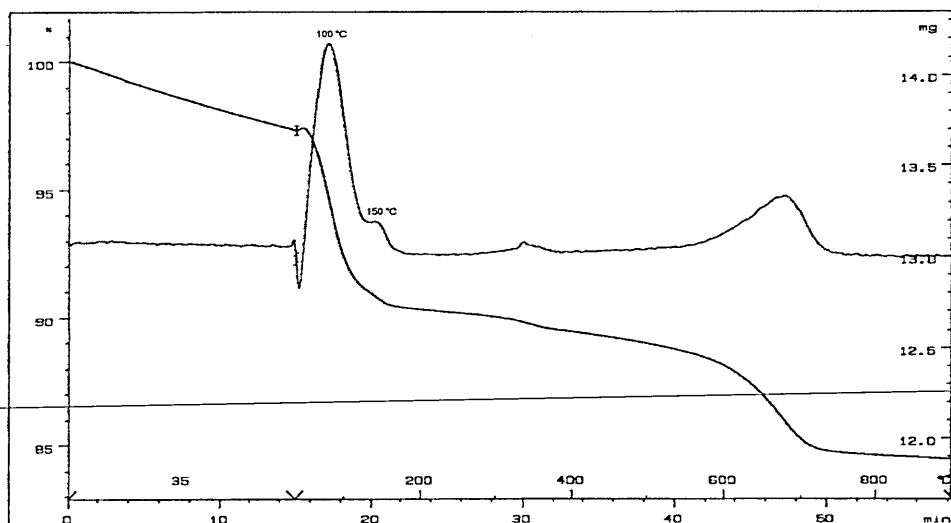
Figure 7.5.1 TG and DTG trace for SWy-2 treated with 2% formaldehyde solution

If SWy-2 is exposed to formaldehyde vapour, (Figure 7.5.2) then this shoulder clearly becomes larger and the sample now loses 18% overall. Both samples clearly show the dehydroxylation of the clay which begins at 600 °C. It is very difficult however, to observe real differences from these analyses.
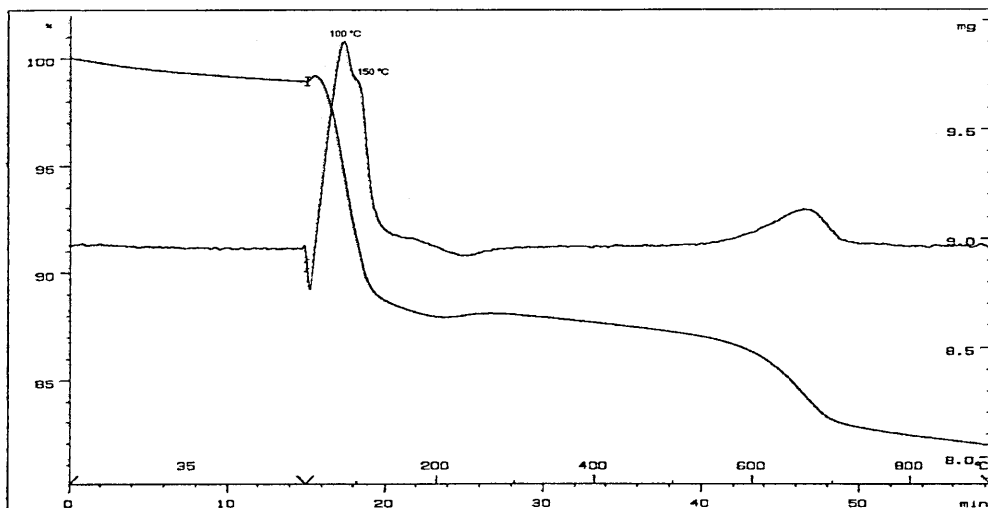
Figure 7.5.2 – Intercalate of Formaldehyde Vapour and SWy-2

The DRIFTS spectrum for the glyoxal intercalate (Figure 7.6) shows bands at 2959, 1609 and 1453, 1418 and 1366 cm^{-1} as well as a characteristic broad and intense O-H stretch for water centred at 3391 cm^{-1}. This spectrum does not change with the length of time that the clay is treated with glyoxal but the most striking feature is the band at 1609 cm^{-1}. This band represents either a shifted OH bending mode (water) or a very large shift in the C=O carbonyl stretch. Evidence for the presence of glyoxal in this sample is provided by the asymmetric CH$_2$ stretch (2959 cm^{-1}) and also CH$_2$ scissoring (1453 cm^{-1}), CH$_2$ bend (1418 cm^{-1}) and CH bend (1366 cm^{-1}). The 1453 and 1418 cm^{-1} bands may be further assigned to –CH$_2$-O- (small ring structure) and –CH$_2$-O- (acyclic structure) vibrations respectively. These latter two assignments are good evidence for glyoxal being present in a polymerised or hydrated form, as they not only indicate the presence of CH$_2$, which is absent in the pure form of glyoxal but also the presence of CH$_2$ bonded to O. However, the IR results can give no indication as to

203

whether these forms of glyoxal are intercalated or surface adsorbed (i.e. how they are interacting with the clay). The SWy-2 – glyoxal intercalate is discussed in more detail later.
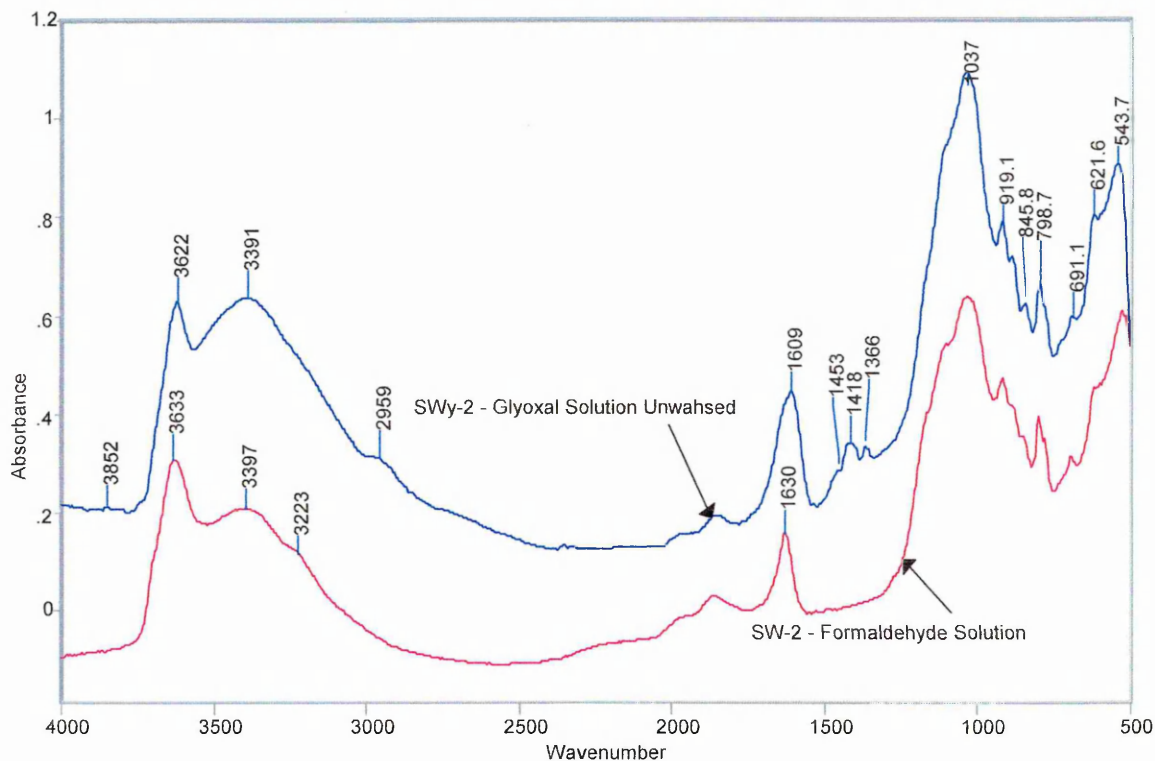
Figure 7.6 – DRIFTS Spectra of Aldehyde Solution – SWy-2 Intercalates.

The DRIFTS spectra for SWy-2 treated with formaldehyde vapour (Figure 7.6.1) and formaldehyde (2%) solution (Figure 7.6) do show marked differences.

For SWy-2 – formaldehyde solution bands are present at 3397 3223 and 1630 cm^{-1} and for the vapour treated sample bands are present at 3381 2979, 2922, 2877 (weak), 2850 (weak), 1697 1631, 1469, 1429 and 1365 cm^{-1}. This would imply that formaldehyde is only definitely present in the vapour treated samples. These bands can be assigned using earlier reports of adsorbed formaldehyde[147-158] (Chapter section 4.4) and its adsorption products as discussed earlier. For the SWy-2 – formaldehyde solution sample, it is difficult to show that any formaldehyde is interacting with the clay – the bands at 3397 and 3223 cm^{-1} can be attributed to water OH stretches and the band at 1630 cm^{-1} the water OH bend ; the increase in interlayer spacing may simply be due to intercalated water.
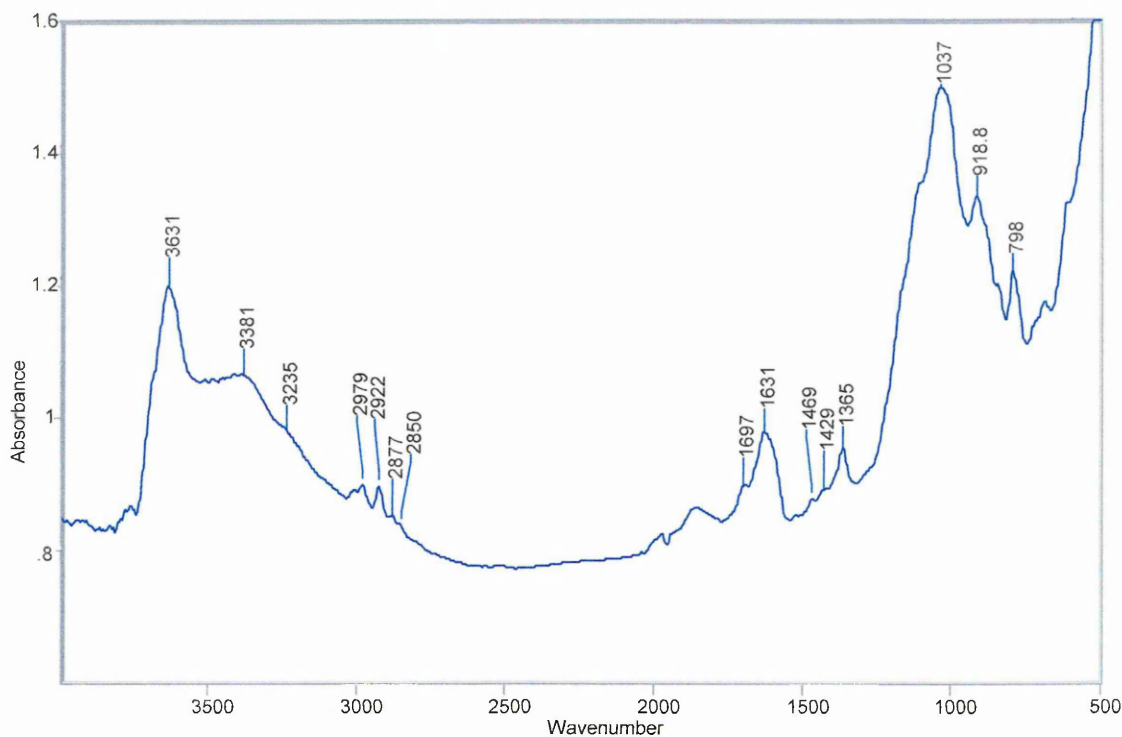
Figure 7.6.1 - DRIFTS Spectrum of Swy-2 – Formaldehyde vapour intercalate

Wavenumber (cm^{-1}) observed	Assignment	Adsorbed Formaldehyde	Polyoxymeth-ylene(POM)	Trioxane
2979	CH$_2$ stretch		2980	2983
2922	CH$_2$ scissoring overtone	2935	2918	2916
2877 (weak)	CH$_2$ symmetric stretch			
2850 (weak)	CH$_2$ symmetric stretch	2850		
1697	C=O stretch or water			
1631	C=O stretching	1610		
1469	CH$_2$ bend (CH$_2$-O-) cyclic	1485	1485	1483
1427	CH$_2$ wag (CH$_2$-O-)		1430	1426
1366	COO$^-$ stretch			1392

Table7.2 – Band Assignments for Formaldehyde Vapour – SWy-2 Intercalate.

As table 7.2 shows as well as adsorbed formaldehyde bands present in this intercalate, there also appears to be some polymerised formaldehyde present.

Bands for polymerised formaldehyde (often attributed to trioxane and polyoxymethlylene (POM)) are observed at 2986, 2919, 1484, 1427 and 1395 cm^{-1} and these bands appear to present a reasonable fit to those observed here with the formaldehyde – SWy-2 intercalates

205

(Table 7.2). However this does not assign all the bands for this complex and the possibility of there being more than one species present must be examined, particularly as there remains a C=O stretch (or water OH bend) at 1631 cm^{-1}, which is not observed in either trioxane or polyoxymethylene.

VT-DRIFTS provides some assistance to the band assignments for this sample (Figure 7.7.1).
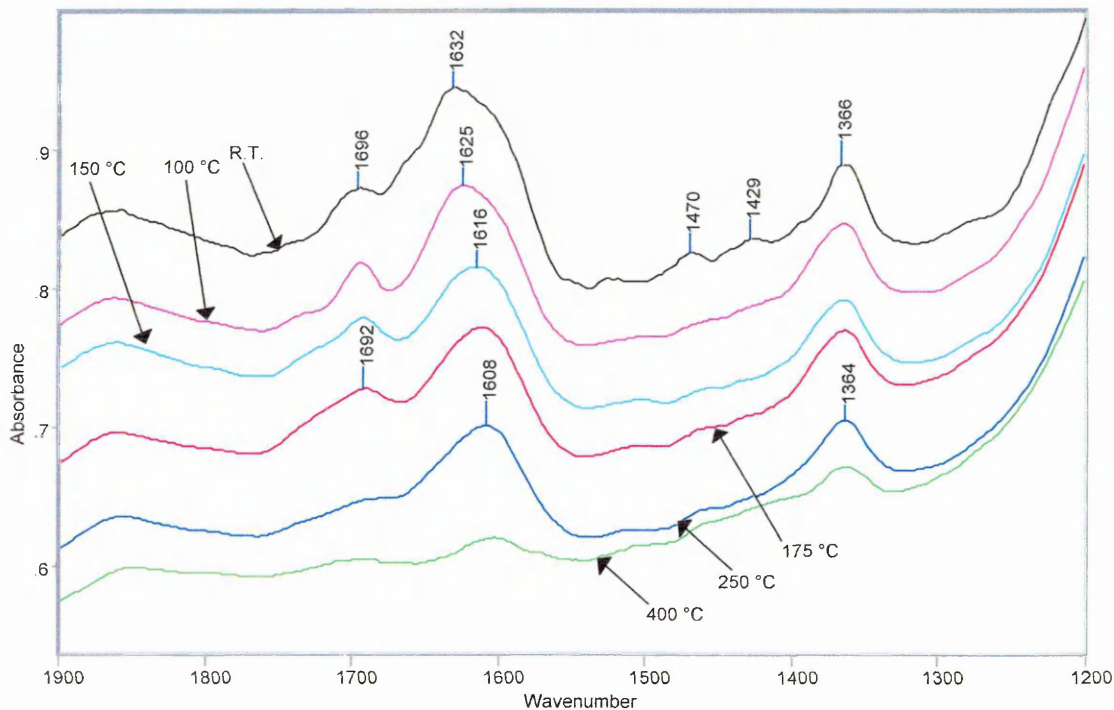
Figure 7.7.1 – VT-DRIFTS of Swy-2 – Formaldehyde Vapour Complex.

As the temperature is increased the 1637 cm^{-1} band decreases in intensity until 150 °C and shifts to 1610 cm^{-1} by 175 °C. However, it is possible that the band at 1637 cm^{-1} arises from water as there is a concurrent decrease in the broad OH stretch (3381 cm^{-1}), characteristic of water (Figure 7.7.2) over the same temperature interval. Therefore, the band at 1610 cm^{-1} is observed as the asymmetry on the low wavenumber side of the 1637 cm^{-1} water OH bend in room temperature spectrum of this sample. The 2980 cm^{-1} band is lost by 100 °C and the CH$_2$ bands (bending modes or deformation) at 1469 and 1427 cm^{-1} are no longer visible by this temperature. The band at 1695 cm^{-1} is no longer visible by 250 °C. The 1610 and 1363 cm^{-1} bands remain until 400 °C after which they are no longer observed. The band at 1366 cm^{-1} may be assigned to either a CH$_2$ bend or the COO$^-$ stretch which is indicative of monodentate formate. If this is the case then the 2922 cm^{-1} could be a CH stretch resulting from the

presence of monodentate formate. This band at 1366 cm^{-1} is still weakly present at 400 °C as is the 2922 cm^{-1} band.
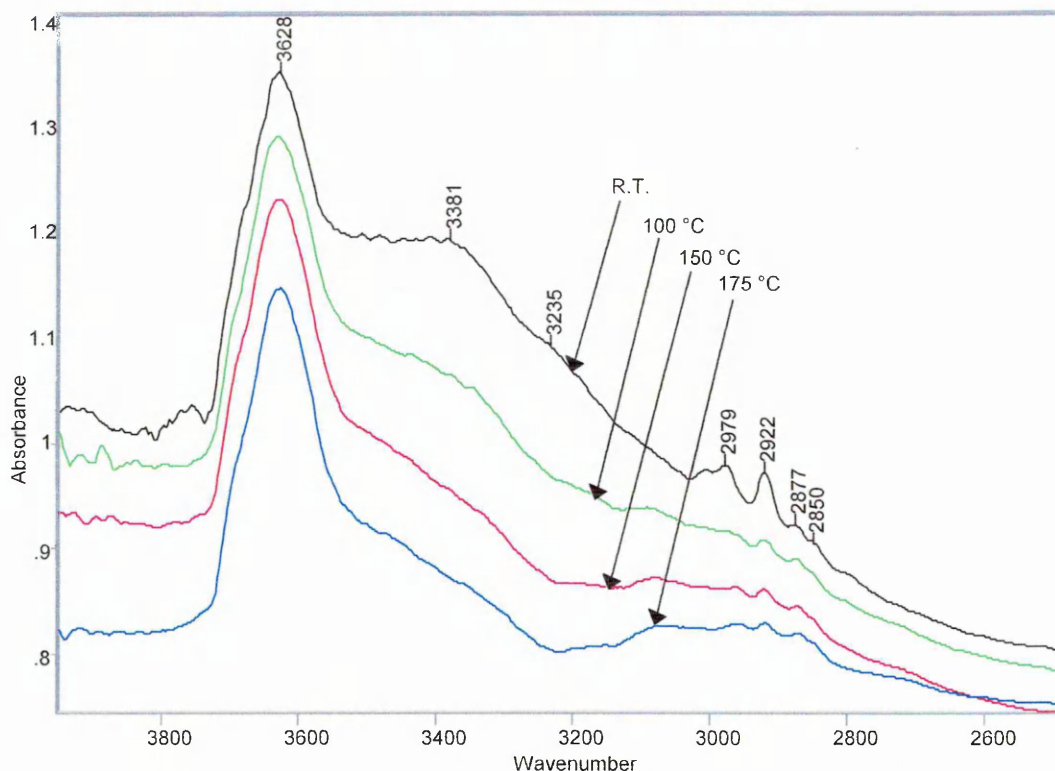
Figure 7.7.2 - VT-DRIFTS SWy-2 – Formaldehyde Vapour Intercalate 3900 – 2500 cm^{-1}.

7.2.2 Summary of Formaldehyde – Clay Data.

These observations lead to the following conclusions. It would appear that the formaldehyde has formed some polymerised species which has formed a relatively strong association with the clay. This is evident from the 2980, 1472, 1428 and 1389 cm^{-1} bands which are all lost at relatively low temperature. There is also water associated with this complex and this is lost by 150 °C, as seen by the 1637 cm^{-1} and broad OH stretch, which both concurrently decrease in intensity. By this temperature, there is also a 10% weight loss observed in the TGA results. Two carbonyl stretching frequencies remain unassigned so far in this discussion at 1695 and 1610 cm^{-1}. The latter is characteristic of chemisorbed formaldehyde, which has characteristically large shifts, and this may be expected due to the strong interaction with the interlayer cations. The former is characteristic of the C=O stretch observed in gaseous formaldehyde – 1689 cm^{-1} (chapter 4, table 4.0). This band cannot be assigned to adsorbed formate (as may be expected due to catalytic reactions with clay) as this species would be

observed at frequencies of 1630 cm^{-1} and lower (Table 4.3). It is also unlikely to be physisorbed formaldehyde on silica or alumina (~1715 cm^{-1} Chapter 4 Table 4.4). The 1695 cm^{-1} band may therefore be assigned to formaldehyde molecules hydrogen bonded to formaldehyde molecules which are interacting with the interlayer cations of the clay. Due to its presence up to 250 °C, it is likely that this band does represent a carbonyl interaction with either the clay or other formaldehyde molecules. The presence of a band at 1366 cm^{-1} also suggests that there is some formate species formed also.

7.2.3 The Glyoxal Intercalate.

The VT-DRIFTS spectrum of the glyoxal – SWy-2 intercalate (unwashed) (Figure 7.8.1) shows bands at 1646 1609, 1455, 1419 and 1367 cm^{-1} at room temperature. By 75 °C however this spectrum has changed considerably. Two new bands at 1742 and 1716 cm^{-1} have now appeared and continue to grow in intensity but are lost by 325 °C (Figure 7.8.2). The emergence of these bands are concomitant with the decrease of the broad OH (water) stretching band (Figure 7.8.3) and a slight decrease in intensity of the 1609 cm^{-1} band, although this band together with the 1646 cm^{-1} band are not lost until 450 °C.
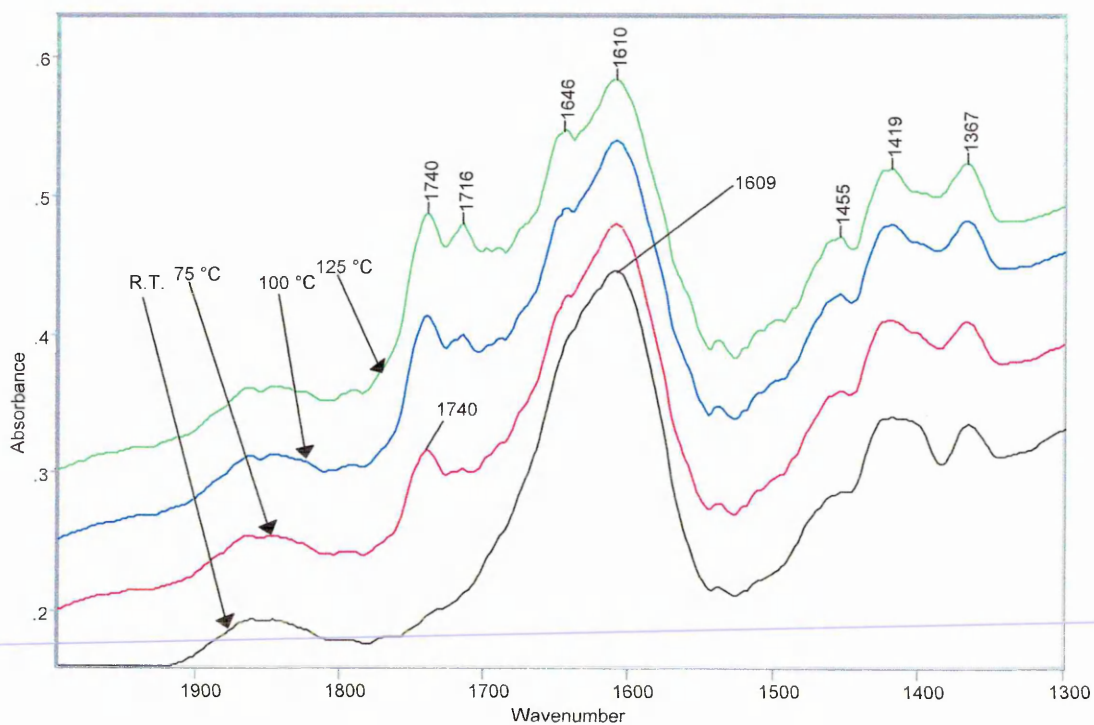
Figure 7.8.1 – VT-DRIFTS of SWy-2 – Glyoxal Intercalate – 2000 – 1300 cm^{-1} R.T – 125 °C.

208

The 1609 cm^{-1} band decreases in intensity and by 125 °C appears to split into two unresolved bands which can be centred at 1643 and 1610 cm^{-1} respectively. It is not clear as to whether this band is real or not from these results, hence deconvolution was utilised (Figure 7.9). It should also be noted that the magnitude of the carbonyl shifts observed here are consistent, if not greater with those reported in literature (e.g. 1640 cm^{-1} for glyoxal on cotton fibres[167]).
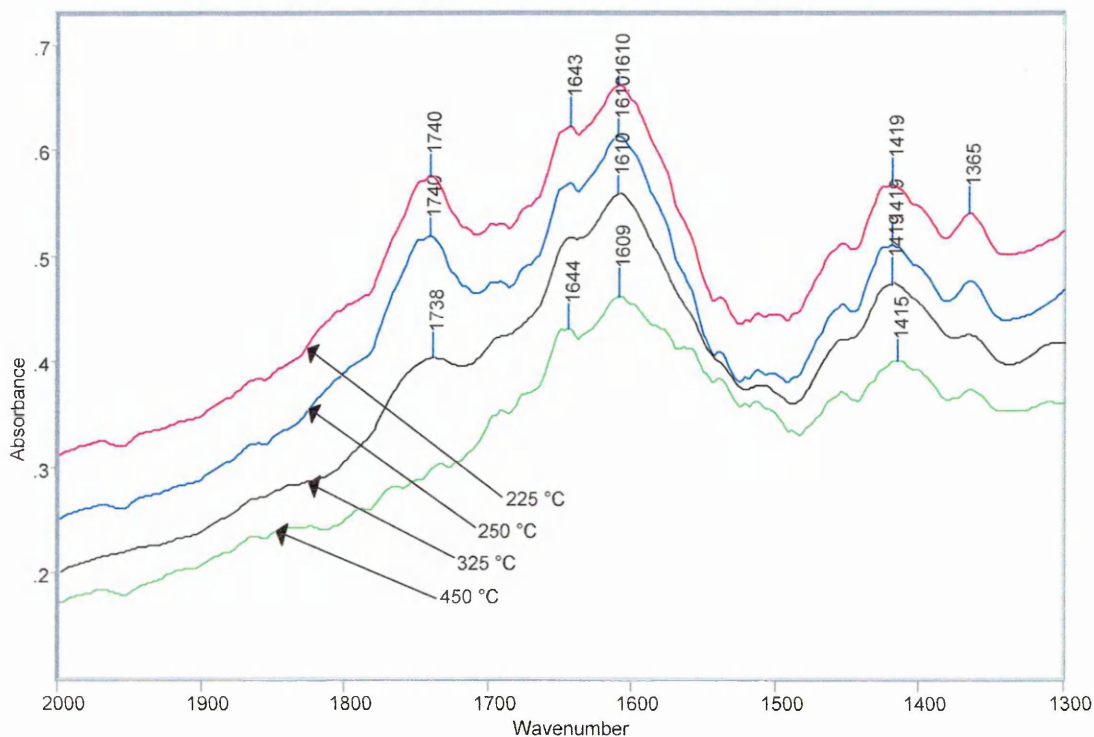
Figure 7.8.2 VT-DRFITS of SWy-2 – Glyoxal Intercalate – 2000 – 1300 cm^{-1}, 200 – 450 °C.

The presence of the bands at 1646 and 1610 cm^{-1} in this sample could merely represent interaction between the carbonyl group of glyoxal and the mixed interlayer cation (Mg^{2+}, Ca^{2+} and Na$^+$) in SWy-2. Alternatively this could represent carbonyl groups interacting with both the interlayer cation and subsequent hydrogen bonding between glyoxal molecules. Furthermore the interaction between glyoxal and the interlayer cations, unlike formaldehyde, may be be via one or both of the carbonyls groups. The large shift of the carbonyl bands at 1643 and 1609 cm^{-1} indicates a strong interaction with the interlayer cation, which is also reflected in its presence at high temperatures in VT-DRIFTS (Figure 7.8.2) and also the TG results. As indicated in the literature review it is also possible that the interaction can take place via both carbonyl groups on the glyoxal molecule which would a particularly strong interaction with the

interlayer cation, involving a torsional rotation of the carbonyl groups from a trans to a cis configuration. Note however that the frequency difference of the carbonyl stretch between the cis and trans isomer[166] is only 1 cm^{-1}.

The 1646 cm^{-1} band appears more clearly resolved as a result of water being lost from this sample.
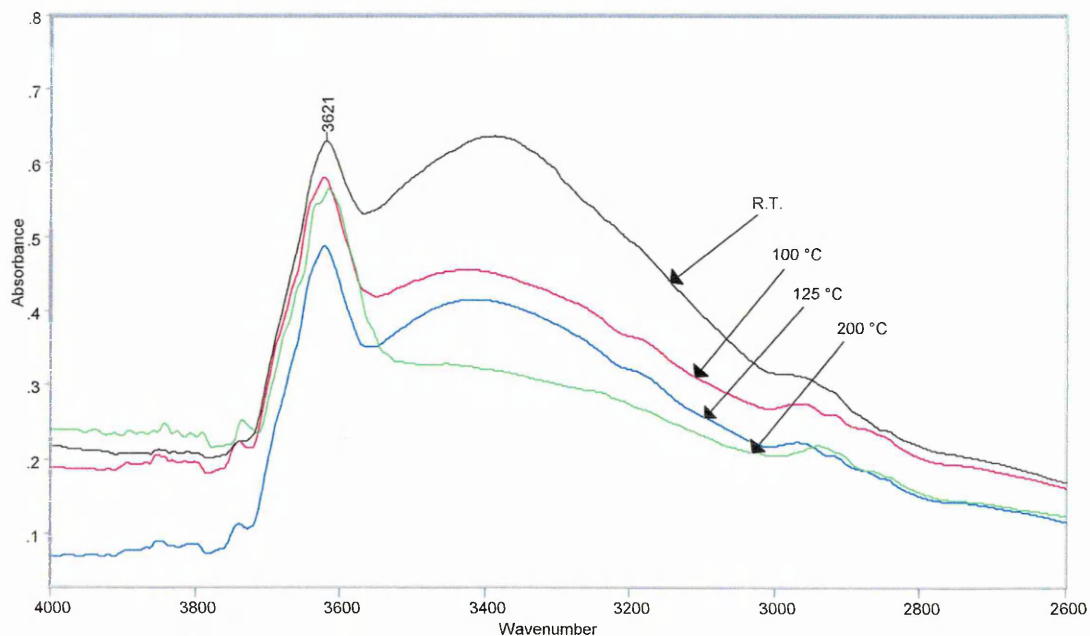
Figure 7.8.3 VT-DRIFTS Glyoxal – SWy-2 intercalate 3000 – 2600 cm^{-1}.
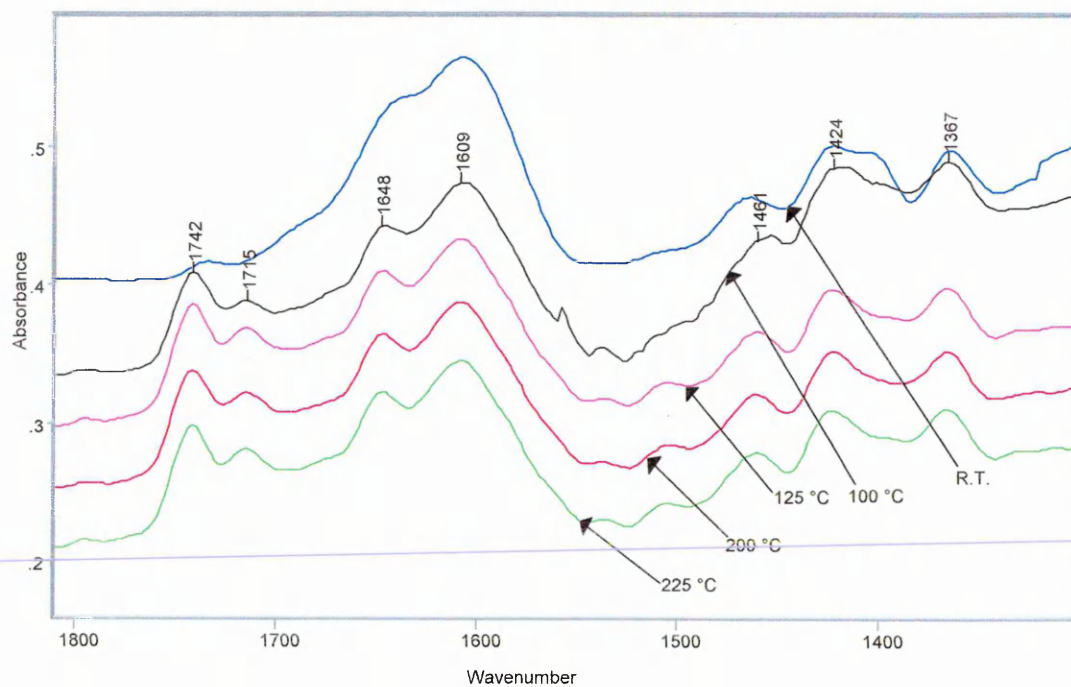
Figure 7.9 – Deconvoluted VT-DRIFTS spectrum of SWy-2 – Glyoxal Intercalate Unwashed.

The deconvoluted spectrum for the Swy-2 – glyoxal intercalate (unwashed) (Figure 7.9) shows that at room temperature there is a shoulder near 1648 cm^{-1} on the 1609 cm^{-1} band. As the temperature is increased this evolves into a distinct band at this wavenumber. Therefore these two bands at 1609 and 1648 cm^{-1} may represent carbonyl groups in two differing interactions with the interlayer cation. The presence to high temperature of these bands (Figure 7.8.2) indicates strong interactions.

The 1609 cm^{-1} band is indicative of an interaction of adsorbed formaldehyde on Cu/SiO_2[150,154] observed at 1610 cm^{-1} (Table 4.2) and also formate on MgO observed at 1605 cm^{-1} (Table 4.3). It is therefore indicative of the type of interaction shown in Figure 7.10 (b).

The 1648 cm^{-1} band is seen in the work of Choi et al[167] in their on cotton fibres treated with glyoxal where the band is present at 1640 cm^{-1}. No firm assignment is given by the authors but the spectrum is described as having no free aldehyde present and it is implied that the easy formation of a five – membered ring is formed with glyoxal and metal ions (Figure 7.10(a)). More appropriate is the work of Para[171], Ibrahim[172] and Kumar[173] and their studies of dialdehyde ligands and metal ion. Para[171] found the band for bidentate ligand (dicarbonyl) on interaction with metal ions to be at 1660 cm^{-1}, whilst Ibrahim[172] and Kumar[173] using smaller ligands, (2-furaldehyde semicarbazone for example) showed that this band shifts to lower frequencies, to as much as 1630 cm^{-1} (Chapter 4 section 4.4.2).
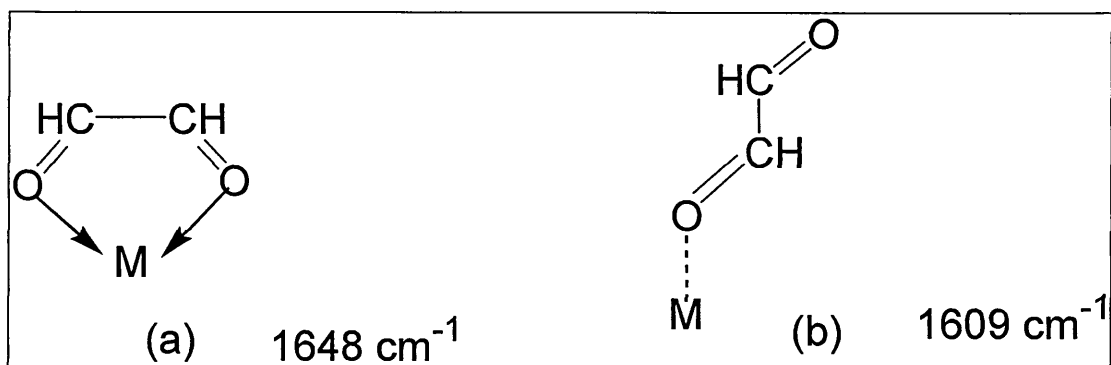
Figure 7.10 – Interactions of glyoxal with interlayer cation.

It should also be noted that the 1609 cm^{-1} band in the VT-DRIFTS of the unwashed intercalate is broad and on heating to 100 °C this band becomes sharper, suggesting that water and / or weakly bound glyoxal may be lost. Note that these bands may also be

211

assigned to similar interactions resulting from dehydrated dimeric and trimeric froms of glyoxal.

The higher frequencies of the 1742 and 1715 cm^{-1} bands suggests that these carbonyl groups are not interacting as strongly with the clay as the carbonyl stretching bands observed below 1700 cm^{-1} and may well be present in clusters of glyoxal more easily removed on heating, or surface adsorbed glyoxal. The 1715 cm^{-1} band is in an almost identical position to that of physisorbed formaldehyde on silica and alumina observed at 1717 and 1718 cm^{-1} respectively (Table 4.4.). It is also in the same position – 1715 cm^{-1} - as the carbonyl interaction with the surface hydroxyls of montmorillonite as described by Sohn[174] and the work on monmorillonite and ketone interactions. This band is not seen until 75 °C however and this may be due to the fact that there may be glyoxal hydrogen bonded to this glyoxal which swamps the signal, and was subsequently lost upon heating. The 1742 cm^{-1} band is in the region of gaseous glyoxal – 1730 – 1745 cm^{-1}. This may imply that either the gas flow in the environmental chamber was not fast enough or that particularly large amounts of glyoxal were being lost from the sample.

A summary of the findings from the VT-DRIFTS of the SWy-2 – glyoxal are presented in Table 7.3, and these results are discussed in more detail in conjunction with the EGA results below, in an attempt to confirm these assignments.

Note that the 1366 cm^{-1} band may be assigned to a CO_2^{2-} stretch, which may indicate the presence of dimeric or trimeric forms of glyoxal.

Observed Band in Intercalate (cm^{-1})	Inference	Temperature Range Observed (°C)
1742	Gaseous glyoxal	75 - 350
1715	Physisorbed / surface adsorbed glyoxal	75 - 325
1648	Dialdehyde – cation interaction (bidentate)	R.T. - 450
1609	Adsorbed Glyoxal (monodentate)	R.T. - 450
1469	CH_2 bend (CH_2-O-) cyclic	R.T. - 450
1427	CH_2 wag (CH_2-O-)	R.T. - 450
1366	CH_2 bend / COO^- stretch	R.T. - 450

Table 7.3 – Band Assignments from SWy-2 – Glyoxal Intercalate (Unwashed)

Several observations are apparent from the EGA of the SWy-2 - glyoxal intercalate. The TIC

(Fig 7.11) shows desorption maxima at 100, 150, 190, 225, 265, 320, 380, 520 and 655 °C.

The major ions detected in this sample are of m / z = 87, 69, 58, 44, 43, 42 and 31 (Figure

7.12). In conjunction with the TG data (Fig 7.3) and the VT-DRIFTS an insight into the thermal

stability can be elucidated.
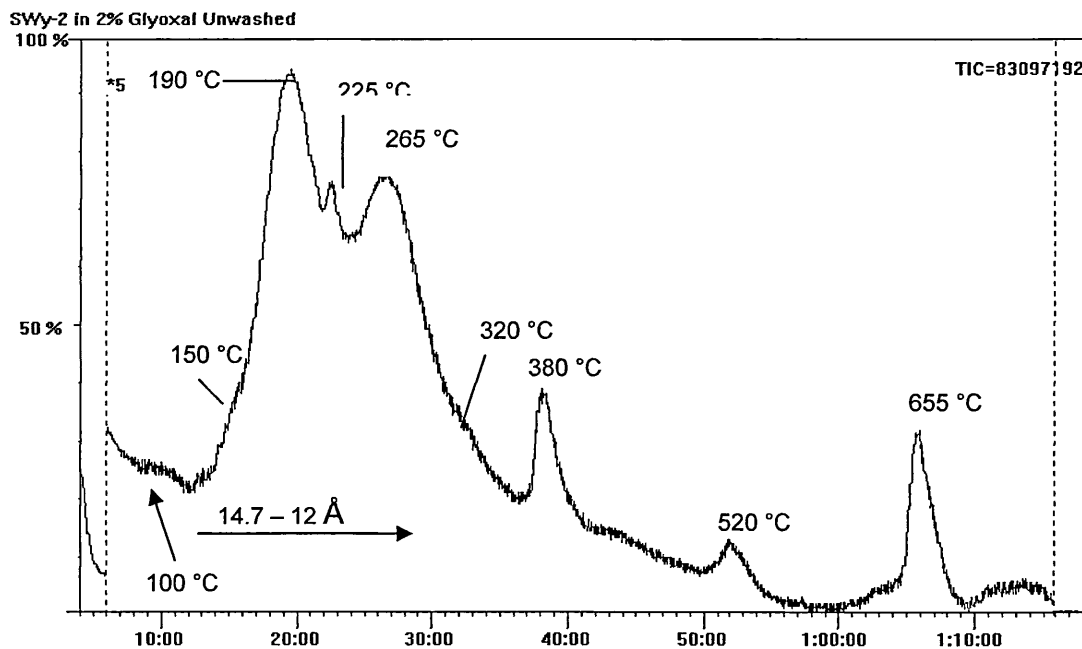
Figure 7.11 – TIC for SWy-2 – Glyoxal Intercalate

Comparison with figure 7.4 shows that the weight loss associated with events at 380, 520 and

655 °C are minimal but obviously produce a high ion yield over a short time. Thus, the major

loss of glyoxal and water occurs between 150 and 360 °C. The data below will show that

unaltered glyoxal is desorbed under the peak at 190 °C, beginning at 140 °C and ending at

300 °C. the second major peak at 265 °C reflects the loss of fragments of glyoxal derived

from polymerised / oligomerised (dimeric and trimeric) species.
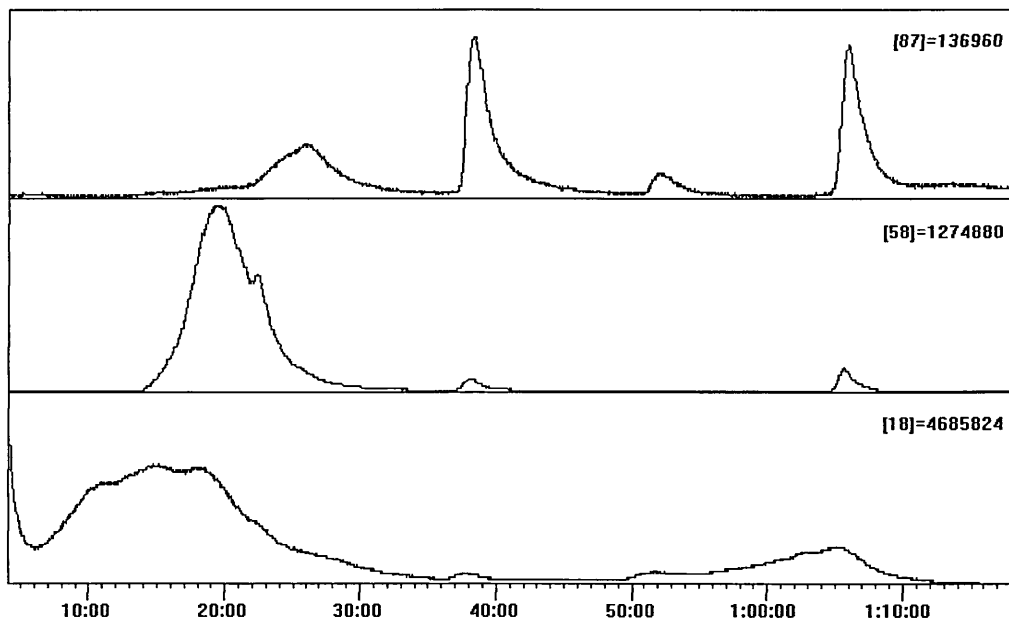
SWy-2 in 2% Glyoxal Unwashed
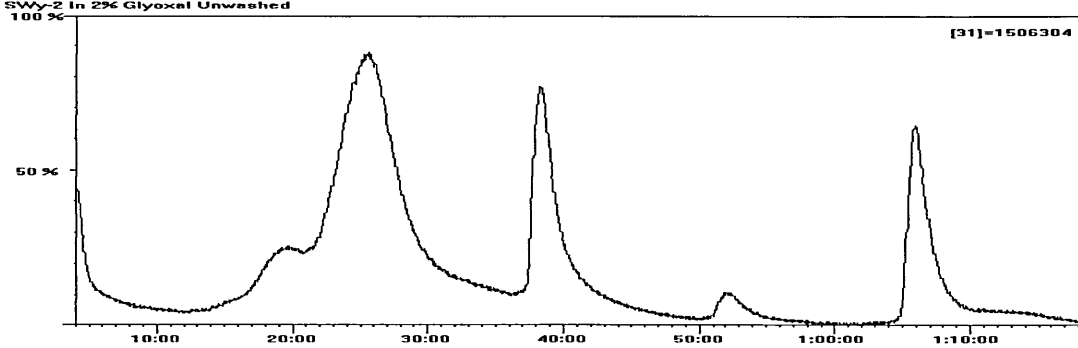
SWy-2 in 2% Glyoxal Unwashed
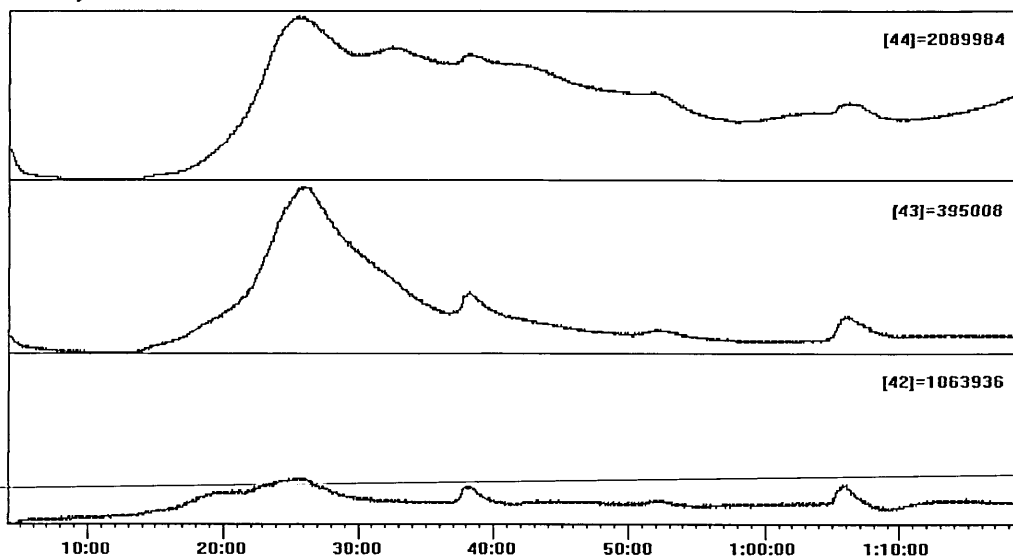
Figure 7.12 – TG – MS Data for SWy-2 – Glyoxal Intercalate

214

	Ion Detected						
Temp (°C)	87	58	44	43	42	31	18
100							√
150							√
190		√				√	√
225		√					
265	√		√	√	√	√	
320			√	√			
380	√	√	√	√	√	√	
520	√		√	√	√	√	
655	√	√	√	√	√	√	√

Table 7.4 – Detection of Ions in TG-MS of SWy-2 – Glyoxal Intercalate.

Examination of the ion $m/z = 18$ (Figure 7.12) shows that water is lost up to a temperature of 350 °C. This may be bridging water – water that is bound to both the interlayer cation and the intercalate. Examination of the VT-DRIFTS for the OH stretching region (Figure 7.8.3) confirms that by 200 °C most of the water has been removed. Differences in temperature are expected when comparing such analyses due to the nature of the increase in temperature – in VT-DRIFTS (and VT-XRD) the increase is stepped, whereas in TG-MS (and TG) this increase is dynamic. If the band assigned to the carbonyl stretch of the intercalate is examined however (1610 cm^{-1}), this does not show any shift to lower frequency as may be expected when such water is removed. There is however a narrowing of this band up to 100 °C especially on the high wavenumber side which may be loss of water seen as removal of the OH bending mode (1630 cm^{-1}). Therefore this water may be bound to the intercalate itself and not the interlayer cation. This is not wholly unexpected given the large quantity of water present in this system. At 200 °C, the VT – XRD shows that this intercalate has gone from a spacing of 14.70 to 13.0 Å. The loss of water is therefore seen in the TG trace as the DTG peaks at 100 and 140 °C, and has a contribution to the peak at 190 °C. The DTG peak at 655 °C is the dehydroxylation of the clay, which occurs as loss of water.

The ion $m/z = 58$ (Figure 7.12) is equivalent to molecular glyoxal (Figure 7.13) (not a polymerised or hydrated form).
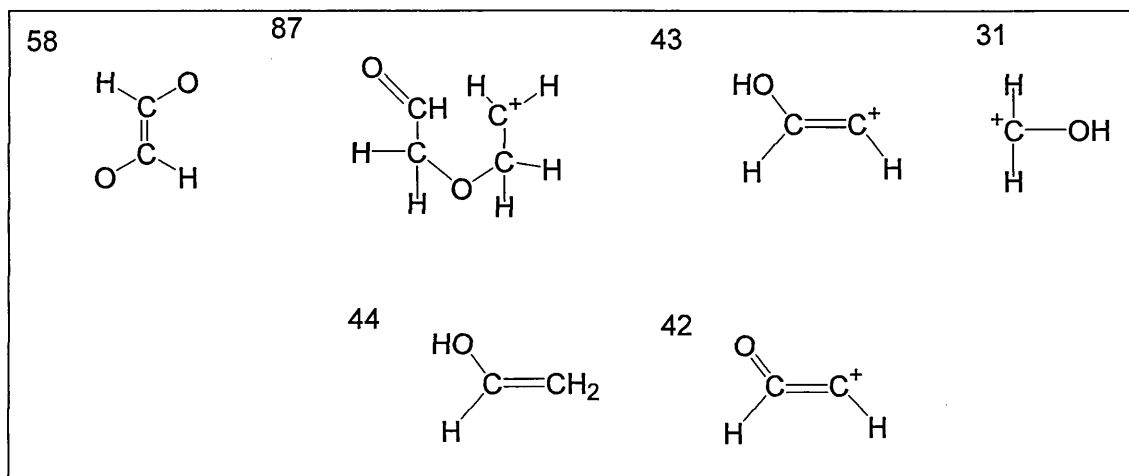
Figure 7.13 – Possible Ion Fragments Resulting from SWy-2 – Glyoxal Intercalate MS data

This ion (m /z = 58) peaks strongly at 190 °C, has a shoulder at 225 °C and is no longer detected by 300 °C. It is detected from 140 °C. The only other two ions which have peaks at 190 °C are m/z = 31 and 18. Over this temperature regime, the VT-DRIFTS shows the detection of the bands at 1742 and 1716 cm^{-1}, although these bands first appear at 75 °C and they are lost at 350 and 325 °C respectively (Figure 7.7). Given the differences in temperature change between these two analyses (VT-DRIFTS and TG-MS) it is still likely that the former assignments for these bands hold true – the 1742 cm^{-1} band may be gaseous glyoxal lost from the sample, whilst the 1716 cm^{-1} is glyoxal adsorbed onto clay surfaces and edges of the clay. This loss is reflected in the DTG peaks (Figure 7.4) at 170 240 and 263 °C and shows a 22% weight loss up to 300 °C. Note also that the VT-XRD shows a decrease in the interlayer spacing from 14.7 to 12.0 Å.

The ion m/z = 31 may be both a fragment of polymerised glyoxal or molecular glyoxal, hence its detection at 170 °C. After 240 °C, the fragment ions detected, m/z = 87, 44, 43, 42 and 31 (Figure 7.13) are assigned to fragments of polymerised glyoxal. Some small amounts of glyoxal (m/z = 58) are detected but this may be glyoxal lost as breakdown products of the polymer. The polymerised glyoxal continues to degrade and is not completely lost when the clay reaches dehydroxylation, and there are peaks from these ions at this temperature, 620 °C (Table 7.4). The ions 87 and 31 show sharp peaks at 380 and 520 (weak) and 655 °C indicating that these ions are detected in short bursts. No explanation as yet can be ascribed to this pattern.

7.2.4 – Summary of SWy-2 – glyoxal intercalate

Glyoxal intercalates SWy-2 to give an interlayer spacing of 14.7 Å which on heating decreases to 12.0 Å by 300 °C. It interacts with the clay via the hydroxyl surface and edge sites (1716 cm^{-1} band) and is intercalated via bidentate (1646 cm^{-1}) and monodentate (1609 cm^{-1}) interaction with interlayer cations. The band at 1716 cm^{-1} together with a band at 1742 cm^{-1} are not detected in the VT-DRIFTS until 75 °C possibly due to hydrogen bonding between glyoxal and water or between glyoxal molecules which swamps these signals. The 1742 cm^{-1} band is assigned to gaseous glyoxal and assignment for this band and the 1716 cm^{-1} is confirmed by TG-MS analysis, which shows glyoxal (m /z = 58) being desorbed over a similar temperature regime. The surface adsorbed glyoxal is lost from the sample by 325 °C and the gaseous glyoxal no longer observed by 350 °C. By this point the TG analysis indicates that 22% of the sample has been lost. Ions detected above that of the RMM for glyoxal and other fragment ions detected by TG-MS indicate that glyoxal may also be present in oligomeric forms, most likely dimeric and trimeric and at high temperature.

7.3 Clay – Amine Intercalates.

7.3.1 – TGA and XRD Analysis

Intercalates of SWy-2 were prepared with 2% solutions of 3NH2, DAP, DAH and EDA. These produced the interlayer spacings (Figure 7.14) shown in Table 7.4.

Amine	Interlayer Spacing Å
3NH2	14.30
DAP	13.20
EDA	13.00
DAH	13.70

Table 7.4 – Interlayer Spacings for SWy-2 Amine Intercalates
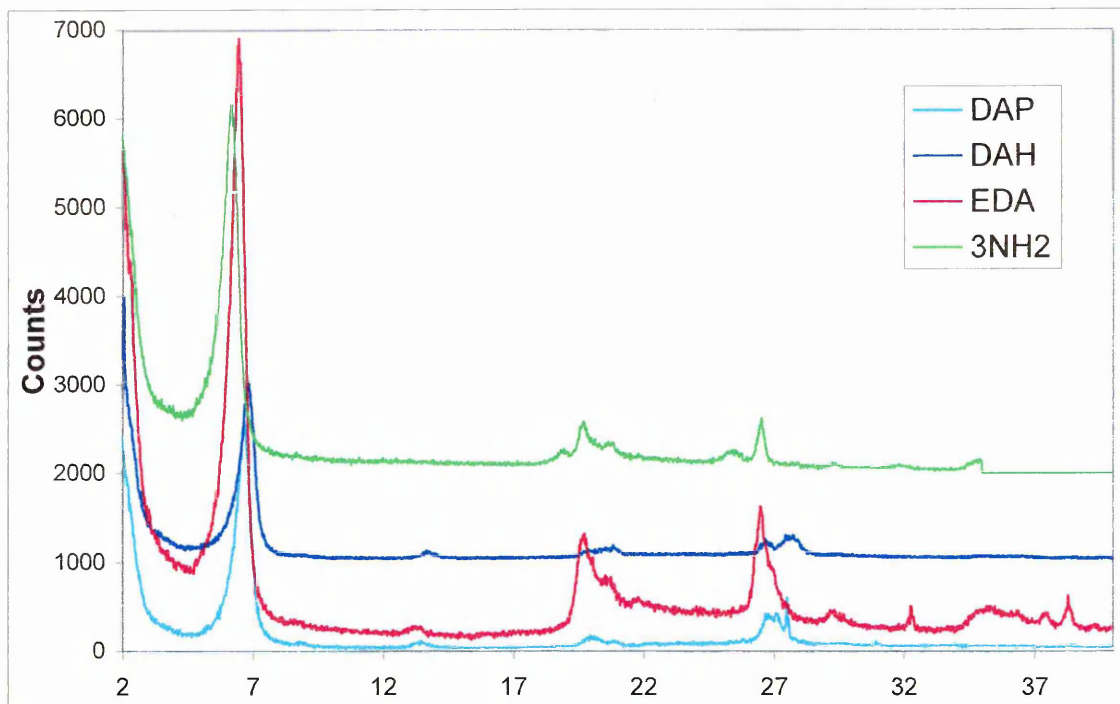
Figure 7.14 – XRD traces of SWy-2 – amine intercalates.

It is interesting to note that the interlayer spacing increases with the chain length of the amine used to form the intercalate (Figure 7.14). The VT-XRD results (Figure 7.15 and Table 7.5 for the 3NH2 intercalate) show a steady decrease in interlayer spacing to 300 °C
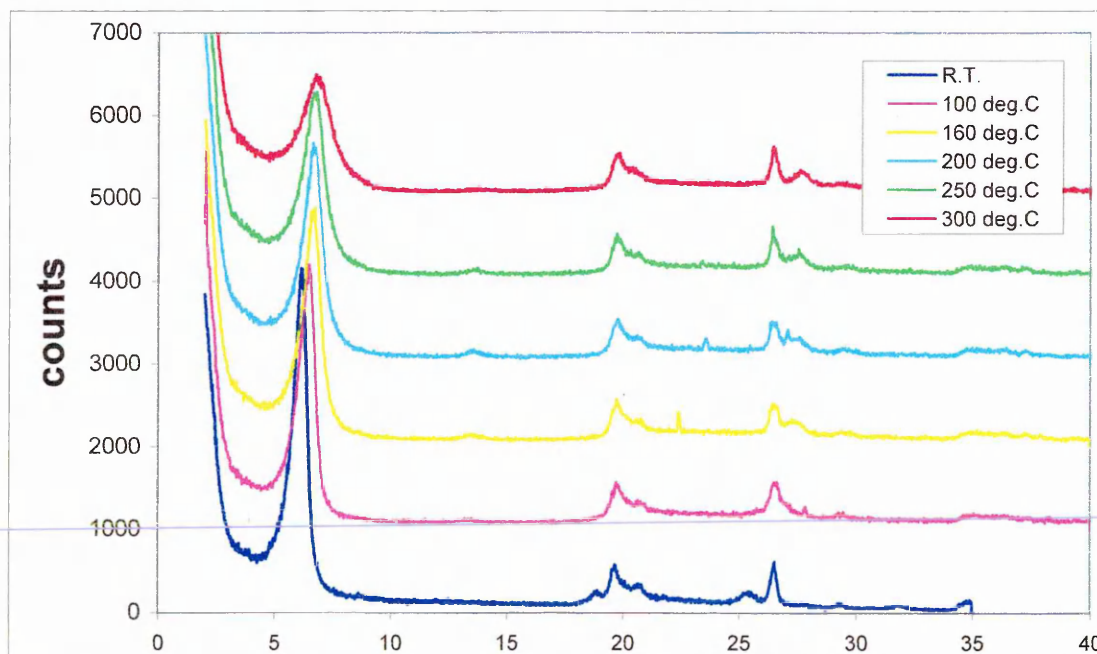
Figure 7.15 – VT-XRD of SWy-2 – 3NH2 Intercalate.

Temperature °C	Interlayer spacing Å
R.T	14.3
50	14.2
100	13.7
140	13.5
160	13.2
200	13.2
250	13.0
300	12.9

Table 7.5 – VT-XRD Analysis of SWy-2 – 3NH2 Intercalate

There is also a steady decrease in intensity of the $d_{(001)}$ of this complex, but it remains stable up to 300 °C. If the TGA of this complex is examined (Figure 7.16, the clay samples which were immersed in 2% 3NH2 solution for 18 hours, 1 day and 2 days show peaks at 100 °C (a shoulder), 132 °C and 188 °C. Also there are broad peaks at 200, 490 and 590 °C, the latter may be the dehydroxylation of the clay. All these intercalates have overall weight losses of 30%.
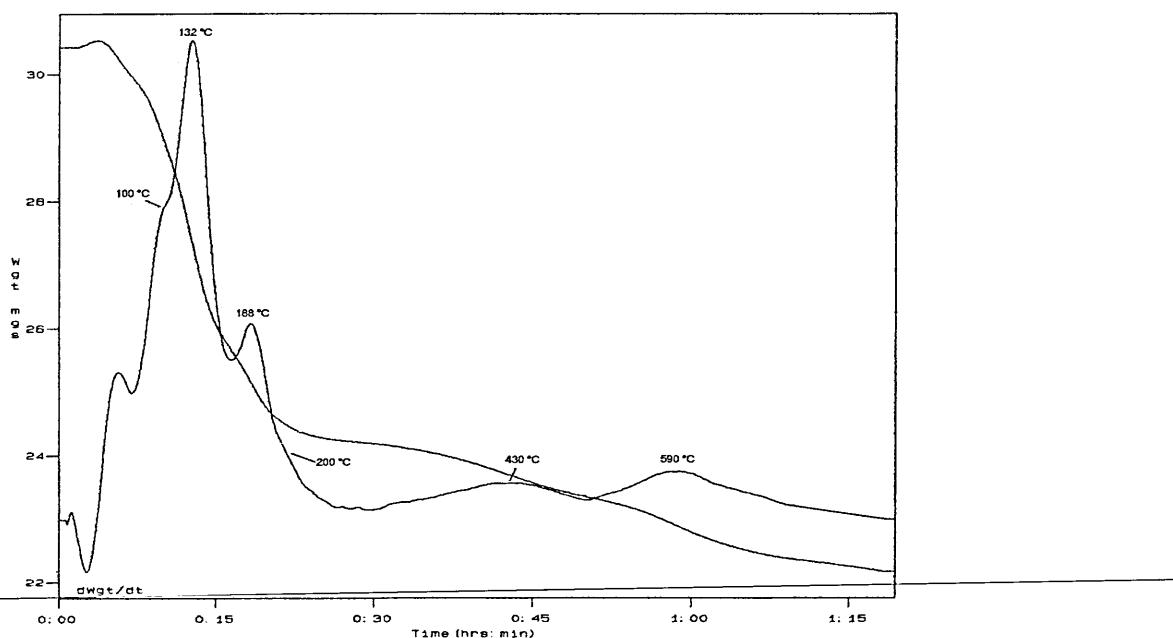
Figure 7.16– TGA of 3NH2 – Clay Intercalate

7.3.2 DRIFTS Analysis

3NH2 liquid (Figure 7.17) has the following bands:-
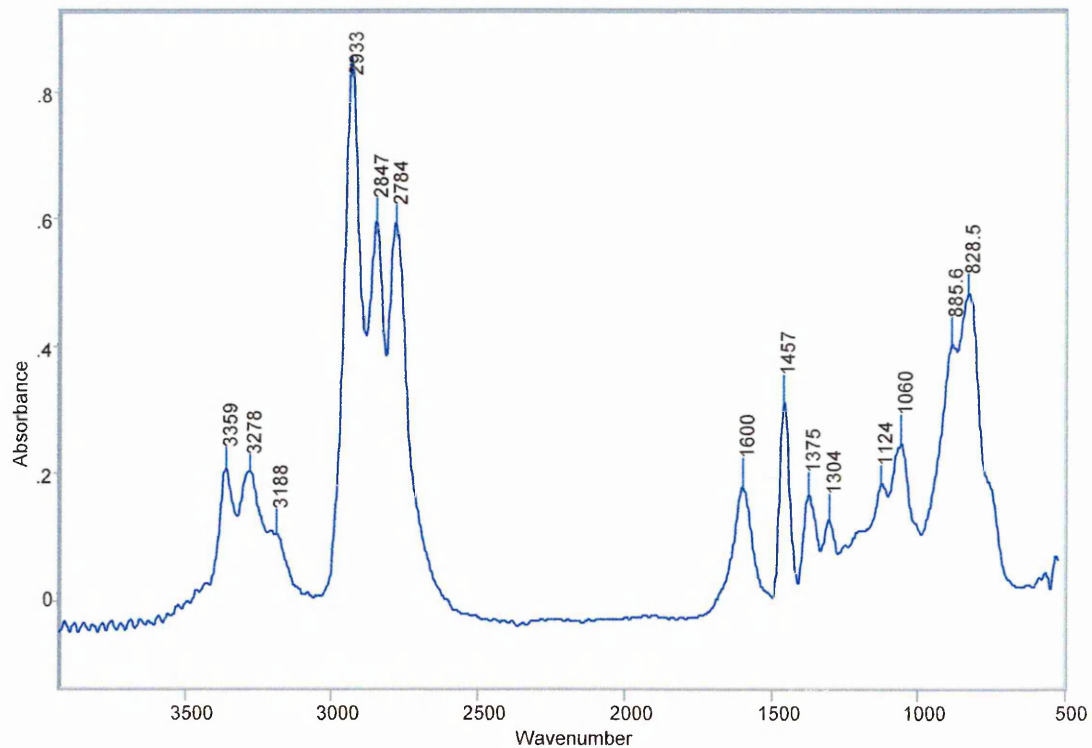
Figure 7.17– FTIR Spectrum of 3NH2 Liquid

Band (cm^{-1})	Assignment
3359	Asymmetric N-H stretch
3278	Symmetric N-H stretch
3188	N-H stretch (free amine)
2933	Asymmetric CH$_2$ stretch
2847	Asymmetric CH$_2$ stretch
2784	Symmetric CH$_3$ stretch
1600	N-H$_2$ scissors
1457	Asymmetric CH$_3$ bend
1375	C-N stretch
1304	CH$_2$ bend

Table 7.6 – Band Assignments for 3NH2 Liquid

The structure of 3NH2 is shown below:-

$$H_2N\text{---}(H_2C)_3\text{---}\underset{\underset{\displaystyle CH_3}{|}}{N}\text{---}(CH_2)_3\text{---}NH_2$$
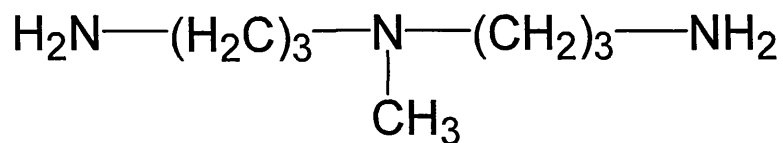
From the position of the central nitrogen atom in this structure this is a tertiary amine. However the presence of the two NH$_2$ groups at either end could also make this a primary amine. This is an important point to consider when studying the IR spectrum of the liquid 3NH2 and its intercalates with SWy-2 and composites with glyoxal.

Recalling that primary amines exhibit two bands in the 3300 – 3500 cm^{-1} region (Chapter 4 section 4.4.4) the two N-H stretching bands at 3359 and 3278 cm^{-1} can be said to be of a relatively low frequency for this amine. This reflects the hydrogen bonding in the liquid 3NH2, which causes the shift to lower wavenumber and is also apparent from the boiling point of 3NH2 –112 °C. Recalling also that the NH$_2$ deformation is located in the region 1590 – 1650 cm^{-1} and is observed here at 1600 cm^{-1}, then this is a consistent observation for hydrogen bonded NH$_2$.

An additional N-H stretch is also observed at 3188 cm^{-1} and this attributed to free amine. This band is only observed as the sample is presented as a neat solution of amine and is consistent with such observations of the IR spectra of such amines (Chapter 4 section 4.4.4). The intercalate prepared from 2% 3NH2 solution (Figure 7.18.1 and 7.18.2) displays the following bands:

Band (cm^{-1})	Assignment
3363	Asymmetric N-H stretch
3300	Symmetric N-H stretch
2950	Asymmetric CH$_2$ stretch
2863	Asymmetric CH$_2$ stretch
2794	Symmetric CH$_3$ stretch
1647	N-H asymmetric deformation / O-H bend
1596	N-H scissors
1468	CH$_2$ scissors
1363	N-C-H bend
1317	CH$_2$ bend

Table 7.7 – Band Assignments for SWy-2 – 3NH2 Intercalate
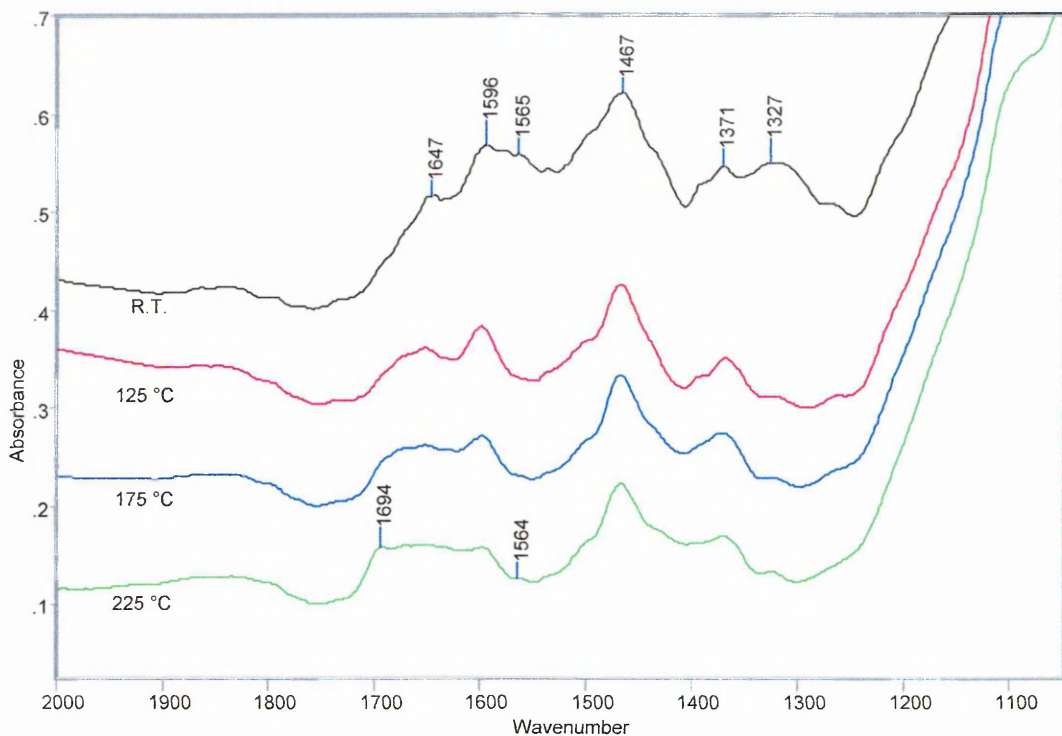
Figure 7.18.1 – VT-DRIFTS of SWy-2 – 3NH2 1900 – 1200 cm^{-1} R.T – 225 °C
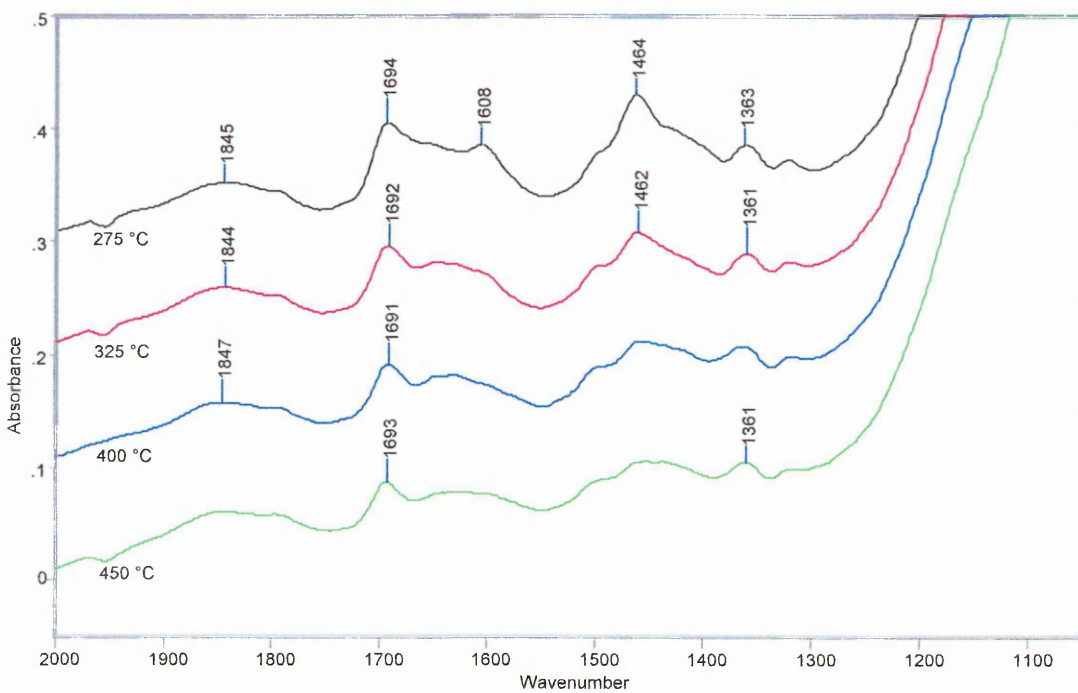
Figure 7.18.2 - VT-DRIFTS of SWy-2 – 3NH2 1900 – 1200 cm^{-1} 275 - 450 °C

The presence of the NH_2 scissors at 1595 cm^{-1} (Figure 7.18.1) is a shift to lower frequency of 5 cm^{-1} from that of the liquid 3NH2. This indicates that it is involved in bonding to the

interlayer cations. This band is stable up to 300 °C and moves to a higher frequency of 1606 cm^{-1} as the temperature is increased (Figure 7.18.2).

A series of bands centred at 1565 cm^{-1} are also observed. Such a shift in the NH_2 scissors (to lower frequency) would imply that these bands are more strongly bound NH_2. However, as they are no longer observed by 125 °C this would appear not to be the case.

The band at 1647 cm^{-1} may be attributed to either water (OH bend) or again the NH_2 scissors. The band is at a high wavenumber for an N-H deformation however and would indicate relatively free NH, leaving the most likely assignment for this band to be water, an O-H bend. Such observations as discussed so far are similar to those of Laura and Cloos [184-186] and their spectroscopic studies of the intercalated EDA (Chapter 4 section 4.4.4.). They observed NH_2 bands at 1592 which were associated with the presence of bridging water (water bonded to the interlayer cation and the EDA and thus acting as a bridge between the two). Hence as this water is removed there is a small shift to higher frequency of this band (the NH_2 is more tightly bound to water than the cation). These authors also observed a shoulder at 1640 cm^{-1} (similar to the band observed in the SWy-2 – 3NH2 intercalate, which was dried in air) in clay samples which they treated with EDA and then exposed to air or water vapour.

A band appears at 225 °C at 1694 cm^{-1}. This is at too high a frequency to be due to NH_2 and is stable to 450 °C. No assignment is as yet given for this band.

The N-H asymmetric and symmetric stretches observed were at 3358 and 3299 cm^{-1} respectively (Figure 7.18.3). These are both lost however by 250 °C as is the CH_3 stretch (2794 cm^{-1}). The CH_2 stretching bands however, remain until 450 °C. These observations of the N-H stretching bands, together with the presence of the NH_2 scissors 1596 cm^{-1}) suggests that 3NH2 is present within the interlayer of the clay to 300 °C. Up to this temperature, the VT-XRD results show that there is a decrease in the interlayer spacing from 14.3 to 12.9 Å.
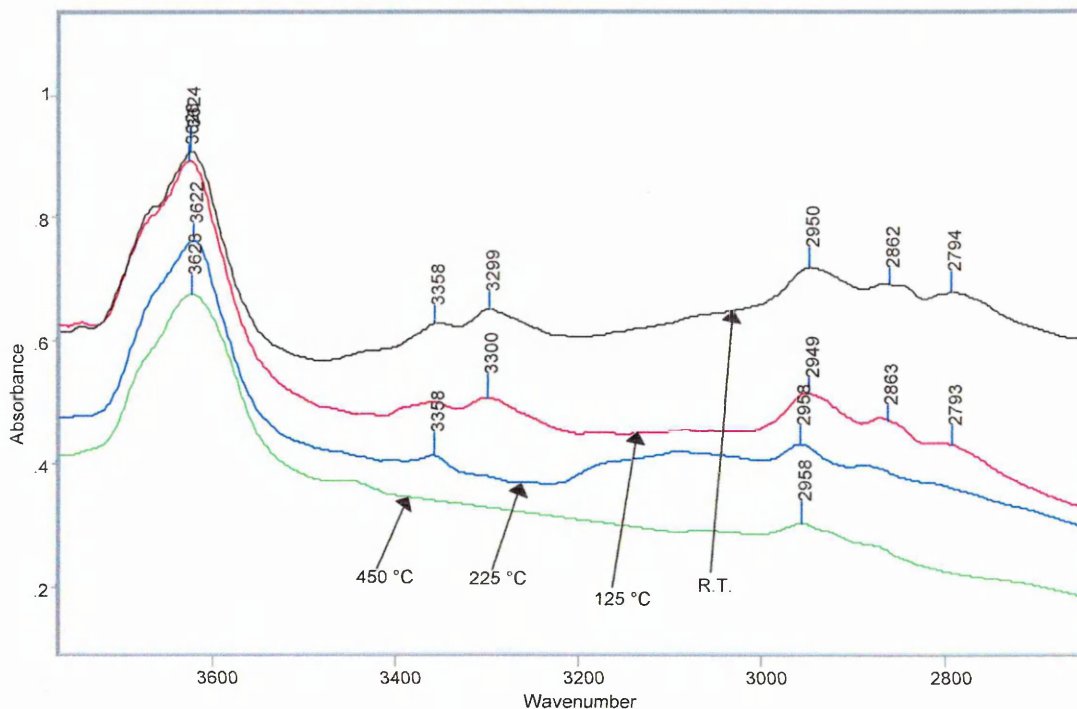
Figure 7.18.3 – VT-DRIFTS of SWy-2 – 3NH2 3500 – 2700 cm^{-1}.

The SWy-2 – 3NH2 intercalate was washed with deionised water, producing differing results. The XRD trace (Figure 7.19) at room temperature displays an interlayer spacing of 13.50 Å at room temperature compared with 14.30 Å for its unwashed counterpart.
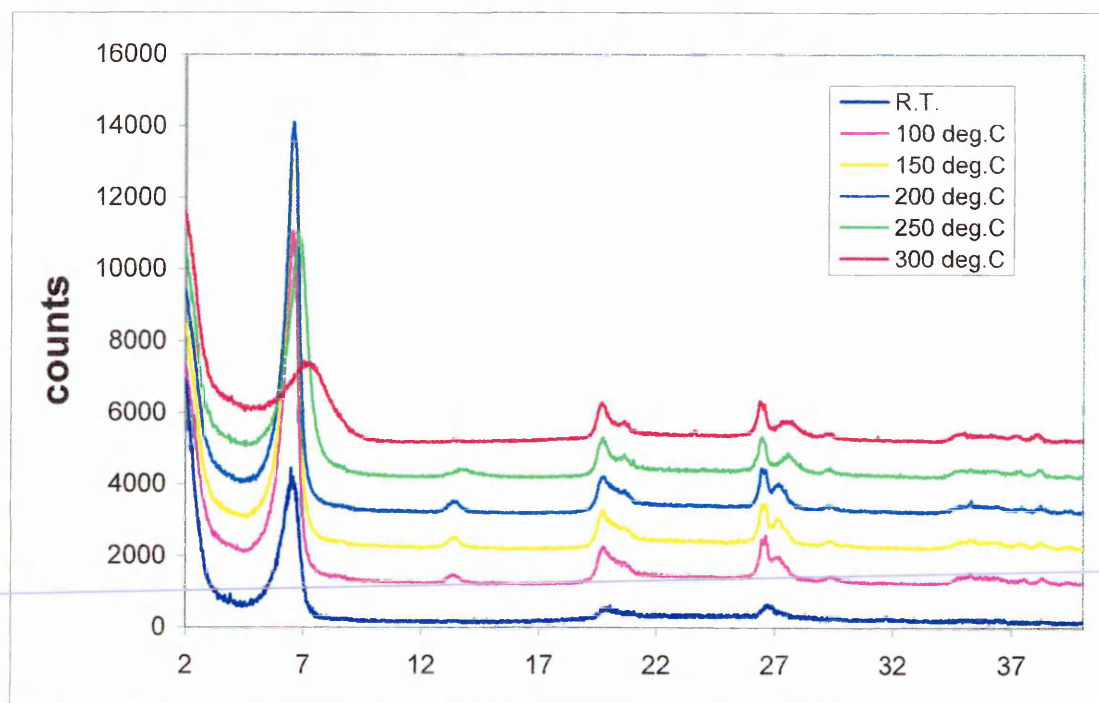
Figure 7.19 – VT-XRD of SWy-2 – 3NH2 intercalate after washing

As the temperature is increased, this spacing decreases to 12.20 Å by 300 °C. DTG analysis of this sample (Figure 7.20) reveals peaks at 60, 200 410 and 620 °C, and is markedly different again to that for the unwashed samples.
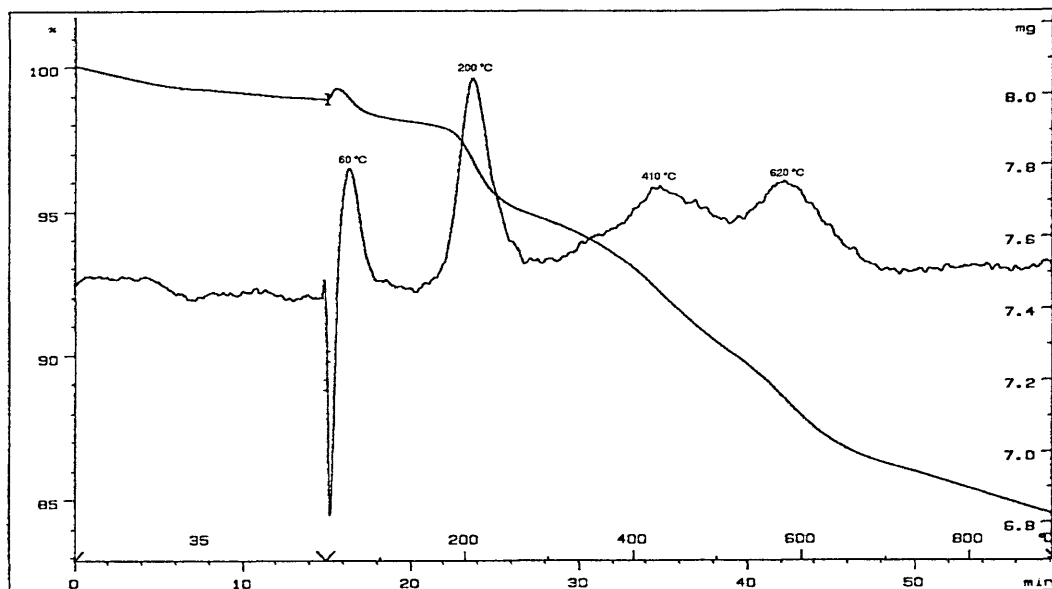
Figure 7.20 – TGA Analysis of SWy-2 – 3NH2 Intercalate after washing

The DRIFTS spectrum (Figure 7.21) shows that the NH_2 scissors (1596 cm^{-1}) is now more intense and clearly resolved at room temperature. The N-H asymmetric deformation is now seen at 1667 cm^{-1} as well a 1596 cm^{-1}, though the former is very weak, whilst two new bands at 3245 and 3196 cm^{-1} are also observed as well as two bands at 3363 and 3303 cm^{-1}. The former two bands at 3245 and 3196 cm^{-1} would indicate N-H stretches but now in a different environment to the unwashed sample, possibly an interaction with the interlayer catrion via a water bridge, hence their relatively lower wavenumber. The broad band at 2550 cm^{-1} is reminiscent of the observations again of Laura and Cloos [184-186] in that they observed a broad diffuse band at 2500 cm^{-1} which they attributed to NH_2 hydrogen bonded to water. Indeed, such broad diffuse regions are often attributed to hydrogen bonding.

Hence the two new NH stretching bands seen at 3245 and 3196 cm^{-1} could now be 3NH2 which is bonded to interlayer cations via a water bridge, most likely as a result of the washing treatment.

225
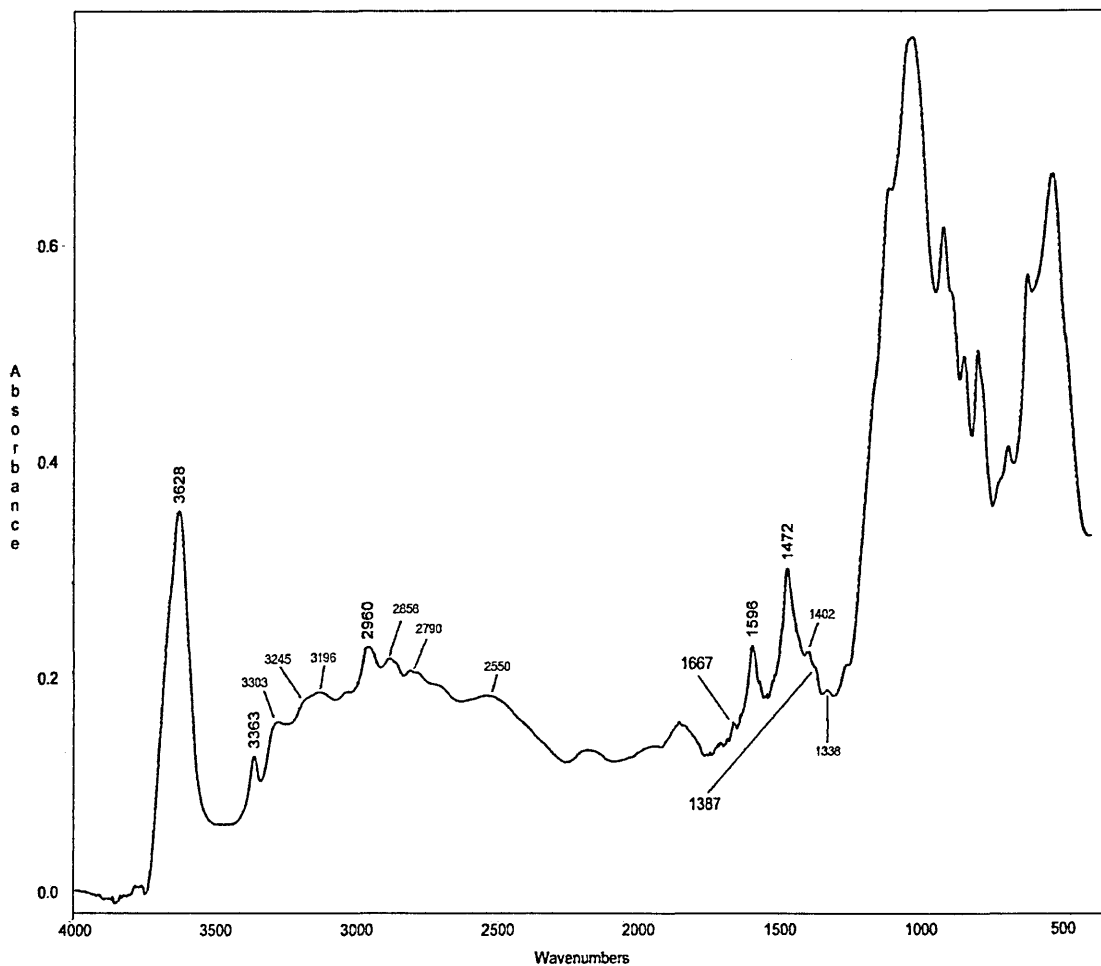
Figure 7.21 – DRIFTS Spectrum of SWy-2 - 3NH2 intercalate after washing.

7.3.3 Summary of SWy-2 – 3NH2 intercalate

3NH2 intercalates SWy-2 to produce an interlayer spacing of 14.30 Å. On heating this decreases to 12.9 Å at 300 °C. Interaction of this amine with interlayer cations is observed in shifts of the NH_2 scissors band to 1595 cm^{-1} which moves to 1606 cm^{-1} as the temperature is increased and is stable to 300 °C. The N-H stretching bands at 3363 and 3300 cm^{-1} in the intercalate are observed at 3359 and 3278 cm^{-1} in liquid 3NH2, but these positions in the liquid reflect hydrogen bonding here. A band at 1647 cm^{-1} in this intercalate is assigned to water and together with the movement of the 1595 cm^{-1} band to higher temperature on heating indicates interaction at room temperature via a water bridge in a situation similar to that observed by other authors[184-186]. The presence of both the NH_2 scissors band and NH stretching bands to 300 °C indicates that 3NH2 is present in the clay to this temperature. The DTG results also show that all the major weight losses have occurred by this temperature.

226

Washing the 3NH2 intercalate shifts the NH stretching bands to lower frequency, 3245 and 3196 cm^{-1} though NH stretching bands still remain at 3363 and 3303 cm^{-1}, indicating that there are some NH$_2$ groups in a different environment possibly interacting via a water bridge. A broad diffuse band at 2500 cm^{-1} observed by other authors[184-186] supports this observation as this is assigned to water hydrogen bonded to NH$_2$.

7.4 Amine – Aldehyde Clay Composites.

Attempts to synthesise clay mineral amine - aldehyde composites were made by immersing the clay in a solution containing equal volumes (3 ml.) of 2% w/w of the aqueous solution of the aldehyde and amine. On mixing the two reactants the resultant solution turned cloudy before clearing. The reaction was also observed to be sufficiently exothermic to warm the reaction vessel. Over time the solution then changed to an orange – brown colour. The resultant composite was the same colour and the texture harder than the original clay upon grinding.

7.4.1 Possible Reaction Products.

In order to understand the full range of potential products produced on mixing the two reactants it is first necessary to identify the possible products that may be formed and the factors affecting their formation. In the examples shown the reaction products are based on the reaction between glyoxal and 3NH2.

7.4.1.1 Reaction of Functional Groups to form imines

As previously discussed, (Section 2.5.3) routes to all the reaction products proceed via the methylol intermediate. If all the amine and aldehyde functional groups were to react and sufficient methylol groups were formed and if the reaction proceeded to form a polyimine the resultant product would be thus:-

227

This is an unlikely scenario (see section below on methylol units). If the polymerisation did not proceed then the simpler imines (b) and (c) would be formed:-

—HC=N—(CH$_2$)$_3$—N—(CH$_2$)$_3$—N=C-C$\overset{O}{\underset{H}{\diagup}}$
         |
         CH$_3$
(b)

H$_2$N—(CH$_2$)$_3$—N—(CH$_2$)$_3$—N=C-C$\overset{O}{\underset{H}{\diagup}}$
         |
         CH$_3$
(c)

If either (a) or (b) was formed then there would be a notable lack of N-H vibrations in the infrared spectrum. If product (c) were to be formed then complications would arise due to overlapping bands from the carbonyl, imine and amine functional groups. These reaction products also serve to illustrate the complexity of the reaction and the subsequent products that may be formed as is illustrated in the following sections. It is worth recapping at this stage the observed band positions for all the functional groups involved as an aid to further discussion:-

NH$_2$ groups – two bands, NH stretching 3500 – 3300 cm^{-1} one band 1650 – 1590 cm^{-1} (NH$_2$ scissoring).

NH – one band 3390 – 3320 cm^{-1} (stretch), one band 1650 – 1510 cm^{-1} (NH deformation).

Imines NH stretch 3350 – 3320 cm^{-1} and C=N stretch 1690 – 1590 cm^{-1}.

Aldehyde C=O stretch – 1740 – 1680 cm^{-1} (and as low as 1610 cm^{-1} on interaction with minerals)

Again it is worth recalling that these band positions may be even lower on interaction with clay minerals.

7.4.1.2   The Methylol Intermediates

It is important to understand the structures of the methylol intermediates when investigating the reaction between aldehydes and amines as ultimately they may determine the end product. As most of the reactant used here – with exception of formaldehyde – are bifunctional then two types of methylol may be formed which depend on the amount of aldehyde present. If the aldehyde is present in approximately equal amounts then monomethylol units may be formed:-

228

$$H_2N-(CH_2)_3-\overset{\underset{|}{CH_3}}{N}-(CH_2)_3-\overset{\overset{H}{|}}{N}-CH\overset{\overset{\overset{H}{|}}{C=O}}{\underset{OH}{}} \quad (1)$$
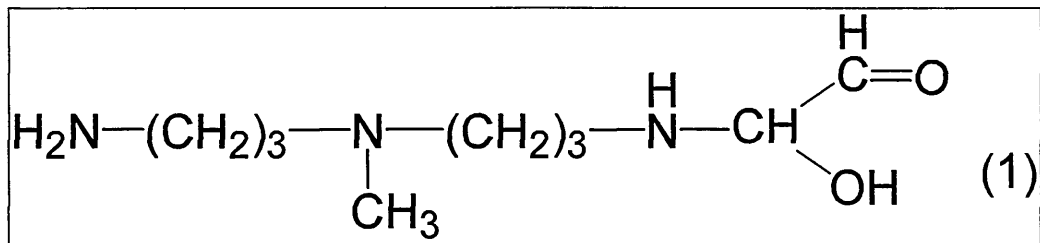
Methylol units are considered to be quite reactive and this unit would easily be characterised

using IR by the OH group giving a strong broad band in the $3600 - 3300$ cm^{-1} region. If

however the aldehyde is present at twice the molar amount of the amine then dimethylol units

are formed:-

$$O=C\overset{\overset{H}{|}}{\underset{HO}{CH}}-\overset{\overset{H}{|}}{N}-(CH_2)_3-\overset{\underset{|}{CH_3}}{N}-(CH_2)_3-\overset{\overset{H}{|}}{N}-CH\overset{\overset{\overset{H}{|}}{C=O}}{\underset{OH}{}} \quad (2)$$
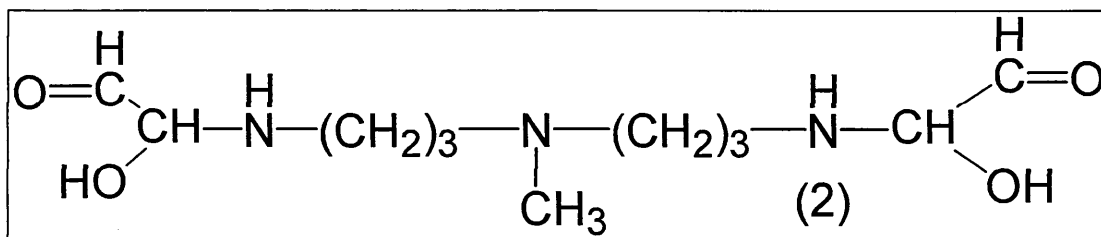
Due to reactive nature of the methylol units it is unlikely – but still possible – that these

products would be observed. The reaction to form methylol units in both cases leads to the

above two intermediates as the most likely to be formed because reaction of the unreacted

carbonyl group is less likely to occur once the aldehyde has formed a methylol unit.

7.4.1.3   Self Condensation of Methylol Units.

The heat generated from the reaction of the aldehyde and amine groups may be sufficient for

the methylol intermediates to react via self condensation to form amino resins, For the

monomethylol units (Structure 1 above) the product is as follows:-

$$(3) \quad H_2N-(CH_2)_3-\overset{\underset{|}{CH_3}}{N}-(CH_2)_3-\overset{\overset{H}{|}}{N}-\overset{\overset{\overset{O}{\|}}{CH}}{\underset{H}{C}}-O-\overset{\overset{\overset{O}{\|}}{CH}}{\underset{H}{C}}-\overset{\overset{H}{|}}{N}-(H_2C)_3-\overset{\underset{|}{CH_3}}{N}-(H_2C)_3-NH_2 \quad + H_2O$$
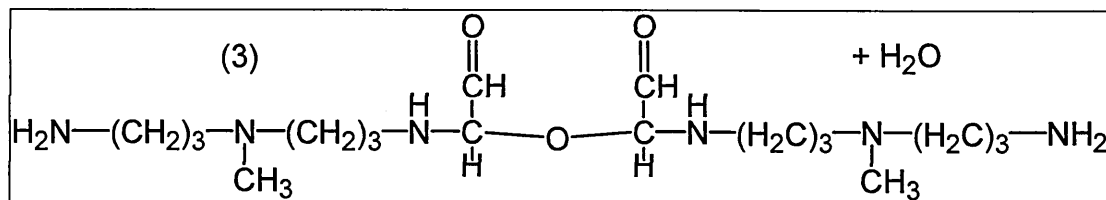
This product is essentially a dimer of the monomethylol units, and polymerisation of

monomethylol units can proceed to yield the following product:-

229

Structure (4):

$$HC\overset{\displaystyle O}{=} \quad HC\overset{\displaystyle O}{=} \quad HC\overset{\displaystyle O}{=}$$
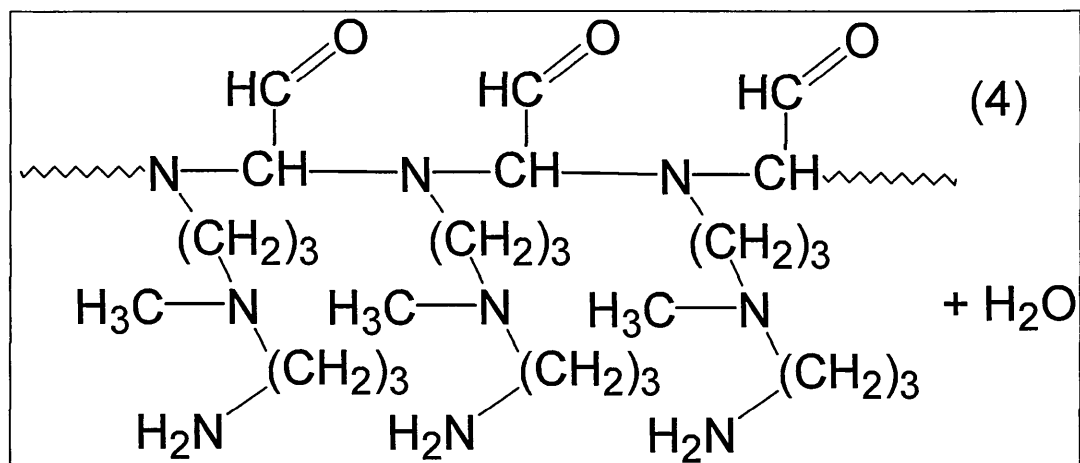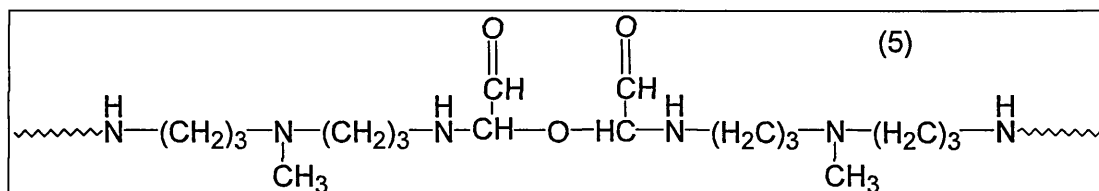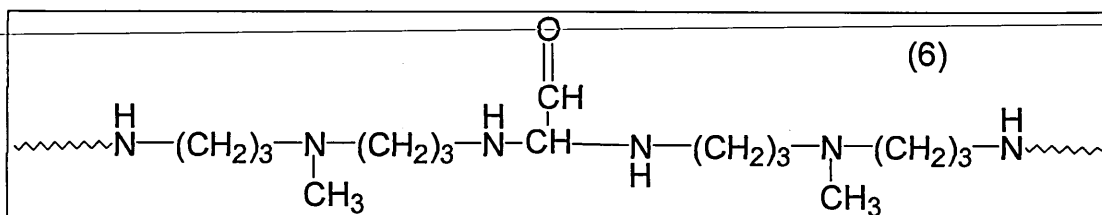
~~~N—CH—N—CH—N—CH~~~
(CH₂)₃   (CH₂)₃   (CH₂)₃
H₃C—N   H₃C—N   H₃C—N   + H₂O
(CH₂)₃   (CH₂)₃   (CH₂)₃
H₂N   H₂N   H₂N

(Structure is $HC{=}O$ groups on CH backbone with $(CH_2)_3$, $H_3C{-}N$, $(CH_2)_3$, H_2N substituents; $+ H_2O$.)   (4)

The self condensation of the dimethylol units (Structure 2 above) can also lead to polymerisation:-

Structure (5):

~~~N—(CH₂)₃—N—(CH₂)₃—N—CH—O—HC—N—(H₂C)₃—N—(H₂C)₃—N~~~
with H on each terminal N, CH_3 on branching N, and $\overset{\displaystyle O}{\underset{\displaystyle \|}{CH}}$ groups.   (5)

In terms of IR analysis the difference between these products would be that the amino resin formed by the monomethylol units would show two bands in the N-H stretching region and the NH₂ scissoring band, whereas the dimethylol product would not exhibit indications of NH₂ scissoring bands, merely one band in the N-H stretching region. Note that there may be two bands in the NH stretching region indicating a chain ending in NH₂ – and the NH deformation seen in both. Some products have a C-O-C ether like bond but this band is observed in the region 1150 – 1060 cm^{-1} so it is unlikely that this band will be observed due to the intense and strong Si-O band seen present due to the clay.

7.4.1.4   Condensation Reactions between Methylol groups and Amines

Alternatively condensation reactions can proceed between the methylol units and amines:-

Structure (6):

~~~N—(CH₂)₃—N—(CH₂)₃—N—CH—N—(CH₂)₃—N—(CH₂)₃—N~~~
with H on terminal N's, CH_3 on branching N's, and $\overset{\displaystyle O}{\underset{\displaystyle \|}{CH}}$ group.   (6)

The product shown above is the same whether the di or mono methylol unit reacts (the dimethylol unit simply adds CHCHO to the end of the above structure). Again there is a lack of NH_2 in the structure, except for the end groups, which may be observed in IR.

7.4.1 XRD Analysis of Composites

The $d_{(001)}$ spacing for the composite made from 1% glyoxal and 1% 3NH2 (Figure 7.25) is 16.40 Å. This value is larger than for the intercalates of both 3NH2 and glyoxal but, if this is an imine polymer a larger value is not altogether unexpected. Subsequent VT-XRD data (Figure 7.22) shows that the interlayer spacing steadily decreases with increasing temperature and at 400 °C has reduced to 13.80 Å. This implies that there may be some degradation of the intercalated material.

Figure 7.22 – VT-XRD traces of SWy-2 + 1% Glyoxal and 1% 3NH2 composite

DTG data for this sample (Figure 7.23) is more complex than others seen so far and shows an overall weight loss of 42% with peaks at 50, 130, 210, 310, 510, 600, 690 and 750 °C. As compared to the DTG traces of the SWy-2 intercalates with 3NH2 and glyoxal alone, the 3NH2 intercalate shares peaks at similar temperatures with this composite at 130, 200, and 600 °C. The glyoxal intercalate at 140 and 300 °C.

Figure 7.23 – TGA trace of SWy-2 + 1% Glyoxal and 1% 3NH2 composite

7.4.2 DRIFTS Analysis of Amine - Aldehyde Composites

An attempt to synthesise the imine polymer was made using 10 % aqueous solutions of glyoxal and 3NH2 without the presence of the clay for subsequent DRIFTS analysis (Figure 7.24).

The product obtained was light brown in colour with a very hard resinous texture. The texture of this product did not allow proper grinding of the sample for DRIFTS analysis as it was so hard. This reflected in the $3500 - 3000$ cm^{-1} region of the spectrum below where detail is lost, due to the background resulting from the poorly ground sample.

Figure 7.24 - Product from 10%Glyoxal and 10% 3NH2 – No Clay

Band Position (cm^{-1})	Assignment
2945	Symmetric CH$_3$ stretch
2841	Asymmetric CH$_2$ stretch
2793	Symmetric CH$_2$ stretch
1661	Imine C=N Stretch / C=O stretch / NH$_2$ scissors
1603	C=O stretch / NH$_2$ scissors
1542	N-H deformation
1463	Asymmetric CH$_3$ bend / CH$_2$ deformation
1312	
1217	C-N stretch
1169	

Table 7.7 – Band assignments for composite made from 10% 3NH2 and 10% glyoxal

The position of the band at 1661 cm^{-1} is high for the NH$_2$ scissors and this leaves the possibility of this being the C=N imine stretch or a C=O stretch. The band at 1603 cm^{-1} is unlikely to be carbonyl as there is no clay present in this sample and the carbonyl stretch has only been observed at such wavenumbers when interacting with minerals. Therefore the NH$_2$ scissors is the most likely assignment. The band at 1542 cm^{-1} is an NH deformation. Hence

233

this sample contains both NH_2 and NH. However, no firm indication of the reaction product can be made from these bands alone. Hence study of the clay composites with these reactants may give further indication of the reaction product formed.

The DRIFTS analysis of a composite made from 1% each of glyoxal and 3NH2 (Figure 7.28) displays the following bands:-

Band (cm^{-1})	Assignment
3389	N-H stretch
3323	N-H stretch
2948	Symmetric CH_3 stretch
2860	Asymmetric CH_2 stretch
2801	Symmetric CH_2 stretch
1674	Imine C=N Stretch or C=O stretch
1655	C=O Stretch
1598	NH_2 Scissors
1538	N-H deformation
1462	Asymmetric CH_3 bend
1364	Symmetric CH_3 bend

Table 7.8 – Band Assignments for SWy-2 + 1% Glyoxal and 1% 3NH2 composite DRIFTS Spectrum

The band at 1655 cm^{-1} could also be an OH bend attributed to water in the sample, but as the VT-DRIFTS analysis reveals (Figure 7.25.1) this band is stable to 400 °C, so this is very unlikely. Other changes which occur as the temperature is increased, are a decrease in the intensity of the CH_2 and CH_3 bends and stretches. The 1655 cm^{-1} band does reduce in intensity by 100 °C but does not significantly decrease in intensity again until 350 °C. Some of this reduction in intensity may be attributed to loss of water. This band is broad and in fact comprises of two bands the second at the higher frequency of 1674 cm^{-1}, equally showing similar thermal stability.

As can be seen from the SWy-2 – glyoxal VT-DRIFTS data (Figure 7.8.1) the 1644 cm^{-1} band also has the thermal stability to that seen of the 1655 cm^{-1} band here. Additionally a weak band is seen at 1740 cm^{-1} as in the glyoxal intercalate, but in this sample this band is lost at much lower temperatures and as stated is much weaker in intensity. The SWy-2 – 3NH2

234

(Figure 7.18.2) intercalate also displays a band (unassigned) at 1694 cm^{-1} with equal thermal stability, but this cannot be comparable when unassigned.
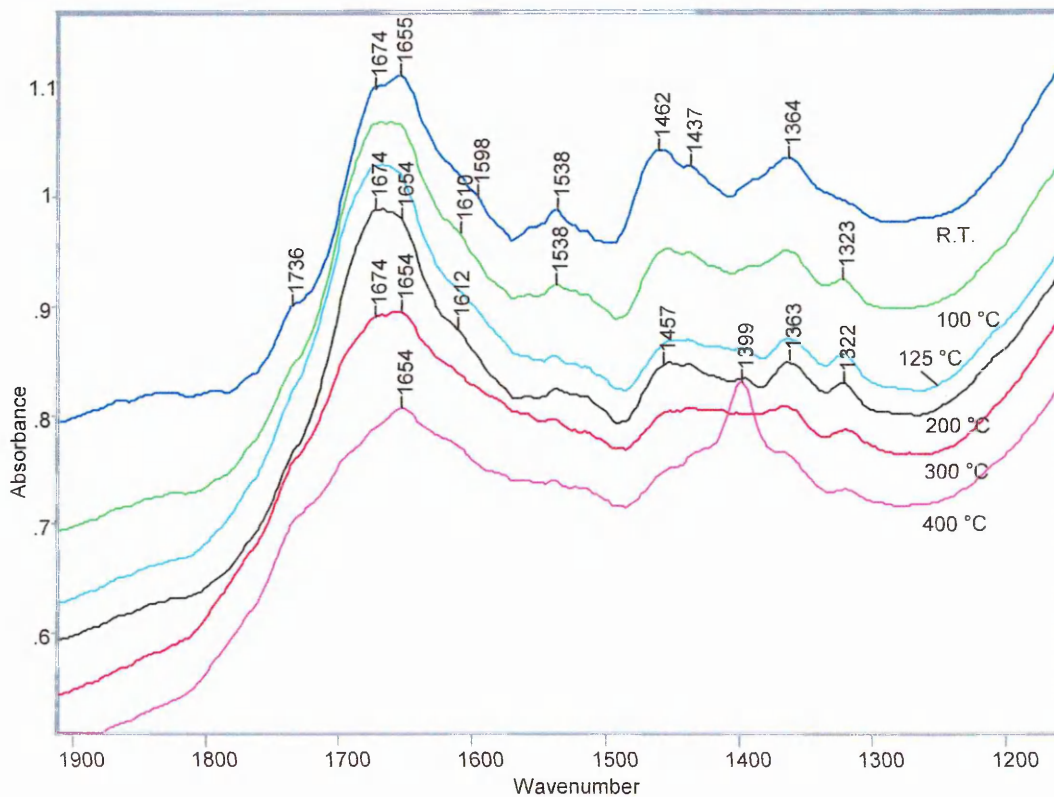

Figure 7.25.1 – VT-DRIFTS for SWy-2 + 1% Glyoxal and 1% 3NH2 composite

A band at 1598 cm^{-1} is visible as a shoulder on the 1655 cm^{-1} band and this moves to 1612 cm^{-1} by 200 °C. However this is barely discernable and weak if at all present. This may be an NH$_2$ scissoring mode and an NH deformation is also seen at 1538 cm^{-1} and lost by 200 °C.

Examining the higher frequency region for this composite (Figure 7.25.2), aliphatic CH stretching bands are observed at 2948, 2860, and 2801 cm^{-1}. The thermal stability of these CH stretching bands matches well the thermal stability of the CH deformations at 1462, 1437 and 1364 cm^{-1} (Figure 7.25.1), both showing a reduction in intensity up to 200 °C. Two bands at 3389 and 3323 cm^{-1} (a shoulder) are also present and may be attributed to an imine stretch for N-H. It is unlikely, that this band is the OH stretching band of water due to its high thermal stability. However it is possible that these bands are N-H stretching bands arising from an amine. The spectrum at 400 °C shows the appearance of two bands at 3020 and 3180 cm^{-1} which are most likely to be excess organic matter on the window of the environmental cell, due to the high organic content of this sample (42%).

235

Figure 7.25.2 - VT-DRIFTS for SWy-2 + 1% Glyoxal and 1% 3NH2 composite 3800 – 2600 cm^{-1}.

However, the fact remains that the spectrum of this composite of 1% Glyoxal 1% 3NH2 and the clay is different not only in terms of band positions, but also in terms of thermal stability to both the washed and unwashed 3NH2 intercalates. All three of these composites / intercalates show different thermal stability displayed in their VT-DRIFTS results. The 3NH2 intercalate is stable to the lowest temperature of the three, whilst the glyoxal intercalate reveals surface bound or perhaps clusters of glyoxal molecules and a significantly shifted carbonyl stretching bands at 1742, 1716 1646 and 1609 cm^{-1} which display higher thermal stability than the 3NH2 – glyoxal composite (Figure 7.25.1). The combination of these factors suggest that at the very least a reaction / interaction has taken place, and therefore the intercalated species is different. Imines are unstable and readily undergo hydrolysis back to their constituent aldehydes and amines as water is a by – product of the reaction. No evidence is apparent of this occurring and the alternative to achieving stability in this system in this reaction is polymerisation. Indeed the bifunctional nature of the aldehyde and amine in

236

such reactions encourages polymerisation at room temperature. As previously stated this composite was also different in appearance and texture compared to the 3NH2 and glyoxal intercalates.

It should be noted here that the amounts of aldehyde and amine used are in weight % and not molar amounts – this stems from initial work completed elsewhere on the hardness and water permeability of these composites. According to the reaction stoichiometry taking place one mol of aldehyde reacts with one mol of amine to produce an imine, amino resin or aminoplast, so an appreciation of the molar amounts involved here would enable a clearer picture of which reactant is in excess.

Therefore when the reactants 3NH2 and glyoxal are present in equal weight amounts (1% in the results presented thus far – VT-XRD, TGA and VT-DRIFTS) the actual molar ratio of glyoxal :3NH2 is 5:1. This is a large excess of glyoxal.

It is important to know which reactant is in excess when identifying the possible reaction products. Recalling that the reaction intermediate is the dimethylol unit if the aldehyde (in this case glyoxal) in excess by 2 mols per mol of 3NH2 then it is probable that this is the reaction intermediate formed here.

Now, in the composite made (1% glyoxal and 1% 3NH2 molar ratio 5:1 respectively) we now know that glyoxal is in excess and hence the dimethylol unit is formed. Hence the reaction products that may be formed are

(5)

which is the self – condensation reaction product or

(6)

which is the condensation product of the dimethylol unit and amine. It is unlikely that much of the latter product above would be formed as the aldehyde is in excess and hence it is unlikely

that the imine is formed for the same reason. If an imine were formed then there would also have to be an absence of NH vibrations in the IR spectrum, yet clearly the NH deformation is seen in Figure 7.25.1.

If the self – condensation product were formed then the 1674 and 1655 cm^{-1} bands would both be carbonyl C=O stretches, or one may be assigned to this product and the other may be excess carbonyl which has not reacted. Two bands may indicate some interaction between the carbonyl and NH groups either intermolecular or intramolecular. The 1538 cm^{-1} band is the NH deformation from the NH seen in the structure. The bands at 3389 and 3323 cm^{-1} could both be the anticipated NH stretching mode. However, there are two bands in this region (two bands indicate NH$_2$) where only one would be expected and also the 1598 cm^{-1} (NH$_2$ scissors), can only just be discerned as a shoulder. The NH$_2$ bands present are not clearly resolved or as intense as the carbonyl or NH deformation and this may be indicate that there is not much present. Hence the NH$_2$ band may be due the chain ends of the oligomers or polymers formed. Alternatively the NH$_2$ band seen may be the result of monomethylol units that have reacted prior to forming dimethylol units. Altering and increasing the 3NH2 content may resolve this issue.

In order to ascertain whether heating the reaction mixture (glyoxal 3NH2 and clay) had an effect on the end product and to determine therefore if the heat generated was sufficient to drive forward the self condensation reaction, the reactants - including clay - were refluxed at 70 °C, a mild enough temperature that would not degrade the reactants in any way. DRIFTS analysis (Figure 7.26) was then performed
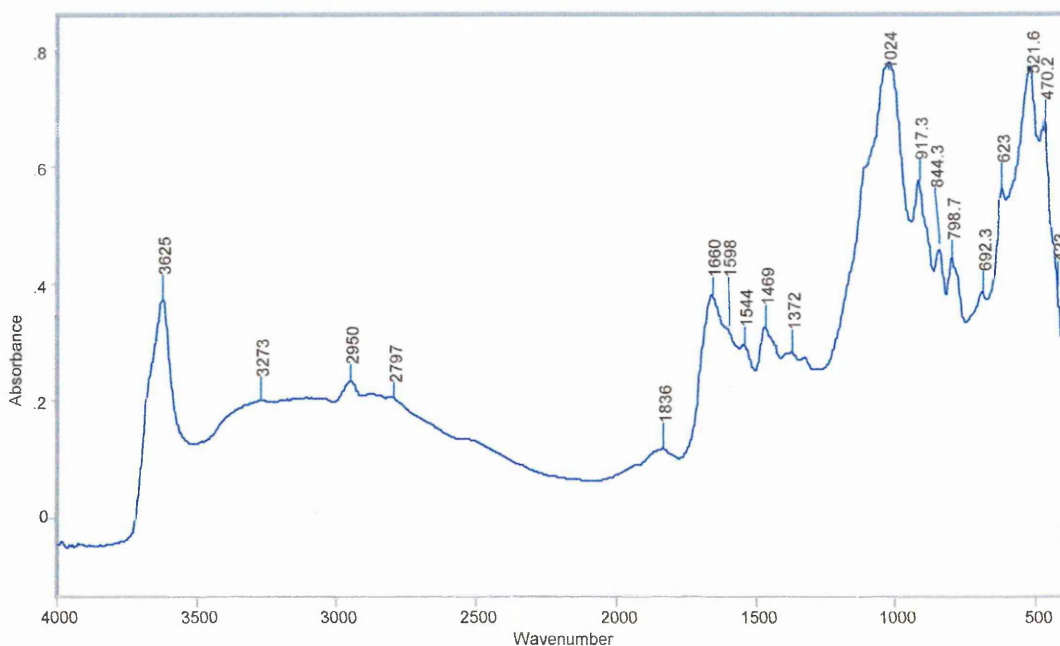
Figure 7.26 - Refluxed mixture of Swy-2 1% glyoxal and 1% 3NH2

The sample remains the same in terms of colour and texture, as its non-refluxed counterpart. The 1660 cm^{-1} band remains broad and may contain two bands but is not as resolved as in the non-refluxed sample. The 1598 cm^{-1} band remains as a weak shoulder on the 1660 cm^{-1} band. A band at 3273 cm^{-1} (NH stretch) is also seen. From the intensity of the 1598 cm^{-1} band (see below for detailed discussion) it would appear that this sample is similar to the non-refluxed sample and the reaction still proceeds via the dimethylol intermediate. Hence it would appear that heating the sample does not influence the product formed or that IR cannot distinguish the difference(s).

7.4.2.1 Summary of Amine Aldehyde Composites made using 1% of each reactant

Glyoxal and 3NH2 react within the interlayer of SWy-2 forming an amino resin as shown below (Figure 7.26.1). The following summarises the properties and of this composite:-

- The $d_{(001)}$ spacing of the composite is 16.40 Å which decreases to 13.80 Å by 300 °C. Significantly this is different to that of either glyoxal (14.7 Å) or 3NH2 (14.3 Å).

- The composite is different in texture – much harder - than intercalates of both glyoxal and 3NH2.
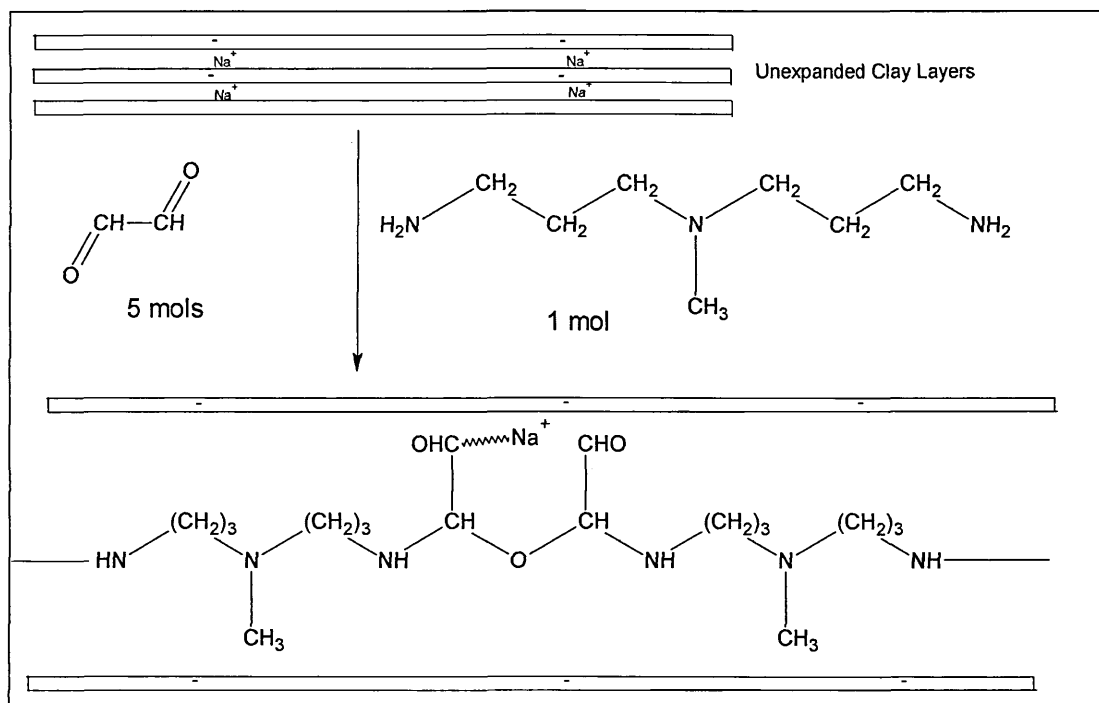

Figure 7.26.1 – Schematic of reaction between glyoxal and 3NH2 and structure of product within the clay interlayer.

From elucidation of the possible reaction products that may be formed and knowledge of the molar ratios of the reactants used it was possible to ascertain that dimethylol condensation products have been formed after study of the DRIFTS spectra.

- Bands at 3389 and 1538 cm^{-1} indicate that NH groups are present which, in turn, indicate that the dimethylol condensation products (Structures 5 and 6 above) are formed.

- There is some evidence for NH_2 in this sample (1598 cm^{-1} and 3223 cm^{-1} both weak and not well resolved) and these may be the chain ends of oligomers or polymers formed or monomethylol units that have reacted quickly with amine before dimethylol units can be formed.

- The bands at 1674 and 1655 cm^{-1} are carbonyl stretching bands and not the imine C=N stretching band as if an imine were formed then there would also have to be an absence of NH vibrations in the IR spectrum

240

- These observations also agree well with the expected reaction products given prior knowledge of the expected reaction (Section 7.4.1).

Hence it was necessary to vary the amine content, and observe changes in the DRIFTS spectrum. Making this sample via refluxing at mild temperature shows that the there is sufficient heat generated at room temperature to drive the reaction.

7.4.3 Altering the 3NH2 Content.

It was considered that if the amount of 3NH2 used in this reaction is increased whilst keeping the amount of glyoxal fixed at 1% the DRIFTS analysis may identify the different products. Figure 7.27.1 shows that the CH_2 and CH_3 bending and stretching bands increase in intensity and the 1656 cm^{-1} band (in the sample where the reactant are at 1% weight each) gradually moves to a higher frequency reaching 1664 cm^{-1} as the 3NH2 content is increased from 1% - 5% This band has also increased in intensity and is narrower. If the 3NH2 content is lowered from 1% to 0.25% the DRIFTS analysis shows that this band has now moved to 1637 cm^{-1} and is much broader and less intense.

Increasing from 1 – 5% of amine also leads to an increase in intensity of the band at 1598 cm^{-1}, which is the NH_2 scissors, initially seen at 1% as a small shoulder.

As the 3NH2 content is increased from a starting point of 1% each of aldehyde and amine (keeping the glyoxal fixed at 1%) then the reaction intermediate formed begins to switch from dimethylol to monomethylol.

At 0.25% amine the band initially at 1664 cm^{-1} at 5% has now shifted to 1637 cm^{-1} and is broader with shoulders on both the high and low wavenumber side of this band. His band appears to be a water OH bend with shoulders on either side the 1609 and 1645 cm^{-1} bands indicative of intercalated glyoxal. In this sample there is therefore insufficient 3NH2 to form enough methylol units and subsequent amino resins, merely an excess of glyoxal. However, the concentration of glyoxal is also greatly reduced now which is why the 1637 cm^{-1} is broad and attributed to water. Decreasing the amine content also leads to the resolving of a band at 1435 cm^{-1}, which is more intense.

The C-O-C ether type bond (in the former structure shown above) would not be seen as this would be observed at 1150 – 1060 cm^{-1} which is in the same position as the intense Si-O band.
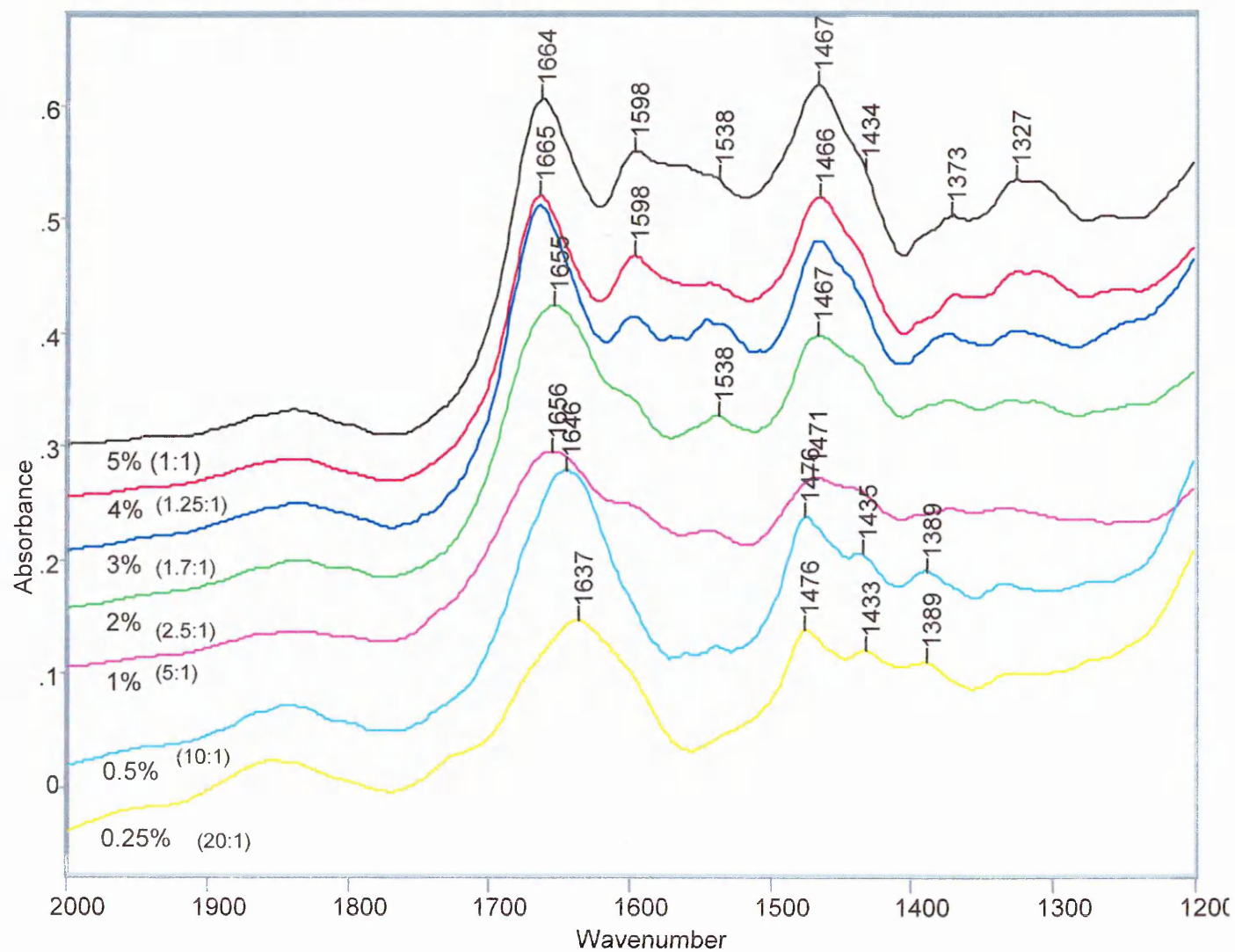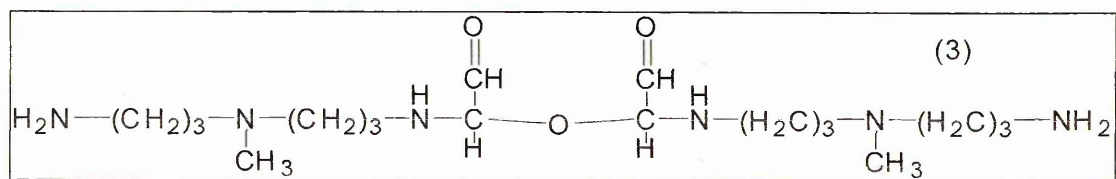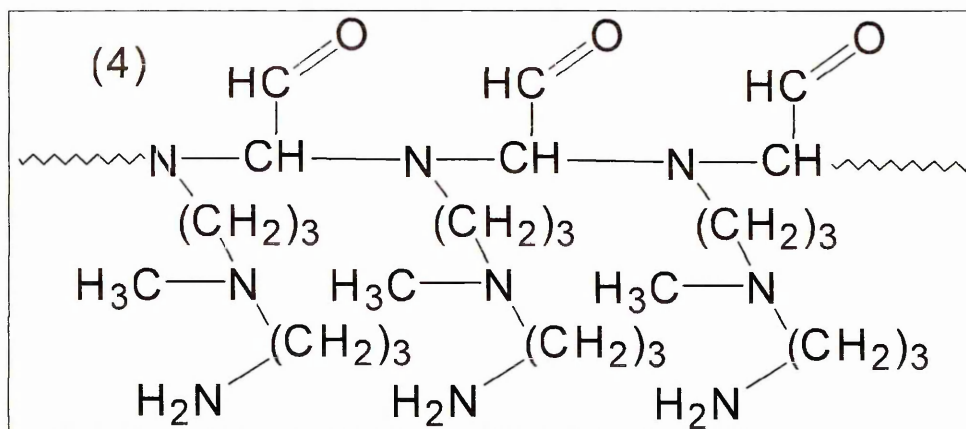
Figure 7.27.1 – DRIFTS Spectra showing the effect of increasing and decreasing amine concentration on composite 2000 – 1200 cm^{-1}. (Molar ratio of glyoxal : 3NH2 is shown in brackets).

The products formed from the monomethylol intermediate would be as follows:-

242

(4)

Both of these have NH_2 groups in the structure. Figure 7.29.1 clearly illustrates that there is an increase in intensity of the 1598 cm^{-1} NH_2 scissoring band, as the amount of 3NH2 – and hence the amount of monomethylol formed – increases. There is also an increase in the 3362 and 3268 cm^{-1} bands (attributable to NH stretches from NH_2) over the same increase in 3NH2 content (Figure 7.29.2).
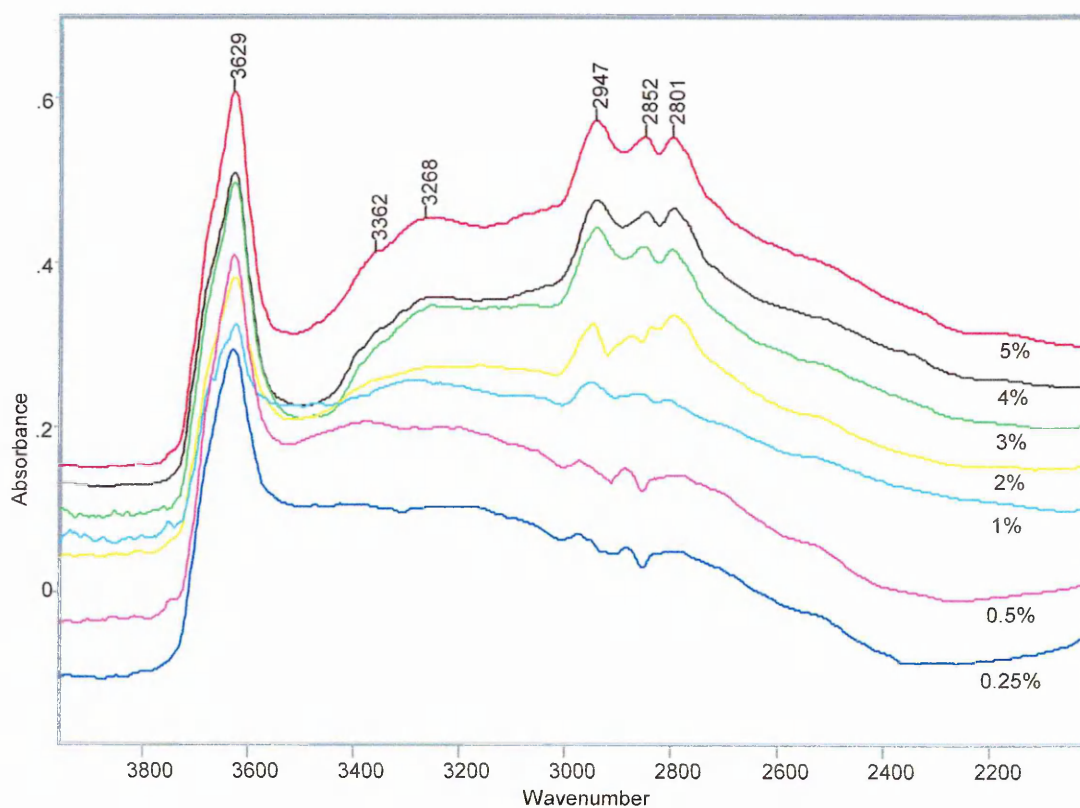

Figure 7.29.2 – DRIFTS Spectra showing the effect of increasing amine concentration on composite 3800 – 2100 cm^{-1}.

Hence as the ratio of reactants reaches equimolar amounts the following occurs within the interlayer of the clay (Figure 7.29.3).
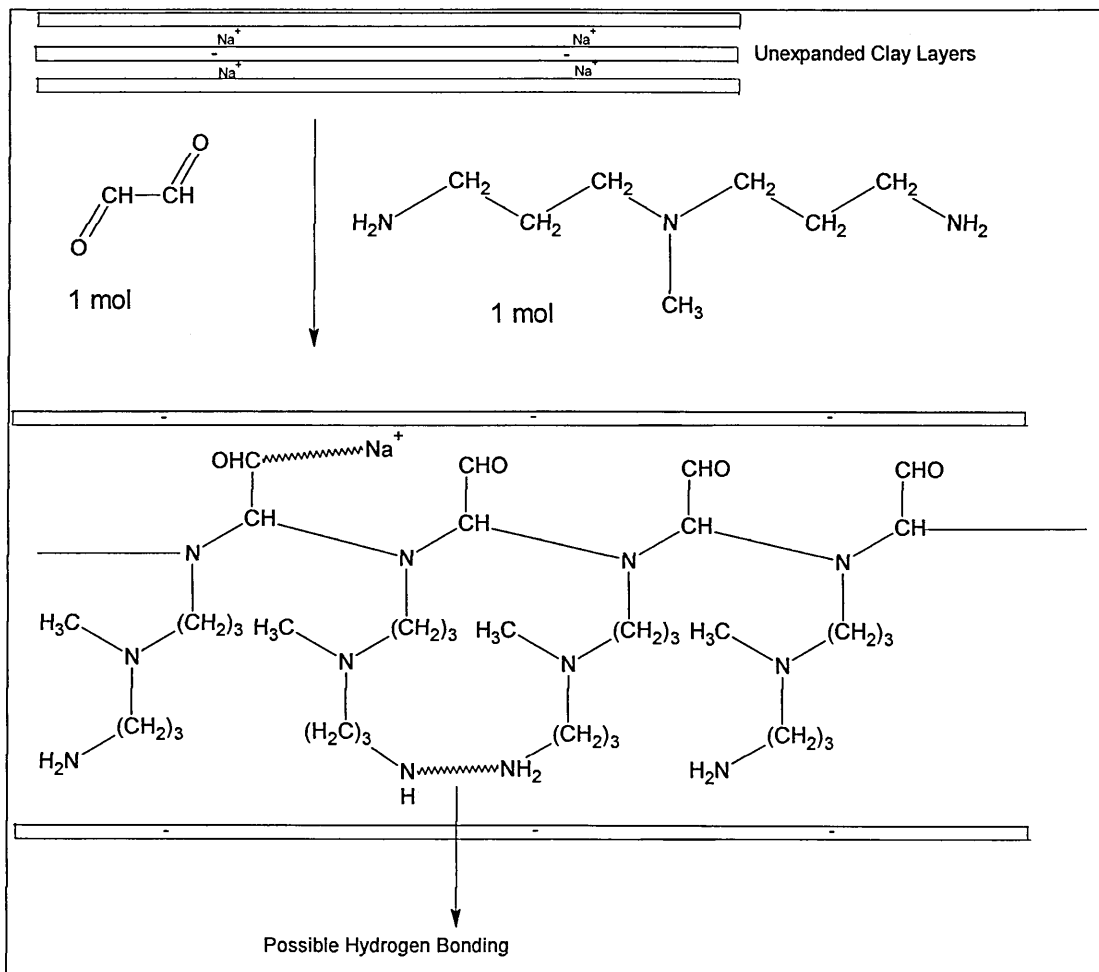

Figure 7.29.3 – Reaction of glyoxal and 3NH2 at equimolar amounts and structure of product with clay interlayer.

Now the following conclusions can be made for the above product:-

* There is an increase in the intensity of the 1598 cm^{-1} band – NH$_2$ scissoring band.

* There is also an increase in the 3362 and 3298 cm^{-1} bands – NH$_2$ stretching bands.

* There is a decrease in the intensity of 1538 cm^{-1} band – NH deformation band.

* The above three points indicate that the reaction intermediate formed has now switched from dimethylol to monomethylol as NH$_2$ is indicate of monomethylol whilst NH is indicative of dimethylol

* The broad nature of the NH$_2$ bands indicates that hydrogen bonding is taking place which is intra or inter molecular (Figure 7.29.3).

7.4.4 Balancing the Molar Ratio of Reactants

If 3NH2 and glyoxal are mixed in equimolar amounts, the interlayer spacing remains at 16.40 Å, and the DRIFTS spectrum (Figure 7.30) indicates the presence of NH_2 in the intercalate via bands at 3368, 3264 and 1602 cm^{-1}. This indicates that the monomethylol units must therefore have been formed.
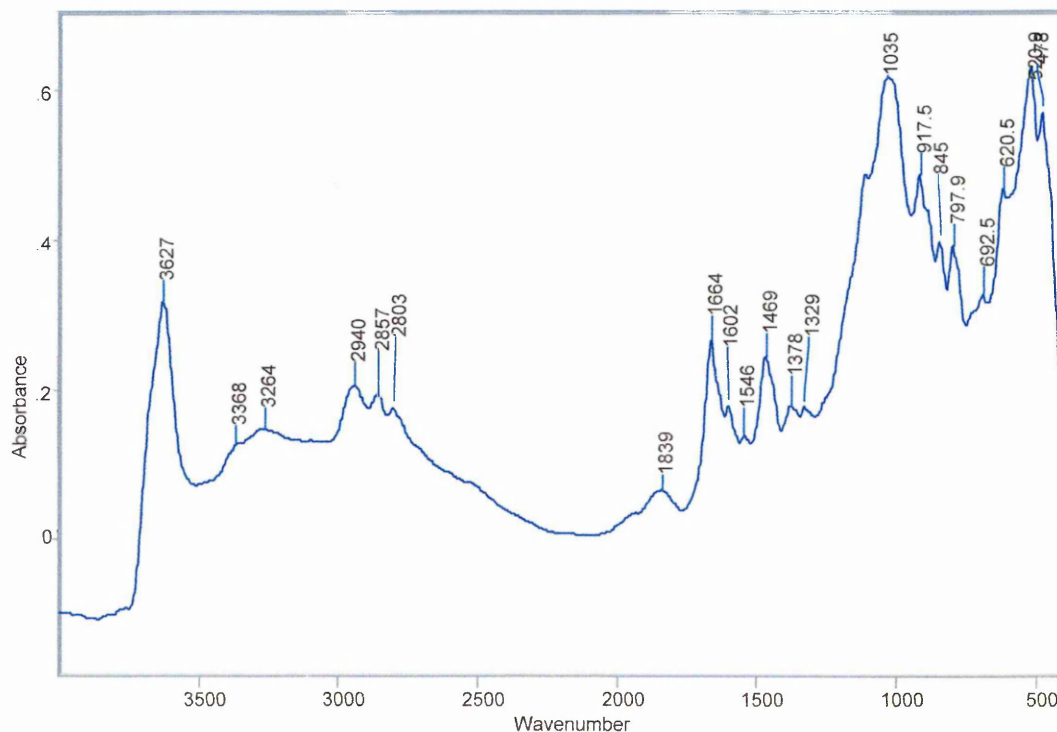

Figure 7.30 – DRIFTS spectrum of composite made from balanced molar ratio of reactants, glyoxal and 3NH2

The DTG for this sample (Figure 7.31) however, shows peaks at 80, 190, 240, 400, 500, 550 and 620 °C. Comparing this to the composite made from 1% of each reactant there is only a peak at 500 °C that the two have in common. The overall weight loss is 25%. If an excess amount of clay is added to this reaction mixture then once again there is no change in these results. In an attempt to create more of the imine polymer and facilitate composite formation, the whole reaction mixture, including the clay was refluxed for 3 hours at 80 °C. The subsequent analysis however, displayed no differences in DRIFTS, TGA or XRD analysis.
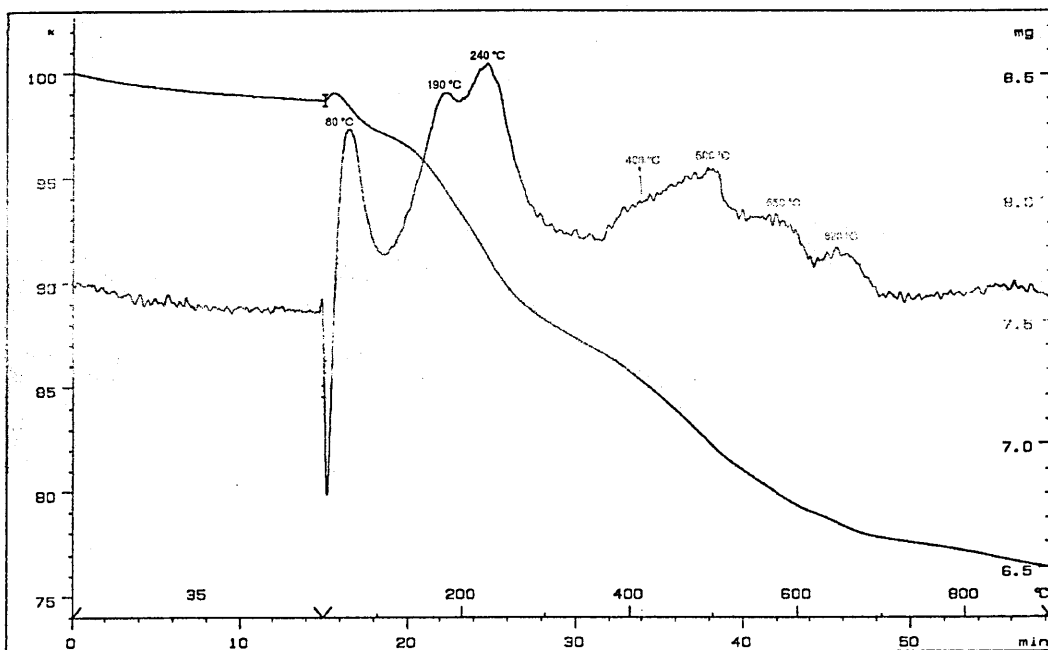
Figure 7.31 – TGA of Composite made from equimolar amounts of reactants

7.4.5 Composites of Different Reactant Combinations

A variety of composites were prepared using different combinations of aldehydes and amines at equal weight percentages (1% of each, aldehyde and amine) and increasing the amine content to 3%. These combinations were formaldehyde and 3NH2, glyoxal and DAP, formaldehyde and DAP and glyoxal and EDA. Hence the molar ratios for these samples were as follows:-

Sample	Molar Ratio (aldehyde: amine)
1% Glyoxal + 1% EDA	2.6 : 1
1% Glyoxal + 1%DAP	3.2 : 1
1% Formaldehyde + 1% DAP	5.5: 1
1% Formaldehyde + 1%3NH2	9.6 : 1
1% Glyoxal + 3% EDA	0.86 : 1
1% Glyoxal + 3% DAP	1.1 : 1
1% Formaldehyde + 3% DAP	1.85 : 1
1% Formaldehyde + 3% 3NH2	3.60 : 1

Table 7.9 Molar Ratios of Reactants

246

The purpose of such an investigation was to confirm and test the hypothesis of the reaction product that would be formed on altering the molar ratios of the reactant aldehyde and amines, whilst using different reactants. These reactants are not all bifunctional reactants as are 3NH2 and glyoxal. Hence it would be of interest to note whether this would affect the final product formed.
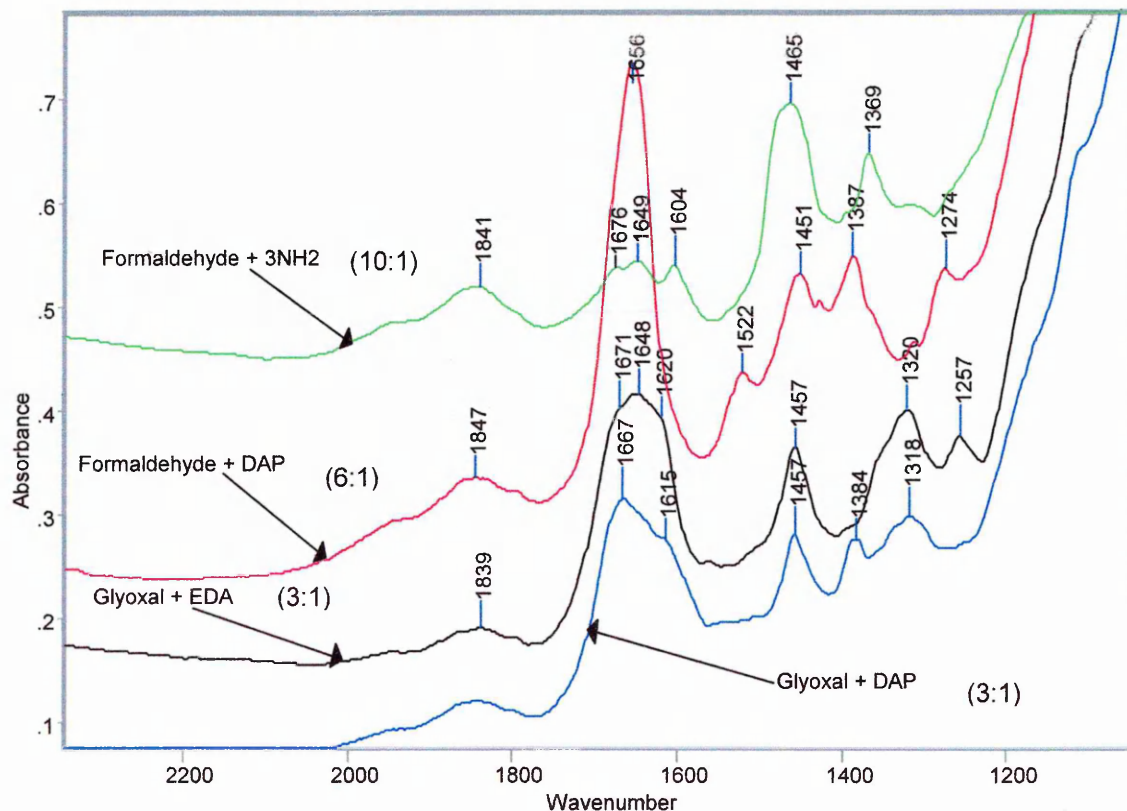

Figure 7.32.1 – DRIFTS spectra of composites made from different reactants and clay at 1% of each reactant – 2300 – 1100 cm^{-1}.

The composite made from 1% formaldehyde and 1% 3NH2 has a huge molar excess of formaldehyde (Table 7.9). This reaction mixture will undoubtedly form dimethylol units but the sheer excess of formaldehyde means that the aldehyde will still be in excess even if these dimethylol units proceed further to a self – condensation reaction to form an amino resin. There are bands observed at 1676, 1649 and 1604 cm^{-1}. The 1604 cm^{-1} band is in good agreement for adsorbed formaldehyde or the NH$_2$ scissoring band. The 1676 and 1649 cm^{-1} bands may be assigned to either hydrogen bonded formaldehyde (hydrogen bonded to groups directly coordinated to the interlayer cation for example) and free carbonyl groups resulting from such hydrogen bonding. This is possible in this sample due to the large excess

of formaldehyde. These are not however the expected bands for polyoxymethylene for example which is the polymerised form of formaldehyde in solution. Examination of the higher frequency region for this sample (Figure 7.32.2) shows a weak band at 3365 cm^{-1} which may be an N-H stretch and evidence of some reaction to form an amino resin condensation product from the dimethylol units. It should be noted that the condensation product resulting from the reaction of formaldehyde will not have any free carbonyl groups unlike the glyoxal related products, hence any carbonyl bands observed would originate from formaldehyde molecules.

The composite made from 1% formaldehyde and 1% DAP shows an intense band at 1656 cm^{-1} and NH deformation at 1522 cm^{-1}. The NH deformation seen here is significant as if the 1656 cm^{-1} band were to be an imine then there could be no NH left in the resultant imine product. Once again however the excess of formaldehyde is immense, and it is likely that although the dimethylol units will be formed the excess of aldehyde means that in this case the 1656 cm^{-1} is likely to be a carbonyl stretch. The intensity of this band favours such assignment also. There is no evidence of any NH stretching from the higher frequency region of this sample (Figure 7.32.2).
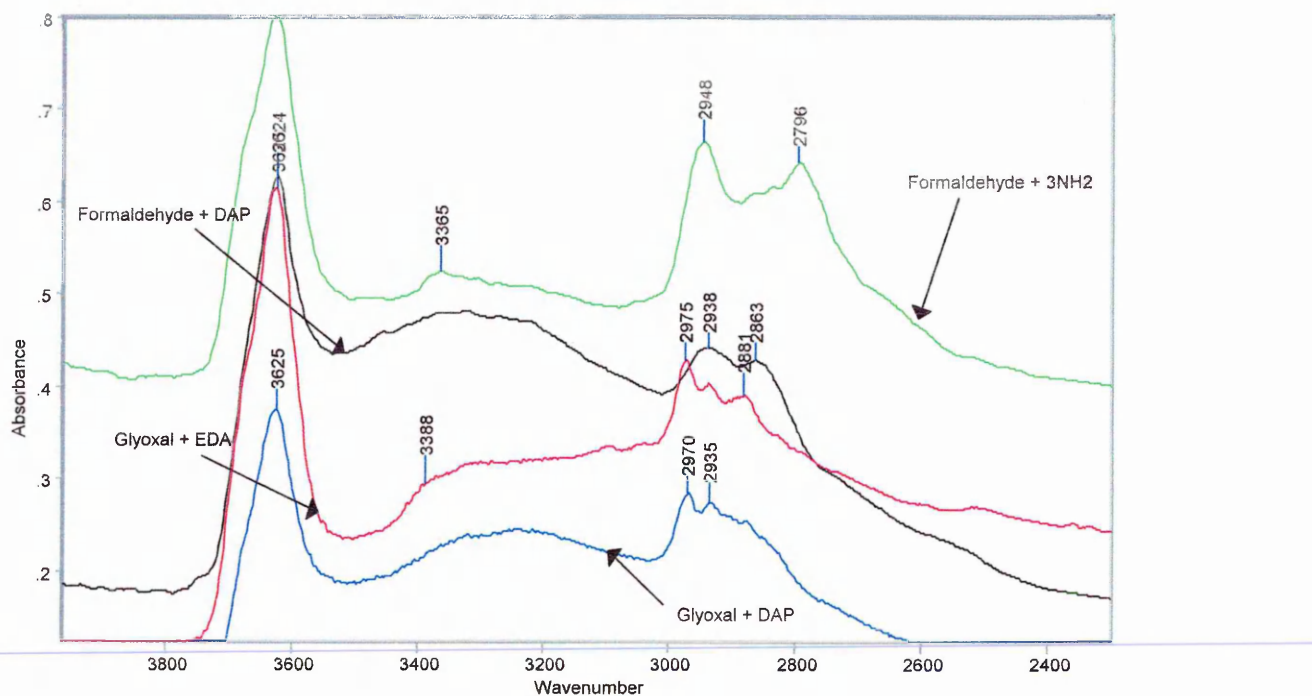

Figure 7.32.2 – DRIFTS spectra of composites made from different reactants and clay at 1% of each reactant – 3800 – 2400 cm^{-1}.

248

The composites made from 1% each of glyoxal and EDA and glyoxal and DAP are consistent with the observations made from the composite containing 1% glyoxal and 1% 3NH2 above. The molar ratios of these composites however are not as great as 5:1 at 1wt. % of each reactant as in glyoxal and 3NH2 (Table 7.9), but the excess of aldehyde is still sufficient to favour the formation of dimethylol units. The glyoxal – EDA sample exhibits an overlapping series of three bands which may be centred at 1671, 1648 and 1620 cm^{-1} though these are difficult to distinguish. The former two are likely to be carbonyl stretches from the condensation product and excess aldehyde and the latter band at 1620 cm^{-1} may be either an NH deformation or excess adsorbed aldehyde intercalated in the clay. The glyoxal – DAP sample has a band at 1615 cm^{-1} to which the same assignment can be made and also a band at 1677 cm^{-1} and possibly another on the low wavenumber side of this to which again the same assignments can be made (excess aldehyde and carbonyl groups from the condensation product). There are no NH stretches observed in either of these products (Figure 7.32.2).

If the amine content is now increased to 3 wt % in all these composites the following DRIFTS results are obtained (Figure 7.33).
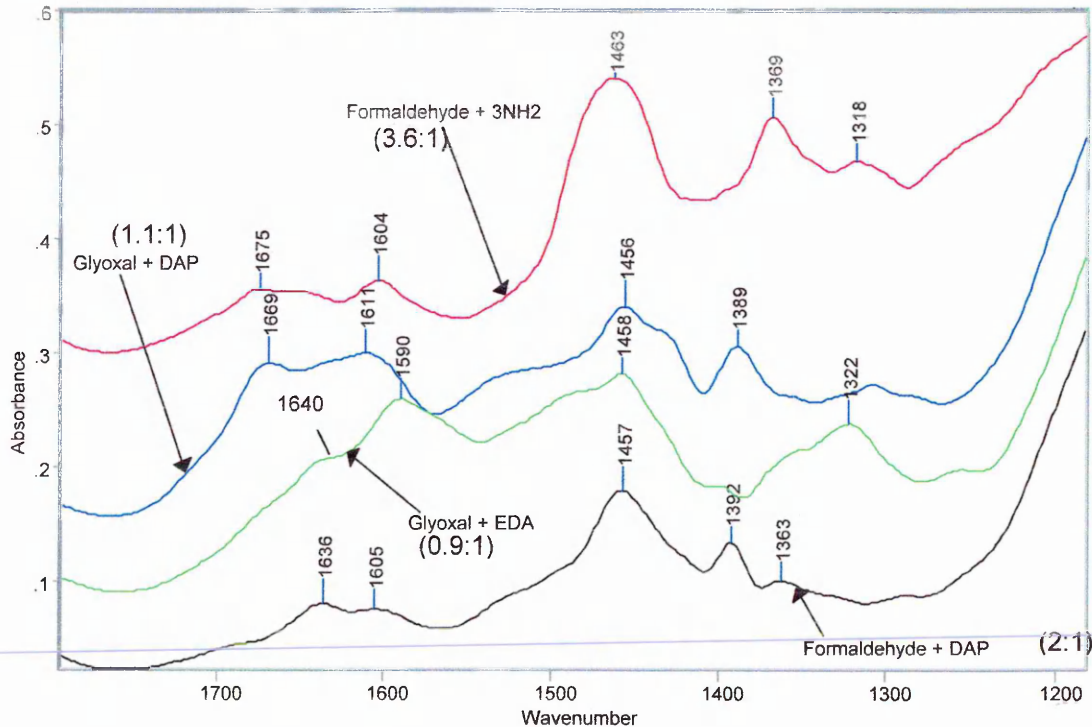
Figure 7.33.1 – DRIFTS Spectra showing the increase in amount to 3% of amine 1800 – 1200 cm^{-1}

The formaldehyde – 3NH2 composite still has an excess of aldehyde and will form dimethylol units. There appears to be little change in the IR spectrum of this sample however (Figures 7.33.1 and 7.33.2) though as stated before the condensation product of this sample would not have any free carbonyl in it. The formaldehyde - DAP composite however has lost the intense 1656 cm^{-1} and now displays two weak bands at 1636 and 1605 cm^{-1}. As the aldehyde is almost at a 2:1 ratio in excess (Table 7.9) this reaction mixture will predominantly still be dimethylol units, but as the higher frequency region for this sample shows (Figure 7.33.2) two NH stretches are clearly visible at 3316 and 3274 cm^{-1}. The 1605 cm^{-1} band in this sample may therefore be the NH$_2$ scissors indicating that a significant portion of monomethylol units must have been formed.
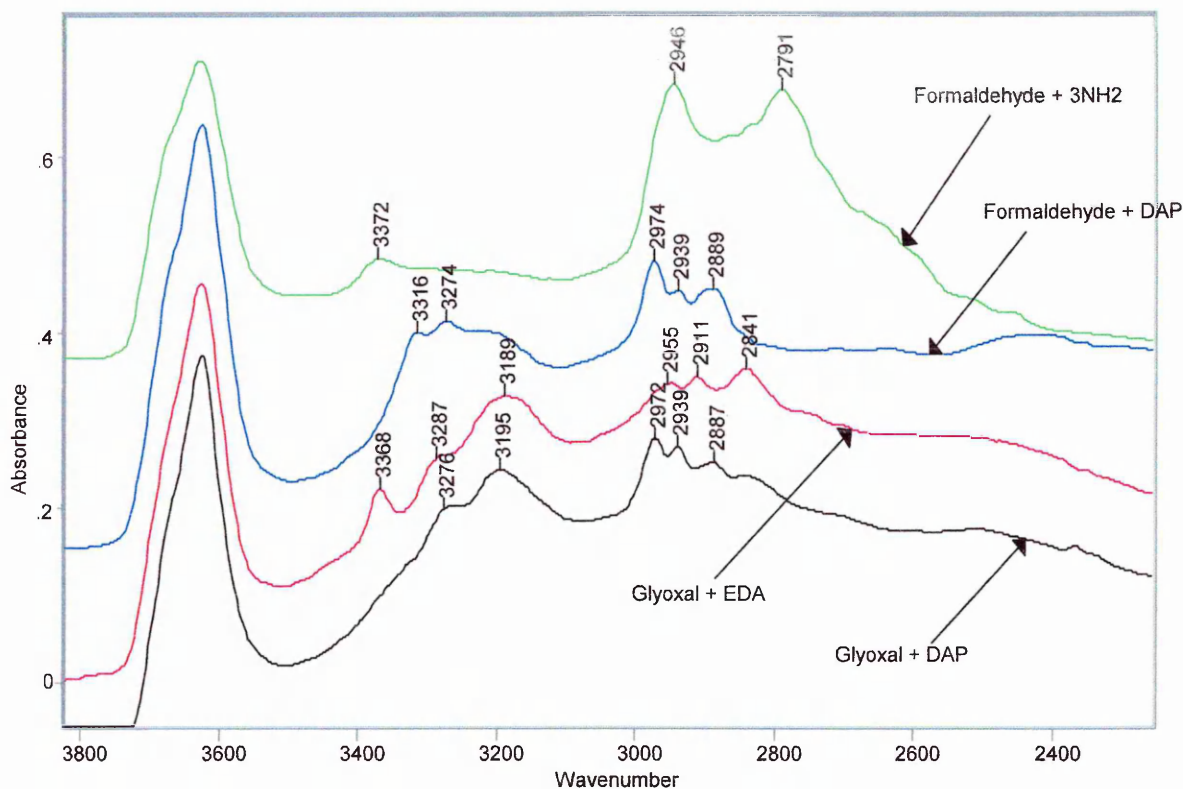

Figure 7.33.2 – DRIFTS Spectra showing the increase in amount to 3% of amine (aldehyde fixed at 1%) 3800 – 2500 cm^{-1}

The glyoxal EDA and DAP composites also show changes in the NH stretching region with the emergence in both samples of bands at 3276 and 3195 cm^{-1} for the glyoxal – DAP sample

and bands at 3368, 3287 and 3189 cm^{-1} for the glyoxal – EDA (three bands). Two bands in this region indicates NH$_2$ and therefore monomethylol units must have been formed. Indeed the ratio of reactants for these samples (Table 7.9) indicates that at a 3% amine content for these composites the molar ratio of reactants is almost 1:1. Therefore the band at 1611 cm^{-1} in the glyoxal – DAP composite is the NH$_2$ scissors and the 1659 cm^{-1} a carbonyl stretch. In the glyoxal – EDA composite the 1590 cm^{-1} is the NH$_2$ scissors and 1640 cm^{-1} the carbonyl stretch. There is a band present at 3368 cm^{-1} in the glyoxal – EDA sample which can be attributed to an NH stretching band, and this indicates the presence of NH$_2$ and NH in this sample. Therefore this sample may be a mixture of monomethylol condensation product and also the reaction between monomethylol unit and amine, which does have some NH present.

7.4.6 Summary of Composites Containing Varying Amounts of Reactants.

On increasing the amount of 3NH2 in a composite (so the reactants approach equimolar amounts) containing 1% glyoxal and 1% 3NH2 it was anticipated that the reaction intermediate would change from the dimethylol unit to the monomethylol unit as the amount of aldehyde decreases. This means that the product obtained also changes from the dimethylol condensation product to the monomethylol condensation product. In IR spectra it was anticipated that this change would be observed as increase in intensity of bands attributable to NH$_2$ since these are present in the monomethylol condensation product as part of the polymer / Oligomer chain and only present in the dimethylol condensation product as chain ends. This was found to be the case, as an increase in intensity of the NH$_2$ scissoring band at 1598 cm^{-1} was observed as the amine concentration increased together with the emergence of NH$_2$ stretching bands at 3362 and 3268 cm^{-1}.

This observation was reinforced by examination of composites made from differing combinations of glyoxal and formaldehyde and the amines 3NH2, DAP and EDA. When the aldehyde was in excess NH stretching and deformation bands are observed indicating that the dimethylol condensation products were formed. When the amine concentration begins to equal that of the aldehyde the NH$_2$ bands are seen.

It would also appear that the bifunctionality of some of the reactants does not have a bearing on the final product formed.

7.5 Changing the Sequence of Addition

Investigations were made into the altering the sequence of addition of the reactants to the clay. This was achieved by first immersing the clay in a 2% solution of one reactant for one day washing any remaining reactant away with 6ml. distilled water and then treating the clay with the second reactant for a day prior to drying in air.

When the reactants are added together to the clay the concentrations of these reactants may not be equal throughout the various sites in the system i.e. the bulk solution, the pores in clay aggregates and the gallery space of the clay (Figure 7.34).
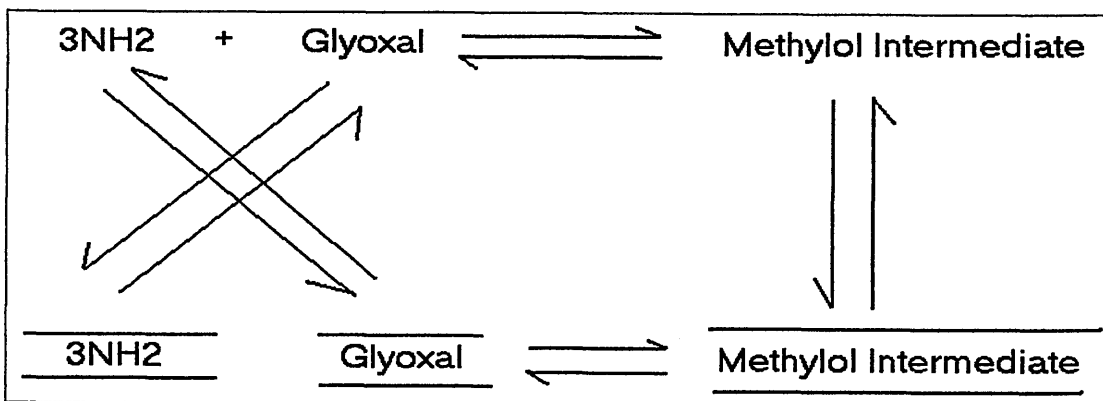

Figure 7.34 – Possible Interaction of reactants at various sites.

From Figure 7.34 it is possible to see that the reactants may react within the gallery of the clay or in the bulk solution and then penetrate the clay layers. One reactant may intercalate the clay prior to reacting with the other, which may be in the bulk, therefore implying that we have mixed intercalates before reaction. This leads to the question of how the concentration of one reactant in the gallery affects the reaction.

7.5.1 Addition of Aldehyde First

This sample however produces an interlayer spacing of 14.50 Å with the $d_{(001)}$ being broad and weak (Figure 7.35), and may easily encompass another peak at higher angle. This value is similar to that of the 3NH2 – SWy-2 intercalate of 14.3 Å.
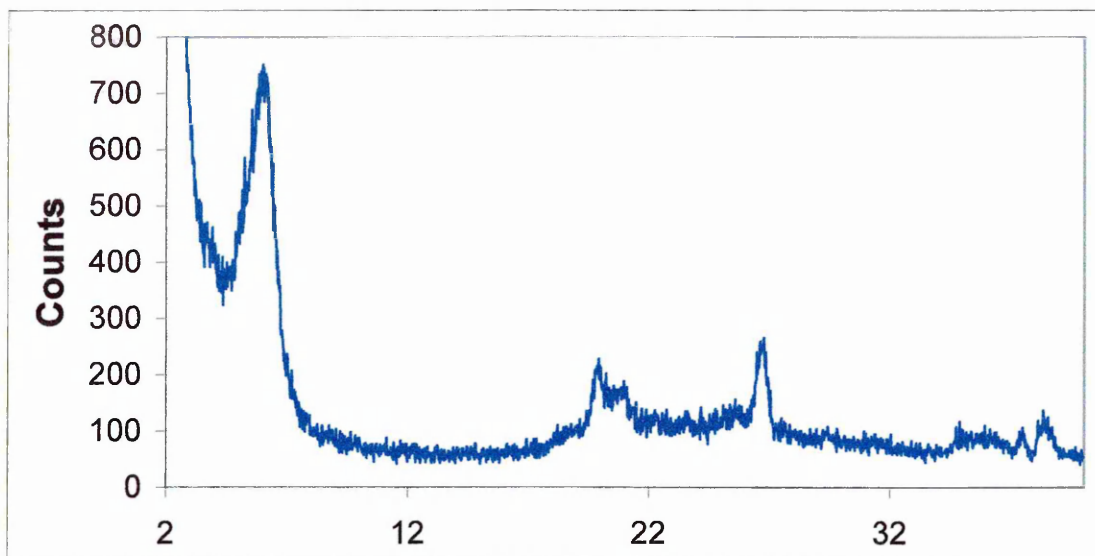
Figure 7.35 – XRD trace of composites prepared adding aldehyde first

In order to determine at this stage the effect of washing the glyoxal treated clay after one day the glyoxal treated Swy-2 was dried after washing for characterisation. The $d_{(001)}$ spacing is already known to be 14.70 Å (Figure 7.1), and the TGA (Figure 7.35) now shows a very different picture after washing.
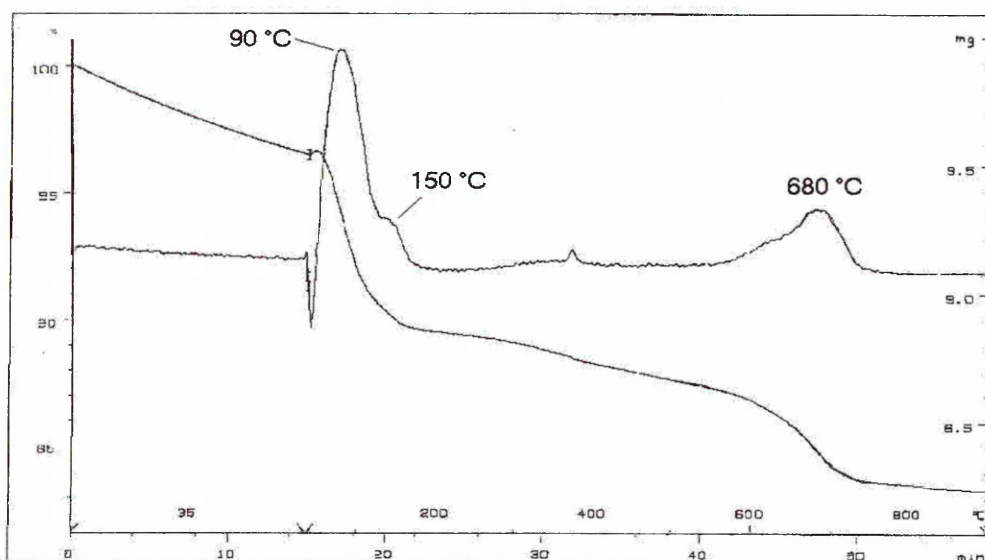

Figure 7.35 – TGA of Swy-2 glyoxal intercalate, washed.

The overall weight loss for the washed intercalate is now 17%, which is half of what was seen originally in the unwashed intercalate. The peaks seen in the washed intercalate at 90 and 150 °C are in similar position to that seen at 100 and 140 °C in the unwashed intercalate.

253

The VT- DRIFTS for the washed SWy-2 glyoxal intercalate (Figure 7.36) also displays marked differences. As the temperature increases the bands at 1740 and 1716 cm^{-1} do not emerge, and the 1648 cm^{-1} band is not observed either. A band at 1634 cm^{-1} is observed, which, by 100 °C has reduced in intensity and shifted to 1622 cm^{-1} (Figure 7.36.1). This band is stable to 375 °C and it is no longer observed by 400 °C. Comparing this band to the one seen at 1610 cm^{-1} in the unwashed intercalate, the 1610 cm^{-1} is stable to 450 °C. It is possible that the 1636 cm^{-1} band in the washed Swy-2 – glyoxal intercalate is water from the washing process, hence an examination of the O-H stretching region (Figure 7.36.2) is required, though there are also signs of CH$_2$ deformation bands in this spectrum (1485, and 1487 cm^{-1}).
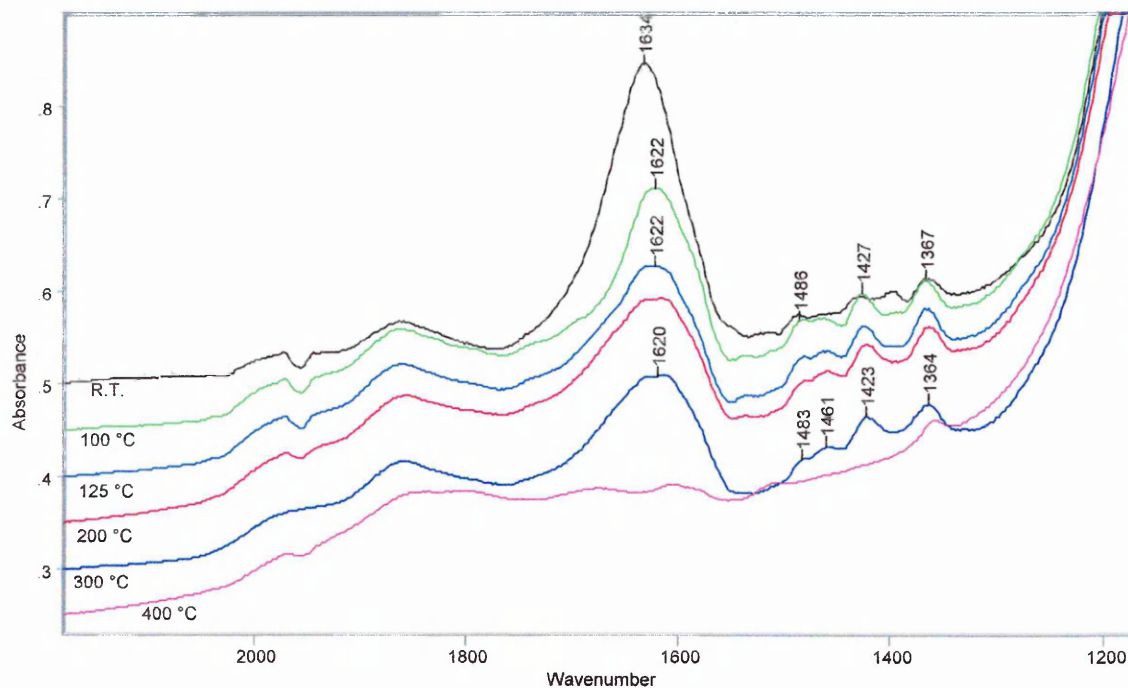

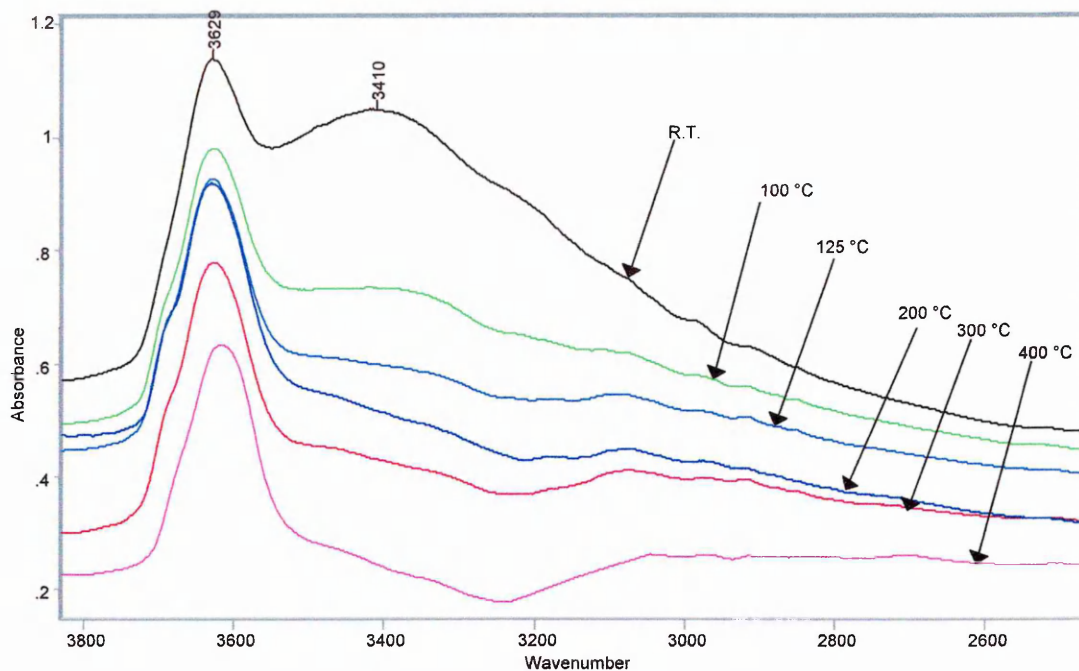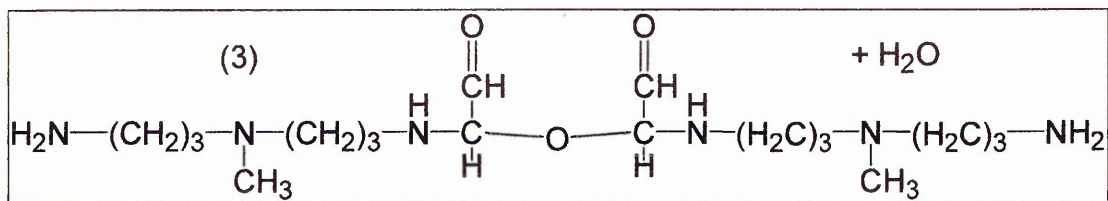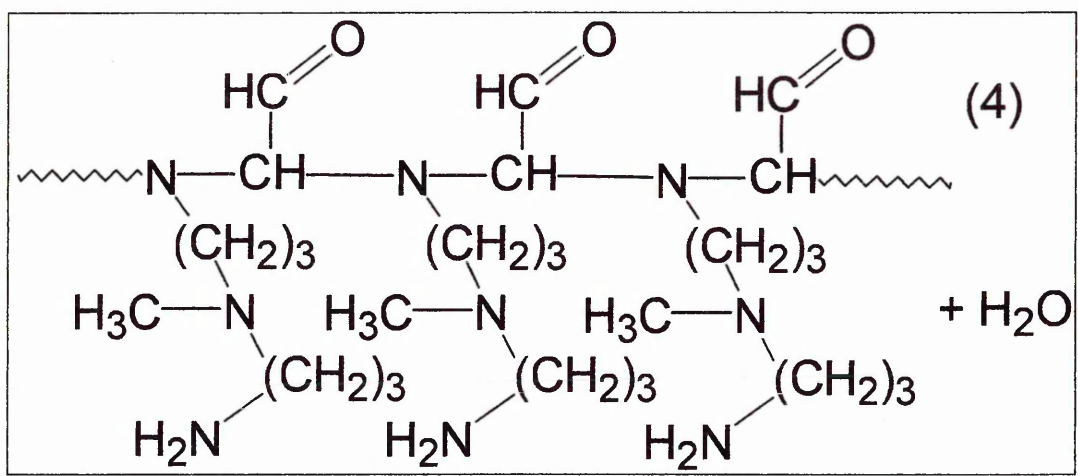Figure 7.36.1 – VT-DRIFTS SWy-2 – glyoxal intercalate washed 2100 – 1200 cm^{-1}

Figure 7.36.2 –VT-DRIFTS SWy-2 – glyoxal Intercalate washed 3800 – 2500 cm^{-1}.

The OH stretching band from water is centred here at 3410 cm^{-1} (Figure 7.36.2) and is seen to be lost by 125 °C. At this temperature the band at 1622 cm^{-1} still remains and the fact that it was originally at 1636 cm^{-1} and has reduced in intensity suggests that this shift and reduction intensity is due to the loss of water from the sample (1636 cm^{-1} being the OH deformation band arising from the presence of water). Hence there may be some glyoxal left in the sample but as the weight loss for this sample (TG) is not as great as the unwashed counterpart here is probably not as much glyoxal. Indeed the main diagnostic band for the carbonyl interaction with the clay is now at 1622 cm^{-1} and this is not as intense as the 1610 cm^{-1} band in the unwashed sample. Recalling that the 1610 cm^{-1} band was originally assigned to monodentate glyoxal interaction with the interlayer cation and was stronger than the 1642 cm^{-1} band assigned to bidentate glyoxal interaction with the interlayer cation, it seem that in this case there is only monodentate species present.

In either case (whether there is or is not as much glyoxal in this intercalate) on the addition of 3NH2 there is a strong possibility that there is now an excess of amine in the sample - the washing process is aimed at removing excess unintercalated glyoxal. Thus if the amine does react with the remaining glyoxal then there should be predominantly monomethylol units produced and hence monomethylol condensation reaction products, which are the dimer: -

(3)

H_2N—$(CH_2)_3$—N—$(CH_2)_3$—N—C—O—C—N—$(H_2C)_3$—N—$(H_2C)_3$—NH_2 $+ H_2O$

(with CH_3 substituents on the N atoms, and CHO / H groups on the central C atoms)

or the oligomer / polymer: -

(4)

Structure showing polymer backbone with HC=O, CH, N, $(CH_2)_3$, H_3C—N, $(CH_2)_3$, H_2N repeating units $+ H_2O$

Subtle changes are apparent from the DRIFTS spectrum for this sample (Figure 7.37.1), when compared to that of the composite prepared from adding the clay to a binary mixture of the two reactants (Figure 7.27).
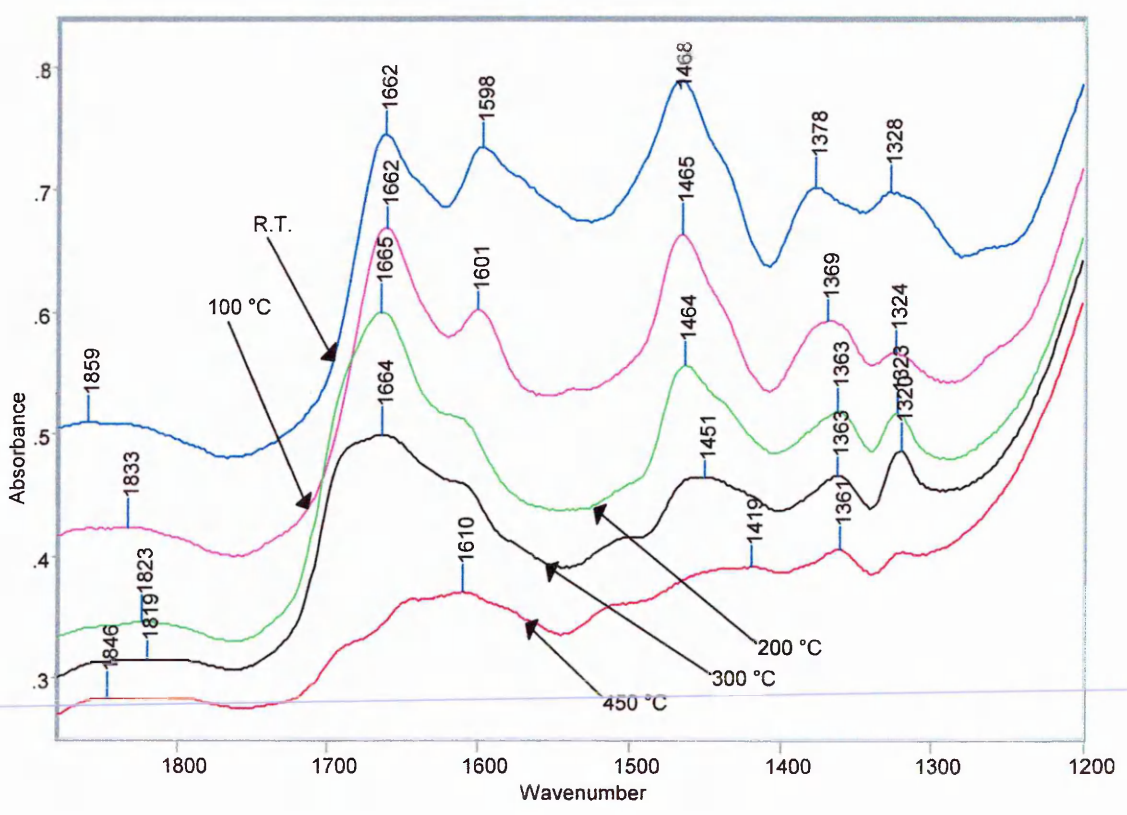

Figure 7.37.1 – VT-DRIFTS of composite prepared on addition of aldehyde first.

256

The 1660 cm^{-1} band has decreased in intensity, whilst the aliphatic CH stretches at 2945, 2849 and 2798 cm^{-1} (Figure 7.37.2) have increased in intensity. Also the 1467 cm^{-1} band attributed to the CH$_3$ asymmetric bend has increased in intensity. As the temperature of this sample is increased, the aliphatic CH bending bands at 1468, 1378 and 1328 cm^{-1} and CH stretching bands at 2945, 2849 and 2798 cm^{-1} decrease in intensity by 175 °C. Relatively, the 1660 cm^{-1} appears to have increased in intensity. BY 200 °C these bands have reduced in intensity, especially the 2847 and 2795 cm^{-1} bands, which are attributed to CH$_2$ stretching vibrations.

At 100°C, the 1660 and 1601 cm^{-1} bands are narrower. By 200 °C the 1660 cm^{-1} starts to lose intensity and broadens. As this band continues to decrease in intensity shoulders appear on both the high (1690 cm^{-1}) and low wavenumber sides of this band before it is lost completely by 450 °C. The 1467 cm^{-1} band is also lost at the same temperature.

A band at 1601 cm^{-1} is also more intense in this sample, than that of the binary mixture (Figure 7.27). This band is sharper by 100 °C but by 200 °C is a shoulder on the 1660 cm^{-1} band.

A band is also observed at 3353 cm^{-1} together with another band at 3274 cm^{-1}, which is lost by 125 °C. The 3353 cm^{-1} band also broadens with increasing temperature.
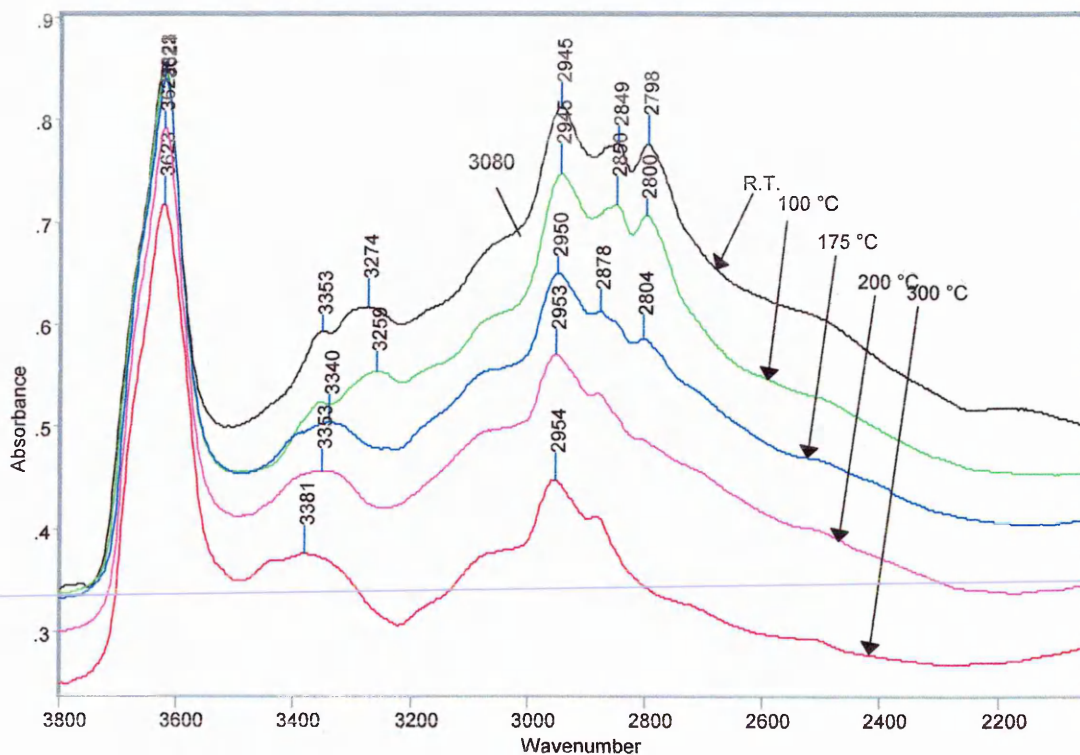

257

Figure 7.35.2 - VT-DRIFTS of composite prepared on addition of aldehyde first 3700 – 2150 cm^{-1}

Several conclusions can now be drawn from this data. The bands at 3353 and 3274 cm^{-1} together with the band at 1598 cm^{-1} represent NH_2 stretching and scissoring bands respectively. Therefore as alluded to earlier NH_2 can only be present if the monomethylol unit was formed, if there is excess 3NH2 present, or as the end groups of Oligomer and polymer chains, and the subsequent product is of the self – condensation reaction. It appears washing the glyoxal intercalate has indeed removed some of the excess aldehyde thus the reactants are only able to form monomethylol units, though there may still be excess amine present. The 1662 cm^{-1} appears to narrow on the low wavenumber side of the band at 100 °C, due to loss of water from the sample (OH deformation at 1630 cm^{-1}).

A band is observed at 3080 cm^{-1} and remains unassigned – this is too low to be an NH stretching band and too high for a CH or CH_2 stretching band, and there is no aromatic in this sample.

It should also be noted however that this sample displays some similarities in VT-DRFITS data to that of the SWy-2 – 3NH2 DRIFTS data (Figure 7.18). In the 3NH2 intercalate, the NH_2 scissoring band (1595 cm^{-1}) is present to 300 °C and the NH_2 stretching bands (3358 and 3299 cm^{-1}) are present to 250 °C. In this sample where the aldehyde is added prior to 3NH2 the NH_2 scissoring band (1598 cm^{-1}) is also stable to 300 °C, whilst the NH_2 stretching bands (3353 and 3274 cm^{-1}) are similarly present to 250 °C. Therefore it would appear that there may also be excess intercalated amine present in this sample also.

The TGA for this sample (Figure 7.38) loses 20% of its weight overall and has discernable DTG peaks at 80 and 195 °C. From 350 – 620 °C there is a broad peak centred at 500 °C accounting for 8% of this weight loss.

Figure 7.38 – TGA of SW-2 and Intercalate adding glyoxal first then 3NH2

The EGA for this sample (Figure 7.39) is again complex with assignment of the fragment ions not possible. M / z = 18 shows its first desorption maxima at 80 °C which is in agreement with the first DTG peak. This may also account for the narrowing of the 1660 cm^{-1} band observed in the VT-DRIFTS. This ion also has two more desorption peaks, seen at 160 °C and 190 °C (therefore associated with the 195 °C DTG peak), and also another at 580 °C which is associated with dehydroxylation of the clay.

The ion 44 peaks at 100 °C and has another desorption maxima associated with dehydroxylation at 603 °C, though this may be CO_2 released form the intercalate as it degrades.

It would also appear that the bifunctionality of some of the reactants does not have a bearing on the final product formed.

7.5 Changing the Sequence of Addition

Investigations were made into the altering the sequence of addition of the reactants to the clay. This was achieved by first immersing the clay in a 2% solution of one reactant for one day washing any remaining reactant away with 6ml. distilled water and then treating the clay with the second reactant for a day prior to drying in air.

When the reactants are added together to the clay the concentrations of these reactants may not be equal throughout the various sites in the system i.e. the bulk solution, the pores in clay aggregates and the gallery space of the clay (Figure 7.34).

Figure 7.34 – Possible Interaction of reactants at various sites.

From Figure 7.34 it is possible to see that the reactants may react within the gallery of the clay or in the bulk solution and then penetrate the clay layers. One reactant may intercalate the clay prior to reacting with the other, which may be in the bulk, therefore implying that we have mixed intercalates before reaction. This leads to the question of how the concentration of one reactant in the gallery affects the reaction.

7.5.1 Addition of Aldehyde First

This sample however produces an interlayer spacing of 14.50 Å with the $d_{(001)}$ being broad and weak (Figure 7.35), and may easily encompass another peak at higher angle. This value is similar to that of the 3NH2 – SWy-2 intercalate of 14.3 Å.

and bands at 3368, 3287 and 3189 cm^{-1} for the glyoxal – EDA (three bands). Two bands in this region indicates NH$_2$ and therefore monomethylol units must have been formed. Indeed the ratio of reactants for these samples (Table 7.9) indicates that at a 3% amine content for these composites the molar ratio of reactants is almost 1:1. Therefore the band at 1611 cm^{-1} in the glyoxal – DAP composite is the NH$_2$ scissors and the 1659 cm^{-1} a carbonyl stretch. In the glyoxal – EDA composite the 1590 cm^{-1} is the NH$_2$ scissors and 1640 cm^{-1} the carbonyl stretch. There is a band present at 3368 cm^{-1} in the glyoxal – EDA sample which can be attributed to an NH stretching band, and this indicates the presence of NH$_2$ and NH in this sample. Therefore this sample may be a mixture of monomethylol condensation product and also the reaction between monomethylol unit and amine, which does have some NH present.

7.4.6 Summary of Composites Containing Varying Amounts of Reactants.

On increasing the amount of 3NH2 in a composite (so the reactants approach equimolar amounts) containing 1% glyoxal and 1% 3NH2 it was anticipated that the reaction intermediate would change from the dimethylol unit to the monomethylol unit as the amount of aldehyde decreases. This means that the product obtained also changes from the dimethylol condensation product to the monomethylol condensation product. In IR spectra it was anticipated that this change would be observed as increase in intensity of bands attributable to NH$_2$ since these are present in the monomethylol condensation product as part of the polymer / Oligomer chain and only present in the dimethylol condensation product as chain ends. This was found to be the case, as an increase in intensity of the NH$_2$ scissoring band at 1598 cm^{-1} was observed as the amine concentration increased together with the emergence of NH$_2$ stretching bands at 3362 and 3268 cm^{-1}.

This observation was reinforced by examination of composites made from differing combinations of glyoxal and formaldehyde and the amines 3NH2, DAP and EDA. When the aldehyde was in excess NH stretching and deformation bands are observed indicating that the dimethylol condensation products were formed. When the amine concentration begins to equal that of the aldehyde the NH$_2$ bands are seen.

The formaldehyde – 3NH2 composite still has an excess of aldehyde and will form dimethylol units. There appears to be little change in the IR spectrum of this sample however (Figures 7.33.1 and 7.33.2) though as stated before the condensation product of this sample would not have any free carbonyl in it. The formaldehyde - DAP composite however has lost the intense 1656 cm⁻¹ and now displays two weak bands at 1636 and 1605 cm⁻¹. As the aldehyde is almost at a 2:1 ratio in excess (Table 7.9) this reaction mixture will predominantly still be dimethylol units, but as the higher frequency region for this sample shows (Figure 7.33.2) two NH stretches are clearly visible at 3316 and 3274 cm⁻¹. The 1605 cm⁻¹ band in this sample may therefore be the NH_2 scissors indicating that a significant portion of monomethylol units must have been formed.

Figure 7.33.2 – DRIFTS Spectra showing the increase in amount to 3% of amine (aldehyde fixed at 1%) 3800 – 2500 cm⁻¹

The glyoxal EDA and DAP composites also show changes in the NH stretching region with the emergence in both samples of bands at 3276 and 3195 cm⁻¹ for the glyoxal – DAP sample

[18]=7950336

TIC=76465296

10:00   20:00   30:00   40:00   50:00   1:00:00   1:10:00

Figure 7.39 – TG – MS data for composite prepared on adding aldehyde first.

[44]=1630209

[43]=411136

[42]=1189888

[40]=2404352

10:00   20:00   30:00   40:00   50:00   1:00:00   1:10:00

Figure 7.39 – TG – MS data for composite prepared on adding aldehyde first.

[56]=161536

[54]=145920

[53]=418304

[52]=434176

[51]=302336

[50]=171776

Figure 7.39 – TG – MS data for composite prepared on adding aldehyde first.

SWy-2 in 2% Glyoxal then 2% 3NH2 Unwashed

[80]=482304

[68]=119296

[66]=133376

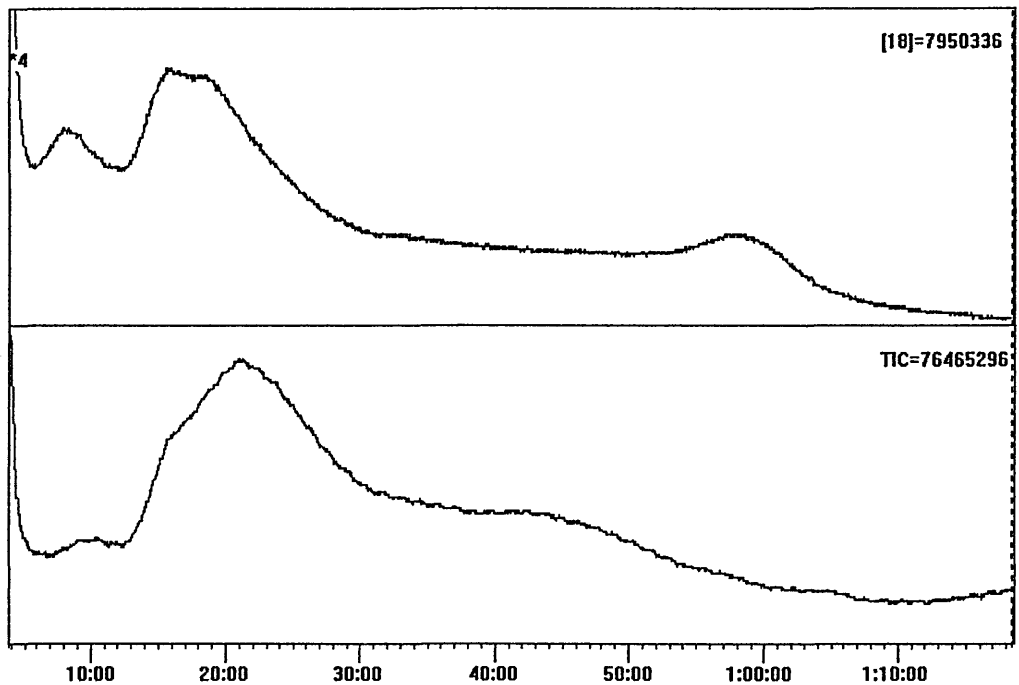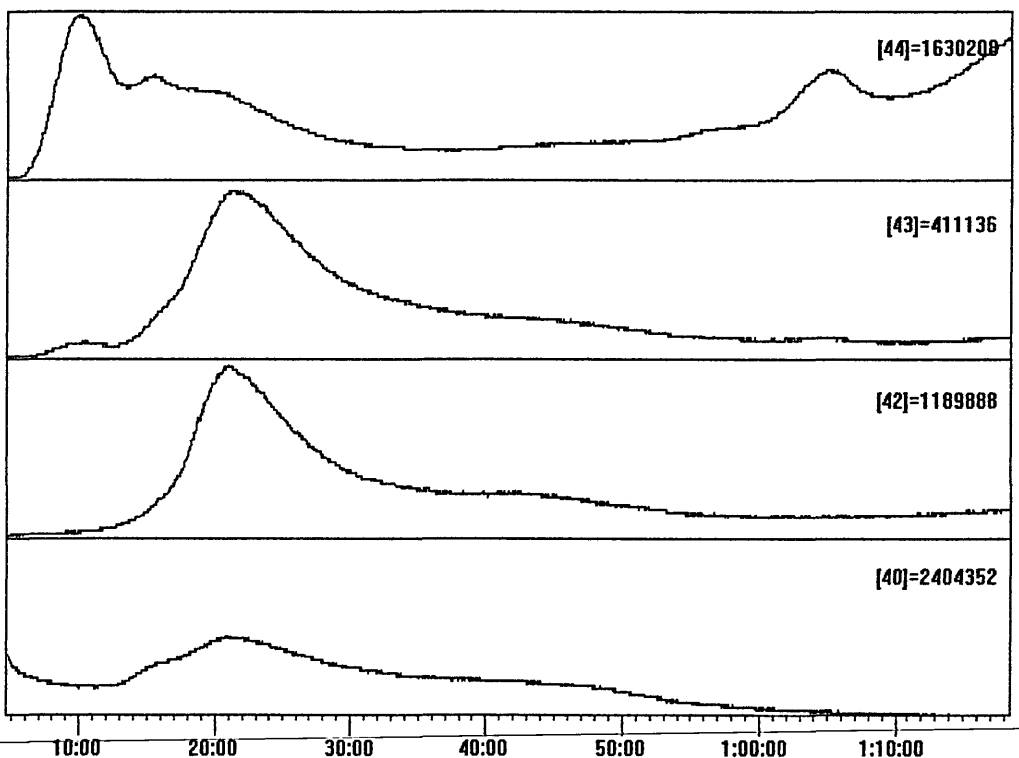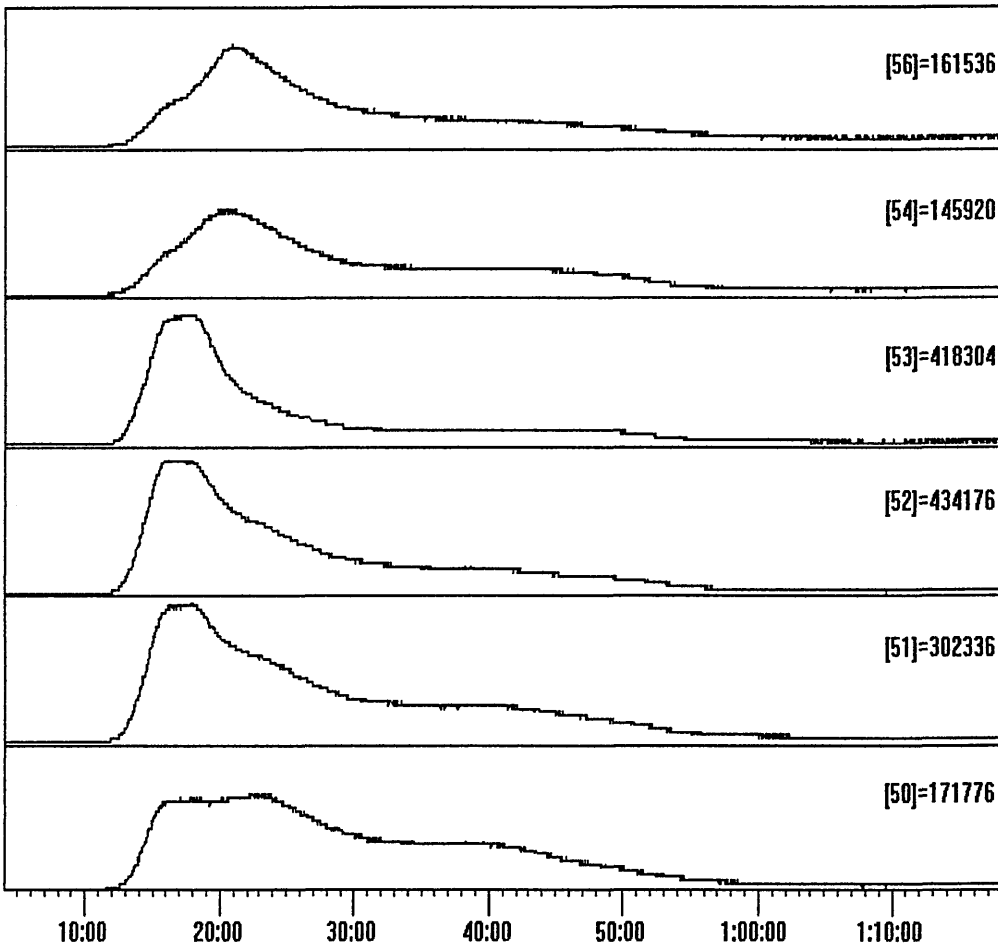Figure 7.39 – TG – MS data for composite prepared on adding aldehyde first.

The ions 43, 42 40, 54 and 56 all have desorption maxima at 210 °C. The ions 51, 52 and 53 all have desorption maxima at 180 °C. Both of these may be associated with the 195 °C DTG peak.

Many of these ions are also observed in the 3NH2 - SWy-2 intercalate but are of a different shape here. These include m/z = 80, 44, 43, 42, 40 and 54.

7.5.2 Addition of the Amine First

XRD analysis shows that the interlayer spacing for this sample is 13.82 Å (Figure 7.40).

Figure 7.40 - XRD trace of composite prepared on adding amine first

This value is closest to that for the washed SWy-2 3NH2 intercalate of 13.50 Å (Figure 7.2).

The TGA results (Figure 7.41) show that this sample loses 16 % of its weight and has five DTG peaks at 80, 210, 380, 410 and 580 °C. This is very different to the composite prepared on adding the aldehyde first and also the SWy-2 – 3NH2 intercalate. The lack of a DTG peak in the region 190 – 200 °C (as seen clearly in Figure 7.20 for the washed SWy-2 3NH2 intercalate) implies that glyoxal can remove 3NH2 where water could not.

Figure 7.41 – TGA trace of composite prepared on adding amine first

From the XRD results (Figure 7.2) and the DRIFTS spectrum (Figure 7.4) for the washed SWy-2 – 3NH2 intercalate we know that after washing the amine treated intercalate the $d_{(001)}$ spacing is 13.50 Å and that there are bands present for 3NH2 in the DRIFTS spectrum indicating that 3NH2 is present and intercalated via a water bridge.

The VT-DRIFTS results for composite prepared by adding 3NH2 first and after washing, glyoxal (Figure 7.42), show a band at 1644 cm^{-1}, at room temperature. By 100 °C this band has reduced in intensity and three poorly resolved bands are visible here at 1675, 1652 and 1610 cm^{-1} (a shoulder). At higher wavenumber, is a weak band at 1740 cm^{-1}. This is barely discernable at room temperature as a small shoulder, but increases a little in intensity as the temperature is raised to 100 °C and is lost by 200 °C. This band was previously assigned to gaseous glyoxal and may originate from very weakly held glyoxal in this sample. The former three bands are no longer present after 300 °C, and the 1740 cm^{-1} is lost by 200 °C. No NH stretching bands are observed in this sample (Figure 7.42.2) and the broad OH stretching band attributed to water has gone by 100 °C. It should also be noted that the CH$_2$ deformation (1470 cm^{-1}) is also observed up to 300 °C in this sample.

263

Figure 7.42.1 – VT-DRIFTS of composite prepared on adding amine first – 2000 – 1100 cm^{-1}.

Figure 7.42.2 – VT-DRIFTS of composite prepared on adding amine first – 3800 – 2200 cm^{-1}.

264

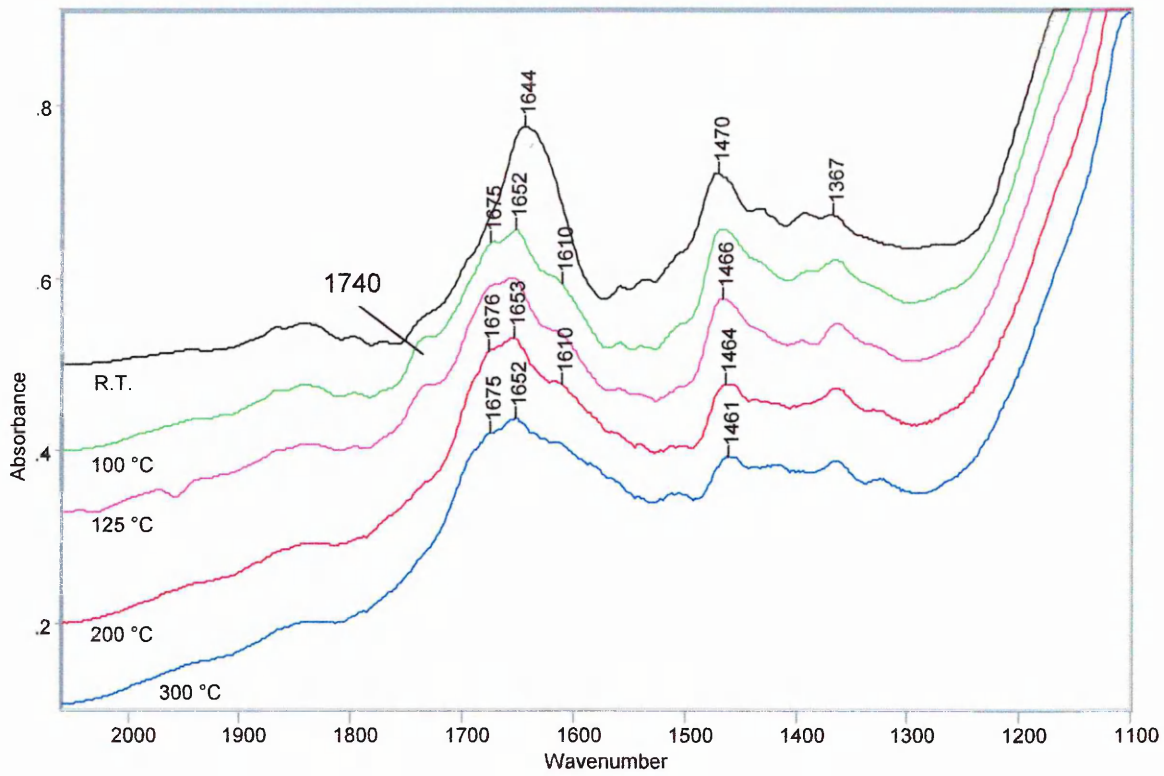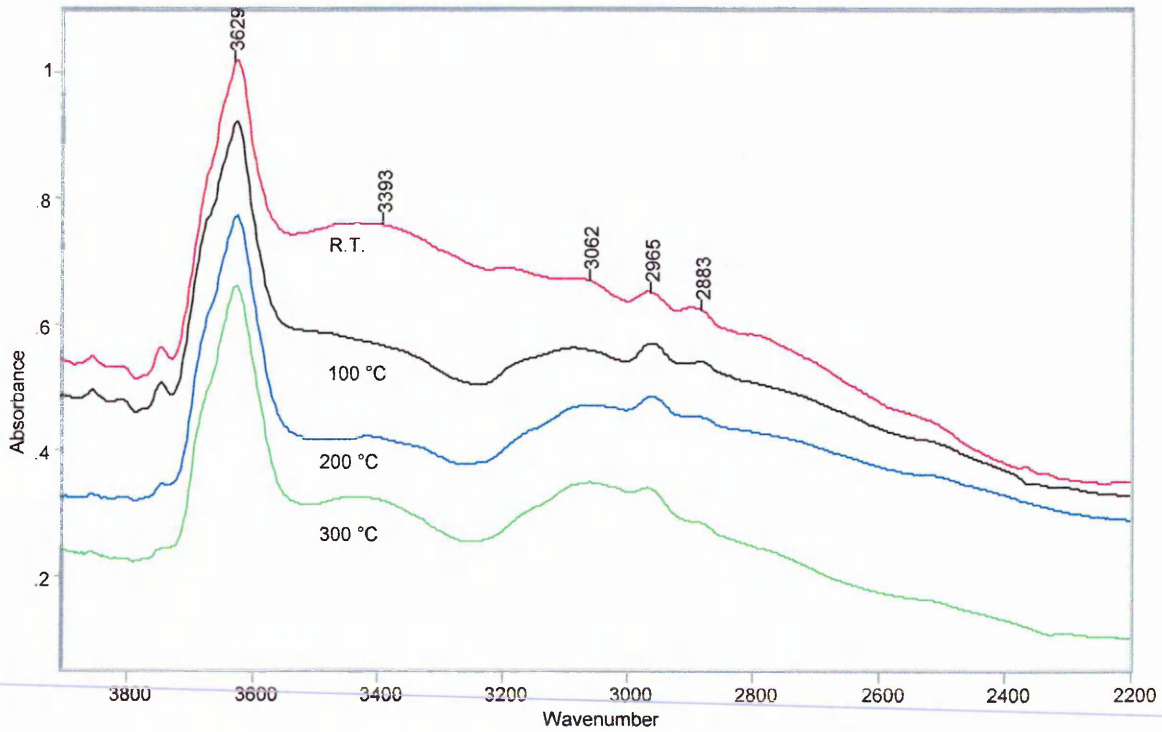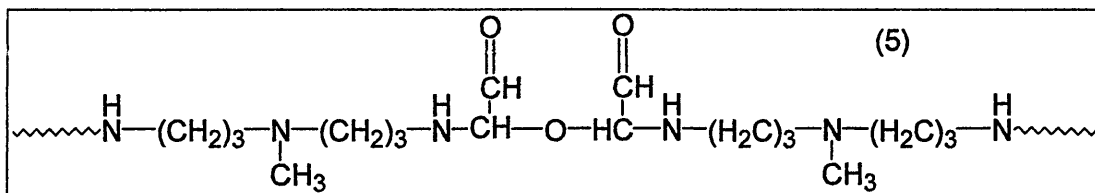Much of the intensity associated with the 1644 cm^{-1} band must initially be attributed to water (OH deformation at 1630 cm^{-1}), as the OH stretching region illustrates. What is most striking in this sample however is the change in the spectra of the washed 3NH2 intercalate (Figure 7.4), which displays NH stretching and deformation bands with some clarity after washing. After treatment with glyoxal (Figure 7.42) these bands are clearly not visible, though no VT-DRIFTS was performed on the washed SWy-2 – 3NH2 intercalate. It is expected that the washing process would again remove excess amine and subsequent treatment with glyoxal would result in there being excess aldehyde, which results in the dimethylol units being formed and then the dimethylol self – condensation reaction product: -

In the above spectra there is no evidence of this occurring as there are no NH deformations (previously seen at 1538 cm^{-1}) and no NH stretching bands.

By 100 °C the VT-DRIFTS spectrum shows a pattern that is similar to the SWy-2 – glyoxal intercalate VT-DRIFTS results (Figures 7.8 and 7.9). There are bands present at 1740, 1675, 1652 and 1610 cm^{-1}. In the glyoxal – SWy-2 intercalate there are bands observed at 1740, 1715, 1646, and 1610 cm^{-1}. However, the thermal stabilities of these two samples are not similar, the glyoxal intercalate displaying the higher thermal stability.

Therefore, it would appear that the glyoxal has displaced the 3NH2 from the clay interlayer, and that there remains too little 3NH2 for any possible reaction to occur, or that can be detected by FTIR.

7.5.3 Summary of Composites Made on Change of Sequence of Addition

Composites of SWy-2 were made again with glyoxal and 3NH2 but by treating the clay first with one reactant, washing with distilled water and then subsequent addition of the second reactant prior to drying in air (Figure 7.43).

When glyoxal was added first the following observation are made:-

- The intercalate obtained produced a $d_{(001)}$ spacing similar to that of the 3NH2 intercalate (14.3 Å) of 14.5 Å.

Figure 7.43.1 – Structure of product formed after addition of glyoxal to clay first.

- The washing process indicates that some glyoxal is still present - a band at 1622cm^{-1} was stable to 300 °C and assigned to monodentate glyoxal interaction with the interlayer cation. However TG analysis reveals that there is not as much glyoxal present as in the unwashed counterpart.

- VT-DRIFTS of the sample after treatment with 3NH2 shows that as anticipated there are bands indicative of the monomethylol self – condensation products (NH2

stretching and scissoring bands at 3353, 3274 and 1598 cm^{-1} respectively). This could equally be assigned to intercalated 3NH2, whose VT-DRFITS bands display similar thermal stability, but the presence of the aldehyde carbonyl stretching band at 1662 cm^{-1} would indicate that a reaction has taken place.

The situation is very different if the amine is added first (Figure 7.43.2).

Figure 7.43.2 – Addition of amine to clay first and subsequent displacement by aldehyde.

- When 3NH2 was added first it appears that glyoxal displaces it from the interlayer, as the presence of 3NH2 in the clay after washing has been confirmed by prior analysis.

- However the product obtained is mainly intercalated glyoxal and water with a d – spacing of 13.80 Å. Water is observed in this sample by the OH bending mode at

267

1644 cm^{-1} in the VT-DRIFTS and is rapidly lost on heating to 100 °C, to leave weak carbonyl stretching bands at 1675, 1652 and 1610 cm^{-1}.

- In addition the DTG for this sample has no peak in the 190 – 200 °C region as seen in the washed SWy-2 – 3NH2 intercalate.

- There is too little of either reactant present for a reaction to occur.

Chapter 8 – Conclusions

8.0 Introduction

The composites prepared within this thesis share some similarities but also display a range of differing properties and qualities each of their own significance. These are discussed in this chapter in terms of the method of preparation and the physical properties of the nanocomposites produced. The analytical results obtained upon characterisation are briefly summarised first. Included also within this discussion, are avenues for further work.

8.1 Results of Characterisation

8.1.1 HPPA and KPPA Intercalates

Halloysite adsorbed twice as much PPA as kaolin in a much shorter time. Both PPA intercalates formed an expanded phase which exhibited remarkable thermal stability. Note that the increase in spacing is almost twice the layer spacing for these clays and therefore is quite a significant change. The PPA moiety decomposed via the loss of the phenyl ring at temperatures above which layer dehydroxylation has ended. Complementary TG – MS and variable temperature DRIFTS data showed that the HPPA and KPPA complexes retained water in three different sites within the intercalate. It would be interesting to compare the behaviour of PPA on intercalation in montmorillonite as the interaction with the interlayer in this clay represents a different one than that with kaolin or Halloysite.

8.1.2 VFA – Clay Composites

VFA intercalates montmorillonite in a manner similar to the amides NMF and DMF. Composites of montmorillonite (MCBP) and VFA may be prepared without the use of an organoclay to produce an intercalated nanocomposite. Employing the use of a polar activator to swell the clay prior to initiation of the intercalated monomer enables an exfoliated nanocomposite to be produced as no $d_{(001)}$ peak is seen in the resultant XRD trace as the amount of polar activator added is increased. The use of NMR would be beneficial here to ascertain the structure of the VFA before and after the use of the polar activator. Unlike the

other composites prepared in this thesis the VFA composites were more suited to XRD and TG study than DRIFTS.

8.1.3 Aldehyde – Amine Composites

Intercalates of the aldehyde glyoxal and the amine 3NH2 have both been characterised by VT-DRIFTS, TGA and XRD. Subsequently these reactants have been added in a binary mixture to montmorillonite (SWy-2) and sequentially (treating the clay first with one reactant and then another), both approaches using DRIFTS to characterise two very different scenarios (discussed further below). The concentration of the reactants also has a bearing on the final product produced. This study would benefit from the application of electron microscopy to confirm the formation of an intercalated nanocomposite and enable a view of how much polymer formation may be present on the surface of the clay.

8.2 Methods of Preparation

The three composites vary greatly in the ease in which they may be prepared. The easiest composite to prepare was the aldehyde – amine composite. These were prepared by simply diluting the aldehyde or amine or amine in water to produce the required concentration and then adding them to the clay. The supernatent was then decanted off and the intercalated clay left to dry in air. No heating was required and the polymer formed at room temperature without the need for initiator. The resultant composite was thought to be an intercalated nanocomposite. This method can be said to be relatively simple and straightforward. The reactants required are easily available and therefore this composite was cheap to prepare. Indeed as previously discussed, glyoxal (and formaldehyde) is used in a number of other industrial applications and readily available and cheap. The method can be varied in terms of the concentration of the reactant used and this has a direct effect on the polymer formed in the final nanocomposite i.e. the monomethylol or dimethylol condensation polymerisation product. Furthermore changing the sequence of addition (treating the clay with first one reactant and then another) or adding both reactants together also has a significant bearing on the final polymer produced within the interlayer of the clay. There exists here an opportunity to explore in more detail the properties of these two products especially the hardness and

270

barrier properties of these two polymers when formed as nanocomposite with the clay. Perhaps also as these composites have applications in wellbore consolidation the reaction should be carried out under higher pressure, temperature having already being examined.

By contrast, the VFA – clay composites required heating under nitrogen to initiate polymerisation using the initiator AIBN. These composites were however the quickest of the three to prepare, as the clay was intercalated first by stirring with VFA and then expanded further by the addition of the polar activator propylene carbonate and AIBN. The polymerisation process was usually complete in twenty minutes and required drying afterwards. Note however, that this method of manufacture was also the only one to produce an exfoliated nanocomposite. More importantly however, this method allows control over the type of nanocomposite produced – if the composite is prepared with 50 % polar activator then an intercalated nanocomposite is produced. If 75 % polar activator is used then an exfoliated nanocomposite is formed. This is a flexibility in production not seen in the other two methods employed in this thesis. Furthermore, VFA as a monomer is attracting more attention and therefore becoming cheaper. This method is more involved than the aldehyde – amine one but still relatively simple to employ.

The intercalates of PPA with halloysite and kaolin were the most time consuming and involved to prepare. The kaolin – PPA required five weeks under reflux with acetone and water whereas the halloysite one week under the same conditions. Prior to drying these intercalates also required a lengthy centrifugation regime not needed in the other two types of composite prepared. Although the resultant complex was an intercalated clay there remains most scope within these intercalates to explore the possibility of intercalating a monomer – such as VFA - within these intercalated and promoting hence, polymerisation and hence nanocomposite formation. The choice of monomer may well prove to be critical. The clay is already expanded a great deal for a 1:1 mineral and this may well have some bearing on the monomer that may interact with the PPA moiety already present. This study has also contributed to current knowledge on the fate of water when used as an entraining agent.

Note also that these are three very different methods of preparing nanocomposites, and that the ease or method of manufacture has neither a positive or negative impact on the nanocomposite formed, but changes the type of nanocomposite that may be formed. Each

method may be employed to suit particular needs, but all methods enable the manufacture of nanocomposites without the use of an organoclay as a starting material as most approaches currently employ. This is a significant cost advantage over more conventional methods such as ones which simply mix the organoclay with a polymer melt.

8.3 Physical Properties

The physical properties of the three composites are significantly different also. The HPPA and KPPA intercalates display a remarkable thermal stability of greater then 500 °C despite the loss of water (which is expected) at lower temperatures. This is easily the best thermal stability of the three composites prepared. Halloysite also absorbs twice as much PPA than kaolin in a shorter time. Note however, that these clays are 1:1 clays and this in itself departs different properties to the clay than the 2:1 montmorillonite used to prepare the other two composites. In this case this is the incorporation of an intercalate into the hydrogen bonding network of kaolin and halloysite, which in itself is imparts a high thermal stability to the clay alone. In montmorillonite the interaction is via the interlayer cation. If, as previously discussed, a monomer could be intercalated into these intercalates and polymerisation initiated to form a nanocomposite, this may well be one with exceptional thermal stability.

By contrast, neither the VFA, nor aldehyde – amine composites exhibit such high thermal stability.

A property not studied in these composites is the hardness and tensile strength. From DRIFTS analysis alone – which is not a measure of either hardness or tensile strength – but requires grinding of the composites, the aldehyde – amine composites would appear to be the hardest. The VFA composite prepared using 50 % polar activator was also noted to be particularly hard however.

Another property not studied was water permeability which is most important in the aldehyde – amine composites considering applications in wellbore consolidation. This would have to involve films on the composite being formed. Furthermore this study should be applied to the actual rock samples that may be encountered in wellbores

An interesting property of the VFA composites is the water solubility and these composites are water-soluble. Bearing in mind that VFA itself has good conductive properties there remains some applications possible in this area.

8.4 Concluding Comments

The composites in this study have been prepared by differing means and show a variety of properties.

The HPA and KPPA intercalates were prepared via the use on an entraining agent and, in the case of HPPA, in a relatively faster time. Both these intercalates however, display remarkable thermal stability at over 450°C. There also remains scope to graft onto these intercalates an organic monomer, such as VFA to enable polymerisation and nanocomposite formation.

The VFA – montmorillonite composites may be polymerised to produce what may be an exfoliated nanocomposite. Unlike most methods of synthesis which rely on the use of an organo-clay precursor the method produced here uses a polar activator to pre-swell the clay.

The montmorillonite composites prepared with the aldehyde and amine combinations may be made by either adding both reactants together to the clay or first adding the aldehyde and then amine. The results produce an intercalated nanocomposite which is stable to 300°C, and should therefore be suitable for shale stabilisation.

9.0 References

1. R.P. Steiger and P.K. Leung, *Quantitative Determination of the Mechanical Properties of Shales*, (1992), SPEDE 181, Trans., AIME, 293,.

2. T.J. Ballard, S.P. Beare and T.A. Lawless, *Fundamentals of Shale Stabilisation: Water Transport Through Shales*, (1991) Society of Petrochemical Engineers 24974.

3. Baroid Oil Mud Manual, Borehole Instability (1985).

4. L. Bailey, P.I. Reid, J.D. Sherwood. *Mechanisms and Solutions for Chemical Inhibition of Shale Swelling and Failure* (1994). Proceedings of the 5th International Conference on Chemistry in the Oil Industry. Royal Society of Chemistry.. 13 – 27.

5. L. Bailey, M. Keall, A. Audibert and J. Lecoutier, Langmuir 10 (1994), 5.

6. Baroid Oil Mud Manual, *Fundamental Characteristics of Drilling Fluids* 1985.

7. Department of Energy, *Development of Oil and Gas Resources of the UK*, 1988.

8. R. Bland. Oil and Gas Journal 90, 26 (1992) 54-59 .

9. G.R. Gray, H.C.H. Darley. *Composition and Properties of Oil Well Drilling Fluids*. 1980 4th Edition, Gulf Publishing Co. Houston.

10. J. Dorman, E. Banka. *Development and Application of Cationic Polymer Drilling Fluids for Shale Stabilisation* (1994). Proceedings of the 5th International Symposium on Chemistry in the Oil Industry. Royal Society of Chemistry, 56-70.

11. P.I. Reid, G.P.Elliot, R.C. Minton, B.D. Chambers, D.A. Burt. Society of Petroleum Engineers 25989 (1993).

12. C.O. Oriakhi. J.Chem.Ed. 77 (2000), 9.

13. B.Z. Jang. Compos. Sci. Technol. 44 (1992), 333.

14. J.E. Sohn. J.Adhes. 19 (1985), 15.

15. M. Alexandre, P. Dubois. Materials Science and Engineering. 28 (2000), 1-63.

16. S. Mann. Nature. 365 (1993), 499.

17. K. Gonsalves, X. Chen, Materials Research Soc. Symposium Proceedings; Materials Research Society, Warerendale P.A. 435 p55 1996.

18. S. Komarneni. J. Mater. Chem. 2 (1992), 1219.

19. M. Lerner, C. Oriakhi, *Handbook of Nanophase Materials*. (1997) A. Goldstein., Ed.; Dekker: New York.

20. N. Herron, D.L. Thorn. Adv. Mater. 10 (1998), 1173-1184.

21. J.E. Mark. Polym. Eng. Sci. 69 (1996) 2905-2920.

22. E. Reynaud, C. Gauthier, J. Perez. Rev. Metall./Cah. Inf. Tech. 96 (1999), 169-176.

23. T. von Werne, T.E. Patten. J. Am. Chem. Soc. 121 (1999), 7409-7410.

24. P. Calvert. T.W. Ebbesen (Ed), Carbon Nanotubes, 1997 CRC Press, Boca Raton, FL, 277-292.

25. V. Favier, G.R. Canova, S.C. Shrivastava, J.Y. Cavaille. Polym. Eng. Sci. 37 (1997), 1732-1739.

26. L. Chazeau, J.Y. Cavaille, G. Canova, R. Dendieval, B. Boutherin. J. Appl. Polym. Sci. 71 (1999), 1797-1080.

27. H.H. Murray. Appl. Clay Sci. 17 (2000), 207-221.

28. J. Konta. Appl. Clay Sci. 10 (1995), 275-335.

29. B.K.G. Theng. The Chemistry of Clay Organic Interactions (1974). Adam Hilger Ltd. London.

30. K.J. Range, A. Range, A. Weiss. Proc. Int. Clay Conf. Tokoyo, Japan (1969). (L.Heller Ed). Israel University Press 1, 3 – 13.

31. S.W. Bailey. Proc. Int. Clay Conf. Strasbourg, France (1989). (V.C. Farmer & Y. Tardy, eds.) Sci. Geol. Mem. 86, 89.

32. C.T. Johnston. Sorption of Organic Compounds on Clay Minerals: A surface Functional Group Approach. (1996) CMS Workshop Lectures 8 The Clay Minerals Society (B. Sahney Ed.) Boulder CO, 1 – 45.

33. P.J.R. Unwins, I.D.R. Mackinnon, J.G. Thompson, J.E. Yago. Clays & Clay Miner. 41 (1993), 6, 707-717.

34. H.W. van der Marel, H. Beutelspacher. Atlas of Infrared Spectroscopy of Clay Minerals and their Admixtures (1976). Elevier Scientific Publishing Company (Amsterdam).

35. V.C. Farmer. The Infrared Spectra of Minerals (1974). Adlard & Son Bartholomew Press (Surrey).

36. J.M. Hollas. Modern Spectroscopy. (1992) 2nd Edition, John Wiley & Sons.

37. J.M. Chalmers, G. Dent. Industrial Analysis with Vibrational Spectrscopy. RSC Analytical Spectroscopy Monographs. The Royal Society of Chemistry, Hertfordshire (1997).

38. Griffiths & De Hasser. *Fourier Transform Infrared Spectroscopy*. John Wiley & Sons (New York) 1986.

39. W.O. George, P.S. Mc Intyre. *Infrared Spectrscopy*. John Wiley & Sons (London) 1987.

40. W.W. Wendlandt, H.G. Hecht. Reflectance Spectroscopy. New York: John Wiley and Sons 1966.

41. D.L. Wetzl. Anal. Chem. 55 (1983), 12 1165a – 1176a.

42. Spectra – Tech technical note TN-2 : Introduction to DRIFTS.

43. M.B. Mitchell. Structure – *Property relations in Polymers* 1883

44. P.B. Coleman. *Practical Sampling Techniques for IR Analysis* (1993) CRC Press London.

45. M.P. Fuller, P.R. Griffiths. Anal. Chem. 50 (1978), 1906.

46. I.M. Hamadeh, S.A. Yeboah, K.A. Trumball, P.R. Griffiths. Appl. Spectrosc. 38 (1984), 486 – 492.

47. M.P. Fuller PhD dissertation, Ohio University, Athens, Ohio, 1980.

48. D.J.J. Fraser, P.R. Griffiths. Appl. Spectrosc. 44 (1990), 193 – 199.

49. S.A. Yeboah, S.H. Wang, P.R. Griffiths. Appl. Spectrosc. 38 (1984), 259.

50. Z. Krivacsy, J. Hlavay. Talanta 41 (1994), 1143 – 1149.

51. J.A. de Haseth. Appl. Spectrosc. 36 (1982), 544 – 552.

52. R.L. White. Anal. Chem. 64 (1992), 2010 – 2013.

53. R.S.S. Murthy, J.P. Blitz, D.E. Leyden. Anal.Chem. 58 (1986), 3167 – 3172.

54. D.N. Todor. *Thermal Analysis of Minerals,* 1976 Abacus Press, Tunbridge Wells 21 – 23.

55. D.M. Moore, R.C. Reynolds. *X-Ray Diffraction and the Identification and Analysis of Clay Minerals*. 1997 2nd Edition. Oxford University Press, Oxford, New York.

56. C. Breen, P.M. Last, M.Webb. Theromchimica Acta 326 (1999), 151.

57. R.L. Frost. A.M. Vassallo. Clays, Clay Miner. 44 (1996), 635 – 651.

58. V.C. Farmer, J.D. Russell. Spectrochimica Acta 20 (1964), 1149 – 1173.

59. V.C. Farmer, *The Infrared Spectra of Minerals,* 331 0 363 The Mineralogical Society, London 1974.

60. R.L. Frost. Clay Minerals. 32 (1997), 65 – 77.

61. D.L. Bish. Clays Clay Miner. 41 (1993), 738 – 744.

62. V.C. Farmer. Clay Minerals. 33 (1998), 601 – 604.

63. R.L. Frost. Clays Clay Miner. 46 (1998), 280 – 289.

64. J.K. Range, A. Range, & A. Weiss. *Proc. Int. Clay Conf. Tokoyo* 1 (1969), 3 – 11.

65. K. Wada, H. Yamada. Am. Mineral. 53 (1968), 334 – 339.

66. G. Lagaly. *Clay Organics Reactions. Phil. Trans. R. Soc.* London a311 (1984), 315 – 332.

67. J. Kristof, R.L. Frost, A. Felinger, J. Mink. J. Mol. Structure. 410 – 411 (1997), 119 – 122.

68. J. Kristof, M. Toth, M. Gabor, P. Szabo, R.L. Frost. J. Thermal Analysis. 49 (1997), 1441 – 1448.

69. R. L. Frost. T.H. Tran. J. Kristof. Vib. Spectrosc. 13 (1997), 175 – 186.

70. R. L. Frost. T.H. Tran. J. Kristof. Clay Minerals. 32 (1997), 587 – 596.

71. M.D. Ruiz Cruz, F.I. Franco Duro. Clay Minerals 34 (1999), 565 – 577.

72. R.L. Frost, J. Kristof, J.N. Paroz, T.H. Tran, J.T. Kloprogge. J. Coll. Interf. Sci. 204 (1998), 227 – 236.

73. C.T. Johnston, D.L. Bish, J. Eckert, L.A. Brown. J. Phys. Chem. B. 104 (2000), 8080 – 8088.

74. R.L. Frost, D.A. Lack, G.N. Paroz, T.H. Tran. Clays, Clay Miner. 47 (1999), 297 – 303.

75. R.L. Frost, J. Kristof, E. Horvath, J.T. Kloprogge. Spectrochimica Acta. A 56 (2000), 1191 – 1204.

76. A. Novak. Struct. Bonding. 18 (1974), 177.

77. R.L. Frost, J. Kristof, E. Horvath, J.T.Kloprogge. J. Coll. Interf. Sci. 226 (2000), 318 – 327.

78. R.L. Frost, J.Kristof. Clays & Clay Miner. 45 (1997), (4), 551 – 563.

79. R.L. Frost. Clays & Clay Miner. 46 (1998), (3) 280 – 289.

80. Y. Sughara, S. Satokawa, K. Yoshioka, K. Kurada, C. Kato. Clays & Clay Miner. 37 (1989), 143.

81. J.J. Tunney, C. Detellier, Clays & Clay Miner. 42 (1994), 552.

82. J.J. Tunney, C. Detellier, J. Mater. Chem. 6 (1996), 1679.

83. J.J. Tunney, C. Detellier, Clays & Clay Miner. 4 (1994), 473.

84. R.L. Frost, J. Kristof, E. Horvath, J.T.Kloprogge. Spectrochim. Acta. A. 56 (2000), 1711 – 1729.

85. R.L. Frost, J. Kristof, J.N. Paroz, T.H. Tran, J.T. Kloprogge. J. Coll. Interf. Sci. 208 (1998), 216 – 225.

86. J.L. Guimaraes, P. Peralto –Zamora, F. Wypych. J. Coll. Interf. Sci. 206 (1998), 281 – 287.

87. J.L. Guimaraes, C.J. da Cunha, F. Wypych. J. Coll. Interf. Sci. 218 (1999), 211 – 216.

88. J.J. Tunney, C. Detellier, J. Mater. Chem. 6 (1996), 1679 - 1685.

89. Y. Komori, Y. Sugahara, Y. Komori,. Appl. Clay Sci. 15 (1999), 241 – 252.

90. M. Sato. Clays & Clay Miner. 47 (1999), (6) 793 – 802.

91. J.E. Gardolinski, L.P. Ramos. G.P. de Souza. F. Wypych. J. Coll. Interf. Sci. 221 (2000), 284 – 290.

92. J.E. Gardolinski, P. Peralta-Zamora, F. Wypych. J. Coll. Interf. Sci. 211 (1999), 137 – 141.

93. F.M. Vichi, O.L. Alves. J. Mater. Chem. 7 (1997), (8). 1631 – 1634.

94. H. Nijs, A. Clearfield, E.F. Vansant. Microporous & Mesoporous Materials. 23 (1998), 97 – 108.

95. G. Alberti, E. Giontella, S. Murcia-Mascaros. Inorg. Chem. 36 (1997), 2844 – 2849.

96. K. Sakamoto, Y. Tsunawaki, A. Nakahira, K. Kitahama, J. Ichilara, S. Yamaguchi. Nanostructured Materials. 12 (1999), 491- 494.

97. L.R. Raki C. Detellier Chem. Commun. (1996), 2475 – 2476.

98. K.J. Frink, R. Wang, J.L. Colon, A. Clearfield. Inorg. Chem. 30 (1991), 1438 – 1441.

99. Y. Sugahara, S. Satokawa, K. Kuroda. C. Kato. Clays & Clay Miner. 36 (6) (1988), 343 – 348.

100. Y. Sugahara, S. Satokawa, K. Kuroda. C. Kato. Clays & Clay Miner. 38 (2) (1990),137 – 143.

101. Y. Komori, Y. Sugahara, K. Kuroda. Chem. Mater. 11 (1999), 3 – 6.

102. J.J. Tunney, C. Detellier. Chem. Mater. 8 (1996), 927 – 935.

103. V. Luca, S. Thomson. J. Mater. Chem. 10 (2000), 2121 – 2126.

104. C. Oriakhi. Nano Sandwiches. Chem. Br. 34 (1998). 59 – 62.

105. P Bala, B.K. Samantary, S.K. Srivatava. Mater. Research Bulletin. 35 (2000), 1717 – 1724.

106. G. Lagaly. Solid State Ionics. 22 (1986), 43 – 51.

107. E. Hackett, E. Manias, E.P. Giannelis. J. Phys. Chem. 5 (1998), 7410 – 7415.

108. G. Lagaly. Appl. Clay Sci. 15 (1999), 1-9.

109. Y. Fukushima, A. Okada, M. Kawasumi, T. Kurauchi, O. Kamigaito. Clay Mineral 23. (1998), 27 – 34.

110. A. Usuki, Y. Kojima, M. Kawasumi, A. Okada, Y. Fukushima, T. Kurauchi, O. Kamigaito. J. Mater. Res. 8. (1993), 1179 – 1183.

111. T. Lan. T.J. Pinnavaia. Chem. Mater. 6. (1994), 2216 – 2219.

112. P.B. Messersmith, E.P. Giannelis. Chem. Mater. 6. (1994), 1719 – 1725.

113. J. Massam. T.J. Pinnavia. Mater. Res. Soc. Symp. Proc. 520 (1998), 223 – 232.

114. T. Lan. D. Padmananda, D. Kaviratna, T.J. Pinnavaia. J. Phys. Chem. Solids 57 (1996), 1005 – 1010.

115. P.C. LeBaron, Z.W. Wang, T.J. Pinnavaia. Appl. Clay Sci. 15 (1999), 11 – 29.

116. X. Kornmann, H. Lindberg, L.A. Berglund. Polymer. 42 (2001), 1303 – 1310.

117. A. Weiss. Angew Chem. Int. Ed. England. 2 (1963)134.

118. X. Kornmann, H. Lindberg, L.A. Berglund. Polymer. 42 (2001), 4493 – 4499.

119. I.J. Chin, T. Thurn-Albrecht, H. Kim, T.P. Russell, J. Wang. Polymer 42 (2001),5947 – 5964.

120. J.M. Brown, D. Curliss, R.A. Vaia. Chem. Mater. 12 (2000), 3376 – 3384.

121. A. Akelah, A. Moet. J. Mater. Sci. 31 (1996), 3589 – 3596.

122. J.G. Doh, I. Cho. Polym. Bull. 41 (1998), 511 – 517.

123. M.W. Weimer, H. Chen, E.P. Giannelis, D.Y. Sogah. J. Am. Chem. Soc. 121 (1999), 1615 – 1616.

124. X. Fu, S. Qutubuddin. Polymer. 42 (2001), 807 – 813.

125. J. Tudor, L. Willington, D. O'Hare, B. Royan. Chem. Commun (1996), 2031 – 2032.

126. J.S. Bergman, H. Chen, E.P. Giannelis, M.G. Thomas, G.W. Coates. Chem. Commun (1999), 2179 – 2180.

127. M. Alexandre, P. Dubois, R. Jerome, M. Garcia – Marti, T. Sun, J.M. Garces, D.M. Millar, A. Kuperman. W.O Patent WO0047598A1 (1999).

128. M. Alexandre, P. Dubois, T. Sun, in Print.

129. P. Dubois, M. Alexandre, F. Hindryckx. J. Macromol. Sci.; Rev. Macromol. Chem. Phys. C38 (1998), 511 – 565.

130. A. Usuki, M. Kawasumi, Y. Kojima, A. Okada, T. Kurauchi, O. Kamigaito. J. Mater. Res. 8 (1993), 1174 – 1178.

131. A. Okada, A. Usuki. Mater. Sci. & Eng. C3 (1995), 109 – 115.

132. Y. Kojima, A. Usuki, M. Kawasumi, A. Okada, T. Kurauchi, O. Kamigaito. J. Polym. Sci. Part A: Polym. Chem. 31 (1993), 983 – 986.

133. P. Reichert, J. Kressler, R. Thomann, R. Mullhaupt, G. Stoppelmann. Acta Polym. 49 (1998), 116 –123.

134. P.B. Messersmith, E.P. Giannelis. J. Polym. Sci.; Part A Polym. Chem 33 (1995), 1047 – 1057.

135. P.B. Messersmith, E.P. Giannelis. Chem. Mater. 5 (1993), 1064 – 1066.

136. T.Agag, T. Koga, T. Takeichi. Polymer 42 (2001), 3399 – 3408.

137. Q. Wu, Z. Xue, Q.F. Wang. Polymer 41 (2000), 2029 – 2032.

138. M.G. Kanatzidis C. Wu. J. Am. Chem. Soc. 111 (1989), 4139 – 4142.

139. M.P. Eastman, E. Bain, T.L. Proter, K. Manygoats, R. Whithorse, R.A. Parnell, M.E. Hagerman. Appl. Clay. Sci. 15 (1999), 173 – 185.

140. F. Bergaya, F. Kooli. Clay Minerals 26 (1991), 33 – 41.

141. K.G. Fournaris, M.A. Karakassides, D. Petridis, K. Yiannakopoulou. Chem. Mater. 11 (1999), 2372 – 2381.

142. K.G. Fournaris, N. Boukos, D. Petridis. Appl. Clay Sci. 19 (2001), 77 – 88.

143. W. Xu. C.T. Johnston, P. Parker, S.F. Agnew. Clays & Clay. Miner.48 (2000), 120 – 131.

144. N.I.E. Shewring, T.G.J. Jones, G. Maitland. J. Yarwood. J. Coll. Inter. Sci. 176 (1995) 308 – 317.

145. R.L. Frost, L. Rintoul. Appl. Clay. Sci. 11 (1996), 171- 183.

146. A. Streitweiser, C.H. Heathcock. *Introduction to Organic Chemistry* (1985). 3rd Ed. Macmillan Publishing Company, New York.

147. D.L. Osborn, D.J. Leahy, D.M. Newmark. J. Phys. Chem. A. 101 (1997), 6583.

148. Q. Cui, K. Morkuma. Chem. Phys. Lett. 263 (1996), 54.

149. P. Blowers, R.I Masel. J. Phys. Chem. A. 104 (2000), 34 – 44.

150. G.J. Millar. C.H. Rochester, K.C. Waugh. J. Chem. Soc. Faraday Trans. 76 17 (1991), 2785 – 2793.

151. M. Kobayashi, R. Iwamoto, H. Tadokoro. J. Chem. Phys. 44 (1966), 922.

152. H. Tadokoro, M. Kobayashi, Y. Kawaguchi, A. Kobayashi. J. Chem. Phys. 38 (1963), 703.

153. J. F. Edwards, G.L. Schrader. J. Phys Chem. 89 (1985), 782 – 788.

154. G. Busca, J. Lamotte, J.C. Lavalley, V. Lorenzelli. J. Am. Chem. Soc. 109 (1987), 5197 – 5202.

155. D.B. Clarke, D.K. Lee, M.J. Sandoval, A.T. Bell. J. Catal. 150 (1984), 81 – 93.

156. I.A. Fisher, A.T. Bell. J. Catal. 172 (1997), 222 – 237.

157. I.A. Fisher, A.T. Bell. J. Catal. 178 (1998), 153 – 173.

158. I.A. Fisher, A.T. Bell. J. Catal. 184 (1999), 357 – 376.

159. A.K.A. Rathi. Chemical Age of India. April (1983), 219 – 223.

160. D.L. Pavia, G.M. Lampman, G.S. Kriz. *Introduction to Spectroscopy*, (1996) 2nd ed. Saunders College Publishing, New York.

161. F. Schweitzer, L. Magi, P. Mirabel, C. George. J. Phys. Chem. A. 102 (1998), 593 – 600.

162. R.K. Harris. Spectrochimica Acta. 20 (1964), 1129 – 1141.

163. A.R.H. Cole, G.A. Osborne. Spectrochimica Acta. 27A (1971), 2461.

164. E. Pebay Peyroula, R. Jost. J. Mol. Spectry. 121 (1987), 167 .

165. H.J. Oelichmann, D. Bougeard, B. Shrader. J. Mol. Struct. 77 (1981), 149 – 163.

166. A. Engdahl, B. Nelander. Chem. Phys. Lett. 148 No2-3 (1988), 264 – 268.

167. H. Choi, J.M. Kim, S. Shin. J. Appl. Polymer. Sci. 73 (1999), 2691- 2699.

168. J.Z. Knaul, S.M. Hudson, K.A.M. Creber. J. Polymer. Sci. 37. (1999), 1079 – 1094.

169. G. Sun, P.W. Geno, H.A. Mottola. Anal. Chim. Acta. 242 (1991), 233 – 240.

170. H.G. Kraft, B.M. Rode. Inorg. Chim. Acta. 47 (1980), 41 – 45.

171. A. Para, S. Karolczyk-Kostuch. Carbohydrate Polymers 48 (2002), 55 – 60.

172. G. Ibrahim, E. Chebli, M. Khan G.M. Bouet. Trans. Metal Chem. 24 (1999), 294 – 298.

173. U.A. Kumar, S. Chandra. Trans. Metal Chem. 18 (1993), 342 – 344.

174. J.R. Sohn, J.T. Kim. Langmuir 16 (2000), 5430 – 5434.

175. M. Onikata, M. Kondo, N. Hayashi, S. Yamanaka. Clay & Clay Miner. 47 5 (1999), 672 – 677.

176. K. Norrish, J.P. Quirk. Nature. 173 (1954), 255 – 256.

177. P. Fusi, G.G. Ristori, M. Franci. Appl. Clay. Sci. 1 (1986), 375 – 383.

178. P. Fusi, M. Franci, M. Bosetto. Appl. Clay Sci. 3 (1988), 63 – 73.

179. A. Pusino, W. Liu, C. Gessa. Clay & Clay Miner. 41 (1993), 335 – 340.

180. L. Calamai, O. Pantani, A. Pusino, C. Gessa, P.Fusi. Clay & Clay Miner. 45 (1997), 23 – 27.

181. S. Olejnik, A.M. Postner, J.P. Quirk. Clays & Clay Miner. 22 (1974), 361 – 365.

182. V. Gutman. Electrochimica Acta. 21 (1976), 661 – 670.

183. M. Onikata, M. Kondo, S. Yamanaka. Clays & Clay Miner. 47. 5 (1999), 678 – 681.

184. R.D. Laura, P. Cloos. Clays & Clay Miner. 23 (1975), 61 – 69.

185. R.D. Laura, P. Cloos, C. Badot. Clays & Clay Miner. 23. (1975), 417 – 423.

186. R.D. Laura, P. Cloos. Clays & Clay Miner. 23 (1975), 345 – 348.

187. K. Morishige, S. Kittaka, S. Takao. J. Che. Soc. Faraday Trans. 1 80 (1984), 993 – 1003.

188. S. Yariv, L. Heller. Israel Journal of Chemistry. 8 (1970), 935 – 945.

189. S. Meijers, V. Ponec. J. Catal. 149 (1994), 307 – 316.

190. S. Samal, N.K. Mohapatra, S. Acharya, R.K. Dey. Reactive and Functional Polymers. 42 (1999), 37 – 52.

191. R. Sokoll, H. Horbert, I. Schmuck. J. Catal. 125. (1990), 276 – 284.

192. C. Breen, F. Clegg, T.L. Hughes, J .Yarwood. Langmuir. 16. 16 (2000), 6488 – 6516.

193. C. Breen, F. Clegg, T.L. Hughes, J .Yarwood. J. Phys. Chem. B. 105. 21 (2001), 4872 – 4878.

194. M. Kroner, J. Dupuis, M. Winter. J. Prakt. Chem. 343 2 (2000), 115 – 131.

195. F. Linhart, W. Auhorn. Das Papier. 46 **V38** (1992).

196. R.K. Pinschmidt Jr., W.L. Renz, W.E. Carroll, K. Yacoub, J. Drescher, A.F. Nordquist, N. Chen. J. Macromol. Sci. A34 **10** (1997), 1885 – 1905.

197. L. Gu, S. Zhu, A.N. Hrymak, R.H. Pelton. Polymer. 42 (2001), 3077 – 3086.

198. S. Spange, A. Madl, U. Eismann, J. Utecht. Macromol. Rapid Commun. 18 (1997), 1075 – 1083.

199. A. Madl, S. Spange, T. Waldbach, E. Anders, N. Mahr. Macromol. Chem. Phys. 200 (1999), 1495 – 1505.

200. H. Uyama, H. Kato, S. Kobayashi. Polymer Journal. 26. **7** (1994), 858 – 863.

201. A. Madl, S. Spange. Macromolecules. 33 (2000), 5325 – 5335.

202. E.E. Kathmann, L.A. White, C.L. McCormick. Macromolecules. 29. (1996), 5268 – 5272.

203. E.E. Kathmann, L.A. White, C.L. McCormick. Macromolecules. 29. (1996), 5273 – 5278.

Appendix

Conferences Attended

Date	Conference	Location
April 2000	Spring Meeting Applied Minerology Group Clay Minerals Society	Exeter
April 2000	5th Infrared and Raman Discussion Group Meeting	Sheffield
September '01	1st Mid European Clay Conference	Slovakia